



UNIVERSITÀ DEGLI STUDI DI TRENTO

Dipartimento di Ingegneria Civile
e Ambientale



QUEEN MARY
UNIVERSITY OF LONDON

**Erasmus Mundus Joint Doctorate School in Science for Management of Rivers
and their Tidal System**

Navid Marofi Fathpour

Interaction among vegetation and morphology in channelized rivers



Autumn, 2016

Doctoral thesis in “Science for Management of Rivers and their Tidal System”,

Cycle (III)

Primary Institution (Department of Civil, Mechanics and Environmental Engineering, University of Trento, Italy)

Secondary Institution (school of Geography, Queen Mary university of London, United Kingdom)

Associate Partner (Edmund Mach Foundation, San Michele, Italy)

Supervisors

Prof. Aronne Armanini, University of Trento

Prof. Maurizio Righetti, University of Trento

Prof. James Brasington, Queen Mary university of London

Academic year 2013/2016

Associate Partner (Advisor):

Dr. Maria Cristina Bruno, F.E.M. institute



Erasmus Mundus
Joint Doctorate Programme

**SMART - Science for Management of
Rivers and their Tidal systems**

The SMART Joint Doctorate Programme

Research for this thesis was conducted with the support of the Erasmus Mundus Programme¹, within the framework of the Erasmus Mundus Joint Doctorate (EMJD) SMART (Science for Management of Rivers and their Tidal systems). EMJDs aim to foster cooperation between higher education institutions and academic staff in Europe and third countries with a view to creating centres of excellence and providing a highly skilled 21st century workforce enabled to lead social, cultural and economic developments. All EMJDs involve mandatory mobility between the universities in the consortia and lead to the award of recognised joint, double or multiple degrees.

The SMART programme represents collaboration among the University of Trento, Queen Mary University of London, and Freie Universität Berlin. Each doctoral candidate within the SMART programme has conformed to the following during their 3 years of study:

- (i) Supervision by a minimum of two supervisors in two institutions (their primary and secondary institutions).
- (ii) Study for a minimum period of 6 months at their secondary institution
- (iii) Successful completion of a minimum of 30 ECTS of taught courses
- (iv) Collaboration with an associate partner to develop a particular component / application of their research that is of mutual interest.
- (v) Submission of a thesis within 3 years of commencing the programme.

¹This project has been funded with support from the European Commission. This publication reflects the views only of the author, and the Commission cannot be held responsible for any use which may be made of the information contained therein

Acknowledgements

I am writing this part, but when I began it I had not realized that time passes quicker than what I thought. As a result, I've already gained too many valuable experiences for my life from whole around me, particularly my supervisors professor Armanini, Righetti and Brasington with their continuous supports of my PhD research, and for their motivation, enthusiasm, and immense knowledge. By the time their efforts is printed and bound in me and I hope one day I will be wise enough to follow their responsibilities. By that time, I think I would take this thesis down from some upper shelf, dust it, and remember the whole nice time I spent with nice people including the SMART family, my friends, and all others who helped me during the last three years. By the end I want to give a special thanks to my parents and my brother that without their sympathy and encouragement this work would have been more difficult to finish.

Navid Marofi Fathpour

September 2016

Abstract

The presence of aquatic vegetation on riverbed and embankments influences flow structure and consequently flow resistance, sediment transport, morphology, and ecology. These influences would lead to a hydraulic diversity, which is a key ingredient of physical habitat in streams. According to this fact, vegetation is commonly incorporated within stream restoration. Although significance of vegetation as an inseparable part of riverine systems is recognized, but yet it is still difficult to predict how the associated influences will respond to the introduction of vegetation and how advantages of vegetation can be optimized to a multitude of different processes.

The primary impact of vegetation is slower flow velocity and thus, reduction in conveyance capacity. In addition to affecting the velocity profile over the full depth, vegetation affects turbulence intensity and diffusion. When mean kinetic energy converts to turbulent kinetic energy within the area planted with stems, turbulence intensity will begin to intensify. As a result of velocity and turbulence changes, aquatic vegetation can affect sediment movement and consequently bed form shapes could be stabilized with new patterns. Bed form characteristics (length, shape, structure, dimensions, stability, etc.) also depend on flow structure and can be divided into different categories according to the bed load materials.

Locations and extension of vegetation in river channels is a fundamental factor should be considered besides the general impacts of vegetation in rivers. Isolated patches of vegetation are more common in practical applications rather than uniform vegetated channels in which the mean properties of the vegetation canopy are independent of the location.

The present study considered the changes in bed forms through semi-circular patches of emergent vegetation, which are located at the banks of the channel. One of the goals is to find out how an island of vegetation modifies the morphology of rivers and mass transport. In particular, this research focuses on the physics of sediment transport and its effect on bed forms, and flow resistance in the presence of a patch of vegetation, by using experimental data and numerical modeling. Providing a physically based model for estimating the effects of vegetation on flow parameters, turbulence dispersion, and sediment transportation, the results of the present study contribute to extending the knowledge of morphology and mass transport in vegetated streams.

Table of Contents

1	Chapter 1: State of art	1
1.1	Vegetation in rivers	1
1.2	Interaction among vegetation and sediment transport	3
1.3	Approaches to use vegetation in restoration projects in terms of sediment management	4
1.4	Review of field investigation about the effects of vegetation on sediment transport	6
1.4.1	<i>Review of experimental modelling of vegetation in flumes</i>	7
1.4.2	<i>Interaction of uniform vegetation in channels and sediment transport</i>	8
1.4.3	<i>Interaction of finite patches of vegetation in channels and sediment transport</i>	8
1.5	Interaction of patches of bank vegetation with river patterns	10
1.6	Review of numerical modelling of vegetation	11
1.7	Research questions	12
1.8	Research objectives	14
1.9	Outline	15
2	Chapter 2: Experimental modelling	16
2.1	Experimental setup	16
2.2	Experimental program	17
2.3	Acoustic Doppler velocimetry	18
2.4	ADV in the present study	20
2.5	Bed profile measurements.....	21
2.6	Bed material characteristics	22
2.7	Simplification and uncertainties	23
2.8	Summary of chapter 2	24
3	Chapter 3: Numerical model	25
3.1	Numerical model setup	25
3.1.1	<i>Model grid and bathymetry</i>	25
3.1.2	<i>Hydrodynamic setup</i>	26
3.1.3	<i>Boundary conditions</i>	28
3.1.4	<i>Physical parameters</i>	28
3.1.5	<i>Implementation of patches of vegetation</i>	33
3.2	Summary of chapter 3	35
4	Chapter 4: velocity results of experiments	36
4.1	Velocity	36
4.1.1	<i>Effects of density of vegetation on streamwise velocity</i>	37

4.1.2	<i>Effects of density of vegetation on transverse velocity</i>	45
4.1.3	<i>Effects of density of vegetation on vertical velocity</i>	53
4.2	Conclusion	57
5	Chapter 5: Morphodynamic result of finite patches of stems	59
5.1	Scouring and deposition process	59
5.2	Characteristics of scouring zone	61
5.2.1	<i>Location of scour holes</i>	61
5.2.2	<i>Depth of scour holes</i>	66
5.3	Characteristics of deposition zone.....	71
5.3.1	<i>Location of deposits</i>	71
5.3.2	<i>Height of deposits</i>	75
5.4	Prediction of affected lateral and longitudinal distance	79
5.5	Conclusions	81
6	Chapter 6: Results of calibrated model, validation and sensitivity analysis	83
6.1	Model calibration	83
6.2	Results of the calibrated model	86
6.3	Validation analysis	91
6.4	Sensitivity analysis of the Variables	96
6.5	Summary and Conclusion of chapter 6	96
7	Chapter 7: Results of calibrated model, validation and sensitivity analysis	98
7.1	Methodology	98
7.2	Installation of mutual patches	99
7.3	Validation of numerical code for mutual patches	106
7.4	Effects of non dimensional lateral distance (W/D) in a channel	111
7.4.1	<i>Velocity impacts</i>	112
7.4.2	<i>Bed profile</i>	116
7.5	Effects of non dimensional longitudinal distance (L/D) in a channel	119
7.6	Estimation of meander pattern	126
7.7	Conclusion.....	130
8	References	133
9	Appendix A: parameter settings	124
9.1	Numerical setting	124
10	Appendix B: Experimental results	127
10.1	Streamwise velocity	127

10.2	Transverse velocity.....	130
10.3	Vertical velocity.....	133
10.4	Ranges of velocities	137

List of Figures

Figure 1.1. Diversity of regions around an island of vegetation inside a river	2
Figure 1.2. Flowchart of the methodology of the study	13
Figure 2.1. (a) Side view and (b) plan of the channel.....	17
Figure 2.2. 3D ADV probe (b) transmitter, receivers and sampling volume location (Velasco and Huhta, 2009)	19
Figure 2.3 Process of sending and receiving the pulses by transmitter and receivers (Doppler technique)	19
Figure 2.4. Location of velocity measurements for a single patch of vegetation	20
Figure 2.5. a: Laser profiler; b: Domain of measurements	21
Figure 2.6. Cumulative grain size distribution of the sediment.....	22
Figure 2.7. Sample of sediment measurement. ($\Omega v=0.05$, $Fr=0.4$).....	23
Figure 2.8. Sample of sediment measurement. Test n. 4 ($\Omega v=0.05$, $Fr=0.4$)	24
Figure 3.1. The computational control volume depth (\bullet), water level (L), velocity (V) (source: Deltares, 2006).....	26
Figure 3.2. Boundary conditions and roughness details	28
Figure 3.3. Shear stress on vegetated and non-vegetated beds	30
Figure 3.4. Morphological update scheme	33
Figure 4.1. Plan view of streamwise component of the velocity in a channel with Fr number=0.2 and density of the patch of vegetation=0.025, (a): at 0.2 h, (b): at 0.8h.....	37
Figure 4.2. Plan view of streamwise component of the velocity in a channel with Fr number=0.2 and density of the patch of vegetation=0.05, (a): at 0.2 h, (b): at 0.8h.....	38
Figure 4.3. Plan view of streamwise component of the velocity in a channel with Fr number=0.2 and density of the patch of vegetation=0.1, (a): at 0.2 h, (b): at 0.8h.....	39
Figure 4.4. Origin of coordinate and longitudinal lines along the channel, which are used to investigate the velocity	40
Figure 4.5. longitudinal transects of depth-average streamwise velocity along two axes of $y/W=0.15$, 0.85 in the channel with $Fr\#=0.1$, $Fr\#=0.3$, $Fr\#=0.4$; (a): $\Omega=0.025$, (b): $\Omega=0.05$, (c): $\Omega=0.1$	41
Figure 4.6. Streamwise velocity along two longitudinal axes of $y/W=0.15$, 0.85 in the channel with $0.1 < Fr\# < 0.4$	42
Figure 4.7. Creation of a shear layer around a patch of vegetation	43

Figure 4.8. Location of the vortices around the patch; a & b: Large-scale vortices and their effects on bed profile; c: location of small-scale vortices along the steady region at the wake of the patch.....	44
Figure 4.9. Plan view of the transverse component of the velocity in a channel with Fr number=0.2 and density of the patch of vegetation=0.025, A: at 0.2 h, B: at 0.8h.....	46
Figure 4.10. Plan view of the transverse component of the velocity in the channel with Fr number=0.2 and density of the patch of vegetation=0.05, A: at 0.2 h, B: at 0.8h.....	46
Figure 4.11. Plan view of the transverse component of the velocity in a channel with Fr number=0.2 and density of the patch of vegetation=0.1, A: at 0.2 h, B: at 0.8h.....	47
Figure 4.12. Comparison of V_y/V_x ratio between 0.2h and 0.8h at different cross sections $Fr=0.4$, $\Omega=0.1$, (a): $x/D=-1$, (b): $x/D=-0.5$, (c): $x/D=0$, (d): $x/D=0.5$	48
Figure 4.13. Longitudinal transects of the transverse velocity in a channel with a patch of density $\Omega=0.025$ - a: along axes of $y/W=0.85$, b: along axes of $y/W=0.5$, c: along axes of $y/W=0.15$. d: comparison of normalized transverse velocity of tests with $\Omega=0.025$ and $Fr=0.1$ & 0.4, e: comparison of normalized transverse velocity of tests with $\Omega=0.025$ and $Fr=0.3$ & 0.4, f: comparison of normalized transverse velocity of tests with $\Omega=0.025$ and $Fr=0.1$ & 0.3.....	49
Figure 4.14. longitudinal transects of depth average transverse velocity in a channel with $Fr=0.1$ and different patches of densities along three axes of a: $y/W=0.85$, b: $y/W=0.5$, c: $y/W=0.15$	51
Figure 4.15. a: lateral transverse velocity profile over the cross section of $x/D=0$ for different density of vegetation; b: lateral transverse velocity profile over the different cross section for a channel with a patch of density of 0.025.....	52
Figure 4.16. Plan view of vertical component of the velocity in a channel with Fr number=0.2 and density of the patch of vegetation=0.025, (a): at 0.2 h, (b): at 0.8h.....	53
Figure 4.17. Plan view of vertical component of the velocity in a channel with Fr number=0.2 and density of the patch of vegetation=0.05, (a): at 0.2 h, (b): at 0.8h.....	54
Figure 4.18. Plan view of vertical component of the velocity in a channel with Fr number=0.2 and density of the patch of vegetation=0.1, (a): at 0.2 h,	

(b): at 0.8h.....	54
Figure 4.19. Ranges of velocity components. (a): $Fr=0.1, \Omega=0.025$, at 0.2h; (b): $Fr=0.1, \Omega=0.025$, at 0.8h; (c): $Fr=0.1, \Omega=0.05$, at 0.2h; (d): $Fr=0.1,$ $\Omega=0.05$, at 0.8h; (e): $Fr=0.1, \Omega=0.1$, at 0.2h; f: $Fr=0.1, \Omega=0.1$, at 0.8h	56
Figure 5.1. Schematic view of scouring and deposition around the vegetation zone (not to scale).....	60
Figure 5.2. (a): extension of scouring across the width and development of erosion and deposition ($\Omega_v =0.025, Fr=0.1$) (b): scouring within and around the patch ($\Omega_v =0.1, Fr=0.4$)	60
Figure 5.3. Contour lines of the scouring downstream the vegetation patches (a) $\Omega_v =0.05, Fr=0.1, D=50\text{cm}$; (b) $\Omega_v =0.05, Fr =0.3, D=50\text{cm}$; (c) Ω_v $=0.05, Fr =0.4, D=50\text{cm}$	62
Figure 5.4. Fitted curves and extracted data with minimum bed elevations in all cross sections from the upstream edge of the patch for different Froude numbers and constant vegetation density	62
Figure 5.5. Fitted curve and extracted data with the minimum elevations along the channel for two different patch densities and same flow Froude number	63
Figure 5.6. Variation of U_1/U_0 with Fr number for different values of the vegetation densities of the patches.....	64
Figure 5.7. Location of extracted data with minimum elevation in all cross sections around the patch over depth-average transverse velocity profile for experiments with $Fr=0.2$; a. $\Omega_v=0.025$; b: $\Omega_v=0.05$; c: $\Omega_v=0.1$	65
Figure 5.8. Longitudinal profile of fitted curves on extracted data with minimum bed elevations	66
Figure 5.9. Longitudinal profile of fitted curves on extracted data with minimum bed elevations	67
Figure 5.10. Shear stress distribution for experiments with $Fr=0.1, D=50\text{ cm}$, (a): $\Omega_v=0.025$; (b): $\Omega_v=0.05$; (c): $\Omega_v=0.1$	68
Figure 5.11. Bed patterns and Contour lines of the scouring downstream of patches ($Fr=0.1, D=50\text{cm}$); (a) $\Omega_v =0.025$; (b) $\Omega_v =0.05$; (c) $\Omega_v =0.1$	69
Figure 5.12. Contour lines of the deposits downstream the vegetation patches (a) $\Omega_v=0.05, Fr=0.1, D=50\text{cm}$; (b) $\Omega_v =0.05, Fr =0.3, D=50\text{cm}$; (c) Ω_v $=0.05, Fr =0.4, D=50\text{cm}$	72
Figure 5.13. The highest elevation of the deposition areas at the wake of the patch of vegetation in all cross sections from the downstream edge of the patch	73

Figure 5.14. Longitudinal profile of the fitted curve on the extracted data with highest bed elevations	73
Figure 5.15. Schematic diagrams for velocity vectors and steady zone; (a): before installation of a patch, (b): after installation of a patch with low density, (c): after installation of a patch with high density	74
Figure 5.16. Relation between the length of the steady region, vegetation density and flow Fr number	75
Figure 5.17. Deposition pattern inside and behind the vegetation zone-(a): $\Omega_v=0.025$, $Fr=0.3$, $D=50$ cm; (b) $\Omega_v=0.1$, $Fr=0.3$, $D=50$ cm.....	76
Figure 5.18. Deposition pattern behind the vegetation zone-(a): $\Omega_v=0.1$, $Fr=0.3$, $D=70$ cm; (b) $\Omega_v=0.05$, $Fr=0.3$, $D=70$ cm	77
Figure 5.19. Experimental data for the normalized dune height as a function of Fr number.....	78
Figure 5.20. Ellipse pattern to identify location of erosion and deposition around the vegetation zone.....	78
Figure 5.21. Definition of lateral and longitudinal effective lengths	79
Figure 5.22. relation among vegetation density, lateral, and longitudinal effective lengths	80
Figure 6.1. Steps in a typical calibration procedure	84
Figure 6.2. Plan of the depth average component of the velocity in a channel with flow from left to right, $\Omega_v=0.05$, $D=50$ cm, $U_0=28.5$ cm/s, $h_0=10.5$ cm, (flow from left to right)- (a): numerical result of streamwise velocity, (b): Experimental result of transverse velocity, (c): Numerical result of streamwise velocity, d: Experimental result of transverse velocity.....	87
Figure 6.3. bed profile of the experiment with $\Omega_v=0.05$, $D=50$ cm, $U_0=28.5$ cm/s, $h_0=10.5$ cm, (flow from left to right). (a): numerical result, (b): experimental result.....	88
Figure 6.4. Comparison between the experimental and numerical data on the values of the depth average streamwise component of the velocity in a channel with $\Omega_v=0.05$, $D=50$ cm, $U_0=28.5$ cm/s, $h_0=10.5$ cm and along three different axes. a: $y/W=0.15$, b: $y/W=0.5$, $y/W=0.85$	89
Figure 6.5. Comparison between the experimental and numerical data on the values of the depth average transverse component of the velocity in a channel with $\Omega_v=0.05$, $D=50$ cm, $U_0=28.5$ cm/s, $h_0=10.5$ cm and along three different axes. a: $y/W=0.15$, b: $y/W=0.5$, $y/W=0.85$	89
Figure 6.6. comparison between the experimental and numerical data on the values of bed elevation in a channel with $\Omega_v=0.05$, $D=50$ cm, $U_0=28.5$	

cm/s, $h_0=10.5$ cm along three different axes. a: $y/W=0.15$, b: $y/W=0.5$, $y/W=0.85$	91
Figure 6.7. Plan of the depth average streamwise component of the velocity in a channel with $\Omega_v=0.1$, $D=50$ cm, $U_0=18.5$ cm/s, $h_0=17.7$ cm, (flow from left to right) – (a): numerical result (b): experimental result	92
Figure 6.8. Plan of the depth average transverse component of the velocity in a channel with $\Omega_v=0.1$, $D=50$ cm, $U_0=18.5$ cm/s, $h_0=17.7$ cm, (flow from left to right) – (a): numerical result (b): experimental result.....	93
Figure 6.9. Plan of the depth average streamwise component of the velocity in a channel with $\Omega_v=0.025$, $D=50$ cm, $U_0=38.5$ cm/s, $h_0=7.8$ cm, (flow from left to right) – (a): numerical result (b): experimental result	93
Figure 6.10. Plan of the depth average transverse component of the velocity in a channel with $\Omega_v=0.025$, $D=50$ cm, $U_0=38.5$ cm/s, $h_0=7.8$ cm, (flow from left to right) – (a): numerical result (b): experimental result	94
Figure 6.11. bed profile of the experiment with $\Omega_v=0.1$, $D=50$ cm, $U_0=18.5$ cm/s, $h_0=17.7$ cm, (flow from left to right); (a): numerical result, (b): experimental result.....	95
Figure 6.12. bed profile of the experiment with $\Omega_v=0.025$, $D=50$ cm, $U_0=38.5$ cm/s, $h_0=7.8$ cm, (flow from left to right). (a): numerical result, (b): experimental result.....	95
Figure 7.1. Location of patches of vegetation and the details of the experimental channel (Origin of coordinate and longitudinal lines along the channel, which are used to investigate the velocity).....	99
Figure 7.2. Location of velocity measurements along the channel	100
Figure 7.3. Depth average component of the velocity along 2 longitudinal axes- (a): transverse velocity along $y/W=0.5$, (b): streamwise velocity along $y/W=0.5$, (c): transverse velocity along $y/W=0.2$ & (d): streamwise velocity along $y/W=0.2$	102
Figure 7.4. bed profile along the experimental channel (density of the patches=0.05, $D=50$ cm)-(a): ($U_0=18.5$ cm/s, $h_0=17.7$ cm), (b): ($U_0=28.5$ cm/s, $h_0=10.5$ cm), and (c): ($U_0=38.5$ cm/s, $h_0=7.8$ cm).....	103
Figure 7.5. bed profile along the experimental channel (density of the patches=0.025, $D=56$ cm)-(a): ($U_0=18.5$ cm/s, $h_0=17.7$ cm), (b): ($U_0=28.5$ cm/s, $h_0=10.5$ cm), and (c): ($U_0=38.5$ cm/s, $h_0=7.8$ cm).....	105
Figure 7.6. bed profile along the experimental channel (density of the patches=0.1, $D=38$ cm)-(a): ($U_0=18.5$ cm/s, $h_0=17.7$ cm), (b): ($U_0=28.5$ cm/s, $h_0=10.5$ cm), and (c):($U_0=38.5$ cm/s, $h_0=7.8$ cm).....	105

Figure 7.7. Comparison of depth average velocity result of the numerical simulation (density of the patches=0.05, $D=50$ cm) ($U_0=38.5$ cm/s, $h_0=7.8$ cm)- (a): Experimental measurements, (b): Numerical results.....	107
Figure 7.8. Comparison of simulated depth average component of the velocity along 2 longitudinal axes of $y/W= 0.2$, & 0.5 (density of patches= 0.05, $D=50$ cm, $U_0=28.5$ cm/s, $h_0=10.5$ cm)- (a): transverse velocity along $y/W=0.5$, (b): streamwise velocity along $y/W=0.5$, (c): transverse velocity along $y/W=0.2$ & (d): streamwise velocity along $y/W=0.2$	109
Figure 7.9. bed profile results of the numerical simulation (density of the patches=0.05, $D=50$ cm) ($U_0=28.5$ cm/s, $h_0=10.5$ cm).....	109
Figure 7.10. Extracted data with minimum bed elevations in all cross sections along the channel.....	110
Figure 7.11. components of the velocity along five longitudinal axes of $y/W=0.1, 0.3, \& 0.5$ in the channel with $W/D = X_w/D$, (a): stream-wise velocity (V_x), (b): transverse velocity(V_y).....	113
Figure 7.12. Transverse velocity of channels with $W/D < X_w/D$ to $4X_w/D < W/D$, (a): $y/W=0.1$, (b): $y/W=0.3$, (c): $y/W=0.5$	114
Figure 7.13. Stream-wise velocity of channels with $W/D < X_w/D$ to $4X_w/D < W/D$, (a): $y/W=0.1$, (b): $y/W=0.3$, (c): $y/W=0.5$	115
Figure 7.14. Bed profile of the channels with different W/D ratio and equal physical, initial and boundary condition-(a): $W/D=1$, (b): $W/D=2$, (c): $W/D=3$, (d): $W/D=4$, (e): $W/D=6$, (f): $W/D=10$	117
Figure 7.15. Probable bed profile in channels with different W/D ratio.....	118
Figure 7.16. Bed profile and distribution of components of the velocity-(a): Transverse velocity $X_L=0.75$; (b): Transverse velocity $X_L=1.25$; (c): Streamwise velocity $X_L=0.75$; d: Streamwise velocity $X_L=1.25$	121
Figure 7.17. Bed profile and distribution of components of the velocity-(a): Transverse velocity $X_L=1.75$; (b): Transverse velocity $X_L=2.75$; (c): Transverse velocity $X_L=3.75$; (d): Transverse velocity $X_L=5.25$; (e): Streamwise velocity $X_L=1.75$; (f): Streamwise velocity $X_L=2.75$; (g): Streamwise velocity $X_L=3.75$; (h): Streamwise velocity $X_L=5.25$	122
Figure 7.18. Effects of longitudinal intervals on scouring area.....	123
Figure 7.19. Longitudinal components of the velocity along a channel with $y/w=0.1$ -(a): Transverse velocity; (b): Streamwise velocity.....	124
Figure 7.20. (a). Average bed slope of the central part of the experimental channel before and after the installation of patches of vegetation; (b): Comparison of bed slope of the central part and meander part.....	126

Figure 7.21. Comparison of the meander bed forms along one meander wave-length, $D=0.56\text{m}$, $\Omega_v=0.025$, $Fr=0.3$	127
Figure 7.22. Comparison of the meander bed forms along one meander wave-length, $D=0.5\text{m}$, $\Omega_v=0.05$, $Fr=0.3$	128
Figure 7.23. Comparison of the meander bed forms along one meander wave-length, $D=0.38\text{m}$, $\Omega_v=0.1$, $Fr=0.3$	128
Figure 7.24. Effects of vegetation density on meander pattern	129
Figure 10.1. Plan view of the streamwise component of the velocity with Fr number=0.3 and $\Omega_v=0.025$, A: at 0.2 h, B: at 0.8h	127
Figure 10.2. Plan view of the streamwise component of the velocity with Fr number=0.4 and $\Omega_v=0.025$, A: at 0.2 h, B: at 0.8h	128
Figure 10.3. Plan view of the streamwise component of the velocity with Fr number=0.3 and $\Omega_v=0.05$, A: at 0.2 h, B: at 0.8h	128
Figure 10.4. Plan view of the streamwise component of the velocity with Fr number=0.4 and $\Omega_v=0.05$, A: at 0.2 h, B: at 0.8h	129
Figure 10.5. Plan view of the streamwise component of the velocity with Fr number=0.3 and $\Omega_v=0.1$, A: at 0.2 h, B: at 0.8h	129
Figure 10.6. Plan view of the streamwise component of the velocity with Fr number=0.4 and $\Omega_v=0.1$, A: at 0.2 h, B: at 0.8h	130
Figure 10.7. Plan view of the transverse component of the velocity with Fr number=0.3 and $\Omega_v=0.025$, A: at 0.2 h, B: at 0.8h	131
Figure 10.8. Plan view of the transverse component of the velocity with Fr number=0.4 and $\Omega_v=0.025$, A: at 0.2 h, B: at 0.8h	131
Figure 10.9. Plan view of the transverse component of the velocity with Fr number=0.3 and $\Omega_v=0.05$, A: at 0.2 h, B: at 0.8h	132
Figure 10.10. Plan view of the transverse component of the velocity with Fr number=0.4 and $\Omega_v=0.05$, A: at 0.2 h, B: at 0.8h	132
Figure 10.11. Plan view of the transverse component of the velocity with Fr number=0.3 and $\Omega_v=0.1$, A: at 0.2 h, B: at 0.8h	133
Figure 10.12. Plan view of the transverse component of the velocity with Fr number=0.4 and $\Omega_v=0.1$, A: at 0.2 h, B: at 0.8h	133
Figure 10.13.. Plan view of the vertical component of the velocity with Fr number=0.3 and density of the patch of vegetation=0.025, A: at 0.2 h, B: at 0.8h	134
Figure 10.14.. Plan view of the vertical component of the velocity with Fr number=0.4 and density of the patch of vegetation=0.025, A: at 0.2 h, B: at 0.8h	134

Figure 10.15. Plan view of the vertical component of the velocity with Fr number=0.3 and density of the patch of vegetation=0.05, A: at 0.2 h, B: at 0.8h	135
Figure 10.16. Plan view of the vertical component of the velocity with Fr number=0.4 and density of the patch of vegetation=0.05, A: at 0.2 h, B: at 0.8h	135
Figure 10.17. Plan view of the vertical component of the velocity with Fr number=0.3 and density of the patch of vegetation=0.1, A: at 0.2 h, B: at 0.8h	136
Figure 10.18. Plan view of the vertical component of the velocity with Fr number=0.4 and density of the patch of vegetation=0.1, A: at 0.2 h, B: at 0.8h	136
Figure 10.19. Ranges of velocity components. a: Fr=0.3, $\Omega=0.025$, at 0.2h; b: Fr=0.3, $\Omega=0.025$, at 0.8h; c: Fr=0.4, $\Omega=0.025$, at 0.2h; d: Fr=0.4, $\Omega=0.025$, at 0.8h	137
Figure 10.20. Ranges of velocity components. a: Fr=0.3, $\Omega=0.05$, at 0.2h; b: Fr=0.3, $\Omega=0.05$, at 0.8h; c: Fr=0.4, $\Omega=0.05$, at 0.2h; d: Fr=0.4, $\Omega=0.05$, at 0.8h	138
Figure 10.21. Ranges of velocity components. a: Fr=0.3, $\Omega=0.1$, at 0.2h; b: Fr=0.3, $\Omega=0.1$, at 0.8h; c: Fr=0.4, $\Omega=0.1$, at 0.2h; d: Fr=0.4, $\Omega=0.1$, at 0.8h	139

List of Tables

Table 2.1 Summary of experiments of first phase	18
Table 3.1. Properties of bed material.....	31
Table 5.1. Features of scour holes and correspondent transverse velocity	69
Table 6.1. Overview of parameters.....	84
Table 6.2. Summary of the condition of tests for validation	92
Table 7.1. Summary of experiments with mutual patches	100
Table 7.2 Details of simulation variables	110
Table 9.1 Applied parameters in simulations	124

1 Chapter 1: State of art

Using of in-stream structures is common for stream restoration with variety prospects from geomorphic modification to improving the ecosystem services. The applied materials of these structures can be artificial such as concrete and metals or natural such as rocks and woods or a composition of them. Recently and due to environmental aspects, the use of natural elements for river engineering projects promote considerably. Vegetation represents an ecologically sensitive and multifunctional alternative to in-stream structures composed of natural materials.

This chapter reviews the relevant studies to understanding the interaction of aquatic vegetation in river channels. The main purpose of this chapter is to explain the usage of vegetation in river restoration programs and classify the role of vegetation on river morphologies due to their position in a channel. Finally, the gaps are defined and the research questions are presented.

1.1 Vegetation in rivers

Flow resistance could change due to shear stress induced mainly by variation of grains and bed forms. But in the presence of vegetation, the additional resistance exerted by plants reduces the mean flow within vegetated regions (Kadlec, 1990; Shi et al., 1995). Vegetation could grow and spread in river channels and floodplains, and alter flow condition and morphology, habitat, and water quality (Yager and Schmeckle, 2013; Everard and Quinn, 2015; Termini, 2016; Platts and Nelson, 1985; Dosskey et al., 2010). Riparian vegetation is a ubiquitous feature of riverine landscapes controlling sediment and nutrients which are an inseparable part of the food chain in fluvial system (Hey & Throne, 1986).

Decelerated flow at the wake of an island of vegetation might be ecologically important, because it acts like a wake of boulders and woody debris in shallow flows and provides shade and a refuge to fish (figure 1.1). Basically, multiple species of fish prefer areas with low velocity and turbulence because they consume less energy and also accumulation of fine particle in these areas provides a good source of macro-invertebrates (Harrison and Harris, 2002). In fact, this region provides a low turbulence zone, which acts like a pool and might be appropriate for fishes to spawn and also other aquatic organisms to live and proliferate (Schlosser, 1982). On the other hand, associated scour holes around

the vegetation patches may also be a suitable refuge for small fish, which are mostly like to live in ripples (Gerstner, 1998).

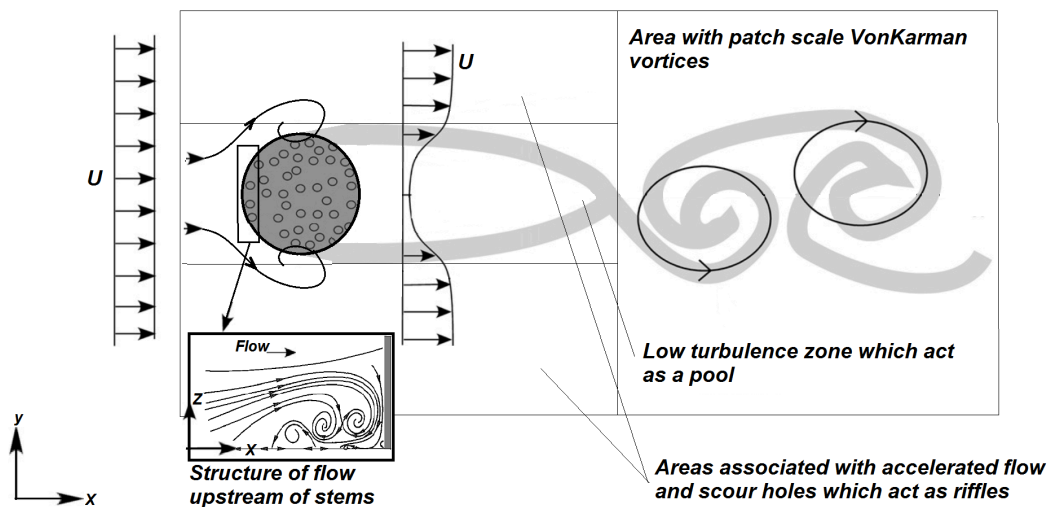


Figure 1.1. Diversity of regions around an island of vegetation inside a river

The influences of vegetation in water bodies depend on flow characteristics (velocity, depth, shear stress, and turbulence), vegetation features (flexibility, density, and submersion rate), and bed material (roughness, and grain size) (Ghisalberti and Nepf, 2006; Bouma et al., 2007; Armanini et al., 2010). Generally, the negative and positive effects of vegetation can be classified separately:

The negative effects:

- Increase flow resistance and reduce flow conveyance which is important factor in flood risk management (Wilson, 2007).
- Promotes erosion under some special conditions like acceleration of flow along the vegetation edges, which could cause local erosion (Bouma et al., 2007).
- Enhance difficulties in inspecting and maintaining the structural integrity of flood embankments (Darby, 1999).

The positive effects:

- Improving water quality by removing nutrients and releasing oxygen to the water column (Wilcock et al., 1999).
- Promotes habitat diversity by creating a diversity of flow regimes (Platts and Nelson, 1985).
- Stabilizing the bed and bank of the rivers (Vargas-Luna et al., 2015).

-
- Trapping the sediment and increasing sedimentation because of reduction of the flow velocity (Bouteiller and Venditti, 2014).
 - Enhance the growth of ridges and islands (Pietsch and Nanson, 2011).

1.2 Interaction among vegetation and sediment transport

Overlay studies about the interaction between vegetation and flow have indicated that within vegetated areas, flow velocity is reduced while turbulence intensity is increased. Hence, vegetation can be considered as a factor of increasing the flow resistance and reducing the transport capacity of the flow (Fischenich, 1997; Wilson, 2007). However, flow characteristics besides the size, shape, density and flexibility of vegetation, and the degree of submergence determine the effects of vegetation in fluvial systems.

Generally, in terms of sediment management, endlessly changing currents, influence the ongoing sedimentation and erosion processes and make the related analysis more complicated. Despite the variability of bed load flux in vegetation areas, there is a stable scouring and deposition pattern of sediment around each stem and each patch of vegetation, which can be explained by considering variability of lateral and vertical components of the bed load flux in upstream side of each stem, and balancing them with stream-wise component in downstream side of the stem.

Scouring and deposition have been defined as a function of turbulent kinetic energy which is related to the porosity of the vegetation. (Follett and Nepf, 2012) High local velocities and generated vortices at the vegetation interface may increase the local erosion and this maybe lead to uprooting the plants (Rominger et al., 2010). On the other hand, increasing the local deposition may also bury the plants (Hupp and Bazemore, 1993). Understanding of these dynamic processes, that govern sedimentation and erosion on rivers, helps scientists to improve the knowledge about the interaction of vegetation and sediment.

Interaction of flow and vegetation generates local vortices and causes promotion of turbulence through generating a variety of coherent flow structures. Generated structures can be classified into three different groups: 1 Horseshoe vortices which are usually generated immediately upstream sides of the vegetation and cause local scour at these parts (figure 1.1) (Dargahi, 1990); 2 Von Karman vortices which are created due to the flow separation downstream of vegetation (Zong and Nepf, 2010); 3 Kelvin Helmholtz vortices which are produced by inflectional instability in the mean velocity at the interface between vegetated and non-

vegetated areas (Poggi et al, 2004). In addition to the associated vortices and their magnitude, sediment movements in vegetation is a function of bed grain size, sediment supply, vegetation density and species, and vegetation location.

Due to the distribution of bed material, different bed pattern could be formed from armored bed to fine deposited bed, because variability in grain size could alter the spatial patterns in bed load flux (Bridge, 2003). Coarser grains are rarely erodible, than fine sediment, while coarser bed provides greater near-bed turbulence. Local pattern of sedimentation is important from different points of view. First of all, recruitment and survival of plants, because the creation of scour hole immediately adjacent to the stems reduce the stability of vegetation. Survival of vegetation close to these scour holes depends on scour depth and root strength. On the other hand, associated deposition of sediment could bury the smoother and short seedlings and change the characteristics of vegetation. Burial of some seedlings could provide more uniform stem pattern instead of clustered pattern (Arens et al., 2001). Second, the fixed pattern of sedimentation associated with patches provides more complex profile, which could enhance the diversity of habitat species (Pollock et al., 1998). However, the elucidation of complex interaction between turbulence generation, bed material, and vegetation features require more investigation.

1.3 Approaches to use vegetation in restoration projects in terms of sediment management

River channels and their corridors are important systems from ecological, flood safety, and aesthetic perspectives. During the last centuries, most of the engineering projects in densely populated areas have been aimed to enhance the agricultural production and promote the protection of assets from flooding. Most of these activities have not only decreased the flood risk, but also resulted in ecological degradation of sensitive riverine habitats (Wiklund et al., 2009). This resulted in broad range of activities like restoration programs to protect river ecosystems. Restoration proposals aim to solve problems associated with anthropogenic-induced channel aggradation and degradation (Brookes and Brierley, 2004).

Protective management of fluvial systems is complicated due to addressing of multiple motives simultaneously. Generally, these motives include ecosystem restoration, flood control, bank and bed protection, sediment management, water quality, aesthetics and recreation. Neglecting of each motive could lead to more associated problems. For example, previous efforts for flood controls mostly tried

to increase channel capacity and conveyance ability by removing the vegetation and channelization of rivers. But river channelization could disrupt and degrade stream systems by reduction of wetland and isolation of main channels from natural flood retention areas and provide flashy hydrographs, steep banks, excessive sediment loads, wide and straight channels, and shallow water (Ganoulis, 2003). In the other word, intensified catchment land-use has even increased the propagation of flood waves (Jarvela et al., 2006).

Sediment management has long been considered in river engineering, and more recently in river restoration. Although sediment management may not be the only restoration motive, but in order to increase the efficiency and achieve better responses, it should be considered in all restoration projects (Sear, 1994). Substantial time lags and non-linearity in channel response could compile with permanent alteration of sediment source and constrain the recovery potential. According to these facts and considering the associated sediment problems, Sear et al. (2003), classified the sediment management techniques into different groups:

1. Erosion control: Stabilize bed and bank erosion by reinstatement or introducing of practical methods to protect threatened assets
2. Gravel Trap: Control and catch the coarse fraction of the sediment load by designing the structures to maintain downstream facilities
3. Re-alignment: Increase the conveyance capacity by regarding and re-sectioning to decrease flood risk.
4. Re-grade: Modify the channel slopes and long profiles based on regime theory.
5. Re-section: Modify and return the cross sections to design configuration, including re-profiling bed and banks.
6. Dredge: Enhance the flood defense and secure navigation activities by removing of deposits to a suitable degree
7. De-silt: Enhance the flow conveyance by removing the fine accumulated sediments.
8. Shoal removal: Flood control by removing of individual shoals.

Each of these techniques has been a widespread practice to achieve certain goals like improving the agricultural drainage, flood conveyance, and navigation system.

Recently, river health and ecologically management encouraged restoration projects to use more environmental options like vegetation. The incorporation of vegetation can be classified into three different categories: 1. Plantings of aquatic vegetation such as live cuttings, dormant willow posts, grasses and other kinds of

macrophytes; 2. Combinations of rocks, stones and vegetation such as bioengineered revetments with vegetation; 3. Usage of wooden material such as engineered log jams and woody debris (Neary et al., 2012). In addition, understanding of the broad consequences of using vegetation as a practical tool for restoration projects has been focused scientist's attention for finding effective methods to increase the efficiency of these projects. Different environmentally approaches have been proposed to use vegetation in restoration projects to improve water bodies from different aspects like increasing the bank and bed stability, providing shade and refugees for aquatic organisms, and controlling morphological changes by stabilizing migration rates. Environmental appeals of bioengineering approaches have promoted the motivation of understanding more details about the interaction among flow, vegetation and sediment transport with improved monitoring devices and data elaboration (Klaassen, 2002).

1.4 Review of field investigation about the effects of vegetation on sediment transport

In organic wetland systems, vegetation grows on deep organic sediment and forms the margins and the bed of river channels (Gurnell, 2013). Also the growth of vegetation on dry-land river channel beds, trap sediment particles and lead to formation of stable ridge-shaped islands which can change water and sediment transfer (Pietsch and Nanson, 2011). Dabney et al. (1993), described the aspects of application of vegetation barriers, which control water and sediment of surface runoff. Different parameters influence the interaction of vegetation and sediment. Huang and Nelson (1997), divided the effects of the vegetation in fluvial system between bed and bank vegetation.

Due to the location of the vegetation on bed or bank of the rivers, their influence and the effective parameters on sediment processes would be different. Increasing of the density of bank vegetation causes narrower and deeper channels, while dense vegetation within the channel can change the effective cross section that conveys the flow and leads to wider channels and significantly influence flow velocity and fate of sediment (Huang and Nelson, 1997; Hicks et al. 2006). Bouma et al., (2007), considered epibenthic structures as a physical structure in river streams and monitored them for two years at different locations with different type of vegetation (Bamboo cane and spartina tussocks). They supposed that the presence of these structures could change the local flow pattern and modify the erosive forces that water exerts on the sediment. Edwards et al. (1999), observed scouring around islands in Tagliamento river.

The effects of vegetation on bank stability cannot be easily quantified or statistically tracked, because not only the growth of vegetation consists of complicated stages, but also interacting factors like geomorphic characteristics and vegetation species play complex roles (Rowntree and Dollar, 1999; Antonarakis et al., 2009). The development and growth of riparian vegetation in sensitive areas could establish significant maintenance burdens against flood (Afzalimehr and Dey, 2009), but it should be considered to minimize flow resistance to reduce the risk of flood at these areas (Darby, 1999). On the basis of field experimental results, Wilson (1967), presented the trapping rate of fine sediment in flood events on different grass covered slopes, and reported the effectiveness role of grass filtration for reducing sediment in flood water. Protective effects of riparian vegetation on bed and bank of a channel have been studied in various rivers (i.e. British Columbia studied by Beeson and Doyle, 1995).

The interaction of flow between the main channel and floodplain in vegetated compound channels causes additional energy losses (Thornton et al., 2000). Jeffries et al., 2003, investigated erosion and deposition processes in both vegetated and non-vegetated channel and found greater deposition in vegetated areas.

Field observation is especially useful for situations in which it would be unacceptable to manipulate the independent variable. Although it is easier to generalize from field results, but weak control of extraneous and independent variables besides time-consuming and costly procedures, coupled with advances in measurement instruments and have led the studies into flume experiments.

1.4.1 Review of experimental modelling of vegetation in flumes

Field observation on sediment patterns helps to clarify the morphological changes, but defining the underlying processes in detail needs accurate hydrodynamic measurements, which are achievable in flume experiments (through proper scaling) and numerical simulation. For example, Bouma et al. (2007), explained field sediment motion by the laboratory patterns of bed shear stress.

According to the location and extension of the vegetation in river channels we classified the related literatures into three different groups which contain uniform vegetation, finite patches in the main channel and bank vegetation. This classification may help to improve our understanding of morphological growth due to vegetation in fluvial systems.

1.4.2 Interaction of uniform vegetation in channels and sediment transport

It is difficult to scale and model all the features of vegetation in a flume, but in order to clarify the poorly understood factors it can be simplified or considered at a certain condition. For example, although turbulence intensities for the flow in an experimental flume is generally lower than the similar simulated flow in the field (Bouma et al., 2007), but by preparing a steady flow condition, turbulence levels in field and simulated flume can become reasonably comparable (Hendriks et al., 2006).

The role of uniform vegetation in morphodynamics of the channels has been mostly investigated through cylindrical elements to distinguish the effects of stems on drag force (Li and Shen, 1973; Nepf, 1999; Wu et al., 1999; Ishikawa et al., 2003; Armanini et al., 2010; Tanino and Nepf, 2008; Carmo et al., 2011). Whereas, the presence of leaves and branches have been considered in some other studies (Moghaddam and Kouwen, 1997; James et al., 2004; Jarvela, 2004, 2005; Righetti and Armanini, 2002; Stone and Hung, 2002; Tal and Paola, 2007).

Chen et al. (2012), investigated a patch of submerged vegetation, located across the width of a rectangular experimental channel, and explained the details of its effects on the flow characteristics and bed profile. Bouteiller and Venditti (2014), focused on physics of morphodynamics interactions of vegetation and sand-bed rivers. They investigated the morphodynamics response of fine sediment bed to vegetation by considering total fluid shear stress and grain-related shear stress. Armanini et al. (2010), investigated the effects of vegetation on bed load transport rate and clarified the influences of vegetation in sand bed rivers. Associated turbulence with piers has been studied in details (Kumar and Kothyari, 2012; Debnath et al., 2012), but overlapping wakes of vegetation stems make the scouring and coherent flow structures more complex than flow around a pier.

1.4.3 Interaction of finite patches of vegetation in channels and sediment transport

Patch scale effects received less attention than uniform vegetation. Coulthard (2005), showed different densities of vegetation change flow dynamics and channel morphodynamics which could end up by deposition of islands, which can develop in different shape and size. Flow structure around the vegetation zone and pattern of bed shear stress, control the growth of vegetation in the channel.

Recently, Sediment pattern of erosion and deposition has been investigated around circular patches of rigid vertical cylinders, simulating a patch of reedy emergent vegetation in channels (Meire et al., 2014; Follett and Nepf, 2012; Zong

and Nepf, 2011; Bouma et al., 2007; Dargahi, 1990). As a temporary changes, Follett and Nepf (2012), reported the diverted flow from vegetation area in a middle of a channel could selectively transport the finer grains in a graded sediment bed and create an armor layer by leaving only the bigger grains. Armoring of the bed around the vegetation area can limit island expansion. They hypothesized that pattern of erosion and deposition near the patch could be classified due to created shear layers and turbulence characteristics. In fact, they tried to add information about the bed development on the study of Zong and Nepf (2011), about the interaction of flow structure and circular patch of emergent vegetation at the mid-channel.

Presence of a finite patches of vegetation divert the flow from upstream side of the vegetation area and created a region of high drag which cause separation of the flow around the island of vegetation (Dargahi, 1990). Flow deceleration within and at the wake of the vegetation zone would cause deposition, while the deflected flow from vegetated area to un-vegetated zone would lead to acceleration of the the flow and scouring (Meire et al., 2014). Local flow deceleration upstream of the vegetation area could also be caused a limited area of fine particle deposition (Gurnell et al., 2001, Zong and Nepf, 2010). Bouma et al (2007), prepared an experimental channel and simulated the circular patches of vegetation with different densities and observed higher scouring inside the patch for denser patches of bamboo canes which continued almost to the half of the patch and ended with sedimentation. Follet and Nepf (2012), observed the same effect of stem density, but sediment accumulation was always observed at the wake of the patch of vegetation, which is mostly because of the small size of the circular patches. Vegetation also generates turbulence and enhanced the turbulence levels within and around the vegetation area and if elevated levels of turbulence accompany with notable flow velocity, scouring happens inside the vegetation area (Bouma et al., 2007).

Variability of near bed turbulence intensities contribute to special variability in bed load flux around the vegetation zone (Nelson, 1995). While the area behind a permeable patch increases the functionality of rivers by producing a low turbulence region at the wake of the patch, the solid patch does not provide it (Follet and Nepf, 2012). Rominger and Nepf (2011), proposed a length scale needs for deceleration of the flow within a patch of vegetation which is related to the larger of patch diameter and frontal area.

There are different methods to quantify the effect of important parameters on sedimentation and erosion process, each with its own strength and weakness.

Higher amount of bed load flux has been reported by Yager and Schmeeckle (2013) around a patch of vegetation where higher near-bed Reynolds stress was measured. Four different type of turbulence around simulated stems are reported, which includes bursts, sweeps, inward interactions, and outward (Termini & Sammartano, 2008). It is also reported that bursts and sweeps contribute positively to the bed shear stress and they are more important at upstream of vegetation, where horseshoe vortices can locally increase turbulence (Dargahi, 1990). Outward and inward interactions contribute in contrast with bed shear stress and they are more important downstream side of vegetation, where oscillations of von Karmen vortices disturb the flow (Seminara et al., 2013).

1.5 Interaction of patches of bank vegetation with river patterns

The influence of bank vegetation on morphology of rivers has been simulated in laboratories and represented the remarkable effects of bank vegetation to control alluvial river patterns (Ikeda and Izumi, 1990; Tsujimoto, 1999; Afzalimehr and Day, 2009; Zong and Nepf, 2010). These studies revealed that vegetation alter channel geometry and flow characteristics. According to this fact, bank vegetation has been considered as a practical tool for stabilization of bed and banks of rivers. Vargas-Luna et al. (2015), analyzed the ability of plants as rigid cylinders to reproduce the effects of vegetation on morphodynamics processes. They used physical and numerical models to simulate the consequences of representing rigid cylinders on river banks. Zong and Nepf (2010), investigated the effects of vegetation density on flow and sediment transport in and around a finite patch of vegetation located at the wall of the experimental channel. Due to the flow velocity, they identified different regions around the vegetation area and reported the deposition pattern in specified regions.

Planting cutting of trees, such as willow, is a common way to restore the ecological status of denuded rivers and stabilize their banks and bed, because in a few months, the willow grows in height and forms an extensive root system that binds the soil and reduces the erosion. In order to increase the effectiveness of these systems, it is often convenient to group the vegetation in patches, and plant it on banks and beds to stabilize the morphological characteristics of the river.

Comparing to the available literature about uniform bank vegetation, patches of bank vegetation has been less considered.

Studies on laboratory sand bed channel were showed the migration of alternate bars could be stabilized by planting vegetation, and sediment tends to be

deposited within the vegetation zone (Bennett et al., 2008; Tsujimoto, 1998). Planting the vegetation at the banks of the channel causes the flow separation and diverts the flow across the main channel. Interaction of flow between the vegetated and non-vegetated banks causes the flow within the main channel to meander.

Sediment transportation in natural rivers follows a dynamic equilibrium and this condition for sand bed streams mostly occurs in meandering platforms. Transforming a straight degraded stream into a meandering channel through the use of vegetation has been proposed recently by Bennett et al., (2002, 2004), because it might enhance the functionality of rivers beside recreational opportunities of the corridors. Bennet et al. (2008), considered rivers with stable channel bank, aggrading channel bed with selective recolonization of woody vegetation within riparian zone and used empirical relation for meander wavelength for placement of vegetation at the bank of an experimental channel. They investigated the effects of vegetation density and on flow characteristics and sediment transportation and clarified the contribution of emergent vegetation to the stream processes is dependent on the vegetation density.

Expansion of riparian vegetation on floodplain and bank of channels has been considered recently and sediment deposits around the island of vegetation have been investigated in terms of flood frequency and sediment pollution (Vastila, 2015; Dittrich and Jarvela, 2006; Tsujimoto, 1999). Human intervention in fluvial systems, such as dam construction and dredging activities could change flood frequency and sediment supply, which are crucial factors in morphology of rivers. Tsujimoto (1999), considered sediment sorting around a bank vegetation area along an experimental channel and investigated the long term effects of flood on extension of vegetation area and morphological consequences.

To summarize, restoration projects using the alternating patches of bank vegetation are aimed to adjust the desired plan-forms in rivers like inducing thalweg meanders in highly incised channels. Considering human impacts, there are still some limitations in this part, because sedimentation and erosion processes have not addressed completely the details of effective parameters and the importance of them on local bed profiles.

1.6 Review of numerical modelling of vegetation

Hydrodynamic and morphodynamics modeling could facilitate upscaling the field results, and laboratory measurements and could be significantly helpful for sustainable sediment management strategies beside other ecological and biological motives (Perona et al., 2009). Due to the simplifications, flume

experiments are not able to capture all spatial scales that are relevant to the alluvial vegetation. On the other hand, the proper understanding of associated physical processes of the interaction of vegetation and sediment transport is a crucial factor for development of modeling tools. However, a well calibrated numerical model could help the laboratory's result to reproduce more details.

Experimental data of Tollner et al. (1982), about sediment transportation in a vegetated sand bed channel has been used in Lopez and Garcia (1998) to validate and calibrate the numerical model. Effects of vegetation on suspended sediment modeled by Shimizu and Tsujimoto (1997), and concentration of sediment has been analyzed both in vegetated and non-vegetated areas with different sediment sizes. Nicolle and Eames (2011), simulated single patches of cylinders in channels and investigated about the effects of density and size of the patches on turbulence and Zong and Nepf (2011), added more details on their results and used these details to support a theoretical model. Cheng and Yong-ming (2008), developed a three dimensional turbulence model and investigated the flow in the presence of vegetation.

Recently, numerical models for sediment management and morphological assessment of rivers have been developed to simulate the effects of vegetation on both hydrodynamic and morphodynamics of flows (Klopstra et al., 1997; Tsujimoto, 1999; and Baptist, 2005). Contribution of bed shear stress and vegetation drag through Baptist (2005) method has been reviewed by Vargas-Luna et al. (2015), and morphological changes of experimental channel bed investigated in terms of mean flow velocity. There are different numerical models which can consider the effects of vegetation in sediment transport. For example, the Delft3D-Flow model is an open source numerical model, which is able to simulate flows over three-dimensional spatial grid and it use different formulas and methods to compute roughness.

1.7 Research questions

Comparing the available literatures, it can be concluded that although recently more studies have been focused on morphodynamics of flow patches in intertidal environments (e.g., Luhar et al., 2008; Bouma et al., 2007), but still fewer studies have investigated interactions among flow, vegetation and sediment transport for flow patches in alluvial rivers (e.g., Bennett et al., 2002, 2008; Tsujimoto et al., 1998,1999). Therefore, sedimentation and erosion processes in alluvial rivers with patches of vegetation have not been addressed completely in details and more

investigation is necessary to find effective parameters and the importance of them on local bed profiles.

In this study we want to consider the changes in bed forms through semi-circular patches of emergent vegetation, located at the bank of a channel. The main primary objective will focus on understanding and analysing of the effects of finite patches, to answer the following questions:

- What are the relationships between finite patches and bed profile?
- How strong are the impacts of patch of vegetation on bed morphology?
- How mutual do patches of vegetation impact each other?
- How could manage the patch of vegetation to improve water bodies and increase its restoration efficiency?
- What factors are more important for investigating the effect of patch of vegetation on river morphology?

Figure 1.2 summarizes the methodology of how to reach to answers of these questions in flowchart form.

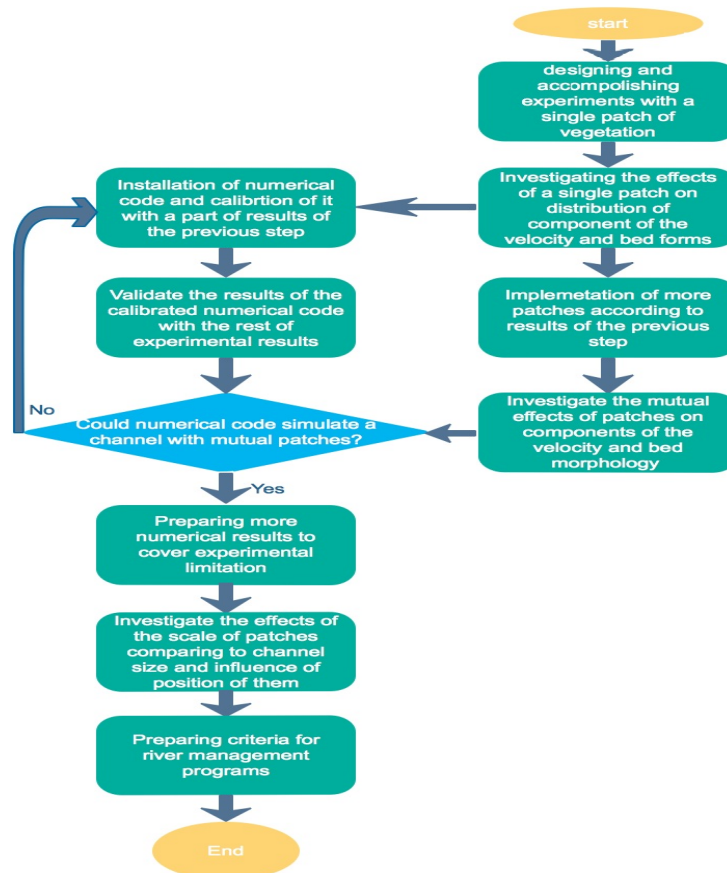


Figure 1.2. Flowchart of the methodology of the study

1.8 Research objectives

While previous studies have revealed the effects of aquatic patches of vegetation in flow structure and sediment transport, they have not provided engineering principles to determine what combination of flow, vegetation, and sediment properties promotes the effects of vegetation in riverine systems (Neary et al., 2012). Thus, further research based on engineering principles should be directed to examination of flow past isolated patches of vegetation, which occurs often in practical applications to provide more information about the sensitivity of morphological processes to address the importance of effective parameters such as the density and size of a patch of vegetation in streams.

The current study builds on the previous studies of bank individual patches and a series of laboratory experiments besides numerical simulations are performed to provide a more detailed description of the heterogeneous bed morphology due to installation of patches of vegetation. Using velocity and bed elevation measurements, this study tends to investigate the effects of vegetation features and positions to prepare useful results for predicting morphological changes, which can be useful especially in river restoration projects.

One of the main aspects of this research is finding out how partly vegetated channel reacts through different flow condition and alters the morphology of a river. To achieve this goal, important parameters that are related to both flow structure and vegetation should be investigated to figure out how the extent of the vegetation patch could be affected in longitudinal and lateral.

In particular, this research focuses on the physics of sediment transport and how distinct patches of vegetation could be used to change the morphology of rivers by eliminating the migration of bars in some part of channels and providing a fixed scour associated pattern. However, bar migration directly influences both hydrodynamic and morphodynamics of channels, and it is necessary to define clearly the effective parameters of finite patch of vegetation on flow fields beside important parameters of mutual patches like the longitudinal and lateral distance between them. For this reason, the investigation aimed to provide a detailed description of the relationship between the flow parameters and the characteristics of the patches of vegetation to improve the understanding of the sedimentation and erosion around the vegetated areas. In addition, the other goal of this research is to prepare useful criteria about the position of the porous obstructions with suitable sizes, shape and densities to get the highest efficiency in restoration projects.

1.9 Outline

Chapter 2 starts with a description of the experimental setup that has been used during this study. Then the channel and material information, measurement instruments, and the plan of the experiments are discussed. In chapter 3, the applied numerical model (Delft3D), important equations, parameters and the processes related to these parameters are explained. Subsequently, the hydrodynamics and morphodynamic results of the experimental measurements are presented in chapter 4 and 5 respectively and the results are discussed in details. In chapter 6, following the presented results of the two previous chapters, calibration and validation of the numerical model are described. Finally, chapter 7 wraps up whole the experimental and numerical morphological development data as a consequence of implementation of the permeable patches in a channel and investigates the important variables.

2 Chapter 2: Experimental modelling

Experiments were performed to study the effective parameters of patches of rigid emergent cylindrical stems on flow field and bed evolution within a straight channel in order to facilitate restoration of river channels particularly in terms of sediment management, habitat resources and aesthetic. This chapter outlines general information about laboratory experiments and discusses measurement equipment. At first the laboratory setup and material are explained and considered simplifications are clarified. Subsequently fundamentals of acoustic Doppler velocimetry and laser scanning are presented. Finally, experimental program and probable measurement errors are reported.

2.1 Experimental setup

Designing of the experiments has been done on a basis of two main factors: Vegetation features (size and density), and flow structure (Fr number). Densities of patches are chosen in different ranges and sizes of the patches are modified due to the preliminary results. Flow parameters are also selected from clear water with fixed bed to live-bed condition, which is considered a typical condition of incised channels. The experiments were carried out in an 18 m long, 1 m wide and 0.7 m high glass-sided flume at the Hydraulic Laboratory of the University of Trento. The bottom was covered by a layer of uniform fine sand, at least 20 cm thick, representing the mobile bed.

The channel was equipped with a recirculating water-sediment system (Armanini et al., 2010), which allowed steady conditions to be reached in a reasonably short period, depending on flow condition. The water discharge was controlled by a choke valve and measured by an electromagnetic flowmeter connected to the inlet pipe. Since the system worked as a closed circuit, the total volume of sediments inside the circuit controlled the sediment discharge. In order to obtain an increase in the sediment transport rate, the volume of sediment had to be increased; to reduce the sediment transport, a certain volume of sediment had to be taken out of the system. This operation was time consuming and required a trial and error approach.

At the entrance of the channel a mesh was installed to eliminate turbulence and secondary currents and to prevent anomalous local scours. Figure 2.1 describes the channel details and Cartesian coordinate system. The origin of Cartesian coordinate system was set at the upstream edge of the vegetation and the top of the smoothed bed. The velocity component in this system are expressed by u , v and w in the x , y and z directions respectively.

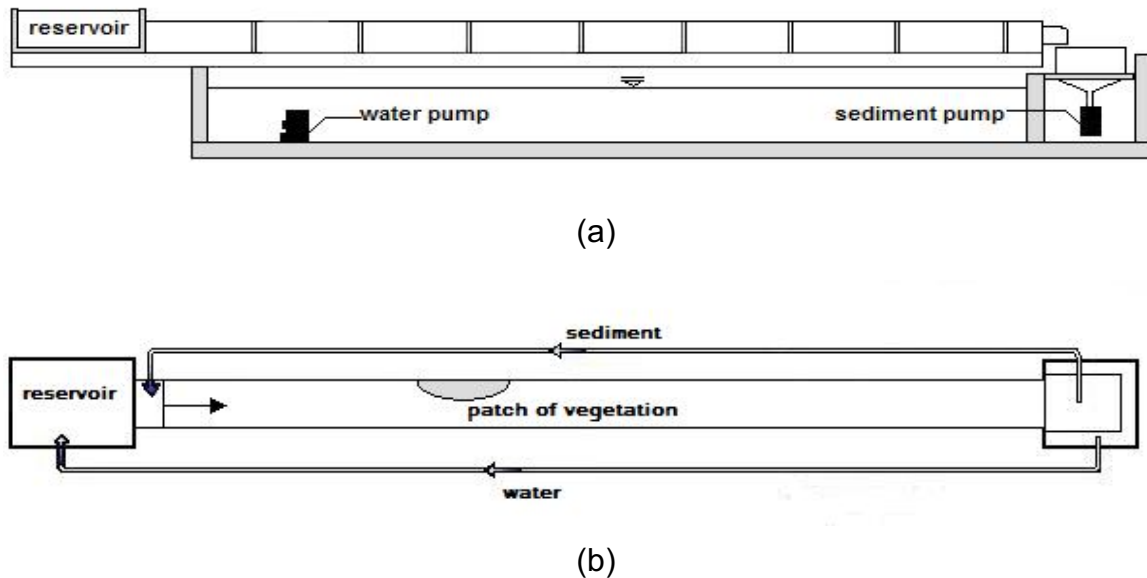


Figure 2.1. (a) Side view and (b) plan of the channel

2.2 Experimental program

In contrast with previous studies (Bennett et al., 2002 & 2008), that assumed the effectiveness of the patches in the channel, in this study experiments divided into two part: at the first part just one patch with different densities and sizes are installed to investigate the local effects of each density of the patch on bed morphology and flow characteristics. Table 2.1 shows the details of these experiments (H is the flow depth, U is the depth average velocity, Ω_v is the stem density, H is the depth of flow, t is the duration of the experiment, and Q_s is the bed load transport without interaction of the patch of vegetation). The velocity distribution and bed profile results of these experiments are presented in chapter 4 and 5 respectively. After a precise analysis of the result of the first part and due to the clarified the influence of each density of a finite patch of stems in the flume, the

other patches were installed with different longitudinal intervals to investigate also the effects of patches on each other.

Following the second phase of the experiments, a set of tests have been designed to study the alteration of bed profiles from straight to meander beds by using 5 semi-circular patches of cylinders with different densities and diameters and also different flow Fr number. More details of these experiments are presented in chapter (7).

Table 2.1 Summary of experiments of first phase

<i>test N.</i>	h_0 [cm]	U_0 [cm/s]	<i>Fr N.</i>	Ω_v	t [h]	q_s [gr/min]
1	17.7	18.5	0.1	0.025	9.5	0
2	10.5	28.5	0.3	0.025	8.5	150
3	7.8	38.5	0.4	0.025	8	950
4	17.7	18.5	0.1	0.05	9.5	0
5	10.5	28.5	0.3	0.05	8.5	150
6	7.8	38.5	0.4	0.05	8	950
7	17.7	18.5	0.1	0.1	9.5	0
8	10.5	28.5	0.3	0.1	8.5	150
9	7.8	38.5	0.4	0.1	8	950
10	9	22	0.2	0.1	9.5	42
11	9	30	0.3	0.1	8.5	180
12	9	45	0.5	0.1	8	1220
13	9	22	0.2	0.05	9.5	42
14	9	30	0.3	0.05	8.5	180
15	9	45	0.5	0.05	8	1220
16	9	22	0.2	0.025	9.5	42
17	9	30	0.3	0.025	8.5	180
18	9	45	0.5	0.025	8	1220

2.3 Acoustic Doppler velocimetry

Since the late 20th century, the acoustic Doppler velocimeter (ADV) has been used as a standard and reliable instrument for both 2D and 3D single point precise velocity measurements for river velocity ranges and up to now it has been applied to many field and laboratory studies (Nikora and Goring, 1999; Chanson et al., 2008). ADV operates on the basis of pulse to pulse coherent Doppler technique with self-adaptive processing algorithms which avoids pulse to pulse interference in cases close to the surface and bed (Miller and Rachwarger, 1972; Zrnica, 1977; Velasco and Huhta, 2009). Comparing to other acoustic techniques such as acoustic travel time or electromagnetic techniques, Doppler technique has more advantages. For example, in terms of calibration, there is no need for regular

recalibration and it has the advantage of being inherently drifted free, and also in terms of acoustic pulses, there is no optical limitation (Lohrmann et al., 1994).

The ADV system has three main modules: measurement probe, signal conditioning, and signal processing module. The measurement probe consists of an acoustic transmitter, receivers (figure 2.2). The sampling volume is located 5 to 10 cm from the tip of transmitter to reduce flow interference. The probe also may include up to 3 different sensors in it to estimate the pressure and velocity, temperature, and compass. The velocity record consist three main elements: the velocity value, signal strength, and correlation value.

In this technique, at first a very short acoustic pulse is being generated by the transmitter and the transmitted pulse propagate through the water. Subsequently, a fraction of the acoustic energy is scattered back by small particles such as suspended sediments or small organisms. The return signal would be detected by a receiver at the sampling volume and the other identical pulses will be transmitted simultaneously. Figure 2.3 illustrate the process of pulse generation (a) and receiving by receivers (b).

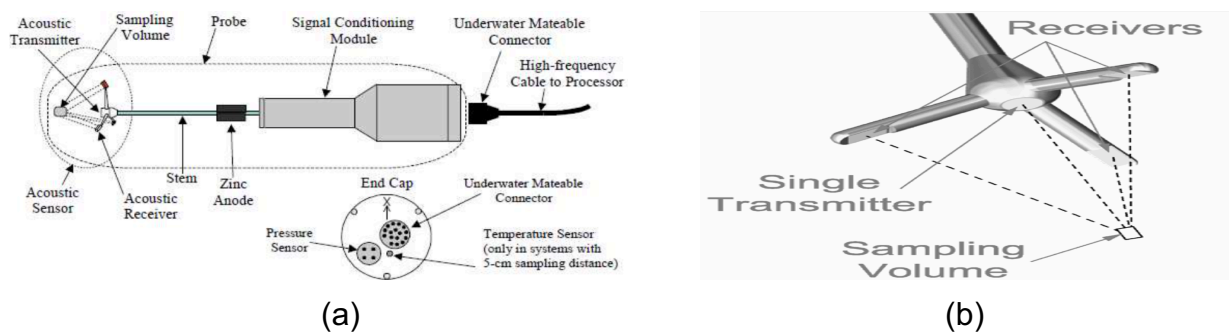


Figure 2.2. 3D ADV probe (b) transmitter, receivers and sampling volume location (Velasco and Huhta, 2009)

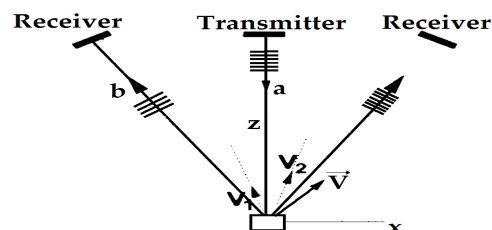


Figure 2.3 Process of sending and receiving the pulses by transmitter and receivers (Doppler technique)

The accuracy of velocity data is mainly depending on velocity range (higher velocity range may provide more noises), and sampling rate (higher sampling rate may provide increases the noises), Doppler noise (noises result from the physical process and they are more important under poor operating condition with low range of signal to noise ratio and correlation value), and probe geometry (sampling volume position and direction of signal transmitters). In order to check and modify the quality of velocity data, the signal strength and correlation values could be checked.

2.4 ADV in the present study

In this study, all flow velocity measurements were done by ADV. Velocity of flow was recorded using a handheld SonTek flow tracker at a sampling rate of 25 HZ over a 240 s interval along the channel. The reason for selecting the long interval is relied on mobile bed condition. In subcritical flow with a small bed perturbation, velocity profile changes due to the movement of bed perturbations (Julien, 2010). Considering this fact and average perturbation speed in different cases, 240 s intervals was chosen to get the average of flow velocity with less uncertainty. Figure 2.4 shows the origin of coordinate and locations of velocity measurements for the first part of experiments. x and y represents the longitudinal and lateral distance from the origin of coordinate and horizontal and vertical axes show respectively the non-dimensional longitudinal distance and non-dimensional lateral distance from the origin of coordinate at upstream side of the patch of vegetation (D is the patch diameter and W is the channel width). The Information of the plan of velocity measurements for the channel equipped by five patches of stems are presented in chapter (7).

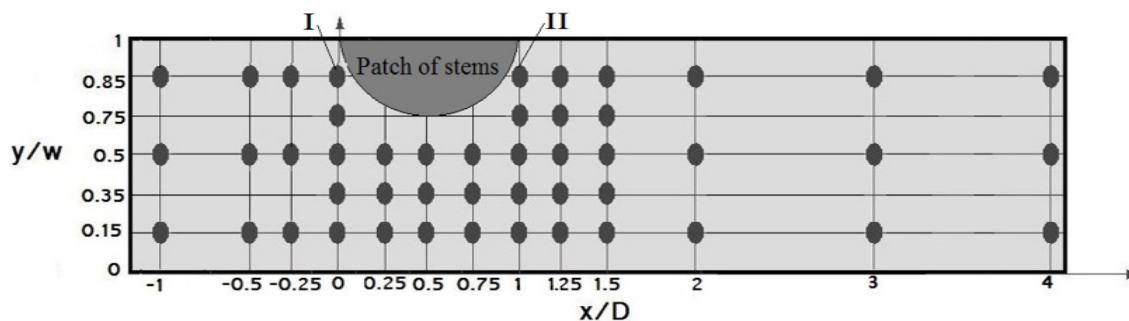


Figure 2.4. Location of velocity measurements for a single patch of vegetation

Velocity measurements were done at 0.2 and 0.8 times of water depth, almost in 5 different points (25, 35, 50, 75, 85 cm from origin of coordinate) in each cross section (less points for far locations to the patch). The mean of two velocities at 0.2 and 0.8 of the flow depth at each point is considered as a depth-averaged velocity. The minimum longitudinal interval was 12.5 cm (near the patch) up to 50 cm (over the area with more than $2D$ distance from the upstream edge). The results of velocity measurements have been presented in chapter 4.

2.5 Bed profile measurements

After drying the channel, the bed topographies were digitized with a M5 laser distance sensor mounted on a motorized track above the channel, using a 25 mm by 1mm grid along the flume. Figure 2.5 shows the details of the laser profiler in the laboratory.

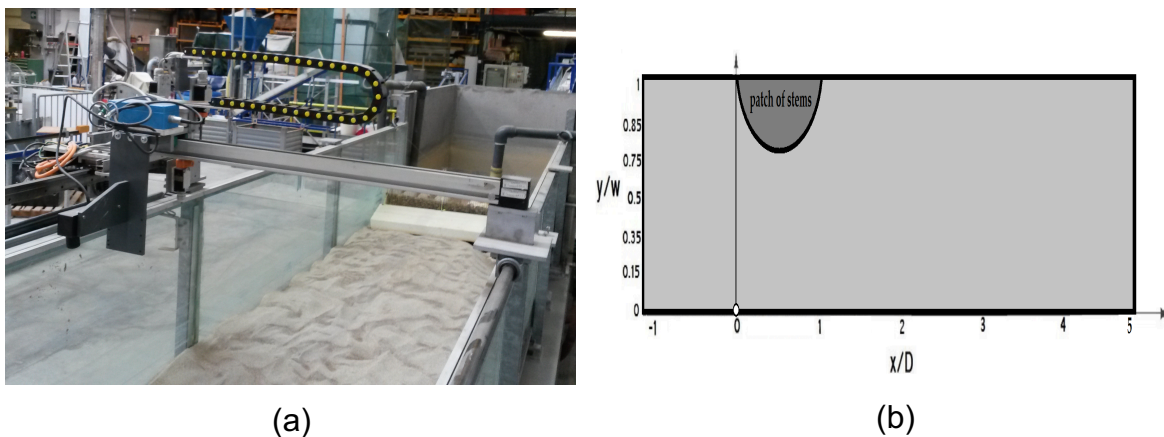


Figure 2.5. a: Laser profiler; b: Domain of measurements

A Matlab code was prepared to interpolate and plot the bed elevation scans. Water surface profile was also recorded by point gage in three longitudinal positions (25, 50 and 75 cm from the origin). The aspect ratio (W/h) of about 25 shows measurements can be classified in wide open channels (Nezu and Nakagawa, 1993), and it corresponds many natural channels (Northwest Hydraulic Consultants Inc., 1987, 1988, 1989). Water depth was calculated by differences between bed elevation and water surface elevation.

2.6 Bed material characteristics

The channel was filled with 20 cm layer of uniform fine sand ($d_{50}=0.5$ mm, $\rho_s=2600$ kg/m³). Figure 2.6 shows the cumulative grain size distribution of the sediment. Standard deviation of sediment size is 1.4, the specific gravity of particles is 2.4 and the angle of sediment repose equals to 30 degrees. Sediment was smoothed before each run using a plate mounted on the movable carriage above the flume and sediment inside the patches was flatted by hand to provide the same initial condition for tests. The average height of dunes moving along the channel bed was 45 mm and 34 mm respectively for experiments with $Fr=0.3$ and 0.4. The critical shear velocity, u_{*c} obtained from the Shields curve (Shields, 1936) was approximately 0.02 m/s. The sediment transport was measured by collecting the samples of sediment at the downstream end of the channel and calculating the mass of the sediment discharged in the unit time.

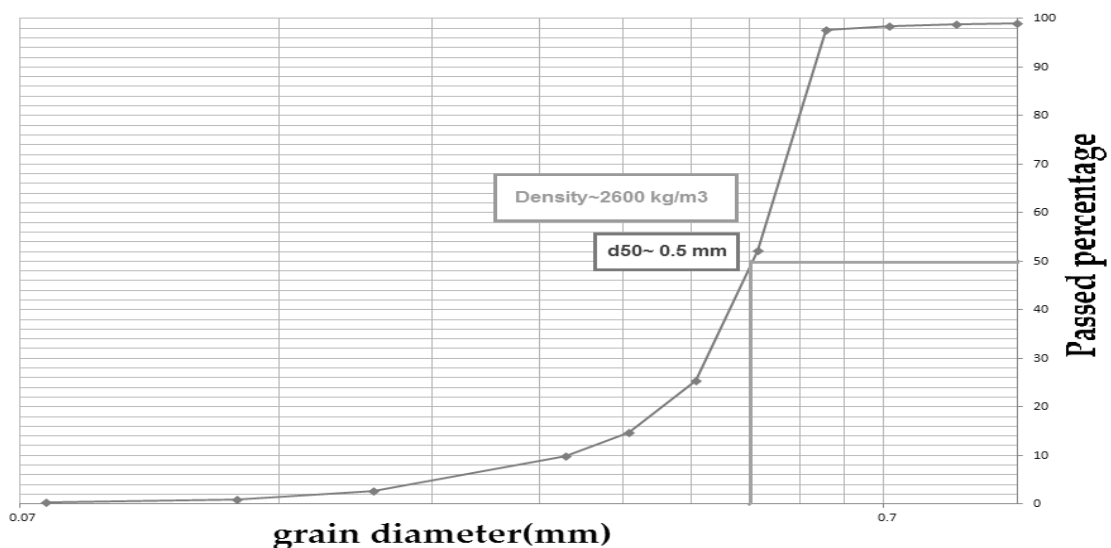


Figure 2.6. Cumulative grain size distribution of the sediment

The tests were conducted both in *clear water condition* (the mobility parameter of the incoming flow under the incipient motion critical value) and in *live-bed condition* (the mobility parameter of the incoming flow above the incipient motion critical value). In experiments with live-bed condition, two ratios of $(u^*/u_{c*}) = 1.5$ and 2.5 have been chosen (respectively for experiments with $Fr=0.3$ and 0.4) to observe the similitude between experiments and reality (Brain et al., 2007).

As expected, the tests in clear water conditions required more time to reach to an equilibrium condition. But most of the relevant experiences showed that approximately 60% of equilibrium condition is obtained after around 2 hours and

relatively 90% after 8 hours (Ataie-Ashtiani and Beheshti, 2006; Dargahi, 1990). Another important parameter in the cases of live bed is the sediment transport rate. In these cases, sediment discharge measured continually with certain intervals till the transport rate become almost constant, which shows the flow is approximately reached to steady state. The samplings were done each quarter of hour. Figure 2.7 shows typical trend of the normalized solid flow rate in function of the normalized time of the sampling.

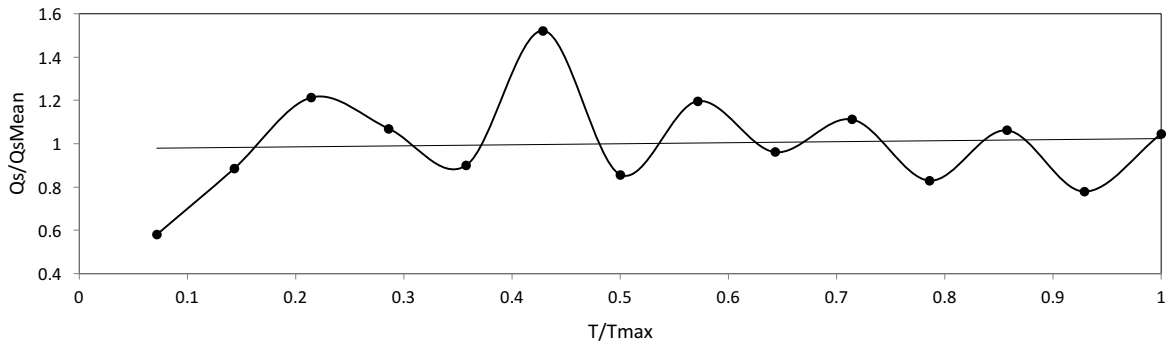


Figure 2.7. Sample of sediment measurement. ($\Omega v=0.05$, $Fr=0.4$)

In figure 2.7 the horizontal trend-line insures that the flow was reached a stationary condition. The minimum time required to reach such condition was 8 hours.

2.7 Simplification and uncertainties

Aluminum cylinders with a diameter 1 cm, mounted on the prepared boards, simulated the vegetation of the patches. Considering the previous literatures, the semi-circular configuration is chosen for each vegetation zone. Density and size of the patches were changeable with planting and harvesting of cylinders. The density of the patch was defined as:

$$\Omega_v = \frac{A_p}{A_{tot}} = n_p \frac{\pi d_p^2}{4} \quad (2.1)$$

where d_p as the diameter of the cylinders and A_p is the area occupied by plants over the total considered area A_{tot} , and n_p is the number of per unit area. The frontal area per unit volume a , was also calculated as $a=n_p \cdot d_p$.

Semicircular patches have been adopted. Two different patch diameters D were considered ($D=70$ and $D=50$ cm). Figure 2.8, shows the configuration of stems

inside the patch and position of patches inside the channel. In order to maximize flow resistance besides conserving the geometric similarity and general hemisphere shape, staggered arrangement had been considered for cylinders.

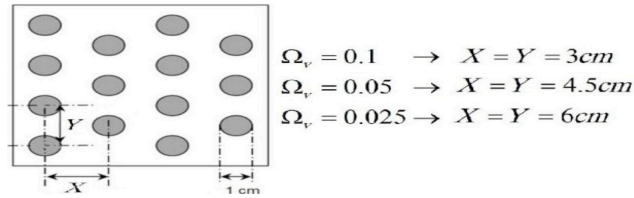


Figure 2.8. Sample of sediment measurement. Test n. 4 ($\Omega_v=0.05$, $Fr=0.4$)

2.8 Summary of chapter 2

Because of improving the knowledge about the interaction between isolated patches of vegetation in open channel flows, the effect of finite patches of vegetation on flow and bed morphology was investigated in a flume at two separate parts. The patch of semicircular emergent vegetation was modeled by cylindrical stems, which mounted on the board located along sides of the channel. The flow conditions are considered for both clear water with fixed bed and movable bed condition.

At the first part of experiments, just one patch of stems is installed. The details about the velocity and bed elevation measurements of the first part of experiments are explained in this chapter. The results of these measurements are presented in chapter 4 and 5. The second part of experiments deals with the mutual effects of the semicircular patches and the important parameters which have significant impacts on planting managements. More details about the measurements and methodology of this part are explained in chapter 7.

3 Chapter 3: Numerical model

This chapter deals with the implementation of patches of vegetation in Delft3D-FLOW. The spatial effects on flow structure and sediment dynamics are studied in simulations with Delft3D-FLOW (from now on referred to as Delft3D). Considering the experimental results in vertical direction and assuming the low turbulent intensity and component of velocity in vertical direction, the 2D depth-average model has been used for simulations. It should be mentioned that a thorough description of comprehensive details can be found in Delft Flow user manual (Deltares, 2010). The goal of this chapter is to explore how to setup the hydrodynamics and morphodynamics process with specific emphasizes on the vegetation modeling in Delft3D.

3.1 Numerical model setup

Delft3D package has been developed by Deltares and provides a platform for computations of coastal, river and estuarine areas. The package is equipped with different modules to be able to simulate different flow conditions, morphological development, waves, and water quality. In order to facilitate the investigation of a partly vegetated river channels, this study uses the flow module that can represent the development of flow and morphology in a channel. To achieve this goal, the model's requirements should be prepared well enough to simulate the effects of vegetation zone on bed profile. The model set-up is explained below.

3.1.1 Model grid and bathymetry

Flow and sediment transport, that result from gravitational forcing is being simulated in the boundary fitted to grids. Delft3D supports both Cartesian and spherical coordinate systems and the Cartesian one is used in this study for simulations. Proper grids should fit to the boundaries perpendicularly and to in order to prevent the inaccuracy errors, their size must almost remain constant. According to the experimental results, rectangular grids are used for simulation. The grids are generated with the Delft3D-RGFGRID module. Due to the hydrodynamic condition, the bed slope of the channel is defined by obtained slopes through the experimental data. The bathymetry is also interpolated to the grid by

using Delft3D-QUICKIN module. The model equations are solved for a control volume, which is quantified by the model grid. A rectangular grid with different dimensions has been set-up for simulation (from 1x1 cm up to 5x15 cm). The dimension of the grids depends on the simulated flume size and the allocated time for the computation. The choice in grid cell dimensions is motivated by the channel dimensions. The disadvantage of the smaller grid is that the time of simulation is increased by more than an order of magnitude. The staggered computational grid on which the model is based is presented in figure 3.1.

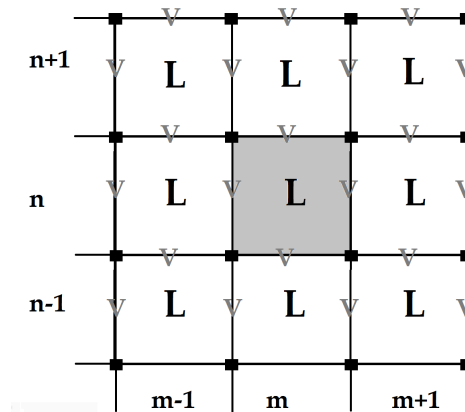


Figure 3.1. The computational control volume depth (\bullet), water level (L), velocity (V) (source: Deltares, 2006).

The hydrodynamic equations are applied on the staggered grid, which is shown in figure 3.1. Each control volume consists of a square with water level surrounded by four depths at the corners of the square and defined by the bathymetry data. The velocities are specified on each sides of the control volume. Depending on the location of the computational point (closed boundaries, open boundaries, and the rest of the domain) different quantities would be considered or calculated for the point.

3.1.2 Hydrodynamic setup

Hydrodynamic effects play a significant role in the vegetated bed channels. The bed level changes in movable bed channels and this fact may cause changes in hydrodynamic condition. For this reason, the interaction of hydrodynamic and morphodynamic should be taken into account at the same time. Assuming the 2D depth average model, the vertical accelerations due to sudden variations in the bottom topography are assumed to be insignificant compared to gravitational acceleration and the momentum equation in vertical direction is reduced to the hydrostatic pressure relation:

$$\frac{\partial P}{\partial \sigma} = -\rho g h \quad (3.1)$$

The system of equations consists of horizontal momentum equations, the continuity equation, and the transport equation. The horizontal momentum equations are:

$$\frac{\partial u}{\partial t} + u \frac{\partial u}{\partial x} + v \frac{\partial u}{\partial y} + g \frac{\partial \eta}{\partial x} + \frac{g|U|u}{C^2(d+\eta)} - \nu \left(\frac{\partial^2 u}{\partial x^2} + \frac{\partial^2 u}{\partial y^2} \right) = 0 \quad (3.2)$$

$$\frac{\partial v}{\partial t} + u \frac{\partial v}{\partial x} + v \frac{\partial v}{\partial y} + g \frac{\partial \eta}{\partial y} + \frac{g|U|v}{C^2(d+\eta)} - \nu \left(\frac{\partial^2 v}{\partial x^2} + \frac{\partial^2 v}{\partial y^2} \right) = 0 \quad (3.3)$$

Where u [LT^{-1}] and v [LT^{-1}] are depth average velocities in x and y direction respectively, g [LS^{-2}] is acceleration due to gravity, η [L] is the water level with respect to datum, $|U|$ [LS^{-1}] is the total velocity rate, C [$L^{0.5}S^{-1}$] is Chézy roughness coefficient, d vertical distance with respect to datum, and ν is horizontal eddy viscosity. The horizontal Reynold's stresses, are determined using the eddy viscosity concept (Rodi, 1984). Equations 3.2 and 3.3 calculate the changes of components of depth averaged velocity, advection of velocity, contribution of surface slope to the acceleration of the fluid, and the loss term due to bed friction in streamwise and transverse direction respectively.

The continuity equation that governs the system by calculation of the total amount of the fluid is:

$$\frac{\partial \eta}{\partial t} + \frac{\partial (d+\eta)u}{\partial x} + \frac{\partial (d+\eta)v}{\partial y} = 0 \quad (3.4)$$

Basically, the inflow and outflow from each cell should be equal. By specification of the boundary condition, the continuity equation would be solved. On the other hand, the considered simplifications to solve the equations introduces parameterizations these equations. These parameters are categorized in hydrodynamic, morphological and sediment parameters. Details of the utilized parameters are presented in physical and morphological sections.

The transport equation reads the advection-diffusion equation:

$$\frac{\partial h_c}{\partial t} + \frac{\partial hu_c}{\partial x} + \frac{\partial hv_c}{\partial y} = h \left(\frac{\partial (D_H \frac{\partial c}{\partial x})}{\partial x} + \frac{\partial (D_H \frac{\partial c}{\partial y})}{\partial y} \right) + hS \quad (3.5)$$

In which c [ML⁻³] is the mass concentration, D_H the horizontal diffusion coefficient, S the source and sink terms per unit area due to the discharge or withdrawal of water.

In order to solve these equations horizontal viscosity (ν_H) and diffusivity (D_H), are assumed to be a superposition of molecular viscosity and turbulence. The molecular viscosity of the fluid is a constant value, but the turbulence is a measure of the horizontal mixing that is not resolved by advection on the horizontal computational grid. The turbulence values may either be specified by the user as a constant or space-varying parameter, or can be computed using a sub-grid model for horizontal large eddy simulation (HLES).

3.1.3 Boundary conditions

By definition of initial and boundary condition, hydrodynamic equations can be solved. For simulation of the flow in a straight channel with patches of vegetation, the initial condition is defined as a uniform water level for all simulations. Also two boundary conditions need to be defined for modeling of the rectangle channel. The upstream and downstream boundaries have been considered as total discharge and water level respectively. The other two boundaries at the sides of the channel have been specified as closed boundaries, see Figure 3.2.

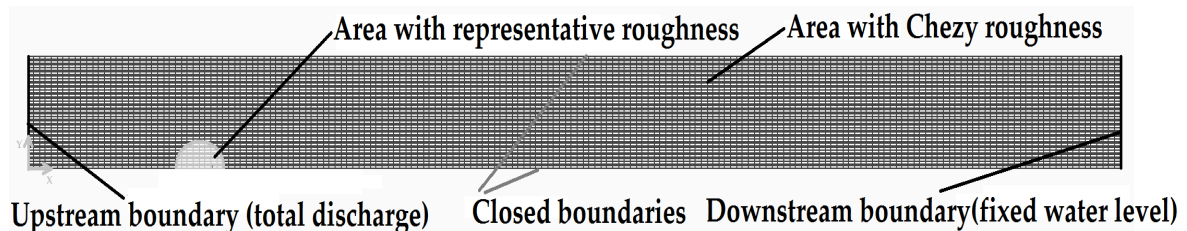


Figure 3.2. Boundary conditions and roughness details

Along closed boundaries, free-slip condition has been considered to set the perpendicular velocity component of the closed boundary to zero.

3.1.4 Physical parameters

Details of physical parameters can be determined in Delft3D. The details of parameters information are presented in Appendix A. Here the parameters that require justification are treated.

3.1.4.1 Diffusion coefficients

Diffusive parts of hydrodynamic equations are determined by component of viscosities and their value can be defined due to the grid size. As the grid cells become smaller, the resolving of advection can happen at smaller scale and less compensation would be required by components of viscosity. Promotion of each of vertical and horizontal viscosities has some effects in outputs.

In multi-dimensional (2D-3D) simulations, a horizontal eddy viscosity and diffusivity have to be specified to consider the loss of energy that is caused both by liquid viscosity and turbulent vortices (eddy). The amount of resistance of the water against forces that causes deformation of it can be represented by molecular viscosity. On the other hand, turbulence induces mixing of water and in order to consider it on the small scales, the Eddy diffusivity is introduced (Deltaras, 2010). For relatively detailed models with grid sizes in the order of centimeters, typical values are in the range of 10^{-3} – 10^{-2} [m²/s] is suggested, whereas for larger grids higher ranges are recommended (Deltaras, 2010).

Also in 3D simulations, multiple vertical layers are introduced in the model. Therefore, two additional terms of vertical Eddy viscosity and diffusivity have to be specified. Increasing of the vertical viscosity enhances the viscosity of flow and can change the velocity profile. Because higher viscose flows provide larger eddies and subsequently easier momentum transfer, which can change the logarithmic distribution of the velocity. Although some scientists parameterized the turbulence and provided some information about vertical and horizontal eddy viscosities (such as Smagorinsky, 1993), but the fine-scale measurements of vertical viscosity 10^{-4} m²/s (recommended by user manual, 2006, p 4-60) is a reliable estimation to start.

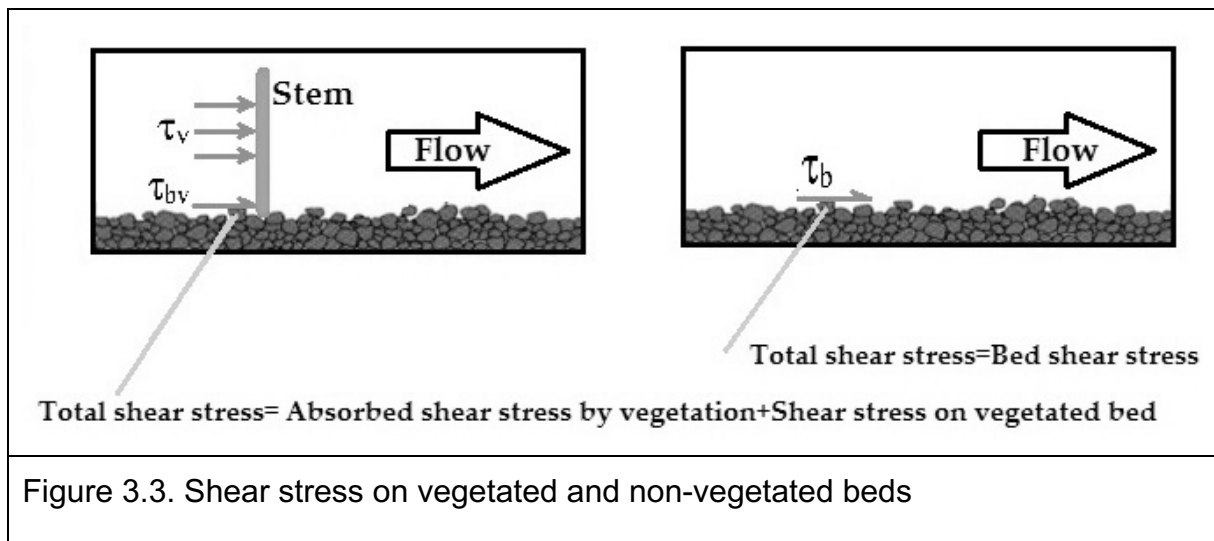
3.1.4.2 Bed roughness

The roughness is implemented as the depth dependent Chézy coefficient (C), which determines for a given depth averaged velocity the bed shear stress induced by the flow. Higher Chézy coefficient describes smoother beds and lower values therefore imply a roughening of the bottom. Considering the experimental bed profiles for different flow condition, uniform bottom roughnesses are imposed in simulations. However, within the cells where the trachytopo functionality introduced to model the effects of vegetation, these uniform values are overruled. The implemented uniform Chézy roughnesses are between 35 to 65. This implies that the model computes bed shear stress using quadratic friction law:

$$\tau_b = \frac{\rho g \bar{U} |\bar{U}|}{C^2} \quad (3.6)$$

Where U represents the magnitude of the depth averaged horizontal velocity and C the Chézy coefficient. The Chézy coefficient also influences the flow itself as a friction term via the momentum equation. There are different methods to estimate the Chézy coefficient. In Chézy formulation, the 2D Chézy coefficient is specified by a uniform value in both streamwise and transverse direction.

The bed shear stress is both exerted on the flow (which experiences drag) and on the bed (which can experience erosion). The shear stress in unvegetated part is smaller than the vegetated part because the representative roughness in this area, which is calculated by trachytopes functionality, is larger than the chezy roughness of unvegetated part. The total shear stress is computed by means of certain depth-average velocity through equation 3.4. The total shear stress consists of the force that can be absorbed by vegetation (τ_v) and the erosive force that related to the spaces between the stems (τ_{bv}) (figure 3.3).



In this study, the bed roughness and flow resistance are specified separately on a sub grid level by the use of Trachytopes function to overrule the roughness at specified time intervals.

3.1.4.3 Morphodynamic setup

Vegetation increases the shear stress on the passing flow. Within the main unvegetated stream flow, the bed shear stress can be quantified by means of roughness coefficients such as Chézy and Manning. The main aim of the model is to simulate the major morphological changes as the consequences of

implementation of the rigid stems in the shape of the semicircle at the banks of a channel. As the morphological processes take larger time scales than the hydrodynamic one, an acceleration factor is considered to be multiplied with the changes of bed level within one step of time and reduce the time of computation. The simulations would be last until the morphological changes become almost constant.

3.1.4.4 Sediment properties

The bed material in sand bed rivers usually consists of the continuous distribution of fine materials. It is always a challenge to capture the variety of sizes of the grains and on the other hand, morphodynamic models are usually simplify the diversity of sediments by considering the main properties of sediments such as the median size of the grains, the specific density of sediment and critical bed shear stress. Regarding to the previous studies about sediment transport in sand bed rivers and according to the experimental material the properties of the sediment in Delft3D have been defined. Table 3.1 represents different properties of the implemented sediment in Delft3D.

Table 3.1. Properties of bed material

Type	Size	Specific density [kg/m ³]	Dry density [kg/m ³]	Median diameter [mm]	Hindered settling [kg/m ³]
Sand	fine	2600	1600	0.5	1600

3.1.4.5 Sediment transport equation

The velocity field calculated by solving the Navier-Stokes equations is used to calculate the sediment transport field. In delft3D the bed-load transport can be calculated by different implemented formula such as Engelund & Hansen (1967), and Van Rijn (1993), at the cell interfaces and corrected according to the slope effects and sediment availability. The magnitude of sediment transport has been calibrated and calculated by the general sediment formula implemented in delft3d and has the structure of Meyer-Peter Müller (1984):

$$S = \alpha D_{50} \sqrt{\Delta g D_{50}} \theta^b (\mu \theta - \xi \theta_{cr})^c \quad (3.7)$$

Where α represents a calibration coefficient, D_{50} the median sediment diameter, g gravitational acceleration $\Delta = \frac{\rho_s - \rho}{\rho}$, b and c constants, μ the ripple factor, θ_{cr} the critical mobility factor, ξ a hiding and exposure factor for the sediment fraction considered, and θ the Shields mobility parameter.

All the powers and coefficients can be adjusted to fit the requirements. Due to experimental results, these amounts were chosen to calibrate the sediment transportation. It should be mentioned that these coefficients have been calibrated by certain experiments and validated by the rest. The Shields mobility parameter can be determined by:

$$\theta = \left(\frac{q}{C}\right)^2 \frac{1}{\Delta D_{50}} \quad (3.8)$$

and the ripple factor also can be specified by:

$$\mu = \min\left(\left(\frac{C}{C_{g,90}}\right)^{(3/2)}, 1.0\right) \quad (3.9)$$

Where $C_{g,90}$ represents the Chézy coefficient related to grains and can be estimated by:

$$C_{g,90} = 18 \log\left(\frac{12h}{D_{90}}\right) \quad (3.10)$$

The bed level in the model is updated at each time step. The following equation represent a balance between the sediment transport and evolution of the bed level:

$$(1 - \varepsilon) \frac{\partial z_b}{\partial t} + \frac{\partial s_x}{\partial x} + \frac{\partial s_y}{\partial y} = 0 \quad (3.11)$$

Where z_b is bed level [L], ε bed proosity (by default 0.4), s_x, s_y [L3L-1T] sediment transport in x and y direction respectively. The update scheme is also presented in figure 3.4.

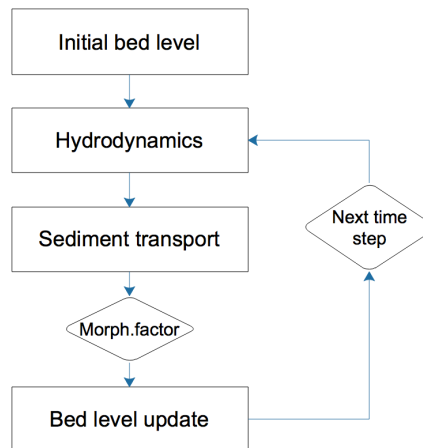


Figure 3.4. Morphological update scheme

This approach allows considering the propagation of morphological features more accurately.

3.1.5 Implementation of patches of vegetation

In vegetated regions, the flow resistance also depends on exerted drag forces by vegetation stems. In order to study the partly vegetated bed influence on the sediment dynamics of a channel using a model the partly vegetated channel needs to be implemented by means of estimation of flow resistance and bed roughness.

3.1.5.1 trachytopes functionality

Compared with non-vegetated flows with the same boundary and physical condition, Implementation of stems causes flow blockage and exerts an extra drag forces, which increases channel resistance by adding large-scale roughness. For example, Nezu and Nakagawa (1993), defined the extra roughness as a wall region, approximately 10 to 15% of the flow depth. Due to the flow regime, exertion of these forces may leads to different bedforms inside and close to the vegetation zone than the other part of the channel. The initial bed elevation can be implemented by simply elevating the bed level in the bathymetry file in Delft3D. This is also allowing capturing the bed slope and computation of bed elevation changes in a morphodynamic model. By definition of the time steps and due to the sediment transport rate, the bathymetry starts to evolve. In such a computation Delft3D itself will calculate the development of deposits and erosion, which could happen relative to the vegetated zone. The bed profile then depends both to the amount of sediment transport rate and the features of the vegetation zone.

Features of vegetation area have been implemented via the Delft3D trachytopo functionality. The trachytopo functionality has been designed to implement both roughness and resistance caused by vegetation in depth averaged model computations by using 3 different roughness classes which are area, line and point (Delft3D user manual). In this study we use the area class, which considers the vegetation variables like stem diameter and height, vegetation density, and drag coefficient by Baptist (2005) formulation.

The specific formulation proposed by Baptist (2005) is based on the assumption that vegetation can be implemented as rigid cylinders and this allows to consider the vegetation variables. Due to Baptist model, in Delft3d the roughness in vegetated area is split into two parts, the first due to vegetation and the second due to the bed. By calculating the effective Chézy bed roughness and considering the Chézy bed roughness, the bed shear stress for vegetated and non vegetated areas are calculated. The representative Chézy roughness is calculated by this formula:

$$C_r = \sqrt{\frac{1}{C_b^{-2} + (2g)^{-1} C_D m D k}} + \frac{\sqrt{g}}{\kappa} \ln\left(\frac{h}{k}\right) \quad (3.12)$$

Where C_r is the representative Chézy roughness coefficient [$m^{0.5} S^{-1}$], C_b is bed Chézy roughness [$m^{0.5} s^{-1}$], C_D is drag coefficient of vegetation structure, m is number of cylinders per unit area [m^{-2}], D is diameter of cylinders [m], k is the height of vegetation, κ is the Kármán's constant, and h is water depth [m].

By assuming a uniform flow in vertical direction, the bed shear stress has been derived as follows (Baptist, 2005)

$$\tau_{bv} = \frac{1}{1 + \frac{C_D m D k C_b^2}{g}} \cdot \tau_t \quad (3.13)$$

Where τ_{bv} is bed shear stress on a vegetated bed [N/m^2], and τ_t total stress on bed and vegetation, which is calculated by the representative Chézy roughness coefficient:

$$\tau_t = \frac{\rho g}{C_r^2} |U|^2 \quad (3.14)$$

Delft3D divides the representative roughness into two parts, which are related to vegetation and bed roughness (C_b). According to this assumption the bed shear stress on a vegetated bed is calculated as follow:

$$\tau_{bv} = \frac{\rho g}{(C_b')^2} |U|^2 \quad (3.15)$$

Where C_b' is effective Chézy bed roughness [$m^{0.5}/s$]

Using C_r as described by equation 3.9 and substituting this into the right hand argument of 3.10, the following expression for C_b' will be achieved:

$$C_b' = C_b + \frac{\sqrt{g}}{\kappa} \ln \left(\frac{h}{k} \right) \sqrt{1 + \frac{C_D m D k C_b^2}{2g}} \quad (3.16)$$

The bed shear stress for non vegetated and vegetated area can be computed by this formula.

3.2 Summary of chapter 3

Numerical modeling could facilitate upscaling the laboratory measurements and could be significantly helpful for capturing the details that experimental can not provide them. In this study, the Delft3D package is chosen to simulate in 2D both flow field and morphological changes of a straight channel, which is equipped with patches of stems. Some important features and parameters of the flow module are explained in this chapter. Patches of vegetation are considered by the trachytopo function, which allows implementing both roughness and resistance caused by stems in depth averaged model. The more detail about uncertain parameters and calibration process and the results are presented in chapter 6.

4 Chapter 4: velocity results of experiments

The hydrodynamics plays a governing role in sediment dynamics and vegetated beds can influence the hydrodynamics in a significant way. Vegetation enhances flow resistance and this would change turbulence and velocity in the flow. Higher flow velocities and turbulence would cause erosion while settling of the sediment on the bed may happen in lower velocities. The mechanisms via which the flow velocity is affected by vegetation are explained in this chapter.

In general, this chapter provides a discussion of hydrodynamic results of laboratory experiments. The effects of vegetation feature on velocity field are expounded upon in light of the experimental data. The primary interest is to discriminate the differences of the effects near the bed and near the surface. Therefore, analyses are made on different components of the velocity both close to the bed ($0.2h$) and to the surface ($0.8h$). The collected data from upstream edge to downstream side of patches is interpolated linearly and plotted by a Matlab code. Effects of the density of vegetation zone are then investigated in terms of distribution of components of velocity, and diversion rate.

4.1 Velocity

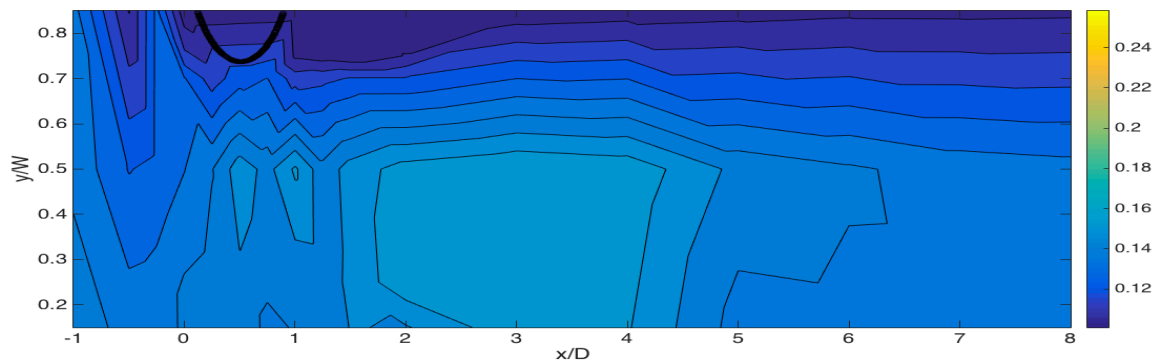
The flow over the bed is hindered by the extra roughness of patches of vegetation and this extra roughness slows down the flow and generates turbulence. Patches of vegetation may become emergent or submerged. In both scenarios the roughness of beds combined with the resistance of stems and may cause significant flow impact. Generally, the physical barrier presented by vegetated area causes flow at the upstream side and in the wake of the vegetation (relative to the flow direction) to slow down, while it is forced to accelerate around the vegetated area and flow velocity increases along the sides of a patch of vegetation. Faster flow causes more bed shear stress and thus the potential for erosion is more. Furthermore, the reduced flow in the wake of a patch of vegetation means that more sediment can be deposited.

Following the figure 2.4, velocity measurements were done at 0.2 and 0.8 times of water depth at each point by using ADV. According to the significant changes of velocity around a finite patch of vegetation and for more detailed investigation the experimental data are interpolated by Matlab and plotted for different component of velocity around the vegetation zone and the effects of stem density, vegetation size

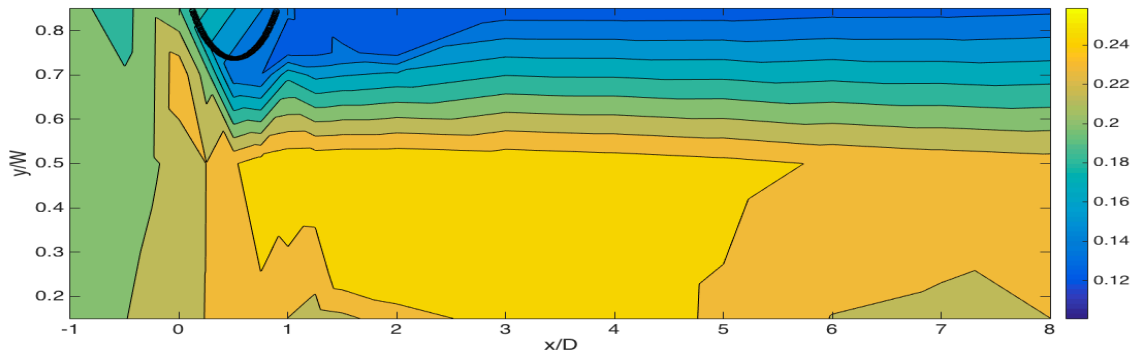
and flow Froude number is investigated on flow velocity. Analyses are made for both 0.2 and 0.8 of the flow depth. The depth-averaged velocity is then calculated and plotted by the means of two velocities at each point.

4.1.1 Effects of density of vegetation on streamwise velocity

The data of the first flow velocity component (V_x) - directed along x , parallel to the channel – (from now streamwise velocity) for different flow conditions are interpolated and plotted at $0.2h$ and $0.8h$ for each vegetation density. Figure 4.1 through 4.3 shows samples of profiles of streamwise velocity around a patch with different densities and same flow conditions. Similar profiles of the rest of the experiments with a single patch of vegetation are presented in Appendix B.

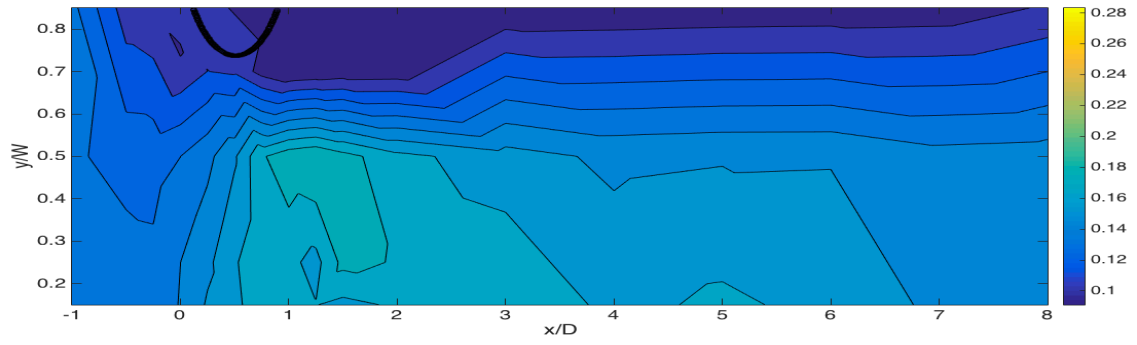


(a)

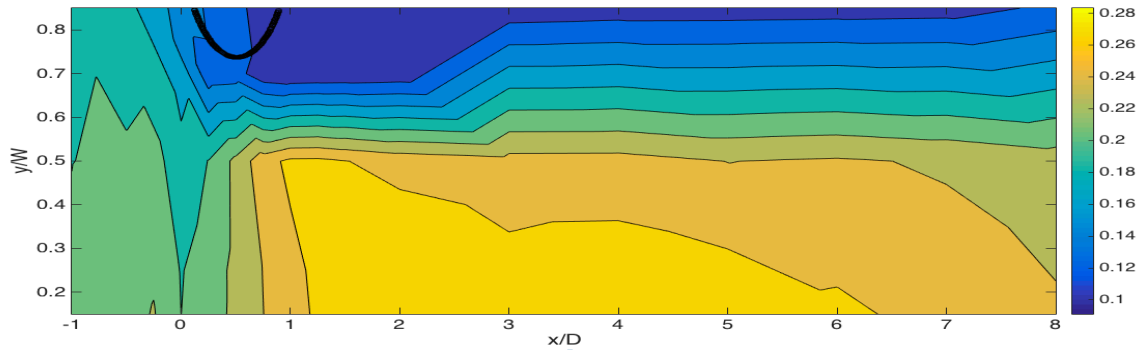


(b)

Figure 4.1. Plan view of streamwise component of the velocity in a channel with $Fr = 0.2$ and density of the patch of vegetation = 0.025, (a): at $0.2h$, (b): at $0.8h$

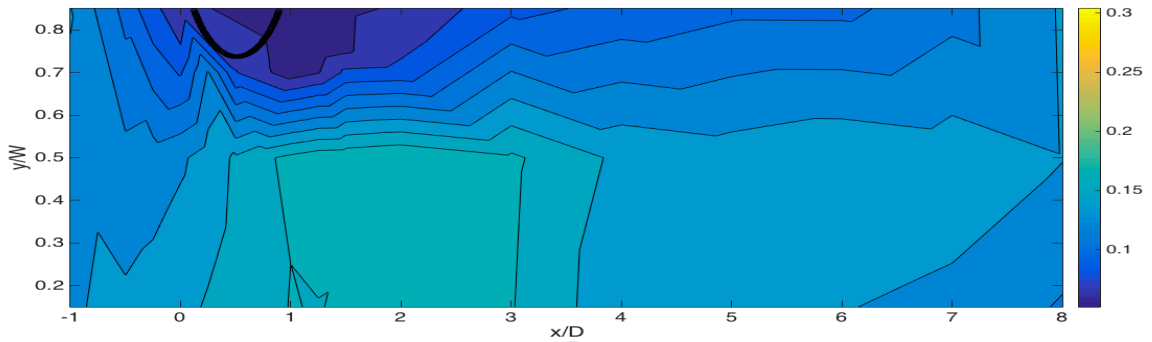


(a)



(b)

Figure 4.2. Plan view of streamwise component of the velocity in a channel with $Fr = 0.2$ and density of the patch of vegetation = 0.05, (a): at $0.2h$, (b): at $0.8h$



(a)

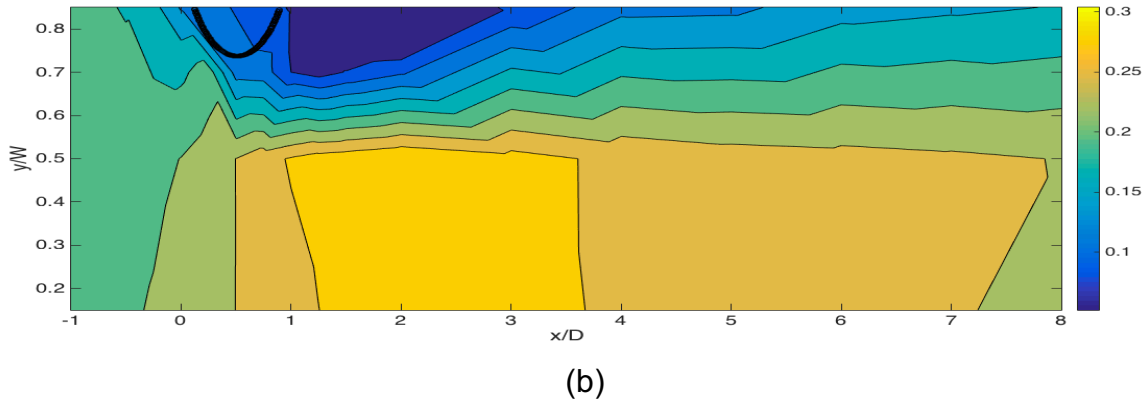


Figure 4.3. Plan view of streamwise component of the velocity in a channel with $Fr=0.2$ and density of the patch of vegetation= 0.1 , (a): at $0.2h$, (b): at $0.8h$

As it was expected, the streamwise velocity shows spatial variation around the patches of vegetation. This variation consists of two different behaviors, which are similar both near the bed and near the surface. The first one is the deceleration of streamwise velocity from the frontal area to the upstream edges of the patch and remaining almost constant for a distance at the wake of the patch. The second one is the acceleration of flow across the channel to the unvegetated side.

Figures (4.1 to 4.3) show that the streamwise velocity decelerates from upstream side of the vegetated zone, and it reaches to its minimum value by the downstream edge of the vegetation zone. In contrast, it accelerates across the channel around the patch of vegetation. Considering these effects in detail, it can be estimated that for the considered ranges of flow Fr number, the decelerated region in the upstream side of the patch is proportional to the diameter of the patch (D), and the region with the minimum velocity behind the vegetation region is a function of vegetation density.

In all tests the deceleration of streamwise velocity starts approximately $1D$ from upstream side of the patch and the rate of reduction depends on density of vegetation. In order to investigate the effects of the patch of vegetation on streamwise velocity, more detail analyses are made on the measured and interpolated depth-averaged streamwise velocity along certain lines with different y/W ratio from the origin of coordinates across the channel. Figure 4.4 shows the location of the lines.

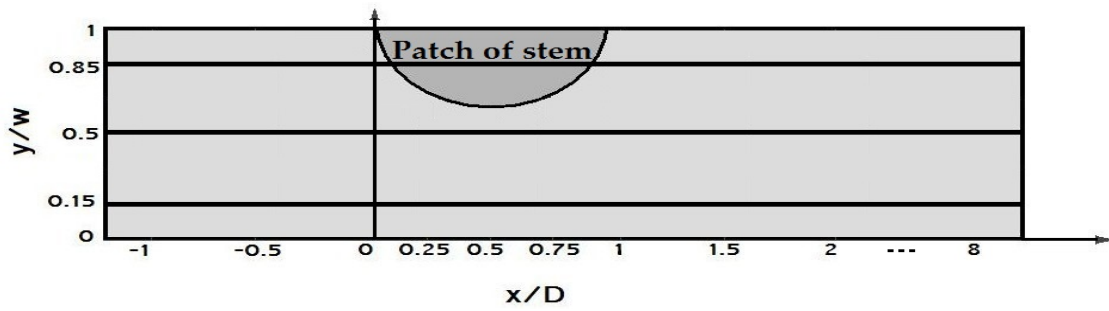
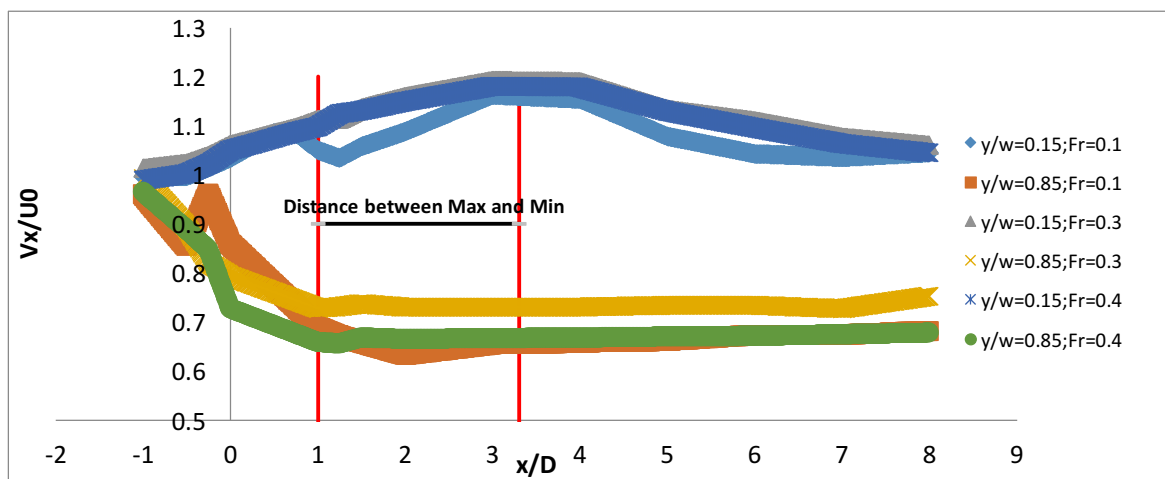
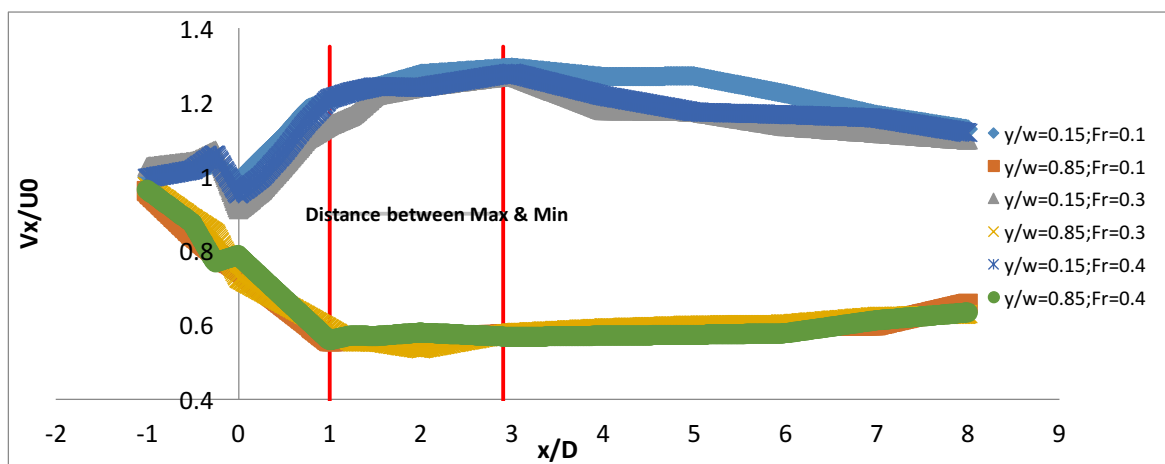


Figure 4.4. Origin of coordinate and longitudinal lines along the channel, which are used to investigate the velocity

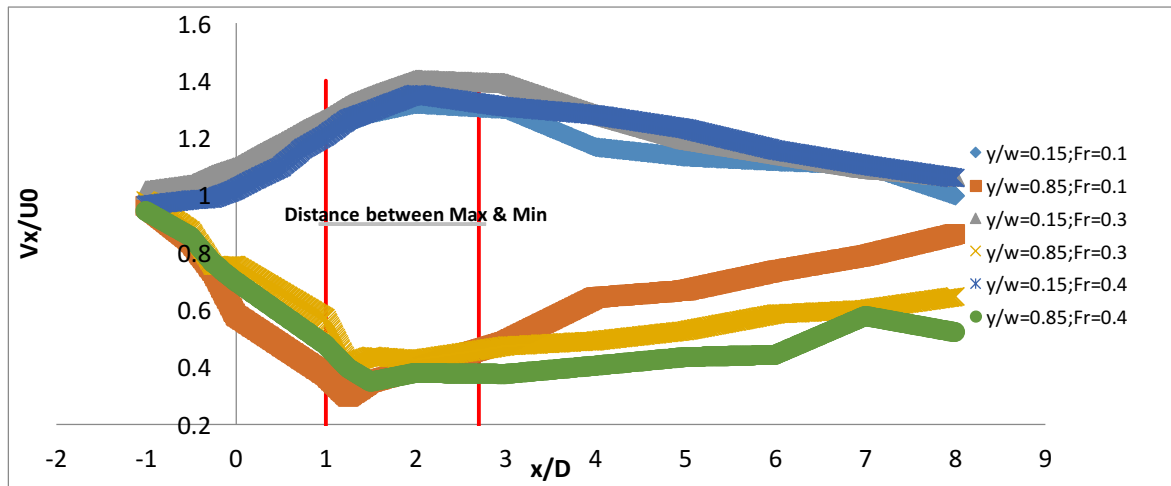
Figure 4.5 (a to c) compares the longitudinal transects of depth-averaged streamwise velocity along two different longitudinal axes of $y/W=0.15, 0.85$ in the channel with different flow Fr number, ranges from $Fr=0.1$ to $Fr=0.4$. The vertical axis presents the normalized streamwise velocity versus the normalized distance from the origin of coordinate.



(a)



(b)



(c)

Figure 4.5. longitudinal transects of depth-average streamwise velocity along two axes of $y/W=0.15, 0.85$ in the channel with $Fr\#=0.1, Fr\#=0.3, Fr\#=0.4$; (a): $\Omega=0.025$, (b): $\Omega_v=0.05$, (c): $\Omega_v=0.1$

In figure 4.5 the streamwise component of the depth-average velocity on both vegetated and unvegetated sides of the channel is investigated in terms of flow Fr number and vegetation density. The patch of vegetation is located between $x/D=0$ and $x/D=1$. For experiments with different Fr number the similar patterns of velocities near patches with a certain density show the velocity distribution is independent from the flow Fr number. This fact proves that the diversion of the flow from vegetated side to the opposite side is not a function of flow Fr number. In the other word, by increasing and decreasing of the flow Fr number, the amount of flow which passes through the patch increases and decreases respectively.

The distances between the minimum streamwise velocity along the vegetated side and the maximum streamwise velocity along the non vegetated side shows that the flow development requires longer length for lower vegetation densities, because the distance between the lowest decelerated flow on the vegetated side and highest accelerated flow along the unvegetated side is longer than the similar length for the higher density (figure 4.5). In chapter 5 by connection of these results to the morphological results, these lengths are used to specify suitable positions for planting the other patches of vegetation. By fitting a polynomial regression through the data for each density of stems, the pattern of velocity on the vegetated side and unvegetated side is found, and then it is used to investigate the effects of density of vegetation on streamwise component of the velocity. Figure 4.6 illustrate the trend line of the velocity along the same longitudinal transects for different vegetation density.

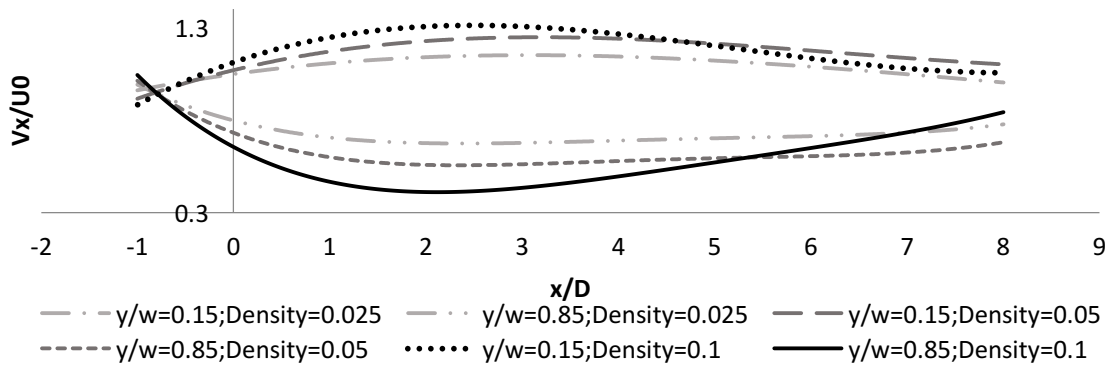


Figure 4.6. Streamwise velocity along two longitudinal axes of $y/W=0.15$, 0.85 in the channel with $0.1 < Fr\# < 0.4$

Different processes along the axes closer to the vegetated side ($y/W=0.85$) and far side of the channel ($y/W=0.15$) are observed. According to the figure 4.6, for the axes of $y/w=0.15$, approaching of the flow to the patch is followed by acceleration of depth average streamwise velocity just around the patch of vegetation and deceleration of it by getting far from the patch till the flow reaches to the initial condition. Enhancement of vegetation density has a direct effect on this process. As the vegetation become denser, more flow diverts to the opposite side and the streamwise velocity increases to a higher amount. For example, the maximum of the streamwise velocity in the channel with density of 0.1 is 25 percent of the depth integrated velocity (U_0) -in a channel without vegetation- while, it is just 7 percent higher than U_0 in the channel with a patch of 0.025 density. In addition, following the pattern of longitudinal transects of $y/w=0.85$, the velocity decreases from the upstream side of the patch and it reaches to its lower amount by the end of the patch and it remains almost constant for a distance in a steady region at the wake of the patch. As the vegetation density increases, the minimum velocity at the downstream edge of the vegetation zone decreases, but the acceleration of the flow happens in the closer region to the vegetated zone and the steady area with decelerated flow becomes smaller. Behind the steady zone, the velocity just starts to increase. The reason of this process is relied on the growth of a shear layer at the wake of the patch which is created because of changes of velocity across the channel. The similar steady region behind a circular isolated vegetation zone is investigated recently for a single patch of cylinders in a wide channel (Ball et al., 1996; Follett and Nepf, 2012). Figure 4.7 illustrates the growth of shear layer around a patch of vegetation.

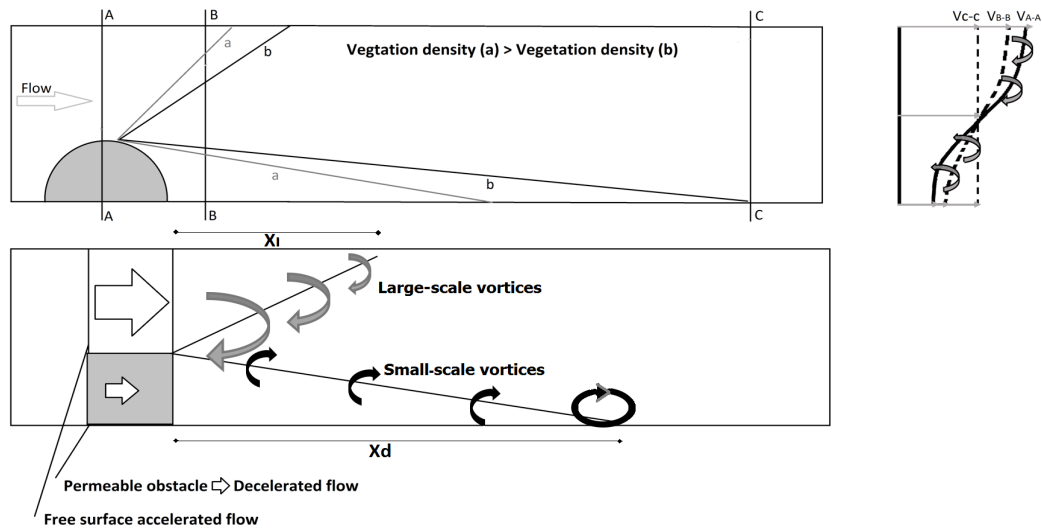
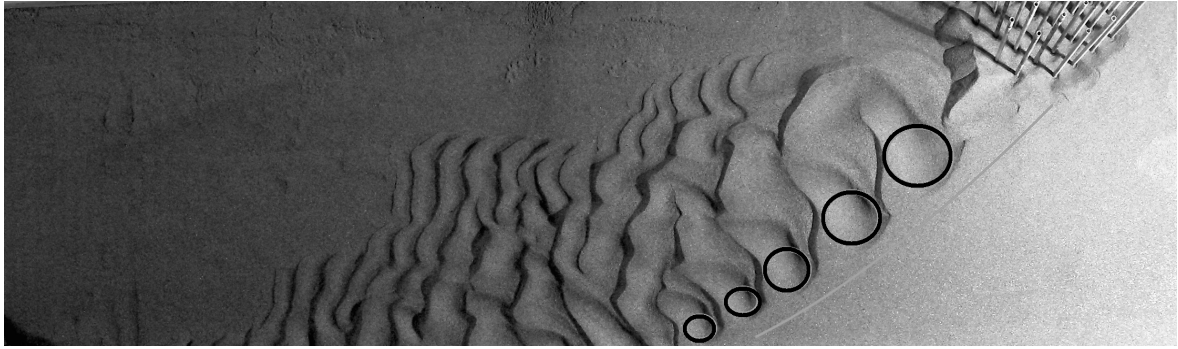


Figure 4.7. Creation of a shear layer around a patch of vegetation

As it is shown in figure 4.7, at the wake of the patch, the shear layer starts to grow up linearly to retrieve the reduction of the velocity and as soon as it reaches to the wall of the channel, large-scale vortices will be generated. By creation of the mixing layer or free shear layer, flow starts to separate along the side of the patch and horizontal vortices with both small and large scales appear along the edges of the mixing layer. In particular, the edges of the mixing layer consist of Kelvin-Helmholtz wave instabilities, which turn into the roller-type vortices (Ghisalberti and Nepf, 2002). Due to the density of the stems, the formed vortices have impacts on bed profile around the vegetation region (figure 4.8).



(a)



(b)



(c)

Figure 4.8. Location of the vortices around the patch; a & b: Large-scale vortices and their effects on bed profile; c: location of small-scale vortices along the steady region at the wake of the patch.

Small-scale vortices have elliptical structures and they spin toward the patch of vegetation (figure 4.8). These vortices form mostly near the apex of the patch and extend to the wake of the patch along the edges of the mixing layer. These vortices are not clearly visible and their observed average sizes are about 10 cm long and 5 cm wide for the patches with density of 0.1. As the density of stems decreases in the patch, vortices become weaker and smaller.

Large-scale vortices have also elliptical structures which rotate toward the vegetation zone and their sizes depend directly on density of the vegetation zone and their distance from the patch. These vortices extend across the channel to the opposite non-vegetated side and formations of them are more probable than small-scale vortices for lower densities. Furthermore, the impacts of these structures on local bed profile are more obvious (figure 4.8). The results of vortices on bed morphology are presented in chapter 5.

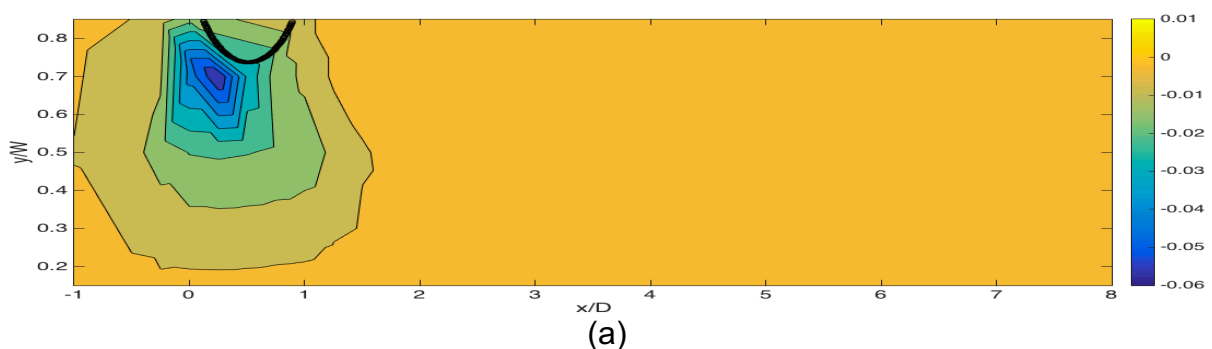
Frequency of vortex shedding can be estimated due to the flow velocity and the size of the patch through Strouhal equation (Levi, 1991):

$$St = \frac{f \cdot D}{U} \quad (4.1)$$

Where the St represents the Strouhal number, f is the vortex shedding frequency, D is the flow length scale before separation, and U is the approaching flow velocity. If the flow length scale would be equal to the constricted flow width ($D=0.5$ m), and the Strouhal number is considered $St=0.159$ (Levi, 1991), the frequency of vortices for different densities would be change from 0.05 to 0.1. The higher frequencies are related to the higher densities. Considering results of depth average velocity distribution, and connecting them with bed profile features, more investigation has been done on physical features such as frequency of vortices which are presented in chapter 5.

4.1.2 Effects of density of vegetation on transverse velocity

The second flow velocity component (V_y) -directed along y , transverse to the channel- (from now transverse velocity) is usually negligible in straight channels with steady and fully developed clear water (Joseph and Tao, 1963). Introduction of the patch of vegetation changes the equilibrium condition and causes significant transverse components of the velocity near the interface between stems and flow. As flow approaches to the vegetated zone, the transverse velocity follows a special variation both close to the surface and the bed, which proves the diversion of the flow. The increase of transverse velocity diverts more flow to the opposite side and changes the velocity distribution. The result of transverse velocity components of experiments at $0.2h$ and $0.8h$ are interpolated and plotted. Figure 4.9 through 4.11 shows samples of profile of transverse velocity around patches with different densities and same flow conditions. Similar profiles for the rest of the experiments are presented in Appendix B.



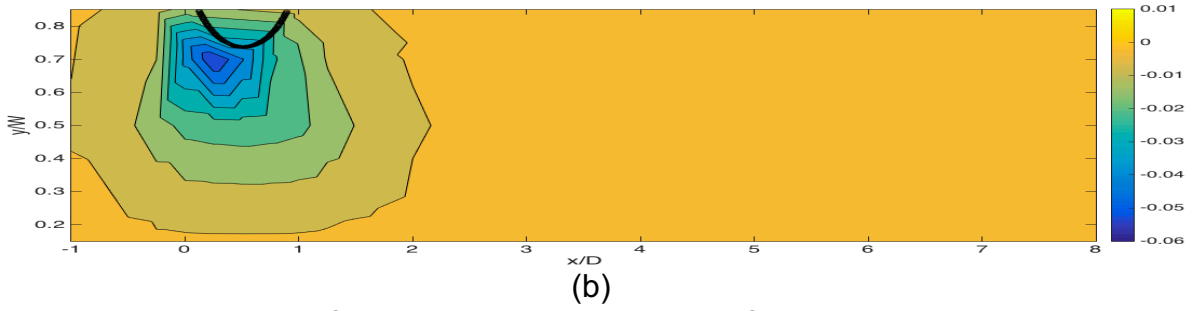


Figure 4.9. Plan view of the transverse component of the velocity in a channel with Fr number=0.2 and density of the patch of vegetation=0.025, A: at $0.2h$, B: at $0.8h$

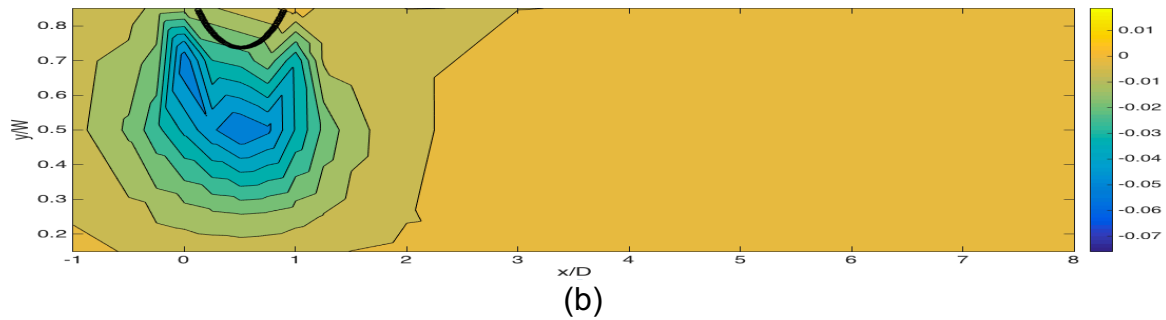
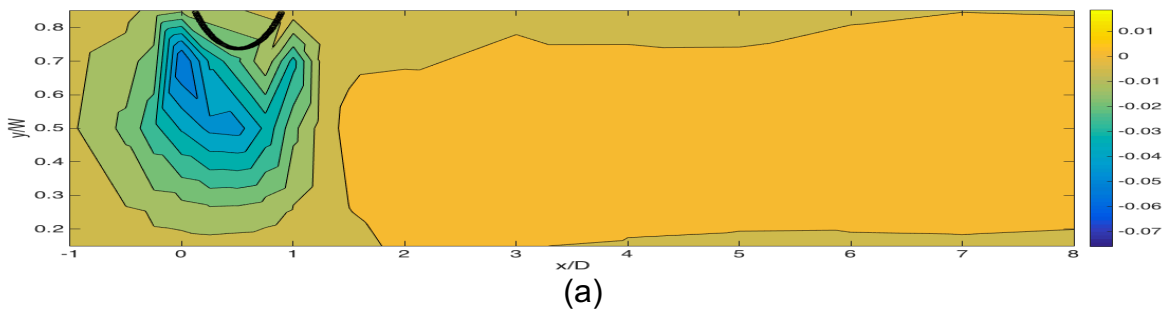
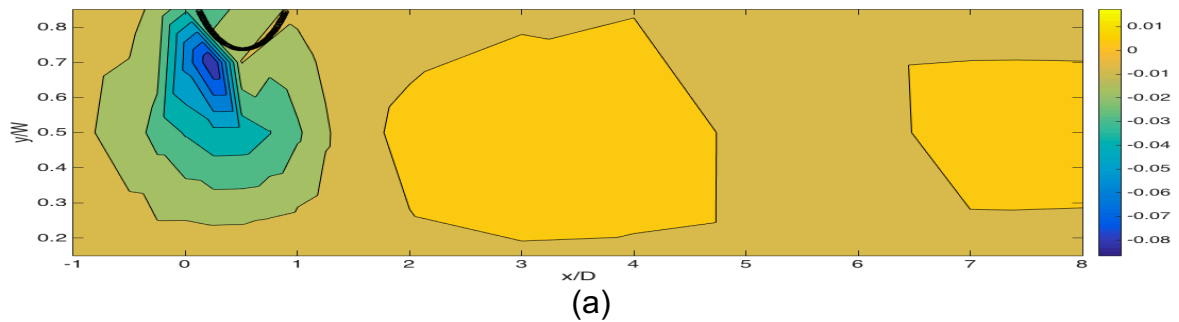


Figure 4.10. Plan view of the transverse component of the velocity in the channel with Fr number=0.2 and density of the patch of vegetation=0.05, A: at $0.2h$, B: at $0.8h$



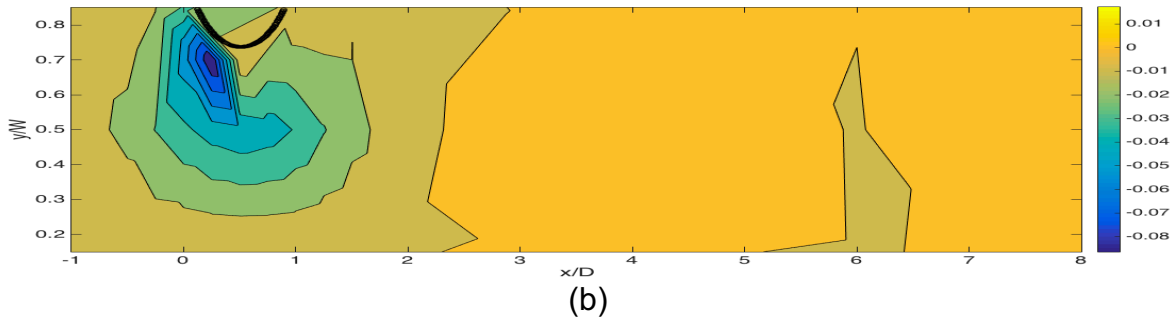


Figure 4.11. Plan view of the transverse component of the velocity in a channel with Fr number=0.2 and density of the patch of vegetation=0.1, A: at $0.2h$, B: at $0.8h$

Transverse velocity distribution follows approximately the same pattern near the bed and near the surface, but in contrast with streamwise velocity the magnitude of transverse velocity in depth of the flow does not necessarily have a logarithmic distribution in areas close to the patch. Comparison of ratio of changes of time average velocities in x and y direction (V_y/V_x) around the patch would help to investigate the effects of patch of stems on distribution of the two main components of the velocity (figure 4.12 a to d).

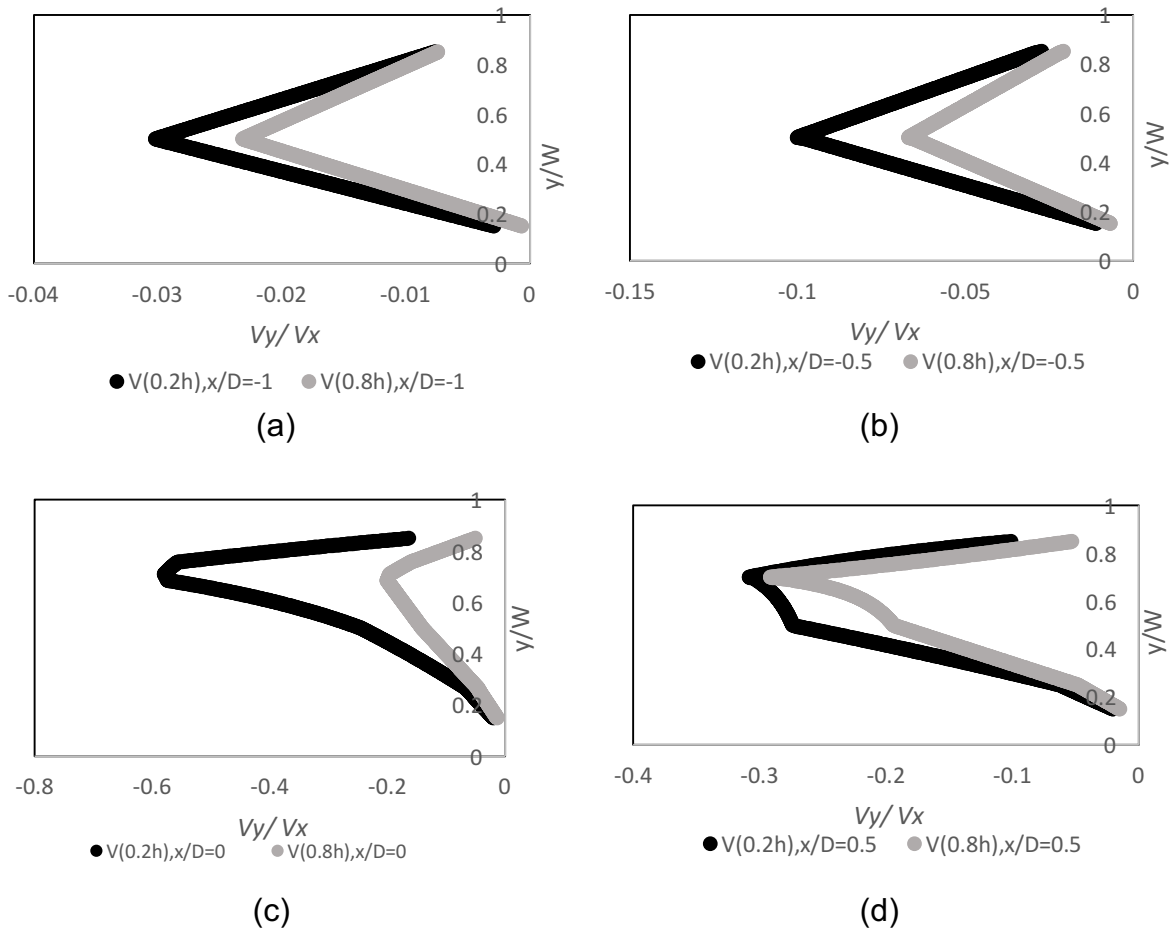
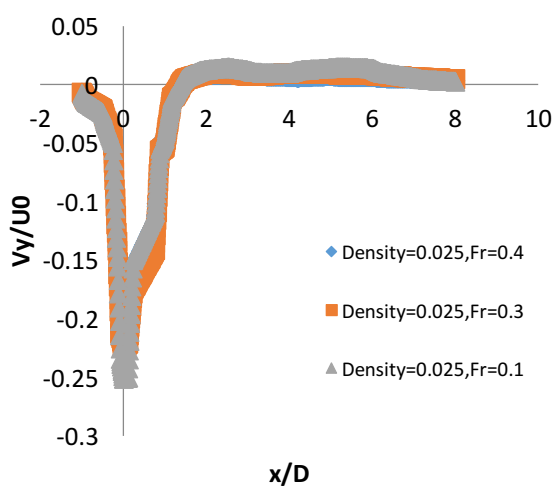


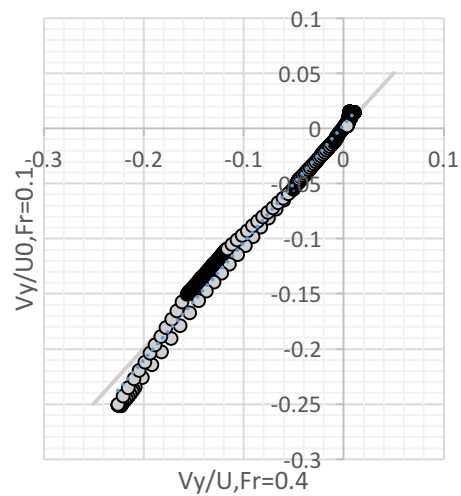
Figure 4.12. Comparison of V_y/V_x ratio between $0.2h$ and $0.8h$ at different cross sections $Fr=0.4$, $\Omega=0.1$, (a): $x/D=-1$, (b): $x/D=-0.5$, (c): $x/D=0$, (d): $x/D=0.5$

In figure 4.12, the non-dimensional ratio of V_y/V_x near the bed and near the surface and along 4 different cross sections of $x/D=-1, -0.5, 0, 0.5$ is presented to investigate the effects of the patch of vegetation on distribution of transverse and streamwise velocity. First of all, the large ratio of V_y/V_x near the bed can be referred to stronger vortices at these regions than the areas close to the surface. Secondly, the differences between the ratio of V_y/V_x start to increase from cross sections behind the patch (figure 4.12 a & b) and it reaches to the highest value close to the upstream edges of the patch, which the highest diversion happens (figure 4.12 c), and it decreases by getting far from this region to the downstream side of the patch. Unfortunately, it was not possible to make velocity measurements within the patch but it is assumed the interpolation of the measured velocities around the patch follows the right velocity distribution.

The flow diversion starts around $1D$ upstream side of the patch and intensifies almost at the first half of the patch, and finish around the end of it. For more clarification about the effects of the patch of vegetation on distribution of transverse velocity, more analyses are made on the detail of the measured and interpolated depth-averaged transverse velocity along different longitudinal transects. Figure 4.13 (a to c) compare the longitudinal transects of depth-averaged transverse velocity along different cross sections in the channel with different flow condition from the range of $Fr=0.1$ to $Fr=0.4$. The transverse velocity is normalized by the upstream uniform depth average velocity (U_0) on the vertical axes and the lateral distance also is normalized by the width of the channel.



(a)



(d)

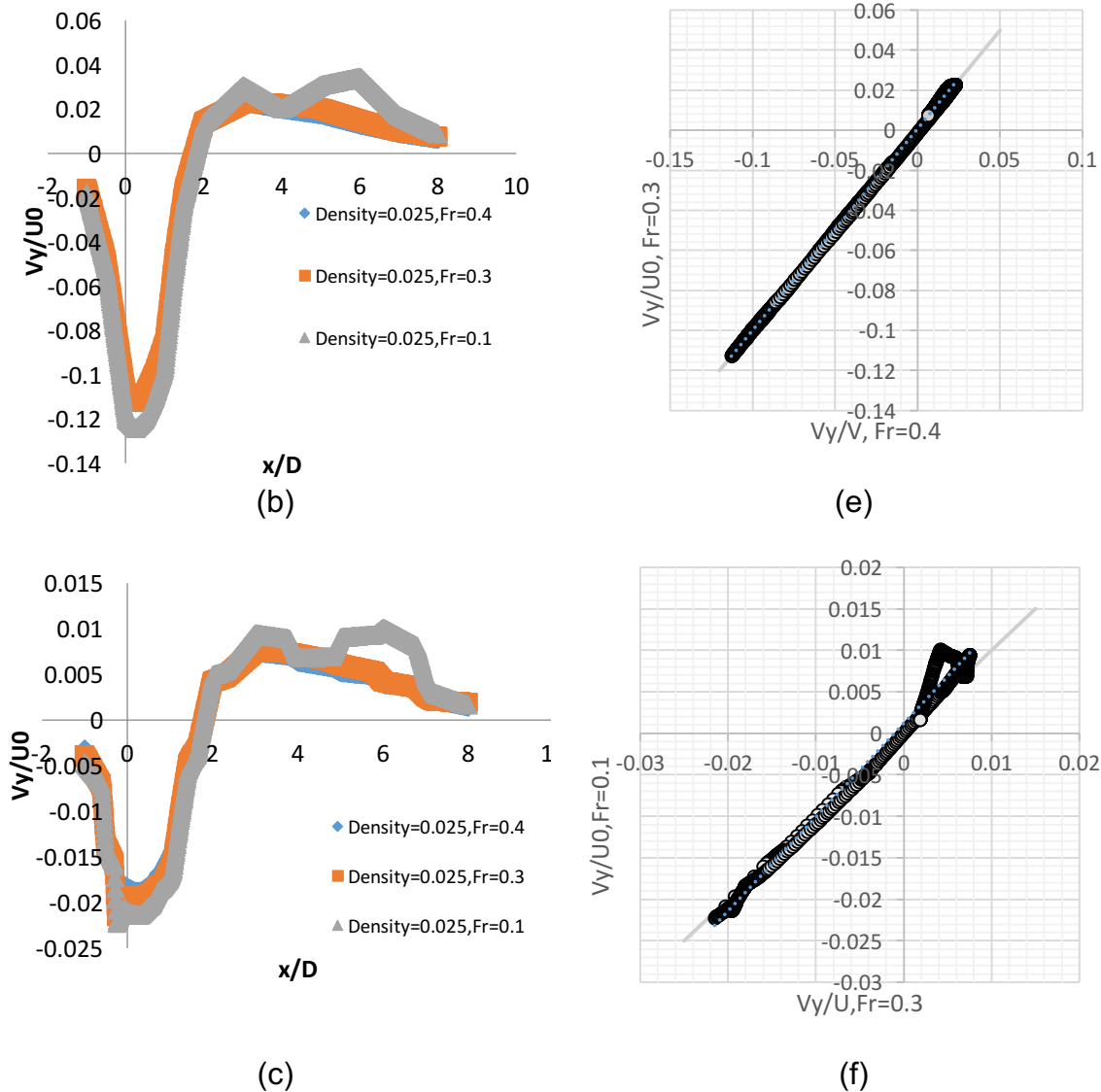
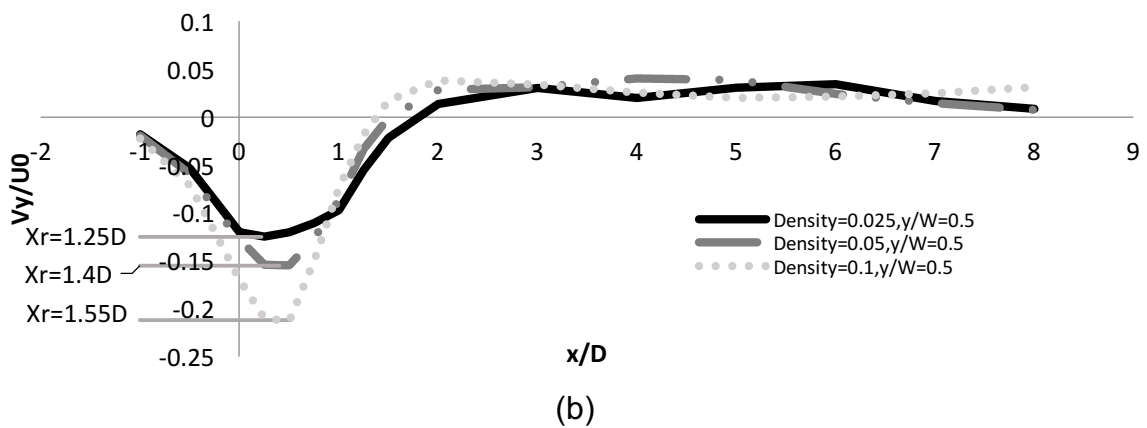
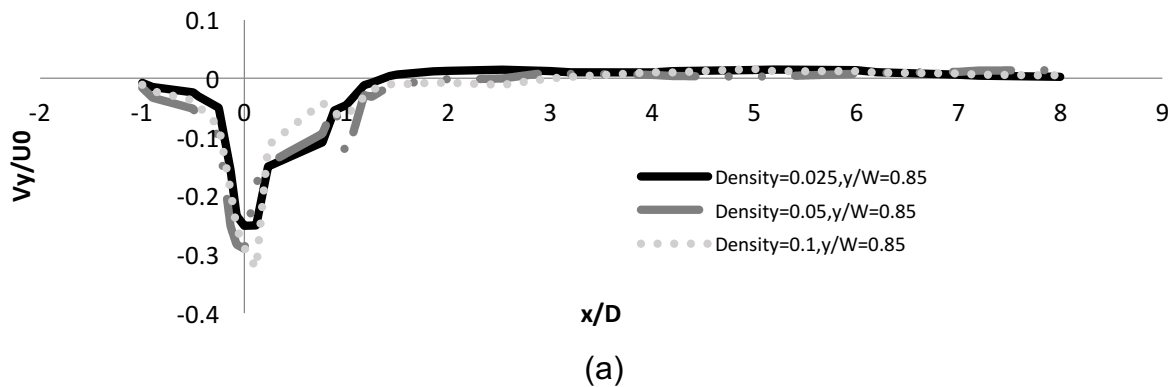


Figure 4.13. Longitudinal transects of the transverse velocity in a channel with a patch of density $\Omega_v=0.025$ - a: along axes of $y/W=0.85$, b: along axes of $y/W=0.5$, c: along axes of $y/W=0.15$. d: comparison of normalized transverse velocity of tests with $\Omega_v=0.025$ and $Fr=0.1$ & 0.4 , e: comparison of normalized transverse velocity of tests with $\Omega=0.025$ and $Fr=0.3$ & 0.4 , f: comparison of normalized transverse velocity of tests with $\Omega=0.025$ and $Fr=0.1$ & 0.3

In figure 4.13 (a to c) the depth average transverse component of the velocity on vegetated side, mid-channel, and unvegetated side of the channel is investigated in terms of flow Fr number in the channel with a patch of density of 0.025. The patch of vegetation is located between $x/D=0$ and $x/D=1$. It is clear that like the streamwise velocity, distribution of the transverse velocity is not a function of flow Fr number, because for experiments with different flow Fr number the similar patterns of velocities near patches with certain density are observed. This fact can also be seen in figure 4.13 (d to f), where the normalized transverse velocity along the similar longitudinal profiles for two of the experiments presented in figure 4.13

(a to c) are compared with each other. The normalized transverse velocity of the tests with Fr number of 0.1 and 0.4 along the longitudinal transects of $y/W=0.85$ are compared in figure 4.13 d, the same data of tests with Fr number of 0.3 and 0.4 along the mid-channel are compared in figure 4.13 e, and finally the transverse velocity of tests with Fr number of 0.1 and 0.3 along the longitudinal transects of $y/W=0.15$ are compared in figure 4.13 f. As it was expected, the differences between the normalized transverse velocities are negligible.

The effects of density of vegetation on transverse velocity is also investigated along the considered longitudinal transects. Figure 4.14 illustrate the longitudinal profile of the depth average transverse velocity along the same three longitudinal transects in channels with different vegetation density.



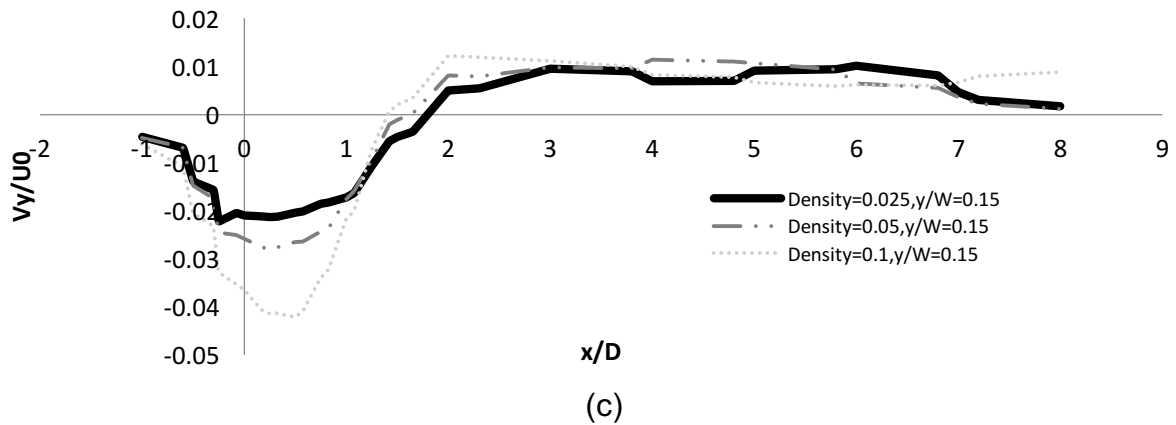


Figure 4.14. longitudinal transects of depth average transverse velocity in a channel with $Fr=0.1$ and different patches of densities along three axes of a: $y/W=0.85$, b: $y/W=0.5$, c: $y/W=0.15$

In figure 4.14 (a to c) the same process for changes of transverse velocity along the axes closer to the vegetated side ($y/W=0.85$), mid-channel ($y/W=0.5$), and far side of the channel ($y/W=0.15$) are observed. For each considered axes, approaching of the flow to the patch is followed by acceleration of the transverse velocity from $1D$ at the upstream side of the patch of vegetation and deceleration of it from the cross sections which passes through the patch and it continues till the transverse velocity magnitude becomes almost zero. The important fact in this process is that the cross section which the acceleration starts is independent from the vegetation density but the cross section that the deceleration happens from there is a function of vegetation density. As the vegetation become denser, the deceleration point is shifted more downstream. For example, if the longitudinal transect along the mid-channel is considered for the tests with density of 0.025 , 0.05 and 0.1 , the acceleration starts almost from the same point (around $1D$) upstream side of the patch and it continues to almost $0.25D$, $0.4D$ and $0.55D$ for respectively (figure 4.14b). In the other word the region that the diversion of the flow happens in it increases by enhancement of the vegetation density and this also proves the increase of flow diversion by vegetation density. Increasing of the transverse velocity by enhancement of the vegetation density under the same initial hydrodynamic condition is also investigated by considering a cross section just at the upstream side of the patch (figure 4.15a).

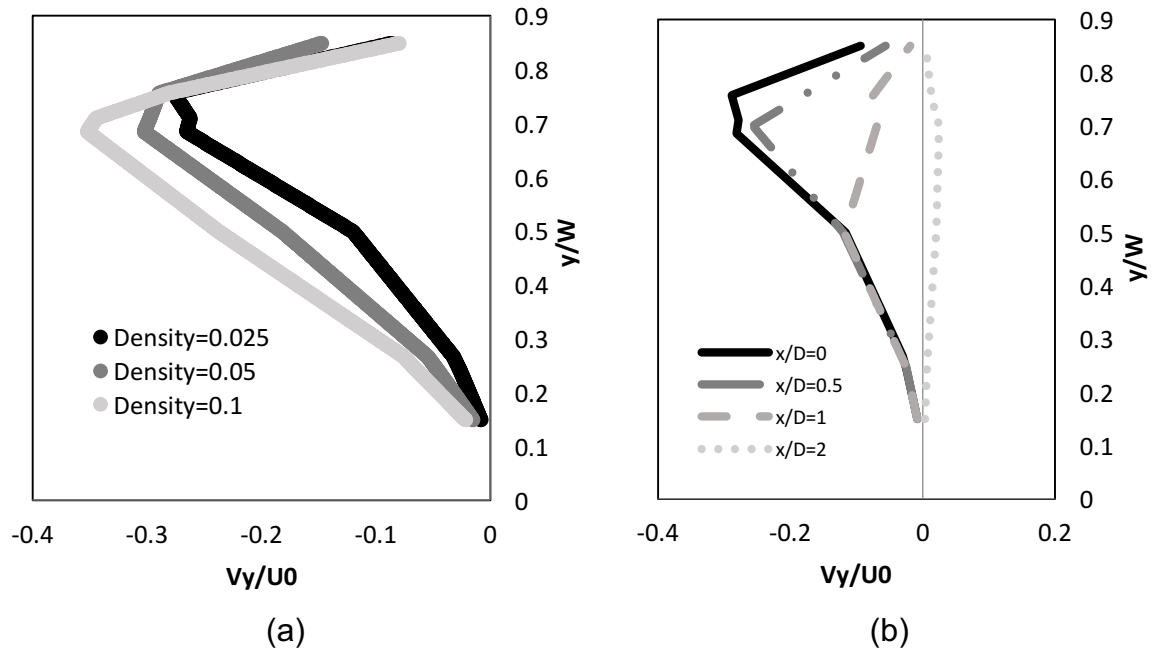


Figure 4.15. (a): lateral transverse velocity profile over the cross section of $x/D=0$ for different density of vegetation; (b): lateral transverse velocity profile over the different cross section for a channel with a patch of density of 0.025

For the cross sections from the upstream affected side to edges of the first half of the patch ($x/D=0$ & 0.05), the highest transverse velocity occurs along the vegetation zone (figure 4.15b). Furthermore, the highest transverse velocity for cross sections from the middle of the patch to downstream side appears in the mid-channel (figure 4.15 b).

Extension of the affected region depends on the density of the vegetation, because as it was mentioned, increasing of the vegetation density intensifies the flow diversion and enhances the transverse velocity and more part of the channel is then influenced across the channel. This is also important in terms of the morphology, because it can change the fate of sediments across the channel and it can also impact the areas close to the other side of the channel.

Connecting transverse velocity profiles to bed profiles in chapter 5, it is found that there is an inseparable correlation between the location and depth of scour holes with the pattern and magnitude of transverse velocity because regions of high transverse velocity around a permeable patch of stems responds to the zone where scouring is possible. More information will be explained about this relationship in chapter 5.

4.1.3 Effects of density of vegetation on vertical velocity

Basically, in non-vegetated channels different components of the velocity are related directly to the bed forms and usually in sand-bed rivers vertical velocity is negligible (Huai *et al.*, 2012). But presence of the vegetation, provide a complicated mechanism of the exerted drag forces which influences vertical component of the velocity as well as other components. In fact, the impact mostly depends on vegetation species, their flexibility, and height of stems. The profile of vertical velocity data for different flow conditions are interpolated and plotted at $0.2h$ and $0.8h$ for channels, which are equipped through patches of vegetation with different densities. Figure 4.16 through 4.18 shows samples of profile of vertical velocity around patches with different densities and same flow conditions. Similar profiles of the rest of the experiments with a single patch of vegetation are presented in Appendix B.

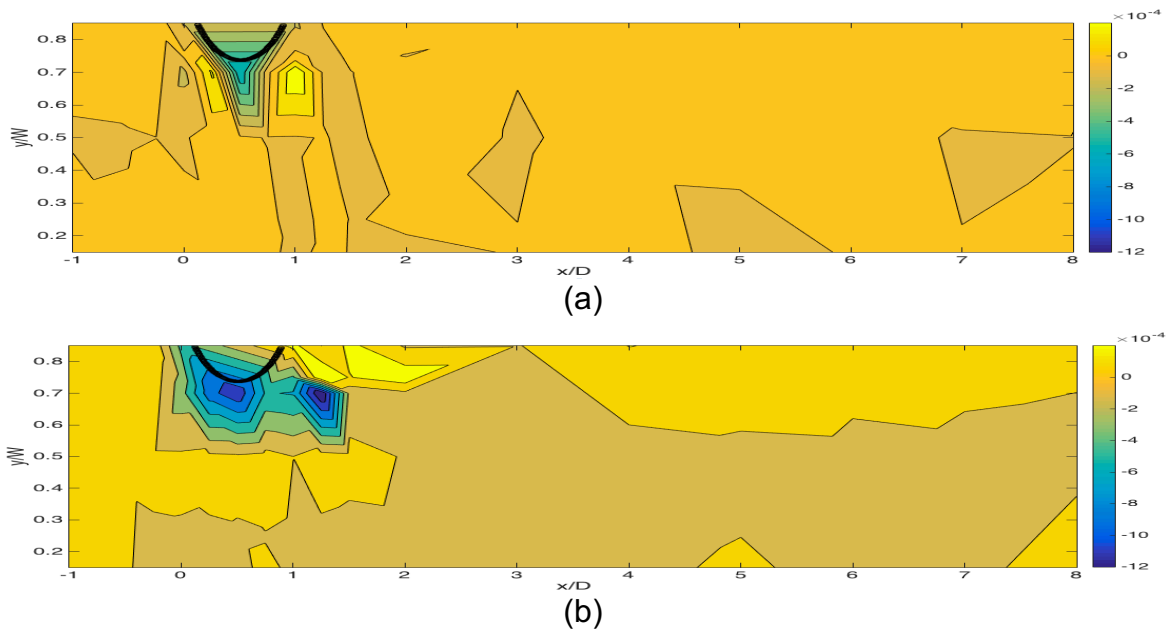
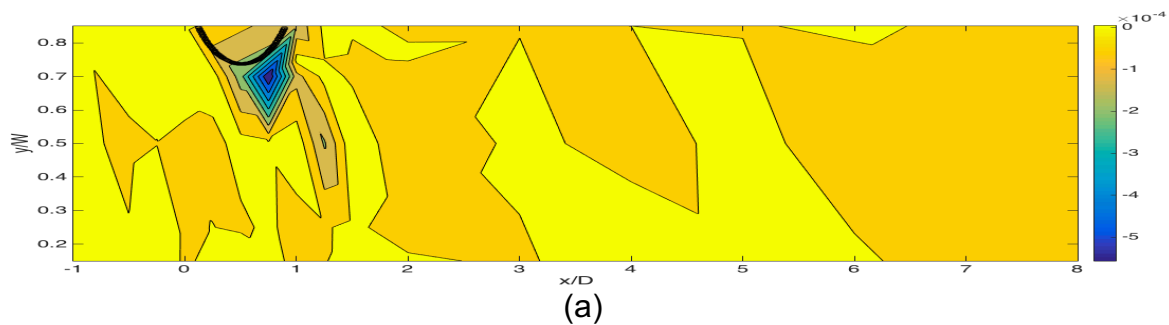


Figure 4.16. Plan view of vertical component of the velocity in a channel with $Fr=0.2$ and density of the patch of vegetation=0.025, (a): at $0.2h$, (b): at $0.8h$



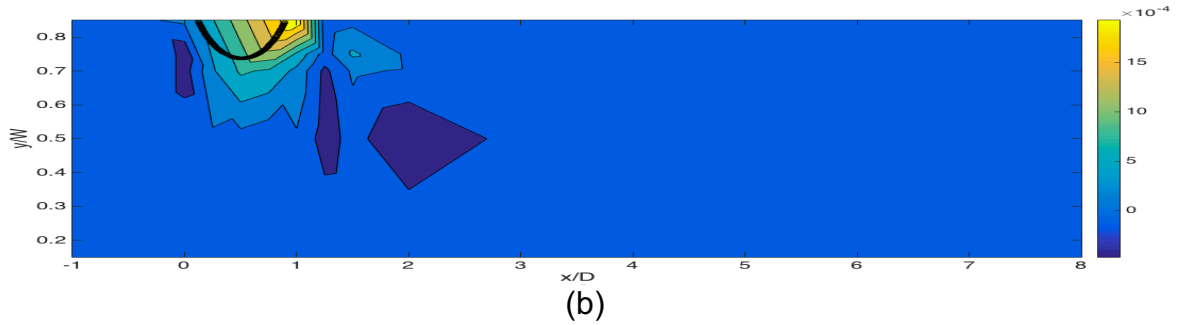


Figure 4.17. Plan view of vertical component of the velocity in a channel with $Fr=0.2$ and density of the patch of vegetation=0.05, (a): at $0.2h$, (b): at $0.8h$

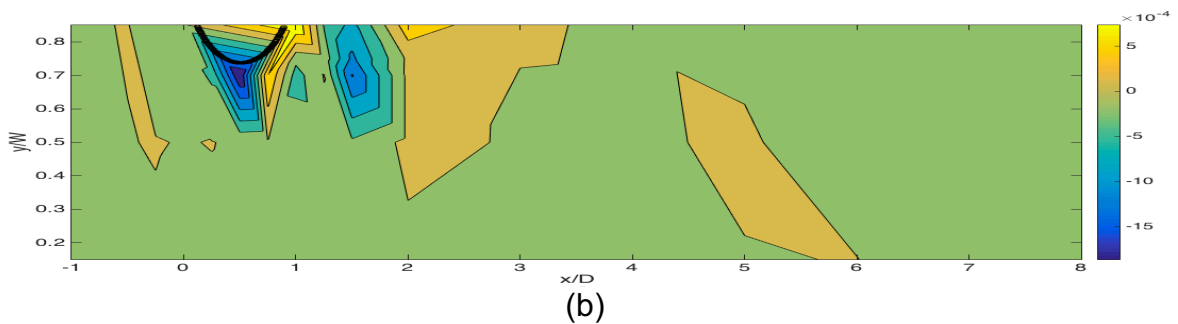
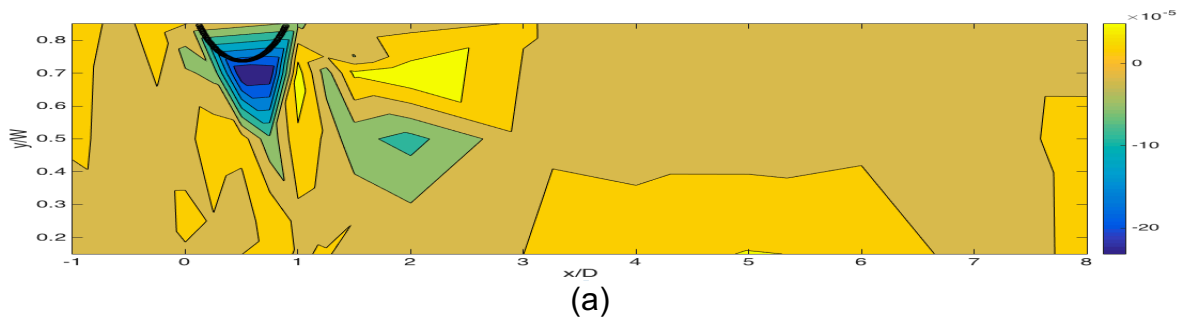
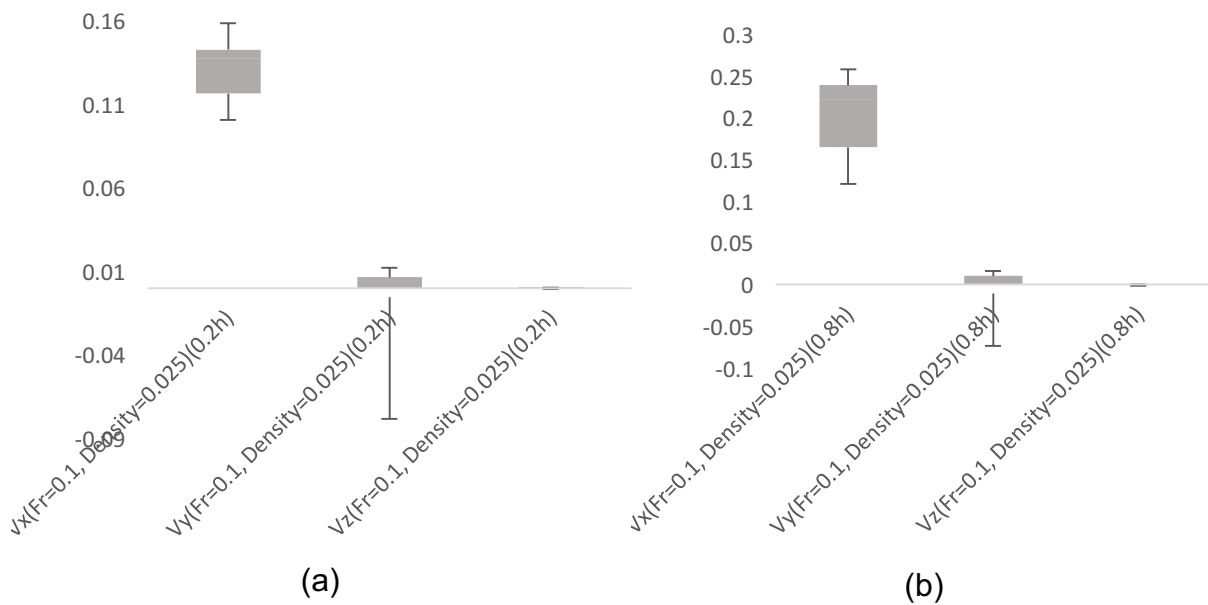


Figure 4.18. Plan view of vertical component of the velocity in a channel with $Fr=0.2$ and density of the patch of vegetation=0.1, (a): at $0.2h$, (b): at $0.8h$

The vertical component of the velocity in the partly vegetated channel could be divided into two separate parts: the unvegetated zone and the vegetated zone. The vertical velocity in unvegetated region is almost negligible but around the vegetated region it depicts a circulation of the flow inside and close to the patch. In fact, when flow reaches to a stem, the boundary layer upstream of the stem must overcome a strong pressure gradient and due to the depth of the flow the vertical component of the velocity intensifies both upward (just near the surface of the flow) and downward (most part of the water column). The upward movement of the flow at the area close to the surface causes the bulk of the flow immediately at the upstream edge of the patch, while the downward accelerated flow creates strong vortices and could finally cause a scour hole around each circular cylinder particularly at the upstream side of it. The process of development of vortices around cylindrical stems both in a fixed-bed and movable-bed channels has been studied in detail by Dargahi 1987, 1989 and 1990.

Generally, by penetration of the flow into the vegetation region and decreasing of the flow velocity, the magnitude of the vertical velocity reduces but the velocity reduction directly depends to the density of stems. For lower densities flow reduction is less than higher densities. In fact, circulation of the flow in the patches with higher density of vegetation is clearer. The reason of this fact relies not only to the exerted drag forces of stems but also the sediment transportation inside the patch. As it will be shown in chapter 5, patches with higher density associated with sedimentation even inside the patch, because higher velocity reduction happens inside the patch and the vertical velocity at the downstream edge of the patch is change completely from downward to upward (figure 4.18).

After primary analysis of velocity components, it is found that except the region close to the patch and inside of it, the vertical component of the velocity is negligible. Figure 4.19 presents the range of different components of the velocity for the experiments presented in figure 4.16 to 4.18. Similar box charts of the rest of the experiments with a single patch of vegetation are presented in Appendix B.



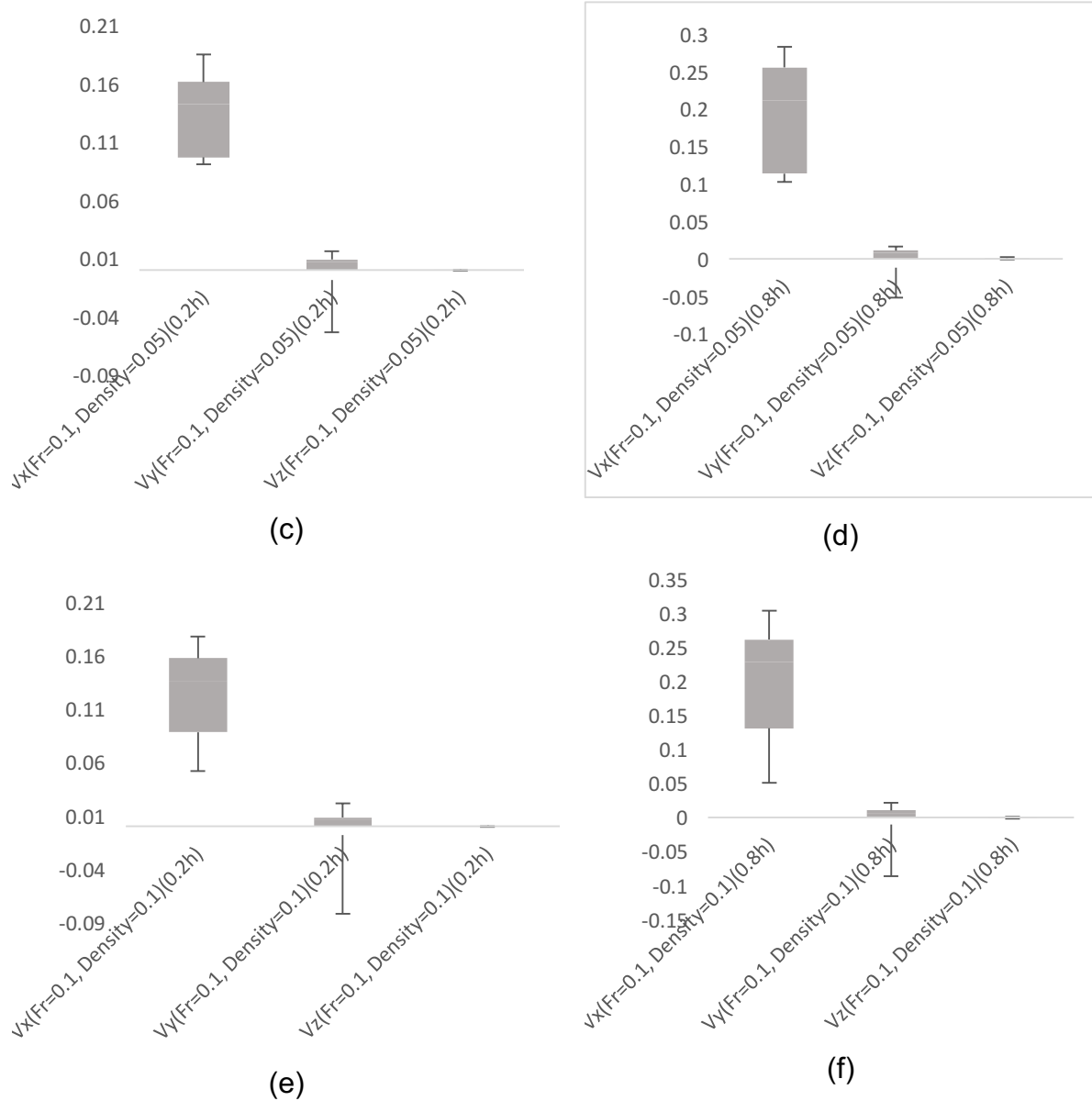


Figure 4.19. Ranges of velocity components. (a): $Fr=0.1$, $\Omega_v=0.025$, at 0.2h; (b): $Fr=0.1$, $\Omega_v=0.025$, at 0.8h; (c): $Fr=0.1$, $\Omega_v=0.05$, at 0.2h; (d): $Fr=0.1$, $\Omega_v=0.05$, at 0.8h; (e): $Fr=0.1$, $\Omega_v=0.1$, at 0.2h; f: $Fr=0.1$, $\Omega_v=0.1$, at 0.8h

In figure 4.19, it is obvious that for the flow with Fr number of 0.1 the range of streamwise velocity is much higher than the transverse and vertical velocity, but on the other hand, by increasing of the stem density the ranges of velocity components promote and the differences between the ranges of components of the velocity, particularly streamwise and transverse velocity decreases. These differences between the ranges of components of the velocity is more obvious near the bed, because as it was shown in this section and section (4.1.2), the transverse and vertical velocity are mostly accelerated by the stems and their values increased almost with the same range simultaneously near the bed and near the

surface. But in terms of the streamwise velocity, the bed roughness has an important role in controlling the velocity and imposes the logarithmic profile along the depth of the flow on this component and because of that the accelerated velocities near the bed and near the surface have different values. Due to the profile of the vertical component of the velocity and as the compared values, it can be concluded that except inside the vegetated region and the area close to it, the patch of vegetation has not significant effects on vertical component of the velocity in a partly vegetated channel.

4.2 Conclusion

In this chapter we discussed about the velocity results of laboratory experiments. Analyses are made on all three different components of the velocity around the patch both close to the bed ($0.2h$) and to the surface ($0.8h$).

The streamwise velocity shows spatial variation by two different behaviors:

1. Deceleration of it from the upstream edges into the patch and remaining almost constant for a distance at the wake of the patch (steady region),
2. Acceleration of flow across the channel and beside the patches of vegetation.

Due to the density of the patch the deceleration and acceleration rates are different and the process of velocity changes near the bed and near the surface are almost the same. Deceleration of streamwise velocity starts approximately $1D$ from upstream side of the patch. Diversion of the flow by the patch of stems is not a function of flow Fr number, but it is a function of vegetation density. Denser patches divert more flow to the opposite side and increase the streamwise velocity to a higher amount.

For lower vegetation densities the effected flow at the wake of the patch requires longer length for development. By connection of these lengths to the morphology results, these lengths can help to specify suitable positions for planting the other patches of vegetation to achieve the certain bed condition.

As the vegetation density increases, the steady area with constant decelerated flow becomes smaller. The velocity increases just behind this region. The reason of creation of this region is relied on the growth of a shear layer at the wake of the patch and separation of the flow at the downstream side of the patch. Eddies with different magnitudes appear along the edges of the shear layer, which can have some impacts on bed profile around the vegetation region.

The transverse velocity in an unvegetated straight channel with steady and fully developed clear water is almost negligible, but Introduction of an isolated patch of stems changes the transverse velocity near the interface between the flow and stems. As flow approaches to the vegetated zone, the transverse velocity follows a special variation. The distribution follows approximately the same pattern near the bed and near the surface, but in contrast with streamwise velocity the magnitude of transverse velocity in depth of the flow does not necessarily have a logarithmic distribution in areas close to the patch.

Changes of transverse velocity also start around $1D$ upstream side of the patch and intensify almost around the first half patch, and finish by the end of it. Extension of the affected region depends on the density of the vegetation, because increasing of the stem density intensifies the flow diversion and enhances the transverse velocity and more part of the channel is then influenced across the channel. The accelerated area is independent from the vegetation density but the decelerated region is a function of vegetation density. It is also clear that like the streamwise velocity, distribution of the transverse velocity is not a function of flow Fr number.

In contrast with other two components of the velocity, the changes of vertical velocity initiate just at the upstream edge of a patch. When flow reaches to a stem, the strong pressure gradient at the upstream side of the stem causes both upward (just near the surface of the flow), and downward (most part of the water column) deflection. The changes of the vertical velocity also directly depend to the density of stems. After primary analysis of velocity components, it is found that except upstream side of the vegetation area, the vertical component of velocity is negligible and can be neglected. According to this fact and due to the time consuming process of 3D simulation, the 2D simulation is chosen for numerical part, which is discussed in chapter 6 and 7. By clarification of the effects of a finite patch of vegetation on flow velocity and turbulent intensities both near bed and near surface, the effects of vegetation areas on each other were started to investigate.

5 Chapter 5: Morphodynamic result of finite patches of stems

In this chapter result of bed profile measurements around a finite patch of vegetation is explained in details. At first, the scouring process around the vegetation area is described and then the bed profiles are separated into erosion and deposition zones and characteristics of each zone is defined to investigate the effective parameters on them in details.

5.1 Scouring and deposition process

Under the control conditions with no patches of vegetation, the flow was uniformly distributed and provided ripples and dunes in the stream-wise direction. However, the presence of the vegetated areas causes a local erosion and deposition around the patches. This process is characterized by two main stages. Initially, scouring results from deflected flow at the upstream edge of the patch, which would create a scour hole around the upstream edge of the patch. Meanwhile, the sediments, located near the wall of the channel, starts to move toward the downstream half of the vegetation zone in the straight path. This trend follows with the movement of sediment into the central part of the channel for the areas closer to the center causes the extension of scouring into both the central part of the channel and the opposite un-vegetated side. As the scouring extends across the width of the channel, the second stage starts. At this stage, sediment moves along a sinuous pattern, starting from the upstream edge of the patch and extend to the opposite un-vegetated side of the channel. The schematic diagram of the development of the bed profile around the patch is shown in Figure 5.1. It should be mentioned that, at the beginning of the experiments in the clear water tests, no sediment movements in the main channel are observed. However, as the scouring extends from the patch to the central part of channel, the erosion pattern becomes obvious around the vegetation zone. For the tests above the threshold of sediment, the mass transportation rate increased locally around the erosion zone and a deeper scour hole creates along the erosion zone. After development of the equilibrium condition no substantial changes in the depth and slope of the scour hole are observed. Figure 5.2 shows the equilibrium condition, inside the patch and the

developed bed profile around the patch for tests with different vegetation density and different flow condition.

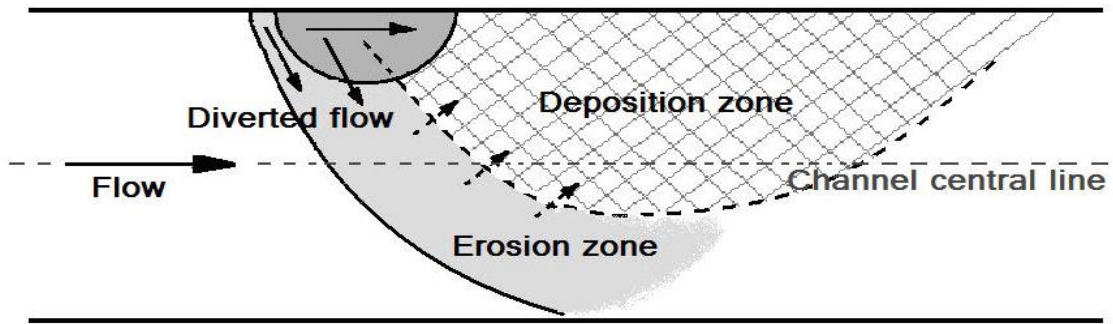
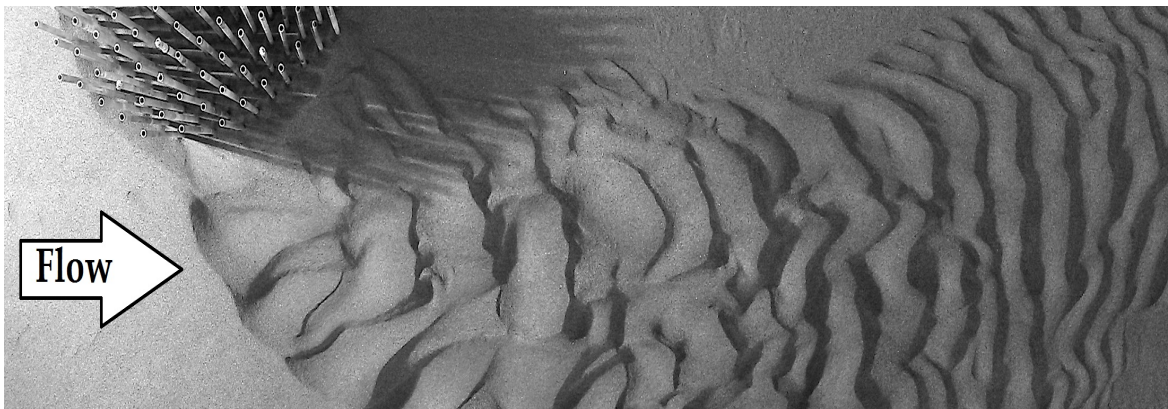


Figure 5.1. Schematic view of scouring and deposition around the vegetation zone (not to scale)



(a)



(b)

Figure 5.2. (a): extension of scouring across the width and development of

erosion and deposition ($\Omega_v = 0.025, Fr = 0.1$) (b): scouring within and around the patch ($\Omega_v = 0.1, Fr = 0.4$)

Interaction of bed morphology and rigid emergent vegetation depends upon the size and density of the vegetation area besides flow characteristics. In order to investigate the local effects of vegetation zone on bed topography with more details, erosion and deposition zones around the patch of vegetation are separated for all cases. These zones are characterized by their location, depth of scouring and height of dunes. Then these features are investigated in terms of flow Fr number and vegetation density and transverse velocity.

5.2 Characteristics of scouring zone

Location of scouring areas are specified by tracing the paths of the minimum elevation at different cross sections along the channel from the upstream side of the patch to the downstream direction and then fitting a second order of polynomial regression through the extracted data, the pattern of thalweg meandering is found.

5.2.1 Location of scour holes

In terms of flow characteristics, the location of the maximum scouring is not influenced by the Froude numbers and it remains approximately constant (Figure 5.4). Figure 5.3 depicts erosion areas around a patch with density of 0.05 in 3 different flow conditions. In figure 5.4, by increasing the Froude number from 0.1 to 0.4 for a certain patch density ($\Omega_v = 0.05$), the location of maximum scouring from the upstream edge of the patch remains constant.

As the vegetation become denser, the scouring migrated slightly upstream and extends more across the channel to the opposite non-vegetated bank. This is likely due to the fact that with increasing of the vegetation density, the flow that is able to penetrate through the vegetation decreases and therefore the lateral component of the velocity upstream of the patches increases. Figure 5.5 illustrates the migration of scouring due to the vegetation density.

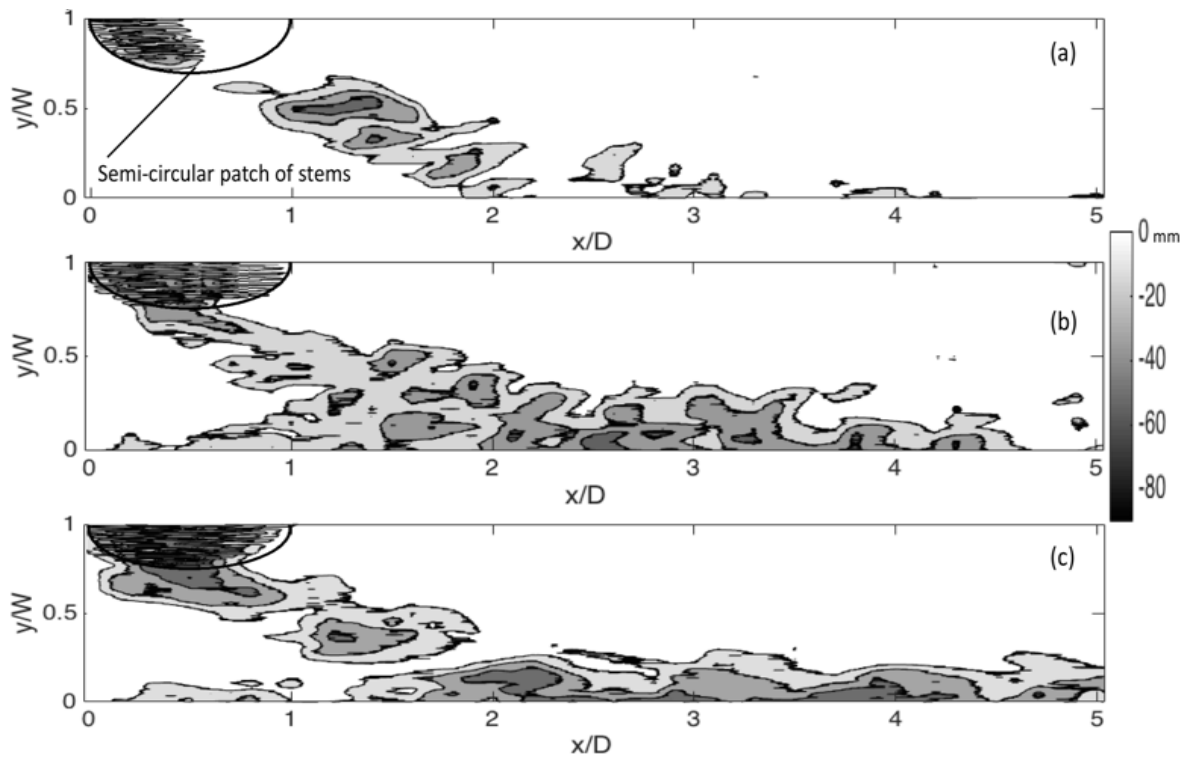


Figure 5.3. Contour lines of the scouring downstream the vegetation patches (a) $\Omega_v = 0.05$, $Fr = 0.1$, $D = 50\text{cm}$; (b) $\Omega_v = 0.05$, $Fr = 0.3$, $D = 50\text{cm}$; (c) $\Omega_v = 0.05$, $Fr = 0.4$, $D = 50\text{cm}$

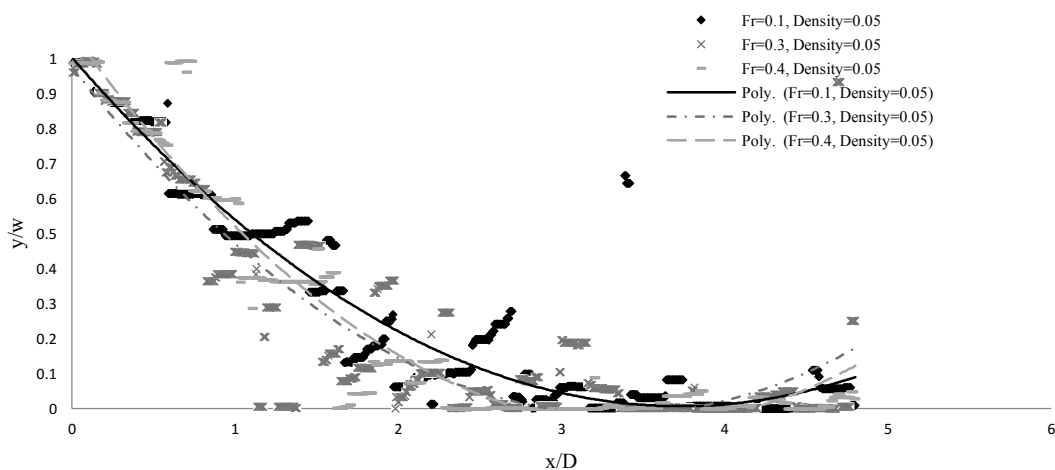


Figure 5.4. Fitted curves and extracted data with minimum bed elevations in all cross sections from the upstream edge of the patch for different Froude numbers and constant vegetation density

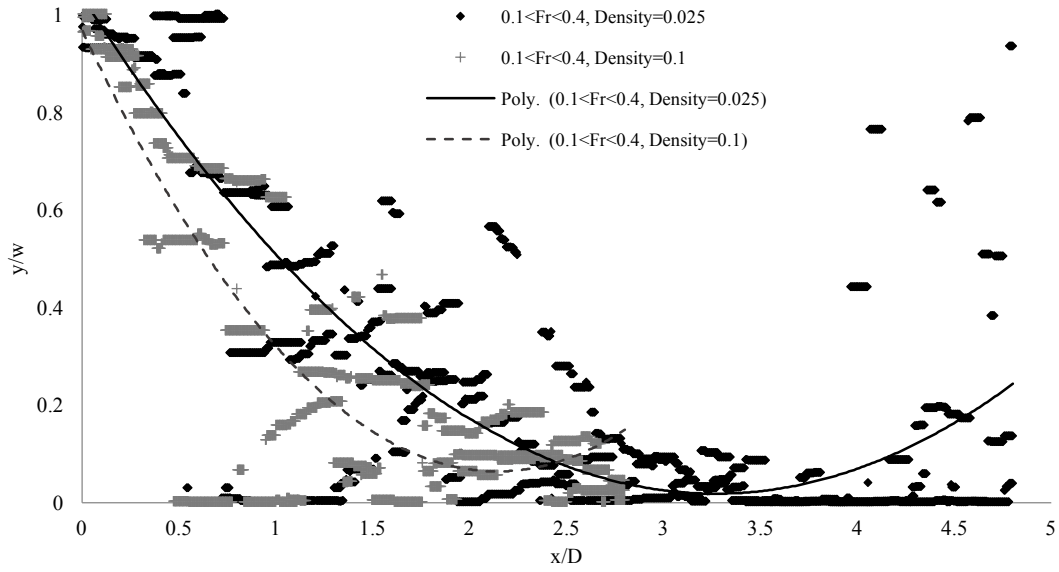


Figure 5.5. Fitted curve and extracted data with the minimum elevations along the channel for two different patch densities and same flow Froude number

Bennett (2004), investigated the vegetation-related turbulent flows and defined a zone for surface waves along side each semicircular patches of stems. The creation of this zone was also connected with the wakes and stacked wakes caused by stems. The angles of propagation of these waves were investigated by observing them in channels with different vegetation densities. Higher densities of their experiments ($\Omega_v > 0.025$) followed by higher propagation angles (angle between waves and x direction) than lower densities ($\Omega_v < 0.006$). The observed propagation angles are also validated by means of the proportion of the velocity of progressive waves over a frictionless bed and highest flow velocity near the upstream edge of the patch through following equation:

$$\theta = \tan^{-1} \left(\frac{\sqrt{gh}}{U_{max}} \right) \quad (5-1)$$

Where \sqrt{gh} is the propagation velocity of infinitesimal gravity perturbations and U_{max} represents the velocity of the flow when approaches to the patch. In addition, at higher vegetation density, the location of surface waves was reported around the upstream half of the patch, while they can be found all along the patches with lower densities. Connecting the results of surface waves with bed morphology, it can be concluded that the angle of propagation of scouring around the investigated patch follows the same principal. At higher vegetation density ($\Omega_v > 0.1$), the propagation of scouring path has angle of about 50 degrees with positive x direction, while the same angle for lower densities ($\Omega_v < 0.025$) is around 40 degrees. Furthermore, as it

is shown in figure 5.16, for lower densities the scouring can happen along the vegetation zone but with increases of the density it would be restricted in space to the upstream half of the patch.

A second parameter, indicative of the effect of the vegetation density on the hydrodynamic field, is given by the ratio between the velocity downstream and upstream of the patches. For this purpose, we have adopted the depth integrated velocity U_0 in a point localized in the cross section immediately upstream of the patches, at a distance $y = 15$ cm from the wall (points I and II in figure 2.4) and the depth integrated velocity U_1 in a point localized in the cross section immediately downstream of the patches, at the same distance from the wall. Figure 5.6 shows how the ratio of U_1/U_0 changes with changing Froude number and vegetation density.

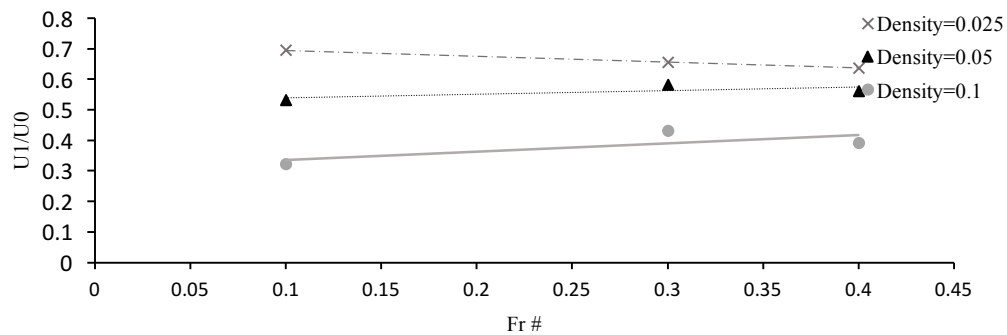


Figure 5.6. Variation of U_1/U_0 with Fr number for different values of the vegetation densities of the patches

In figure 5.6, as expected, by increasing the vegetation density, the diverted flow rate from the vegetated bank towards the non-vegetated bank increases. The ratio enhancement could subsequently pro-mote the bed degradation in the non-vegetated area and increases the meandering feature of the thalweg. However, the ratio weakly depends on the Froude number, while it depends mostly on the vegetation density. Furthermore, the ratio increases with decreasing of the vegetation density.

As it was explained in chapter 4, diversion of the flow is significantly related to the transverse component of the velocity. On the other hand, it is known that regions with higher transverse velocity are more suitable for destabilization of bed sediment. In figure 5.7 a to c, morphological data of tests with different densities of the patch and similar flow condition are connected to distribution of the transverse

velocities by fitting the traced scouring path on the depth average transverse velocity profile.

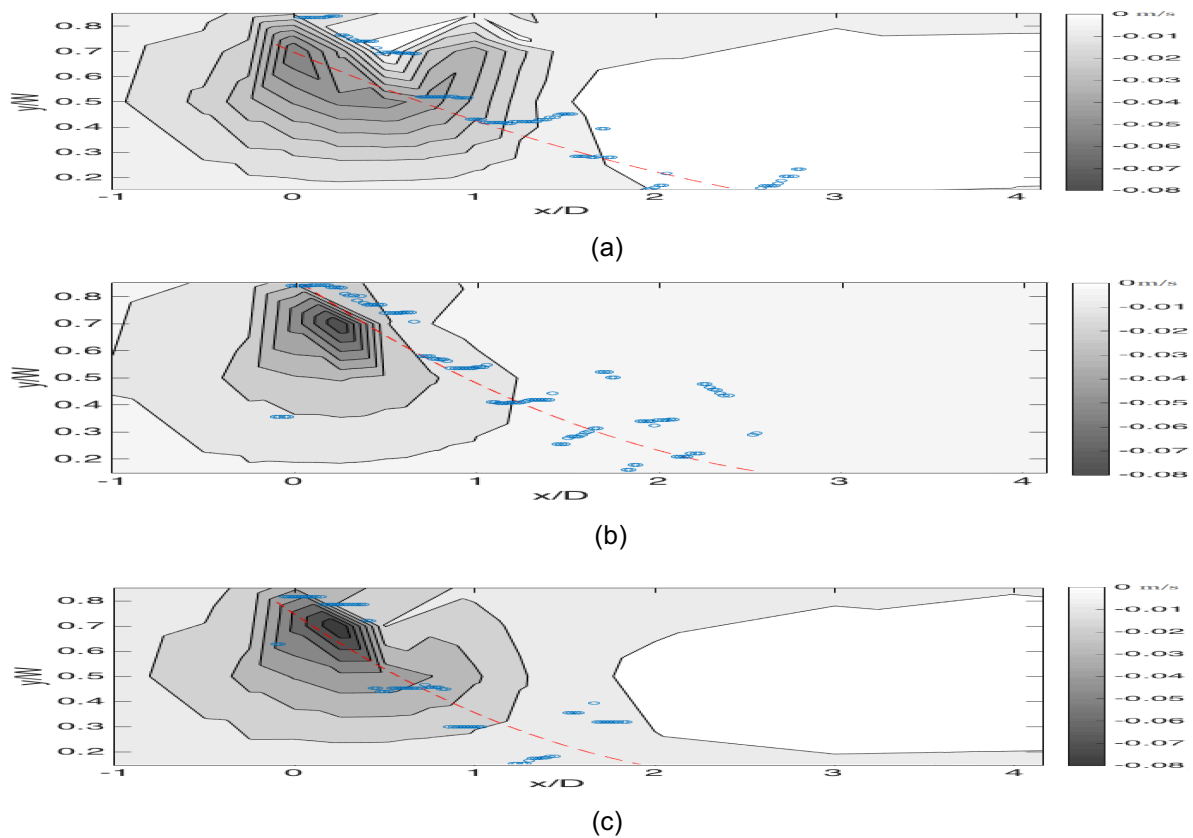


Figure 5.7. Location of extracted data with minimum elevation in all cross sections around the patch over depth-average transverse velocity profile for experiments with $Fr=0.2$; a. $\Omega v=0.025$; b. $\Omega v=0.05$; c. $\Omega v=0.1$

The initial flow condition of the presented tests in figure 5.7 has been chosen to have less bed shear stress than the critical bed shear stress in the absence of the permeable patch of stems. But introducing of the patches with densities from 0.025 to 0.1 causes the increase of the bed shear stress at the patch scale and for all these three cases leads to sediment movement around the patch. The bed shear stress profile and morphological condition of these tests are also shown in figure 5.10 and 5.11 respectively. Comparison of location of scour holes and pattern of v_y around the permeable patch clarify the correlation between transverse velocity and scouring. From distribution of the transverse velocity around each stem, the highest values of the transverse velocity are at upstream side of each stem (Dargahi, 1990), and from connection of the distribution of the transverse velocity with location of scour holes at the patch scale, it is found that the highest values of transverse velocity around the patch responds to the location of associated scouring. The higher the density of the patch is, the stronger the transverse velocity component over the bed is. Furthermore, stronger transverse velocity

destabilizes more bed materials, causes further scour holes across the channel. Considering the flow velocity and bed material and according to the distribution of transverse velocity, scouring can be initiated from 1D at upstream side of the patch and extends to the opposite side of the channel. Correlation between the width of scouring region and density of the patch is discussed in section 5.4.

To summarize the last result, the highest scouring happens near spots with the highest transverse velocity. In the other words, location of scouring within and around the patch is controlled by distribution of the transverse velocity, which is a function of density of vegetation and size of the patch in a channel.

5.2.2 Depth of scour holes

Both of Froude number and vegetation density influence the depth of the scouring hole around the patch of stems. The longitudinal profile of the fitted curve (Figure 5.8) shows that, as the Froude number increases from 0.1 to 0.4, the average depth of the scour holes increases. The reason is relied on the increasing of the bed shear stresses around the patches.

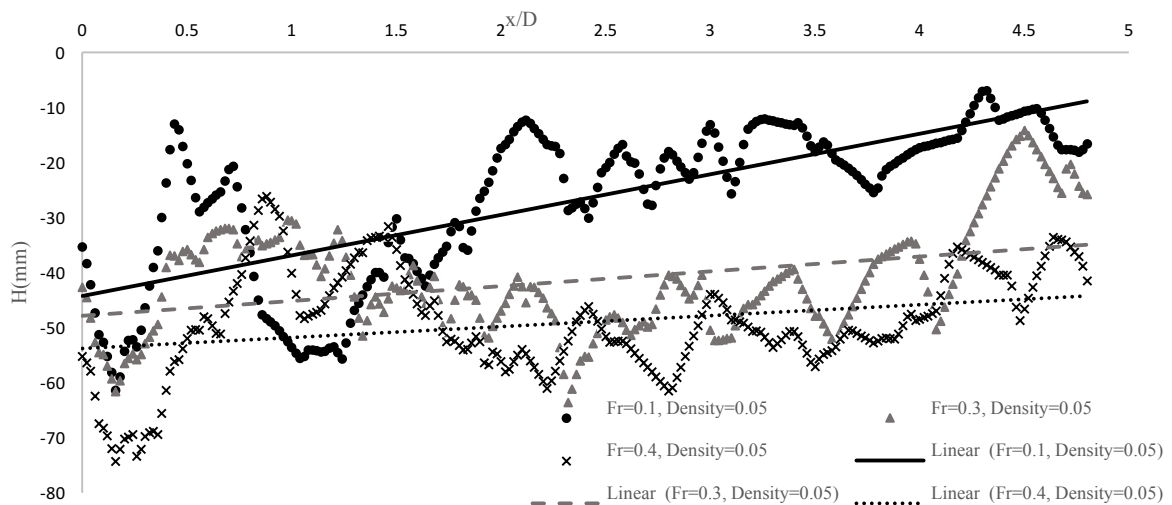


Figure 5.8. Longitudinal profile of fitted curves on extracted data with minimum bed elevations

Furthermore, high vegetation density deflects more portion of the flow and provides stronger lateral and vertical components of the velocity around the vegetation

zone, which cause a deeper scour hole. Figure 5.9 shows the longitudinal profile of the extracted curve for three different experiments with various densities and the same flow condition.

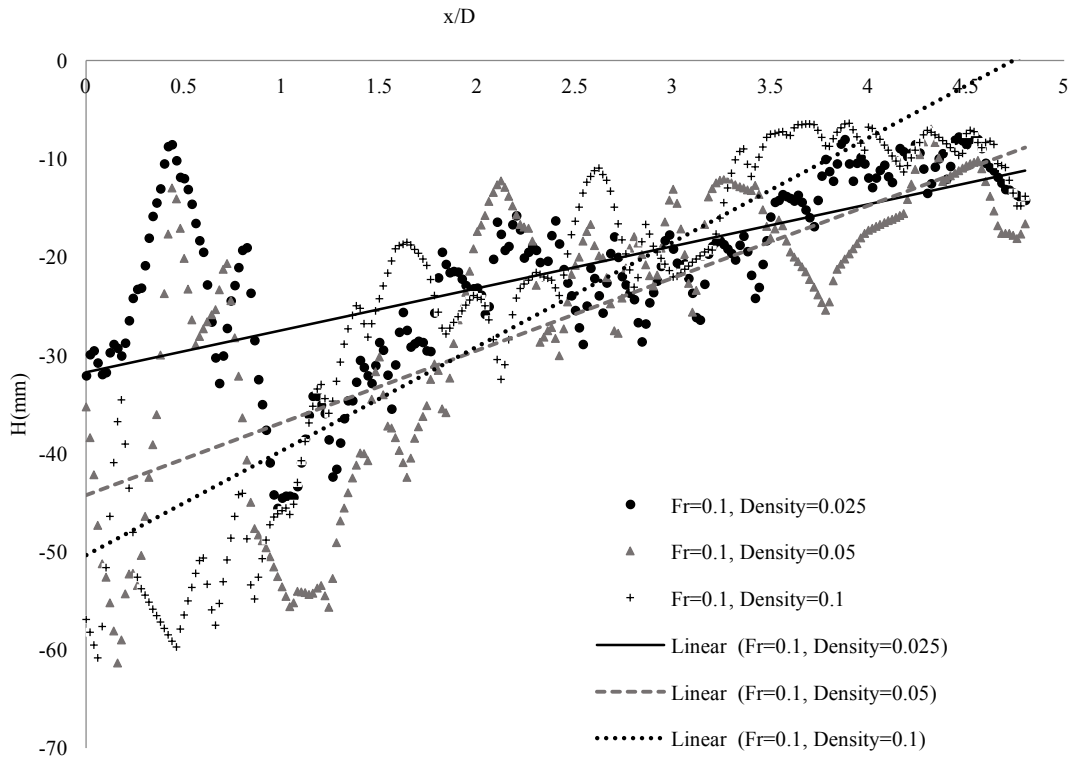
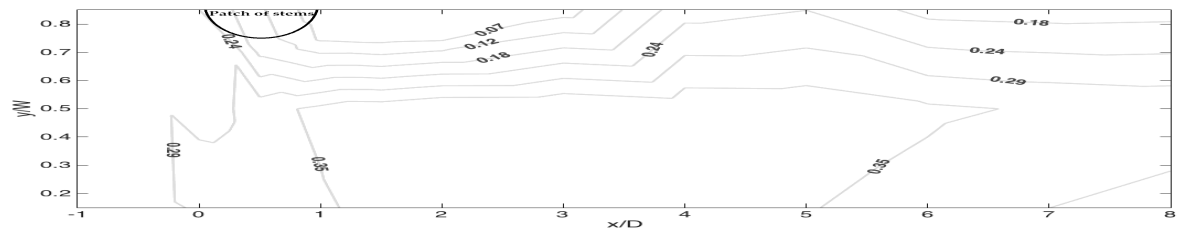
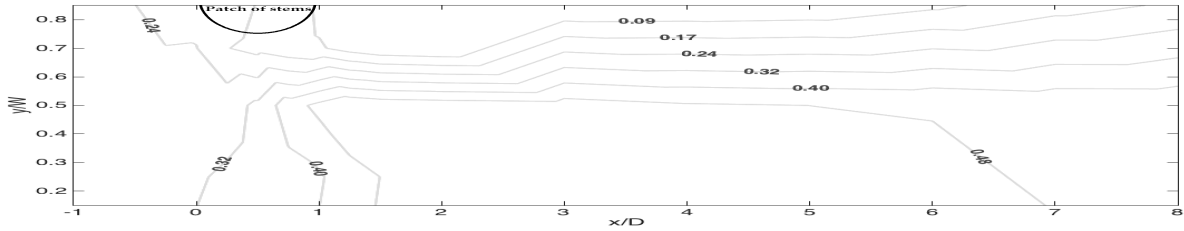


Figure 5.9. Longitudinal profile of fitted curves on extracted data with minimum bed elevations

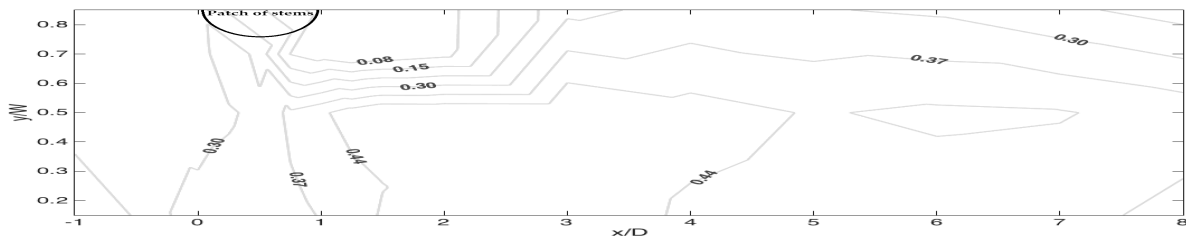
In experiments with clear water ($U_0=18.5$ cm/s, $h=17.7$ cm), dimension of scour holes are measured after drying, and different features of scour holes including the non-dimensional highest and average depth ($h'_{Max}=h_{Max_scour}/h$, $h'=h_{ave_scour}/h$), non-dimensional highest and average length of scour holes ($L'_{Max}=L_{Max_scour}/D$, $L'=L_{ave_scour}/D$), and non-dimensional average area ($A'=A_{ave_scour}/A_{patch}$) is investigated and compared in terms of the transverse velocity. Figure 5.10 and 5.11 illustrate the bed shear stress, bed configuration and scan of scouring regions of the tests with clear water and 3 different densities of the patch. The features of scour holes are also presented in table 5.1 with other information such as the amount of flow deflection.



(a)

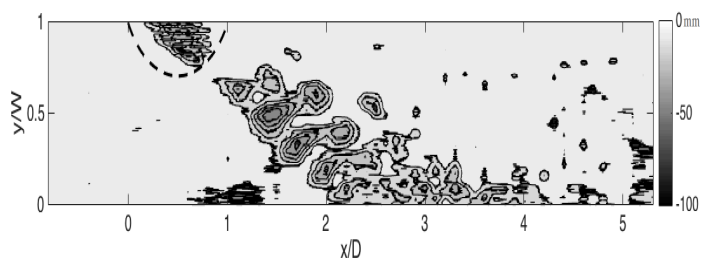


(b)



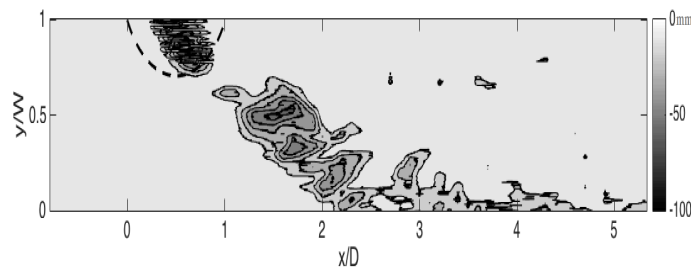
(c)

Figure 5.10. Shear stress distribution for experiments with $Fr=0.1$, $D=50$ cm, (a): $\Omega v=0.025$; (b): $\Omega v=0.05$; (c): $\Omega v=0.1$

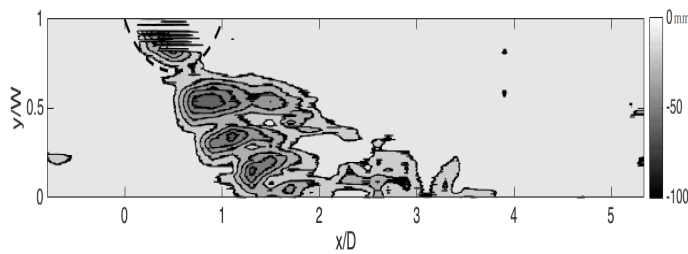


(a)





(b)



(c)

Figure 5.11. Bed patterns and Contour lines of the scouring downstream of patches ($Fr=0.1$, $D=50\text{cm}$); (a) $\Omega\nu=0.025$; (b) $\Omega\nu=0.05$; (c) $\Omega\nu=0.1$

Table 5.1. Features of scour holes and correspondent transverse velocity

Test	Ω	Highest Non dim. length (L'_{max})	Average Non dim. length (L')	Highest Non dim. Depth (H'_{max})	Average Non dim. Depth (H')	Average non dim. Area (A')	Highest non dim. V_y (V_y/U_0)	Average flow deflection
1	0.025	0.56	0.4	0.27	0.13	1.47	0.28	0.66
2	0.05	0.72	0.58	0.36	0.15	2.25	0.37	0.53
3	0.1	0.8	0.72	0.36	0.16	2.85	0.44	0.38

The observation of the tests in figure 5.11 shows the average of normalized scour holes depth (H') in the channel with a patch of density of 0.025 is about 0.27. Increasing of the vegetation density to 0.05 promotes the highest H' to almost 25% more than the lowest density, but it remains almost constant for higher densities. On the other hand, increasing of the vegetation density enhance all of the non-dimensional highest and average scouring lengths and non-dimensional average scouring area. This fact proves the creation of stronger vortices by denser patches. Higher transverse velocity destabilizes more bed material and causes deeper and larger scour holes within and around the patch. By increasing of vegetation density,

vectors of transverse velocity increases and the effects of these changes can be seen in scour holes dimensions (figure 5.11). For tests with lower flow deflection, the transverse velocity is smaller. Hence, local vortices along the shear layer become smaller and in terms of scouring, smaller and shallower holes are created rather than the tests with higher flow deflection.

Immediate oscillation of flow behind each stem produces vortices, which can affect the flow structure at the wake of the stem. However, vortex shedding at the patch scale can be investigated by means of bed profiles. The average dimension of scour holes can be used to depict the vortex length. Bennett (2004) has used the vortex length to estimate the frequency of vortex shedding by using:

$$f_v = \frac{|U|}{L} \quad (5-2)$$

Where U is the flow velocity and L is the vortex length scale. Due to data in table 5.1 and the velocity distribution around patches with different densities, the frequency of large-scale vortices varies from 0.5 to 1.4 (1/s). Higher ranges of these frequencies happen around the vegetation zones with higher densities, while lower densities provide lower frequencies. For example, decreasing of density of a patch with certain diameter from 0.1 to 0.025 causes significant decrease of vortex shedding frequencies. Comparing these results with calculated results of Strouhal equation (chapter 4), it can be concluded that the large-scale vortices occur more frequent and stronger than small-scale vortices at the wake of the patch. Also according to bed profiles, only large-scale vortices are strong enough to cause scour holes around the patch. Kiya et al. (1980), investigated vortex shedding around cylindrical stems by means of two different parameters which are dependent to both flow structure and stem properties:

$$Re_c = \frac{u_v \cdot d}{\nu} \quad (5-3)$$

$$K = \frac{u_* \cdot d}{u_v} \quad (5-4)$$

Where u_v is the approaching velocity to the cylinder and $u_* = (\tau/\rho)^{0.5}$ and d is stem diameters. Vortex shedding can be observed from $50 < Re < 300$ and $0 < K < 0.25$ and increase horizontal diffusivity and small-scale turbulences (Kiya, 1980, Nepf 1997, Cheng et al. 2007). Unfortunately, in this study velocity through rigid emergent patches of stems have not been measured, but according to data of previous similar studies (e.g. Kiya 1980; Bennett, 2002, Nepf, 1997), it can be expected vortex shedding from cylindrical stems is placed in the flow.

5.3 Characteristics of deposition zone

As the flow approaches the vegetation zone, the depth average velocity (U_0) starts to decrease. Within the vegetation zone, although the velocity is reduced, but the turbulence is increased and causes scouring. On the other hand, from the region that no more flow is deflected till the region of recirculation of the flow at the wake of the patch, deposition occurs. The location of the deposition zone and height of dunes investigated in terms of flow characteristics and vegetation density

5.3.1 Location of deposits

Morphological processes usually occur on different time scales (Kirkby, 1990). Installation of a patch has an immediate impact on flow structure at a local scale and consequently the sediment transport regime changes. As a response of changes of sediment transport, channel morphology and finally the channel slope evolve gradually. Furthermore, due to the physical condition, development of the channel with the new morphological system can be accompanied by vegetation growth and extension of the patch in different directions (Watson et al. 1997). In this respect, for restoration or other river management programs, it is vital to figure out the probable location of the deposits to track the extension of the planted islands.

Planting of patches of live cuttings in reality has been proven that patches can extend both longitudinally and laterally inside channels. For example, planting of American water willow along the left portion of bankfull channel of Hurricane Creek, was extended almost over the entire width and more than three times of the channel widths downstream, and resulting in a homogeneous vegetation zone (Neary, 2009). To be able to predict the location of deposits, the extension zones can be predicted.

In contrast with scouring location, sediment deposition depends both on the flow characteristics and on vegetation density. For the cases with $Fr < 0.2$, deposition occurs immediately downstream of the erosion area, while flows with higher Fr number ($0.2 < Fr < 0.4$) transport the eroded sediment further downstream and toward the wake of the patch. Figure 5.12 depicts deposition zones of the patches in 3 different flow conditions and certain patch density.

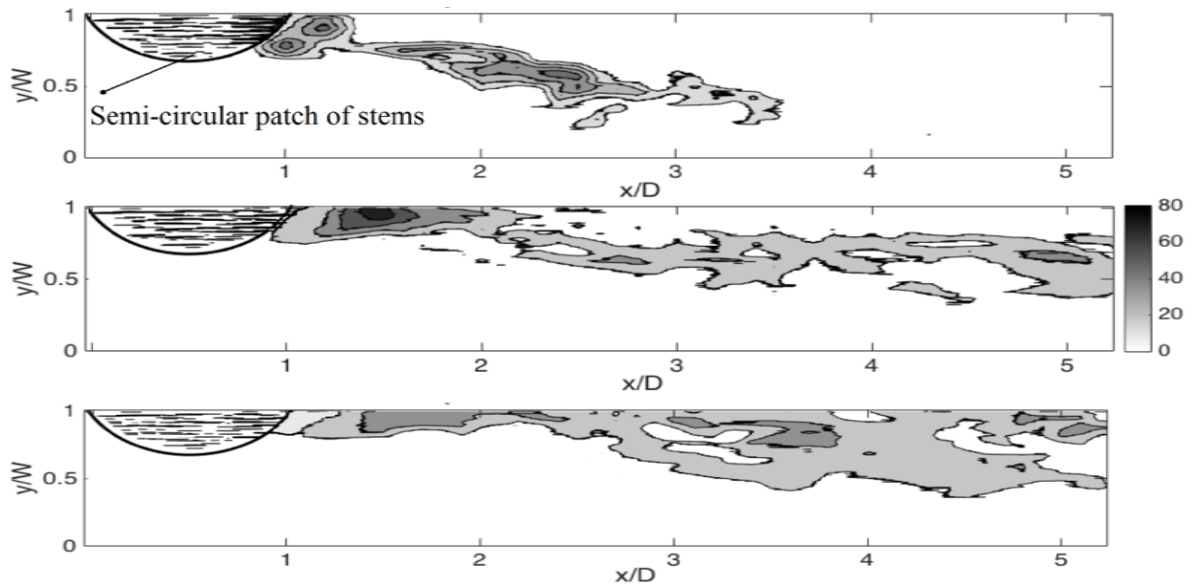


Figure 5.12. Contour lines of the deposits downstream the vegetation patches (a) $\Omega_v=0.05$, $Fr=0.1$, $D=50\text{cm}$; (b) $\Omega_v =0.05$, $Fr =0.3$, $D=50\text{cm}$; (c) $\Omega_v =0.05$, $Fr =0.4$, $D=50\text{cm}$

In order to compare the location of the deposition zones, we plotted the maxima of the deposits in all the cross sections, thus improving the reliability of our findings. The experimental points have then been fit-tered by a linear regression. Figure 5.13 illustrates the location of points with high elevation. It shows 3 different experiments with different vegetation densities and Froude numbers. The linear regression of each series of data shows that with increasing the Froude number, the deposition area tends to move towards the wake of the patch.

To investigate of the interaction between the vegetation density and the location of the deposits, we should consider the characteristics of the flow. In clear water conditions, the tests prove that sediments were deposited immediately after the excavation area.

In section 5.2, it is mentioned that increasing of the vegetation density, change the location of scouring zone to upstream. In clear water, deposition occurs immediately behind the scouring zone hence migration of scouring zone follows by migration of deposition zone. On the other hand, in live-bed conditions, it is found that the deposition mostly occurs inside the wake of the patches. In these cases, by increasing the vegetation density, the deposition area starts to shrink and the deposition crests moves toward the downstream edge of the patch (Figure 5.14).

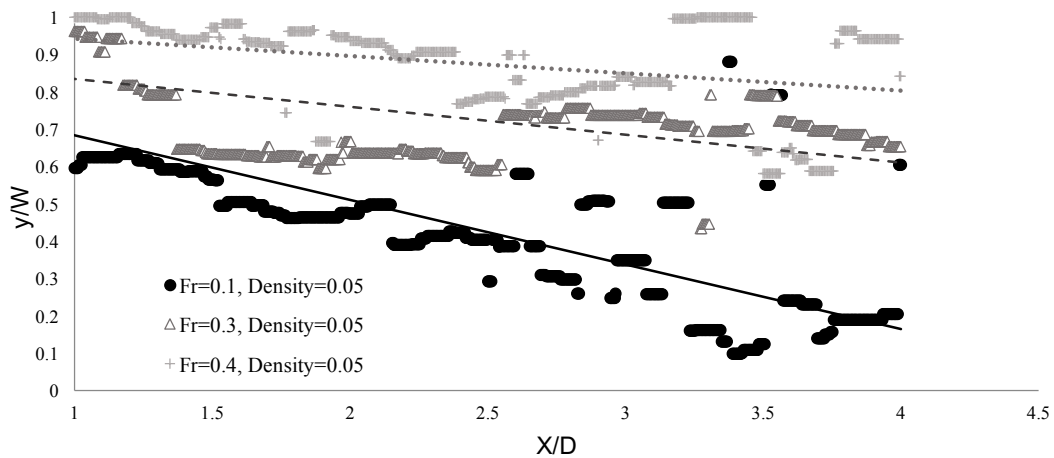


Figure 5.13. The highest elevation of the deposition areas at the wake of the patch of vegetation in all cross sections from the downstream edge of the patch

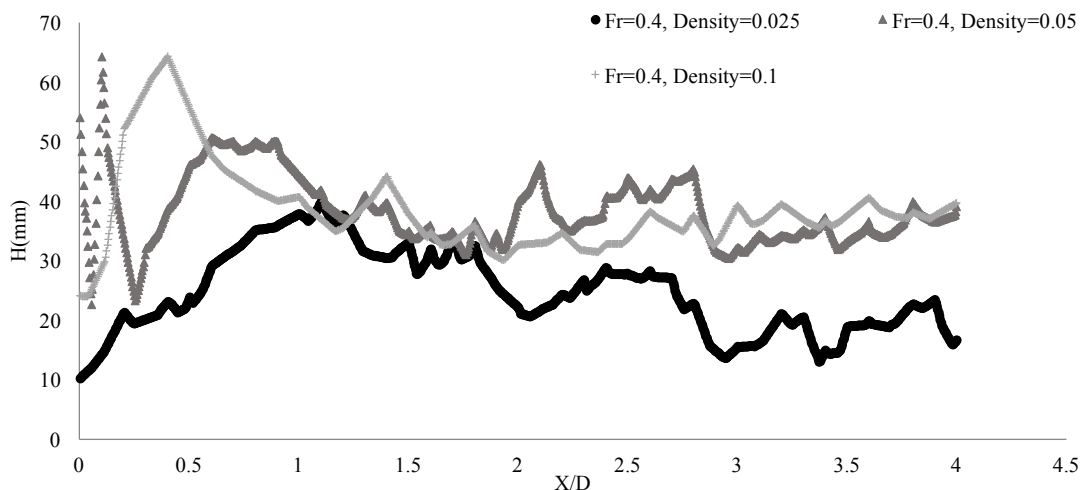


Figure 5.14. Longitudinal profile of the fitted curve on the extracted data with highest bed elevations

In flows with higher Fr number, location of deposits proves that if the other physical conditions are suitable for vegetation growth, the extension of vegetation zone is more probable to occur at the wake of the patch. Also shrinkage of the deposits at the wake of the patch with higher densities shows that the extension of the planted patch is more limited in size for higher densities. Figure 5.14 shows the longitudinal profiles of the deposition crests for different Froude numbers and different vegetation densities. It is obvious that an increase of the vegetation density results in a displacement of the position of the maximum of the deposit toward the downstream edge of the patch. This effect is reasonably corroborated by the vortex

shedding from the vegetation patches (Zong and Nepf, 2010; Follet & Nepf 2012). The shrinkage of the deposition region shows that an increase of the vegetation density moves the recirculation of the separated flow closer to the patches.

As it was explained in chapter 4, the creation of shear layer at the wake of vegetation zone influences the flow and provide a wake fed from the vegetated patch. The velocity magnitude remains almost constant in this region. For flows with higher Fr number ($0.2 < Fr < 4$), due to the density of the vegetation zone, deposition of the both eroded sediment from the scour region and transported mass through the patch of vegetation can takes place both in the whole steady region or just some part of it and the accumulation of deposits appears in this region just behind the vegetation area (e.g. figure 5.12 & 5.17). The width of this region with steady flow is almost equals to the patch diameter, but the length of it depends to the vegetation density and flow structure (figure 5.15).

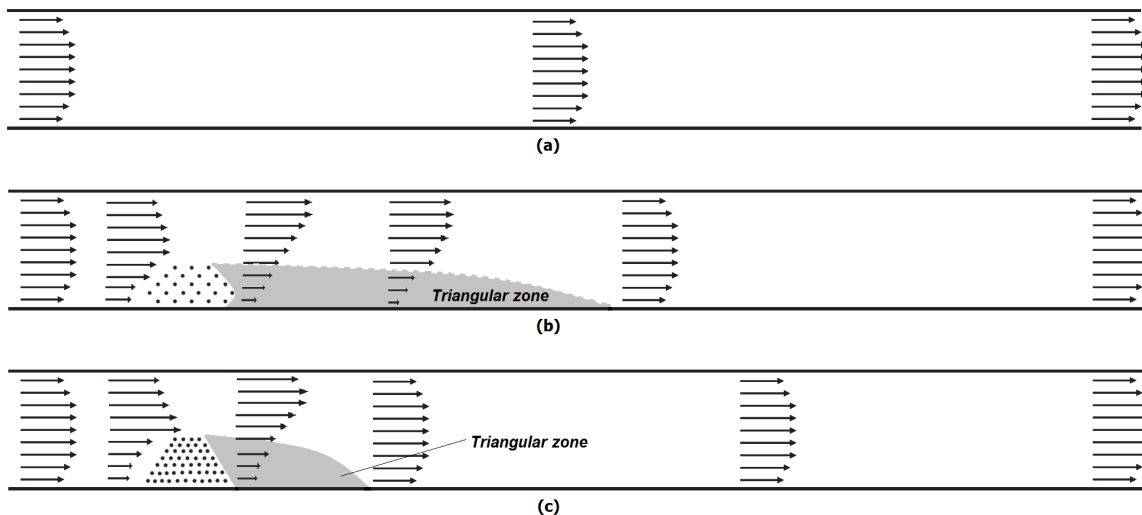


Figure 5.15. Schematic diagrams for velocity vectors and steady zone; (a): before installation of a patch, (b): after installation of a patch with low density, (c): after installation of a patch with high density

Over time, the accumulated deposits in the wake of the patch provide a natural point bar, which can be suitable for growth of vegetation and longitudinal extension of the planted island (Gurnell and Petts, 2006). However, denser vegetation zone causes more perturbation of the flow field than a sparse patch. The induced perturbation determines the size, length and depth of pools and riffles around the patch to attain a dynamic stability of erosion and deposition.

Overall, the length of the induced perturbation is shorter for the dense patch and this fact for the tests with higher Fr number causes shorter deposits at the wake of the dense patch. By considering the velocity and bed profiles for the tests with different Fr number, the steady regions are investigated and their lengths are

measured. Figure 5.16 illustrate the relation between the length of the steady region, Fr number and vegetation density.

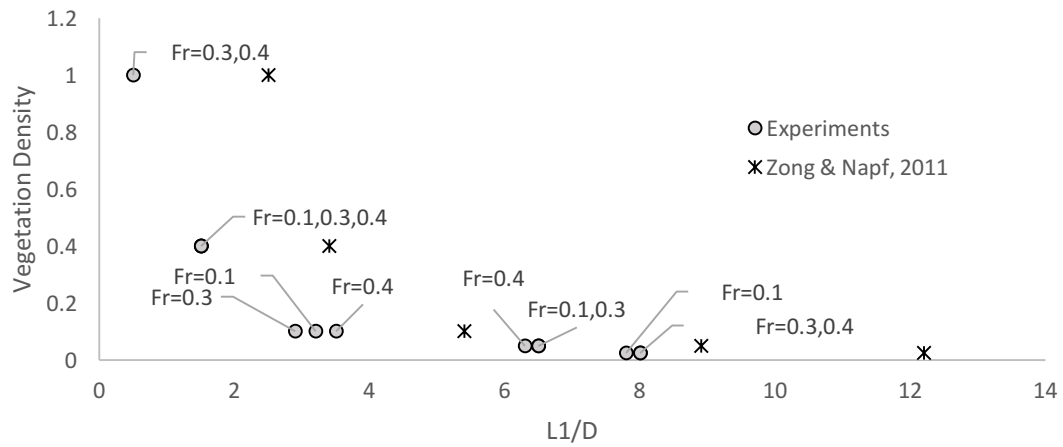


Figure 5.16. Relation between the length of the steady region, vegetation density and flow Fr number

It can be concluded that the length of the steady zone behind the patch is just a function of vegetation density and it is independent from the flow Fr number. As it was explained in chapter 4, by increasing of the vegetation density, more flow diverts to the opposite unvegetated side and due to figure (5-6) the ratio of U_1/U_0 decreases. Zong and Nepf in 2011 used this ratio to estimate the length of the steady region at the wake of the circular patch of cylinders:

$$L_1 \approx 2.5D \frac{(1 + U_1/U_0)}{(1 - U_1/U_0)} \quad (5-5)$$

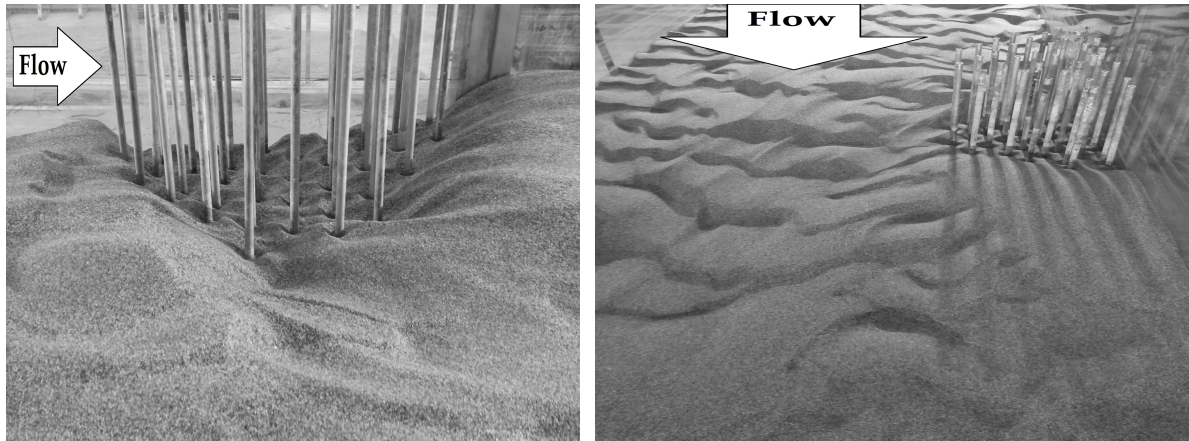
Where L_1 is the length of the steady region.

The results of the calculated length with equation 5.5 are presented in figure 5.16. It is obvious that the increasing of the vegetation density reduces the targeted length but the experimental results are less than the calculated lengths and the reason may rely on the semi-circular shape of the patch.

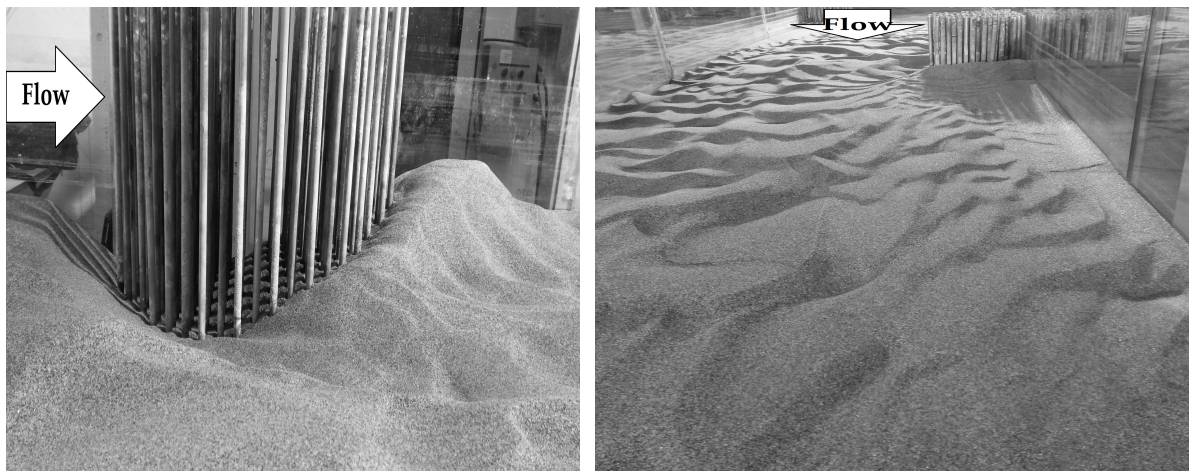
5.3.2 Height of deposits

The deposition height is dominated both by vegetation features, and by the flow characteristics, because the deposition zone at the wake of the patches can be fed both by the sediment transport within the permeable patch and by the eroded sediment from outer edges of the patch and non-vegetated parts. Accordingly, the height of the deposited dunes depends both on to the density of the vegetation zone and on the flow characteristics.

Since an increase in the vegetation density enhances the scouring around the patches, the height of the dune also increases. On the other hand, the sediment transport rate through the sparse patches is higher than through the dense patches, creating higher dunes at the wake of the vegetation (figure 5.17).



(a)



(b)

Figure 5.17. Deposition pattern inside and behind the vegetation zone-(a): $\Omega_v=0.025$, $Fr=0.3$, $D=50$ cm; (b) $\Omega_v=0.1$, $Fr=0.3$, $D=50$ cm

For lower vegetation density, the sediment transport through the patch is the dominant factor. As the vegetation increases, the dominant factor becomes the sediment transport in the main portion of the channel. This process is shown in Figure 5.18.

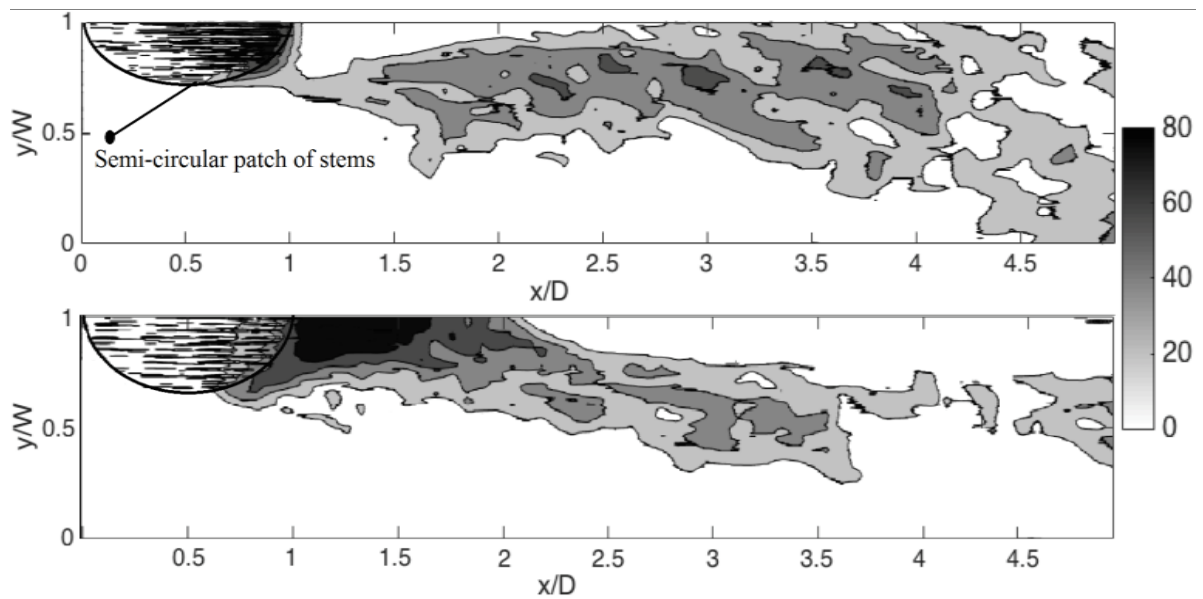


Figure 5.18. Deposition pattern behind the vegetation zone-(a): $\Omega_v = 0.1$, $Fr = 0.3$, $D = 70$ cm; (b) $\Omega_v = 0.05$, $Fr = 0.3$, $D = 70$ cm

In figure 5.18, sediment passes through the vegetation zone and control the dune height at the wake of the patch with lower vegetation density ($\Omega_v = 0.05$), but for the higher density ($\Omega_v = 0.1$) less sediment could move through the vegetation and the deposited sediment is mostly affected by the sediment diffused from the un-vegetated part of the channel to the wake of the patch.

In terms of the flow characteristics, fluctuation of flow velocity follows different scenarios due to the vegetation density. In cases with low vegetation density ($\Omega_v < 0.05$), more than half of the flow, which is approached to the patch, could pass within the vegetation zone and increasing of the flow velocity would cause the decreasing of the dune height. This process is mainly because of the considerable flow velocity at the wake of the patch. On the other hand, in cases with higher vegetation density ($\Omega_v = 0.1$), the velocity of the flow is extremely less than the average velocity in the channel and as it is mentioned, the deposition part is controlled by transported sediment from the main portion of the channel. Considering the promotion of the scouring by increasing the velocity of the flow, dune height increases by enhancement of velocity for cases with the same vegetation density and flow depth (figure 5.19).

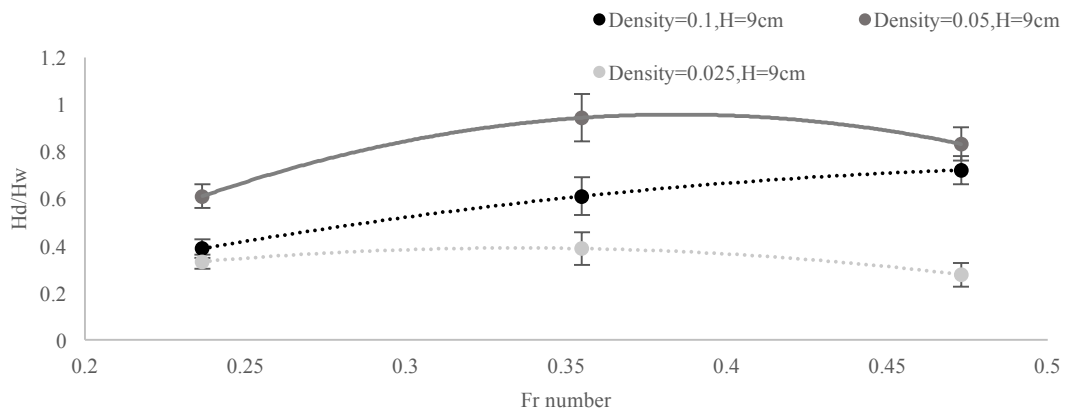


Figure 5.19. Experimental data for the normalized dune height as a function of Fr number

Considering the interaction of the penetrable patch and bed morphology for all cases, erosion and deposition zone was specified by two ellipses (figure 5.20). The bigger ellipse separates the whole affected area from $1D$ upstream of the patch to $7D$ behind the patch. The small ellipse separates the erosion and deposition areas, which starts from the downstream edge of the patch. This classification could help us to diagnose the areas that shear stress is increased and decreased rather than the un-vegetated channel.

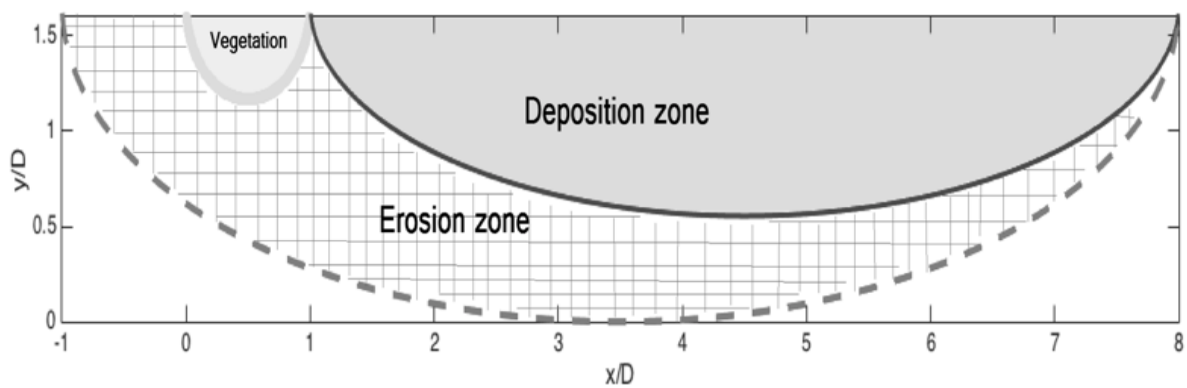


Figure 5.20. Ellipse pattern to identify location of erosion and deposition around the vegetation zone

5.4 Prediction of affected lateral and longitudinal distance

As it was explained, the tests were conducted both in clear water condition (the mobility parameter of the incoming flow under the incipient motion critical value) and in live bed condition (the mobility parameter of the in-coming flow above the incipient motion critical value). In tests with no patches of vegetation in clear water condition, sediment was uniformly distributed and provided a smooth surface. By introducing of cylindrical stems in forms of semi-circle patches, distinct patterns of erosion and deposits are observed. Connecting results of velocity field in chapter 4 with bed profiles two main features have been found for each vegetation regions with various densities. The first one is called the lateral effective length, which is presented by X_w figure 5.21 and shows the maximum scouring length across the channel and the second one is called the longitudinal effective length, which is illustrated by X_L (figure 5.20) and it depicts the maximum scouring length along the channel from upstream edge of the patch. As it was explained in section 5.2, these lengths are a function of vegetation density. Figure 5.22 shows the obtained lateral and longitudinal effective lengths due to different vegetation densities.

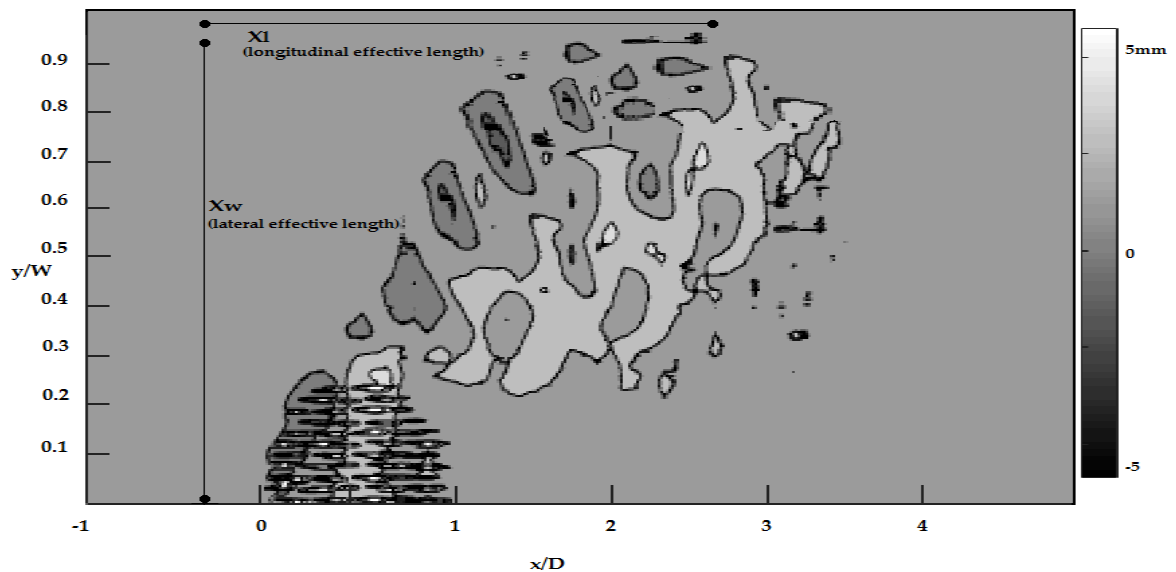


Figure 5.21. Definition of lateral and longitudinal effective lengths

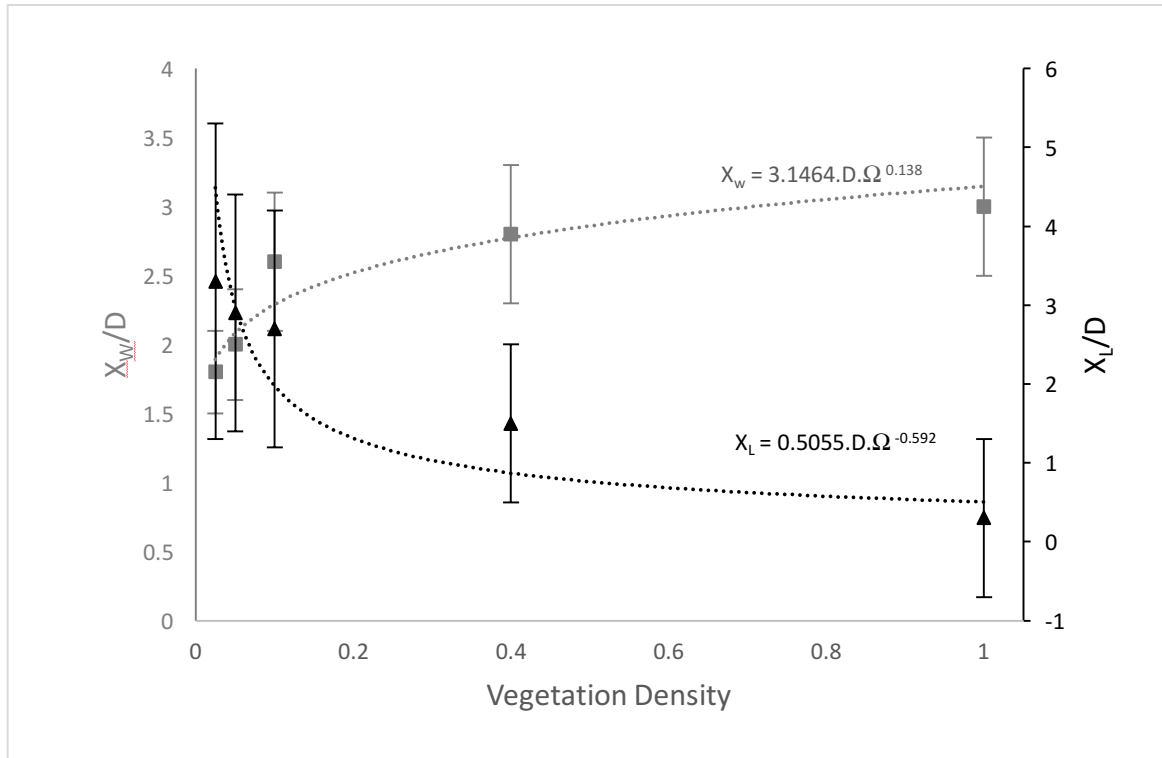


Figure 5.22. relation among vegetation density, lateral, and longitudinal effective lengths

In figure 5.22 the lighter and darker regression lines illustrate the derived power equations fitted the experimental data of effective length across and along the flume respectively from the origin of coordinate. According to this figure, the lateral and longitudinal effective lengths can be estimated using the following equations:

$$X_w = 3.1464D\Omega^{0.138} \quad (5-6)$$

$$X_L = 0.5055D\Omega^{-0.592} \quad (5-7)$$

It is quite obvious to note that the growing of vegetation density follows by upward and downward trend on lateral and longitudinal effective lengths. By increasing the stem density, the lateral effective length X_w starts to increase till it reaches to it's highest amount in case of presence of a block, which is no more permeable. It is also interesting that the enhancement rate of X_w is sharper for lower densities than the higher ones, and it remains almost constant for higher densities ($\Omega_v > 0.4$). On the contrary, as the vegetation become denser, the longitudinal effective length X_L falls gradually and follows a steady decrease. The reason of these trends relies on the amount of the deflected flow from vegetated part to unvegetated regions. As it was explained in chapter 4, enhancement of the vegetation density not only accelerates the transverse component of the velocity around the patch of

vegetation, but also decelerate the stream-wise component of the velocity within the area close to the upstream edge of the vegetation zone, and this would lead to the increasing of the diversion of the flow into the central parts of the channel.

The derived power regressions show reasonable fits on the results. These equations are used to define the position of the other patches of vegetation in the channel to achieve certain goals such as providing a meander bedforms or creating narrower and deeper channels. The results of the implementation of the mutual patches of vegetation on flow field and bed morphology are presented in chapter 7.

5.5 Conclusions

The use of vegetation in river restoration programs enhances the functionality of the projects in different terms, like habitat, aesthetic beauty, etc. Establishment of vegetation influence local channel hydraulic and causes flow deceleration and acceleration, erosion and aggradation of sediment, stabilization of natural colonization of point bars and increasing the biodiversity in various ways over time. In order to utilize vegetation in a practical way to get more efficiency, more details should be known about the interaction between vegetation and bed morphology.

In this study, we investigated the effects of vegetation patches on the bed profiles under various flow condition and vegetation density. According to our results, the vegetation density and the Froude number are important parameters, which influence the processes of erosion and deposition that occur near patches.

At the lowest density ($\Omega_v = 0.025$), nearly 66% of the flow, which faces the vegetation zone, passes through the vegetation, while at the highest density ($\Omega_v = 0.1$), the drag force exerted by the stems increases, and the flow passage percentage reduces to almost 38%.

This severe blockage of the flow causes separation in flow, which induces an acceleration of flow in front of the vegetation patches and a deceleration at the wake of the vegetation zone.

In general, the experiment results indicate that an increase in density of the stems induces a deflected flow and this affects the position of scour hole, location of the dunes, and also the magnitude of the local scour depth and the dune height.

The lowest density of the stems shows the lowest flow deflection. However, the flow intensity has no significant effects on the location of the scour hole, while it changes the location of deposition region and increases the scour depth.

An ellipse pattern is proposed for a range of flows ($Fr < 0.5$) to illustrate the scouring and deposition processes around a patch of vegetation ($\Omega_v < 0.1$). In addition, connecting hydrodynamic and morphodynamic results, two main features have been found for vegetation regions. The first one is called the lateral effective length (X_w) which shows the maximum scouring from the upstream edge of a patch across the channel, and the latter is the longitudinal effective length (X_L) which represents the maximum stream-wise scouring from the upstream edge of the patch. By means of these two features a straight channel can be configured for mutual patches to induce erosion and deposition in desired locations along channels.

6 Chapter 6: Results of calibrated model, validation and sensitivity analysis

To achieve reliable results from the model, precise calibration, validation, and sensitivity analysis is necessary. The explained model set up in chapter (3), gives a 2D model based both on hydrodynamics and morphodynamics, which is accompanied with trachytopes function for considering the effects of the rigid emergent cylindrical stems. In this chapter at first the simulated results of an experiment with the calibrated model will be explained to check if the selected parameter values for sediment transport formula and trachytopes function fit to the experimental results. Then validation of the model will be investigated by applying the calibrated model to another data set. Finally, the assessment of the effects of imprecision or uncertainty in model inputs values on output values will be explained in sensitivity analysis.

6.1 Model calibration

Delft3D is a practical tool to simulate the water and sediment movement in open channels, streams and coastal area. The simplified equations that describe the flow field and morphological changes are getting solved by parameterizations of them. These parameters can be divided into *certain* and *scaling* parameters. The certain parameters represent quantifiable features of the system like the discharge and finally helps to find the hydrodynamics and morphodynamics condition on scales smaller than the spacing of the numerical grid. On the other hand, the simplification of equation introduces scaling parameters, which contain the uncertainty of the system and indicate the relative importance of certain parameters and they have to be calibrated using experimental or field data to fit the model application with reality (figure 6.1). In fact, calibration is an essential part in using a numerical model and according to the number uncertain parameters, it can be a complicated and time consuming process. Objective of this chapter therefore is to calibrate the model to improve performance of application of Delft3D in modeling of the partly vegetated channels.

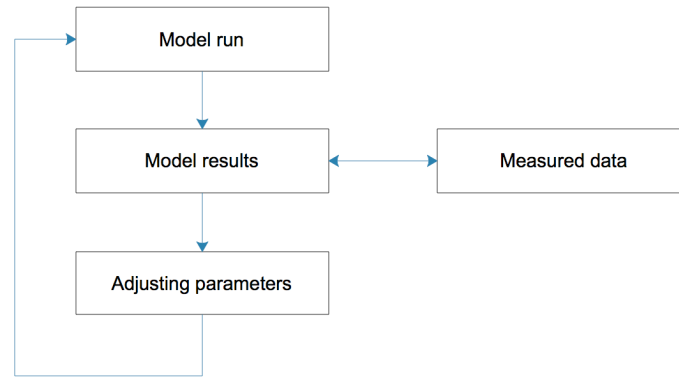


Figure 6.1. Steps in a typical calibration procedure

Ideally, a calibration strategy for modeling a channel with live bed condition consists of calibration of the flow module and calibration of the parameters involved in the sediment transport and morphology module. Each of hydrodynamic and morphodynamics calibration effects the final results. The choice on what data to calibrate is depend to available measured data and different strategies might be applied for calibration. An overview of hydrodynamic, morphological and sediment parameters that have been utilized throughout this study is categorized in Table 6.1.

Table 6.1. Overview of parameters

Module	Parameter	<i>symbol</i>	Description
Flow	Rhow	ρ	Fluid density
	Ag	g	Gravitational acceleration
	Dryflc	-	Threshold depth
	Vicouv	ν_{uv}	Horizontal Eddy viscosity
	Dicouv	D_{uv}	Horizontal Eddy diffusivity
	Ccofu	C_u	Uniform value bottom roughness x-direction
	Ccofv	C_v	Uniform value bottom roughness y-direction
Morphology	Morfac	-	Morphological scale factor
	MorStt	-	Spin-up interval before morphological changes
	SedThr	-	Minimum depth for sediment calculation
Sediment	RhoSol	ρ_s	Specific density
	CDryB	-	Dry density

	SedDia	D_{50}	Median diameter size
	*.tdf	C_d	Drag coefficient
	*.tra	Θ_{cr}	Critical mobility parameter

Numerical results can be also applied to determine the sensitivity of key parameters. Model variables represent the model state, but model parameters are static variables and they must be fixed before initiating the simulation. Model parameters don't change during the solver process. This section investigates the effects of the parameters while the variables are constant. If changes in the value of a parameter would have a significant effect on the final results, the model could be sensitive to the investigated parameter.

Five different parameters are considered for the calibration: the bed roughness, horizontal viscosity and diffusivity, critical mobility parameter, and drag coefficient. The calibration has been done for these parameters by two main changes of the values and comparing the corresponding model results with the measurements. These values are selected to be both higher and lower than the expected values, which are mostly calculated by empirical and theoretical formulas. All final input parameters are given in Appendix A.

As it was explained in chapter 3, the Chézy coefficient represents the roughness in the simulated channel. Changes of this coefficient would cause changes in velocity profiles and consequently the sediment transport and bed slope. Increasing of the Chézy coefficient particularly reduces the velocity near the bed and due to the bed material size and properties it can increase the sediment transport and finally bed slope. So it is critical to find the right Chézy coefficient for the simulation. In order to do this, the experiments with the fixed bed are considered because by introduction of vegetation zone the sediment moves just in the region around the patch, which shows the bed shear stress is just exceeded the critical shear stress in this region (figure 3.2). It must also mention that real patches in natural rivers are usually dense (Watson, 1997; Dawns and Throne, 2000). Hence, the selected densities for the experiments are approximately high. Furthermore, sediment transport rate within most of the tests are negligible. Just in tests with lowest density and high Fr number, the sediment transport rate within the patch is remarkable.

Eddy viscosities and diffusivity are used in the model to simulate the effects of small scale turbulent vortices and mixing of the fluid. The values of horizontal eddy viscosity and diffusivity depend on the flow and grid size. In fact in 2D simulations, forces are distributed in the flow via the horizontal viscosities as a means of mixing

of momentum in the flow. Higher horizontal viscosity provides the larger the area of the flow over which the forces are distributed and it can help the near bed flow to become more developed and this is mainly because of the easier transfer of the momentum of the flow in x and y direction (. Previous literatures suggest the flow development corresponds with the horizontal viscosity rate (Hasselaar, 2006). Due to the grid sizes in the order of centimeter used in simulations, typical values are in range of 10^{-3} - 10^{-2} m²/s recommended by Delft3d user manual.

The chosen sediment transport formula used to calculate morphological developments deals with just the bed load transportation and includes a critical shear stress. Sediment particles motion starts only when the shear stress becomes higher than the critical value. According to the shields diagram, the value of critical mobility factor is estimated to be around 0.047, which is also used in Meyer-Peter-Müller formula.

The presence of stems in bed imposes extra drag on the fluid. The trachytopy functionality has been designed to consider the extra exerted drag in depth averaged model computations. The drag coefficient computed by Armanini et al., 2010:

$$C_{Dp} = \frac{\pi}{2} \frac{1 - \Omega_v}{\Omega_v} \frac{d_p}{h} \left(\frac{gh i_f}{U^2} - \frac{g}{(21.1)^2} \left(\frac{d_{50}}{h} \right)^{1/3} \right) \quad (6-1)$$

Where Ω_v is the density of vegetation, d_p is the diameter of stems, h is the depth of flow, i_f is the slope of flow, $U=Q/W(1-\Omega_v)h$, and d_{50} is the median of the bed material.

6.2 Results of the calibrated model

A reference situation of a channel with a single semi-circular patch of vegetation on the channel bed and at one side of the flume has been set up in chapter (3). For investigation about the results of the numerical model the experiment with the patch of density of 0.05 is chosen to simulate. The certain initial condition of $U_0=28.5$ cm/s, $h_0=10.5$ cm is specified due to the experimental setup. As both components of the velocity are important factors in study of partly vegetated channels, the results of both of the streamwise and transverse components of velocity distribution are presented in figure 6.2. Results of bed profile from the model run corresponding with the experiment are also illustrated in figure 6.3. The numerical results are then compared in the same figures with experimental data to

study whether the imposed parameters indeed can simulate the experimental conditions.

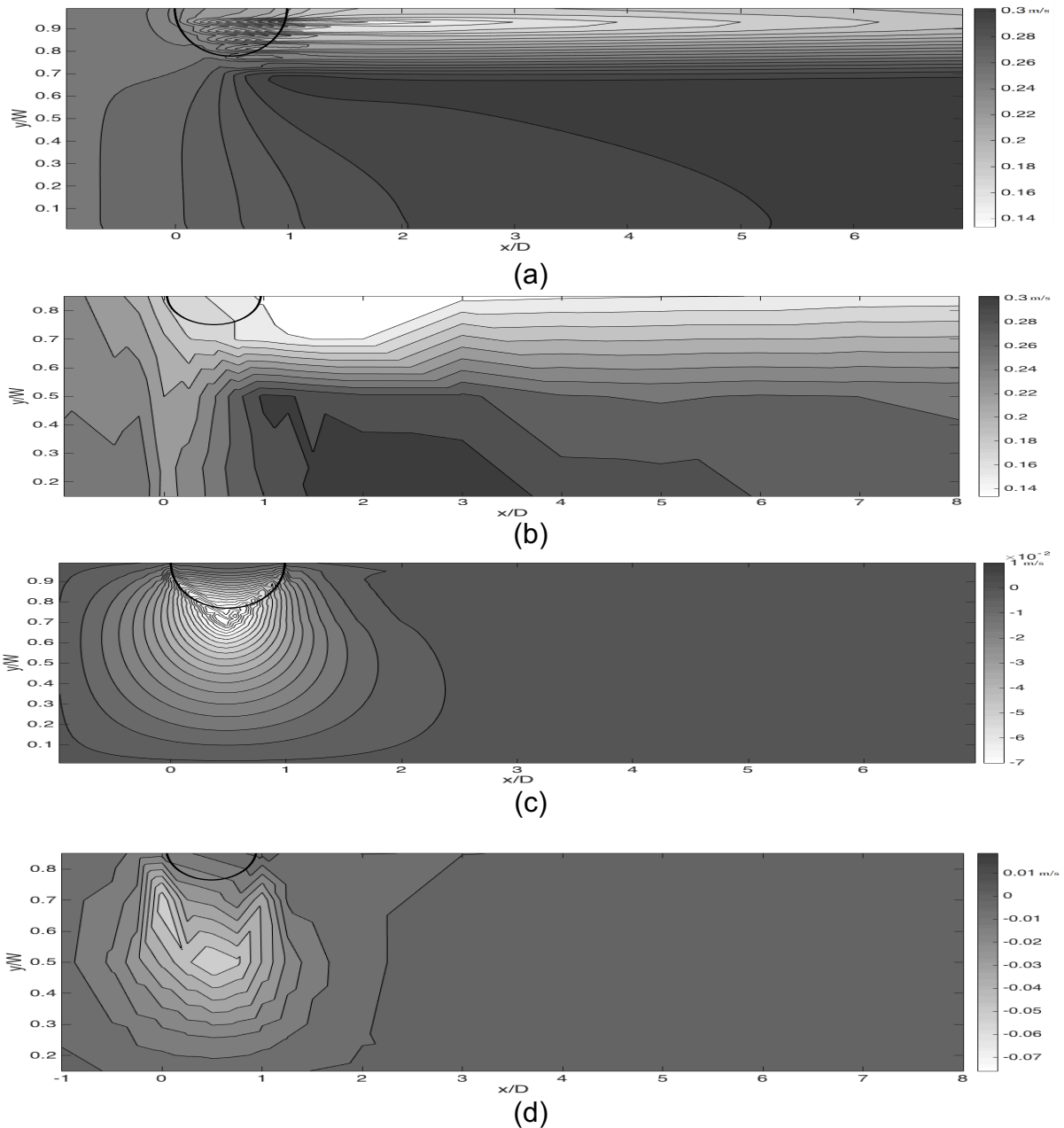


Figure 6.2. Plan of the depth average component of the velocity in a channel with flow from left to right, $\Omega_v=0.05$, $D=50$ cm, $U_0=28.5$ cm/s, $h_0=10.5$ cm, (flow from left to right)- (a): numerical result of streamwise velocity, (b): Experimental result of transverse velocity, (c): Numerical result of streamwise velocity, d: Experimental result of transverse velocity

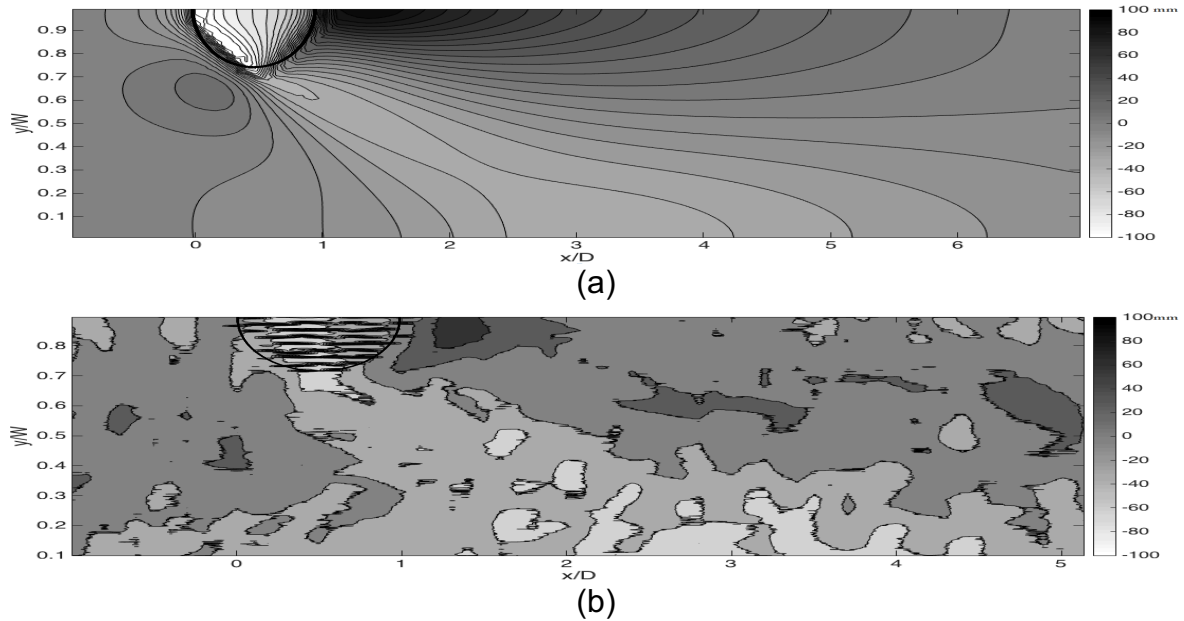


Figure 6.3. bed profile of the experiment with $\Omega_v=0.05$, $D=50$ cm, $U_0=28.5$ cm/s, $h_0=10.5$ cm, (flow from left to right). (a): numerical result, (b): experimental result

The distribution of components of the velocity closely follows the experimental results. Maximum streamwise velocity occurs beside the patch across the flume and the steady region at the wake of the patch extends almost to $7D$ behind patch. Due to the shortage of the experimental data about the flow structure inside the patch, the result of the velocity inside the patch is neglected in this comparison. Furthermore, the transverse velocity starts to increase from around $1D$ upstream edge of the patch and extends to the opposite unvegetated side of the flume. The whole area, which the transverse velocity affected, is almost the same with the experimental results and the values observed in the model comply with experimental data. Also a comparison between the experimental and numerical data on the values of the component of the velocity along different axes of the channel has been done and results presented in (figure 6.4 & 6.5). On the other hand, the harmonic bed profile around the patch of vegetation is also clearly visible and the calculated bathymetry shows relatively good agreement with the measured bed elevation. Scouring starts from upstream side of the patch and it intensifies by approaching to the patch. Just similar to the procedure, that explained in chapter 5, the extension of the scouring to the opposite unvegetated side across the channel is investigated in details by tracing the path of the lowest points at all transects along the channel from $1D$ upstream side of the vegetation zone to $5D$ to the downstream direction figure 6.5. Also more investigation has been done on the longitudinal profile of the bed elevation and the longitudinal transect of the bed elevation is extracted in mid-channel and presented in figure 6.5.

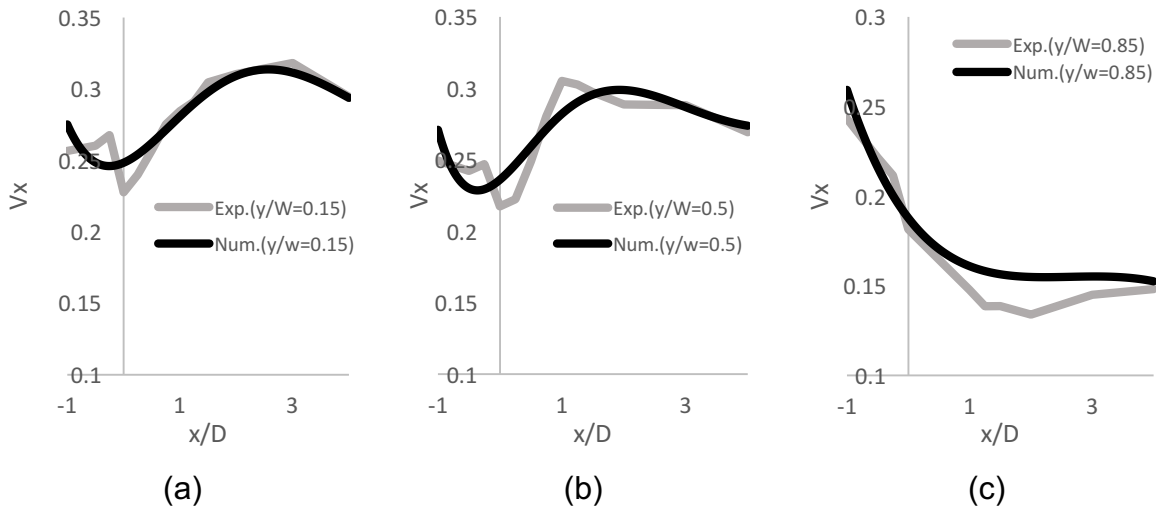


Figure 6.4. Comparison between the experimental and numerical data on the values of the depth average streamwise component of the velocity in a channel with $\Omega_v=0.05$, $D=50$ cm, $U_0=28.5$ cm/s, $h_0=10.5$ cm and along three different axes. a: $y/W=0.15$, b: $y/W=0.5$, $y/W=0.85$.

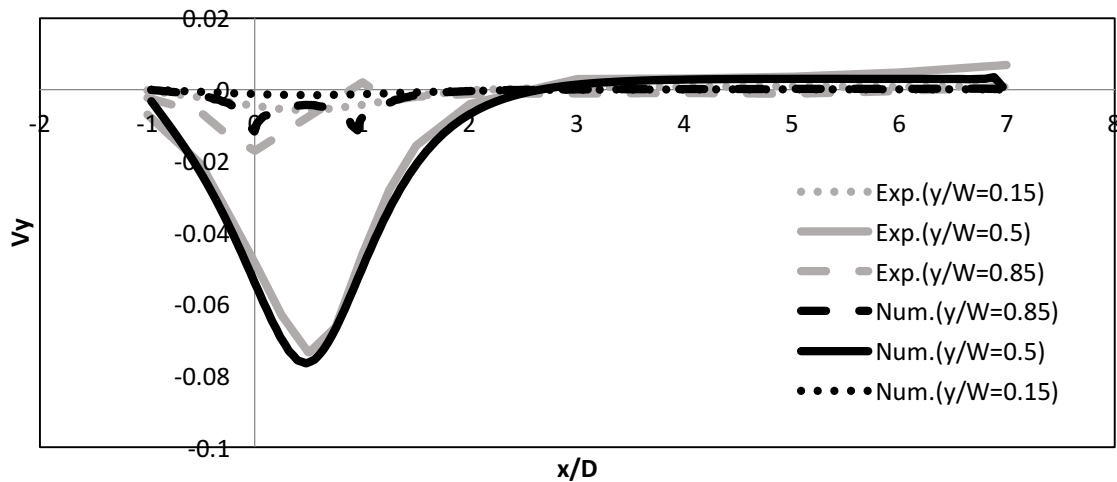
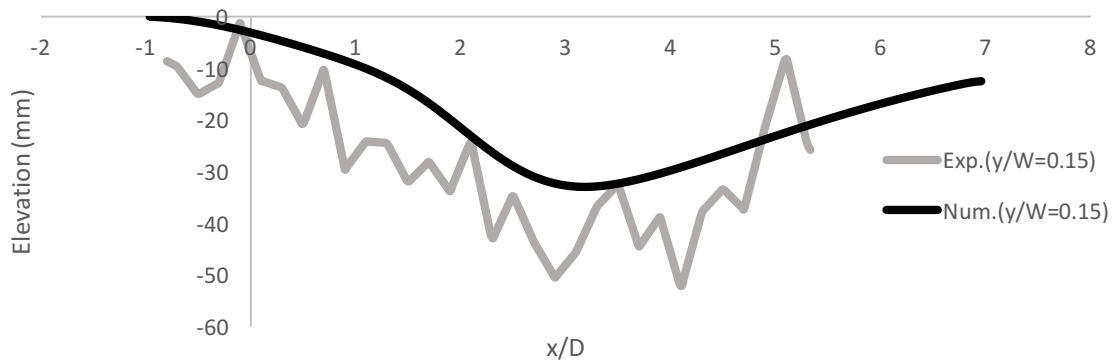


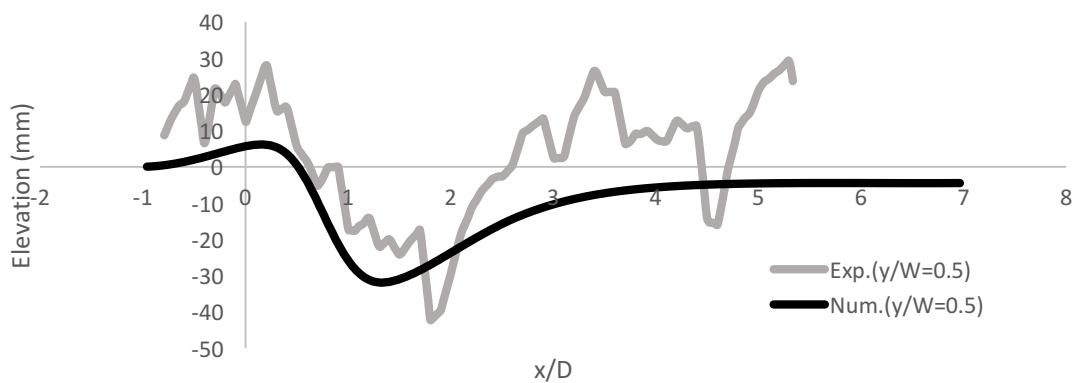
Figure 6.5. Comparison between the experimental and numerical data on the values of the depth average transverse component of the velocity in a channel with $\Omega_v=0.05$, $D=50$ cm, $U_0=28.5$ cm/s, $h_0=10.5$ cm and along three different axes. a: $y/W=0.15$, b: $y/W=0.5$, $y/W=0.85$.

The streamwise component of the velocity is mostly important for controlling the sediment transport rate, while the transverse component of the velocity significantly impacts the location of scouring and sedimentation due to diversion of the flow (see chapter 5). The maximum V_y along unvegetated transects (e.g. $y/W=0.15$ and $y/W=0.5$) depicts the location of the points with high shear stress, and scouring is more probable at these points (figure 5.7). In other words due to experimental

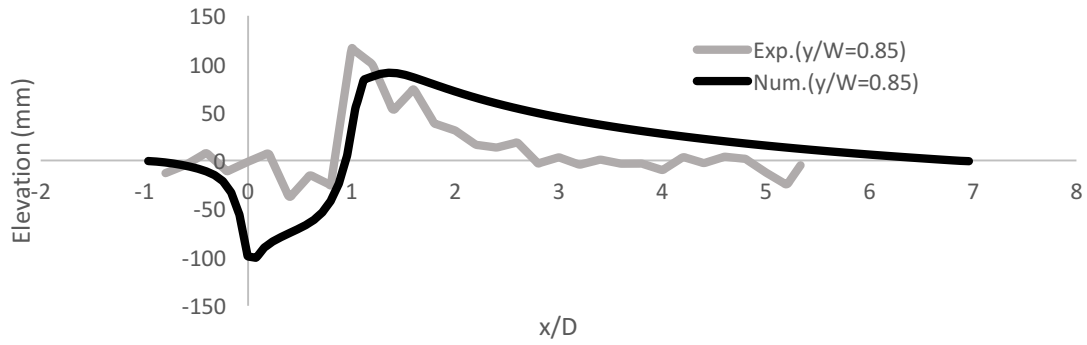
results these areas are the mostly affected regions by the patch and their position is different across the channel. So that, it is critical to catch the right values for each of the components of the velocity. The calculated streamwise and transverse velocity by the model shows correctly the distribution and peaks of components of the velocity along the three different areas of the channel. The patch of stems situated between 0 and 1. The calculated transverse velocity along the transects of $y/W=0.85$, which passes through the patch shows a symmetry behavior near the edges of the patch, which is not true in reality because the measured data shows lower transverse velocity near the downstream edges of the patch (figure 6.2 c & d and figure 6.5). The reason for this relies on sudden changes of the bed roughness (see section 3.1.5). As a direct effect of the symmetry in V_y distribution, flow continues to divert by the downstream edges and more scouring occurs at these regions (figure 6.6 c).



(a)



(b)



(c)

Figure 6.6. comparison between the experimental and numerical data on the values of bed elevation in a channel with $\Omega_v=0.05$, $D=50$ cm, $U_0=28.5$ cm/s, $h_0=10.5$ cm along three different axes. a: $y/W=0.15$, b: $y/W=0.5$, $y/W=0.85$.

The measured and calculated results of different longitudinal transects of the developed bed is presented in figure 6.6 to make further clear the alignment of experimental and numerical result. Peaks in figure 6.4, correspond to peaks in bed elevation in figure 6.6. The higher calculated flow velocity as explained above is carried through the patch of vegetation and caused deeper scour holes inside the patch. On the other hand, slower flow at the wake of the patch allows the sediment to settle on the bed. It is obvious that the model is able to simulate the bed evolution, but the calculated values for bed elevation of the vegetated side is slightly higher than those observed in the channel, while as it gets far to the unvegetated side the calculated bed elevation becomes slightly lower than the measured data. As it will be shown in next sections, if the parameters of morphology would change to fix this problem, the general bed profile result would be also affected. In general, it can be stated in conclusion that the model calculates the bed profile and velocity distribution with relatively acceptable results.

6.3 Validation analysis

Validation of a model refers to the investigation of applying independent data set in the model with calibrated parameters to find the ability of the calibrated model in simulation of the data set. To validate the numerical model, the results of two other experiments with various physical and initial conditions are considered to compare with numerical results. The summary of the condition of selected tests are presented in table 6.2. The reason for selecting these tests relies on the investigated ranges of vegetation density (0.025-0.1) and Fr number (0.1-0.4) to cover the whole ranges.

Table 6.2. Summary of the condition of tests for validation

test N.	h_0 [cm]	U_0 [cm/s]	Fr N.	Ω_v	D [cm]	Sediment transport rate[gr/min]
1	17.7	18.5	0.1	0.1	50	0
2	7.8	38.5	0.4	0.025	50	1220

The numerical results are validated in terms of velocity component and bed morphology. Numerical results of depth average components of the velocity and bed profiles are compared with the measured flume data through figure 6.7 to 6.12 to study whether the model with fixed parameters can simulate the tests with different physical variables.

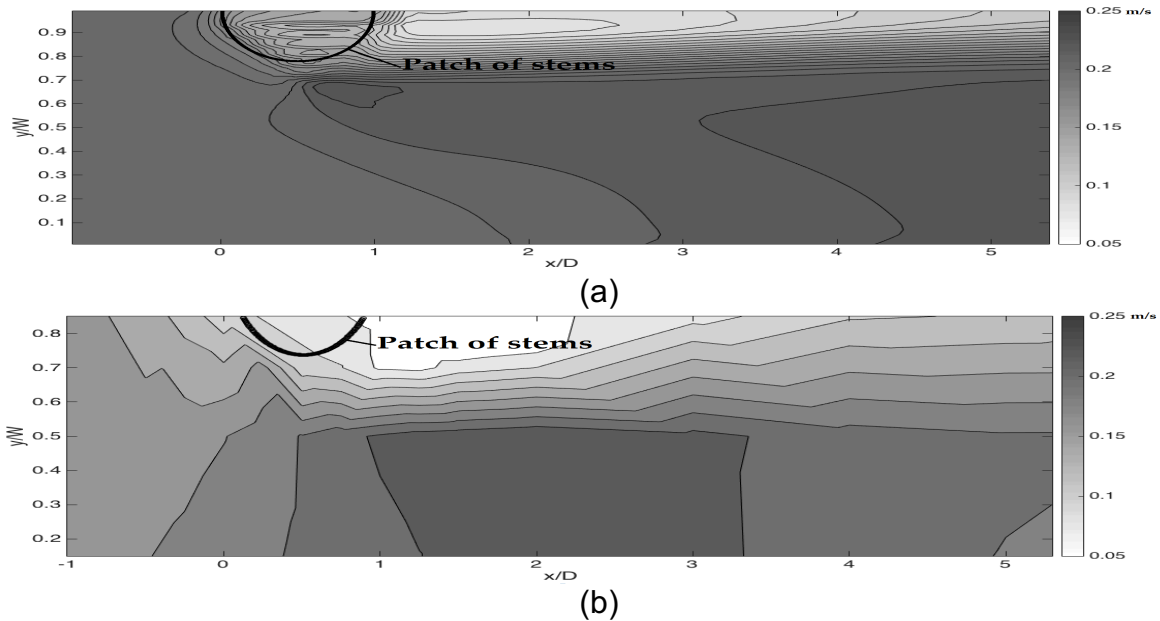
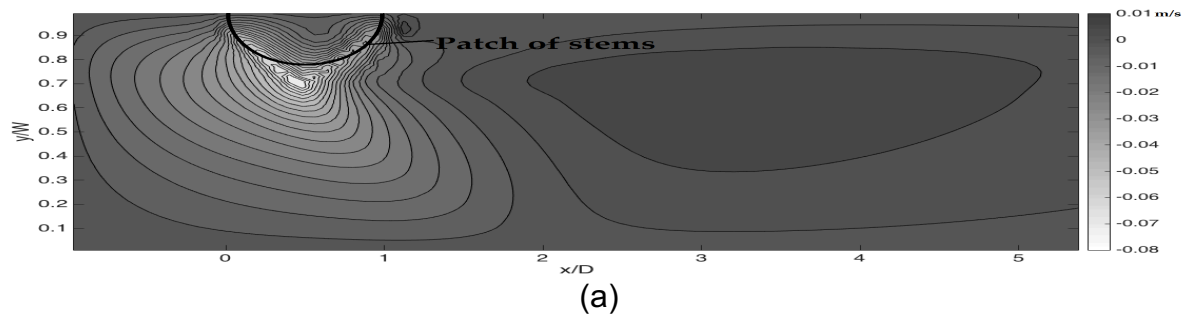


Figure 6.7. Plan of the depth average streamwise component of the velocity in a channel with $\Omega_v=0.1$, $D=50$ cm, $U_0=18.5$ cm/s, $h_0=17.7$ cm, (flow from left to right) – (a): numerical result (b): experimental result



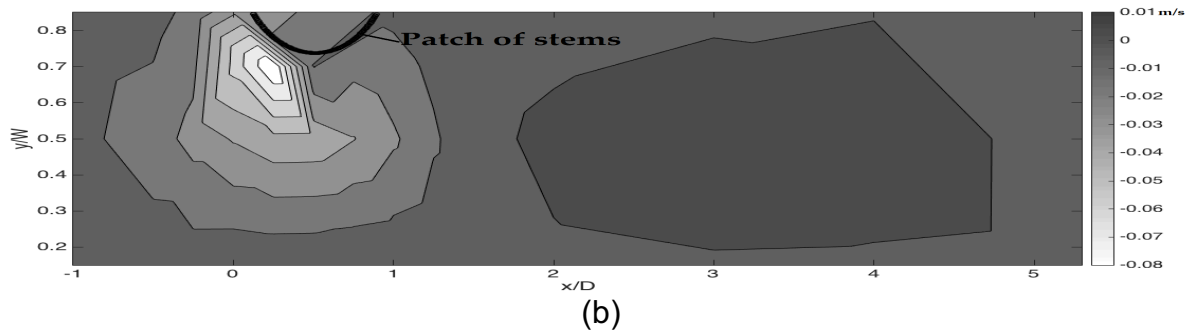


Figure 6.8. Plan of the depth average transverse component of the velocity in a channel with $\Omega_v=0.1$, $D=50$ cm, $U_0=18.5$ cm/s, $h_0=17.7$ cm, (flow from left to right) – (a): numerical result (b): experimental result

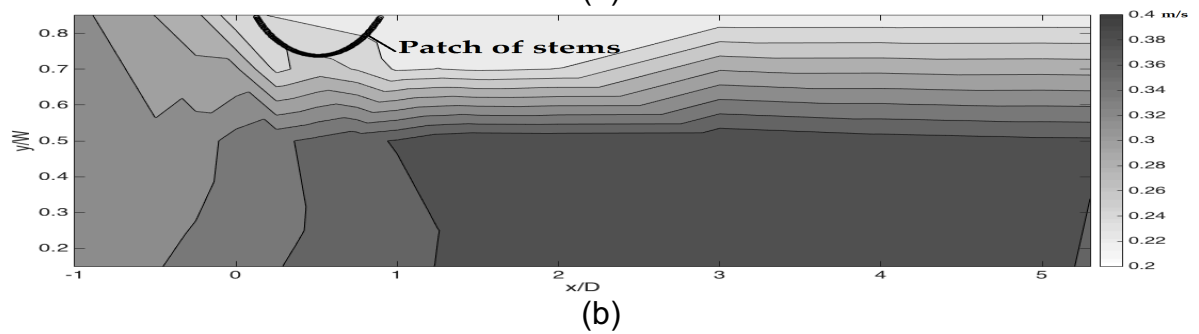
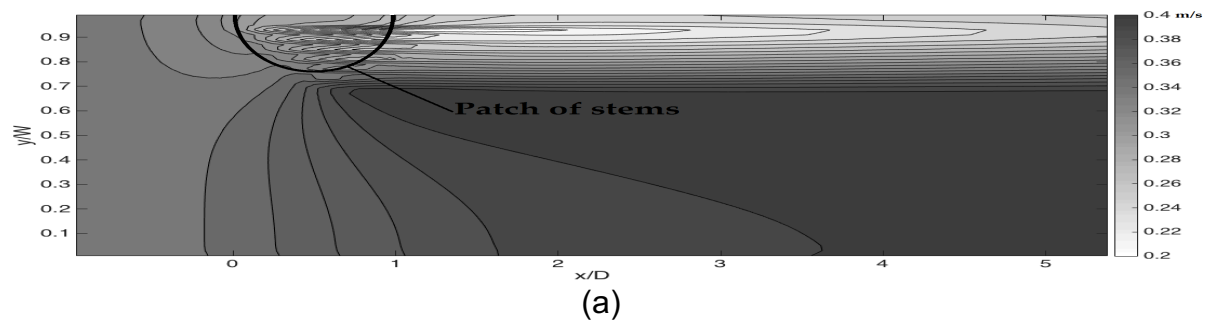
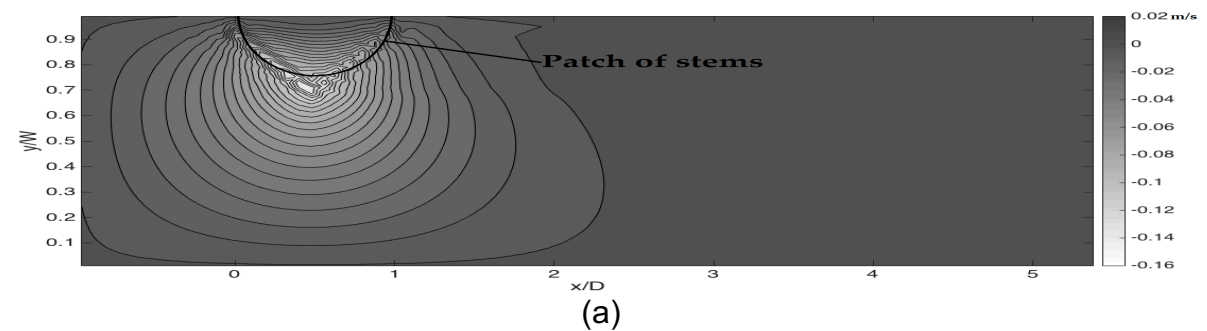


Figure 6.9. Plan of the depth average streamwise component of the velocity in a channel with $\Omega_v=0.025$, $D=50$ cm, $U_0=38.5$ cm/s, $h_0=7.8$ cm, (flow from left to right) – (a): numerical result (b): experimental result



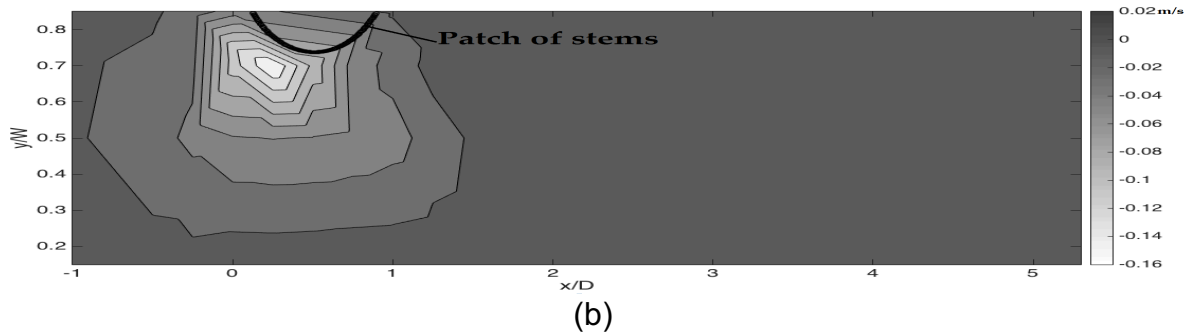
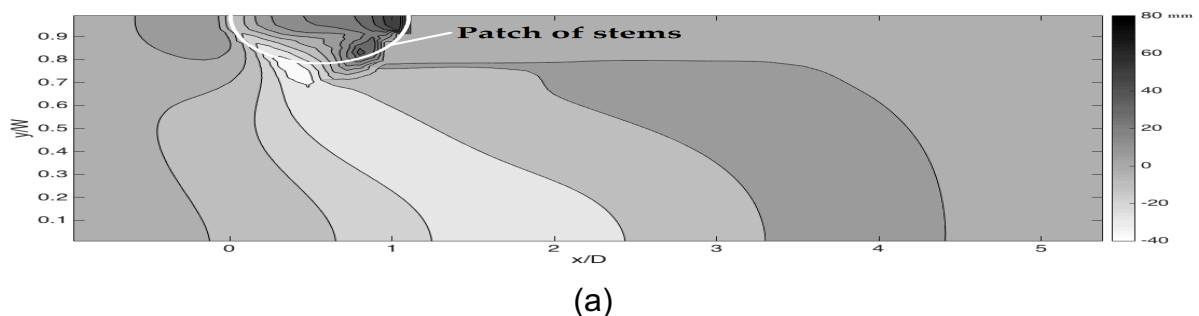


Figure 6.10. Plan of the depth average transverse component of the velocity in a channel with $\Omega_v=0.025$, $D=50$ cm, $U_0=38.5$ cm/s, $h_0=7.8$ cm, (flow from left to right) – (a): numerical result (b): experimental result

As it is evident in figure 6.7 to 6.10, the depth averaged distribution of the component of the velocity and their values follows the experimental results. The location of the highest and lowest components of the velocity predicted well enough. The steady region with constant velocity in the wake of the patch is also clearly developed for both tests and consequently the bar of sediment is created behind the patch (figure 6.12). As it was expected, because of differences of stem densities, the length of this region is different for these two tests. In the first case, it takes more distance for the shear layer to reach to the side of the channel, while by increasing of vegetation density in the second test the streamwise velocity decreases more and acceleration of the flow happens in the closer region to the patch and the area with decelerated flow at the wake of the patch becomes smaller. On the other hand, the transverse velocity shows higher values for the higher vegetation density, which would lead to more flow deflection. But as it was mentioned the symmetry of transverse velocity in numerical results is not correspond with measured data because of the sudden changes in bed roughness.



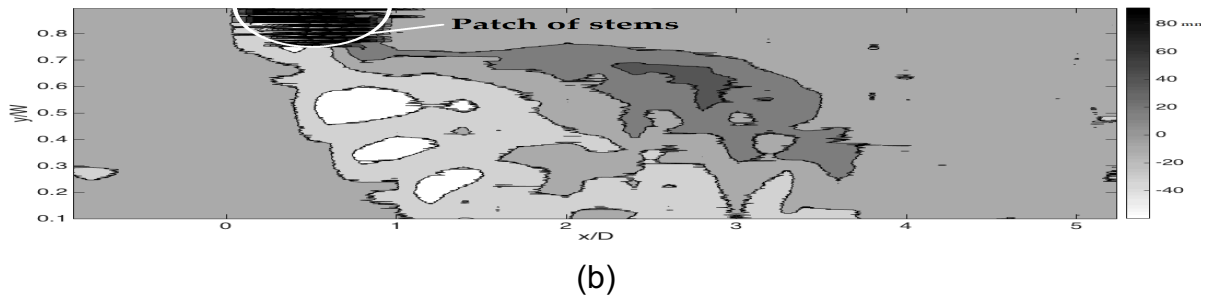


Figure 6.11. bed profile of the experiment with $\Omega_v=0.1$, $D=50$ cm, $U_0=18.5$ cm/s, $h_0=17.7$ cm, (flow from left to right); (a): numerical result, (b): experimental result

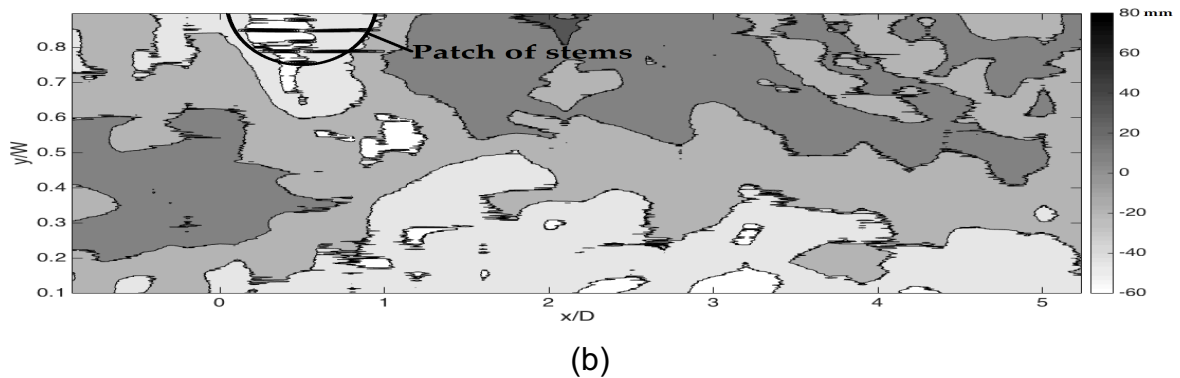
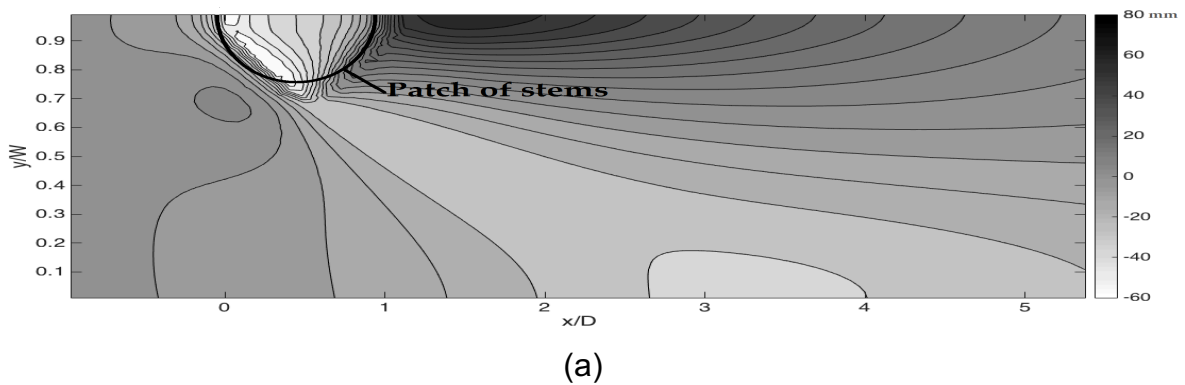


Figure 6.12. bed profile of the experiment with $\Omega_v=0.025$, $D=50$ cm, $U_0=38.5$ cm/s, $h_0=7.8$ cm, (flow from left to right). (a): numerical result, (b): experimental result

As it was explained in chapter 5, due to the flow Fr number and vegetation density the scour holes and deposits location, depth and height can be different. As it was expected, the calculated results for the case with higher density of stems and lower Fr number in the main channel, deposition occurs downstream of the scour holes. Because of the high density of stems and low flow energy less sediment can pass through the patch and it is immediately settle behind the downstream edges of the patch (figure 6.11). On the other hand, the model results for the case with lower vegetation density and higher Fr number shows the transportation of the eroded

sediment further downstream and toward the wake of the patch, which has a steady condition with lower velocity magnitude. Furthermore, because of the low density of stems, sediment is also fed by the transported mass within the permeable patch and the tip of the deposits occurred just behind the patch close to the channel wall, which is indicated as the darker region in figure (6.12 a).

To summarize, despite the differences of the velocity distribution around the edges of the patch, investigated numerical results are relatively similar to experimental data for both tests and the general patterns stand out in spite of changes of variable.

6.4 Sensitivity analysis of the Variables

The sensitivity analysis assesses the response of an output variable to a change in an input variable, and the intensity of the response corresponds to the intensity of the sensitivity to that variable (White and Chaubey, 2005). Three types of variables have been identified in this study: (1) density of stems, (2) flow Froude number, (3) location of patches. In chapter 4 and 5, the development of bed profiles and distribution of components of the velocity and their sensitivity has been investigated in terms of density of vegetation and flow Froude number. But there are some other variables like the location of patches, that can have significant effects on both hydrodynamic and morphodynamic of the flume. Although the experimental setup could provide valuable information, it is costly and time consuming to investigate the effects of the location of patches in a channel. Coupling the experimental data with the results of the numerical model, more analyses are accomplished to investigate the effects of more variables on bed profile and velocity distribution in a channel and the results are presented in chapter 7.

6.5 Summary and Conclusion of chapter 6

Generally, model variables represent the model state, but model parameters are static variables and before starting a simulation with a numerical package it is vital to find uncertain parameters and fix their values on the basis of the available experimental and field measurements, because they can have significant effects in outputs. While the variables are constant, investigates about the effects of the uncertain parameters have been done by considering five different parameters, which include the bed roughness, horizontal viscosity and diffusivity, critical

mobility parameter, and drag coefficient. Simulated results of velocity and bed elevation are studied and compared with the experimental data for a typical case to investigate the result of the calibrated code. Furthermore, to validate the numerical model, the results of two other experiments with different physical and initial conditions are considered and modeled with Delft3D. In the analyzed experiments, the results of the numerical model are in relatively good agreement with experimental data.

7 Chapter 7: Results of calibrated model, validation and sensitivity analysis

Previous literature has mostly neglected the effects of important parameters such as density and size of patches of vegetation, and directly used the empirical formulas for estimating longitudinal and lateral intervals between the vegetation regions (e.g. Bennett 2002, 2008). On the basis of results of experiments with a single patch of vegetation (chapters 4 and 5), this chapter deals with the designing of positions of mutual patches in a channel, and focuses on the effects of longitudinal and lateral intervals between patches. Therefore, the main object of this chapter relies on finding the proper intervals between the patches to provide efficient geomorphic and ecosystem services in the channel. The lateral and longitudinal intervals between the patches are investigated both experimentally and numerically and effects of the scale, density and position of patches are studied in terms of a flow structure, bed morphology.

7.1 Methodology

One of the motivations of this research is to prepare more information to understand the details of using the patches of vegetation to transform a straight channel with low ecological efficiency into a more ecological channel. Based on the results of chapter 4 and 5, density of a simple patch of vegetation has a direct effect on velocity distribution and subsequently on bed evolution around a finite patch of vegetation. Moreover, different features such as lateral and longitudinal affected length are determined for patches with different stem density. This fact is used to investigate the lateral and longitudinal intervals between the patches on both sides of the channel by predicting the interaction among vegetation, flow structure and bed morphology.

At first a set of experiments have been designed to change the bed profile from being straight to meander bed. This is done by using 5 patches of cylinders with certain density and different flow Fr number on both sides of the channel to investigate the capability of equations 5.6 and 5.7 in the channel with mutual patches (figure 7.1). Subsequently, more investigations have been done by

accomplishing experiments with both higher and lower densities. After realizing the reliability of the equations in estimation of positions of the mutual patches, the experiments modeled with Delft3D. This meant to not only study the alignment of the numerical result and experimental result but also the effects of both non dimensional lateral distance (W/D) (W represents the width of the channel and D represents the diameter of the patch of vegetation), and non dimensional longitudinal distance (L/D) (L represents the intervals from upstream to upstream edges of the patches) on bed profiles to recognize the consequences of different lateral and longitudinal intervals between the patches in the channel.

7.2 Installation of mutual patches

In order to study the details of the mutual interaction of vegetation zones, first, patches of vegetation with density of 0.05 are chosen with certain initial condition similar to the tests with a simple patch of vegetation. This is done because according to the diagram 5.17, the lateral affected length (X_w) for the patches with 0.5 m diameter is around 1 m, which is provided by the flume. Also due to the same diagram, the distance of 1.45 m is defined as the longitudinal intervals (X_L) between the patches to plant the cylinders as representatives of vegetation stems on both sides of the channel. The configuration of the patches in the experimental setup is shown in figure 7.1.

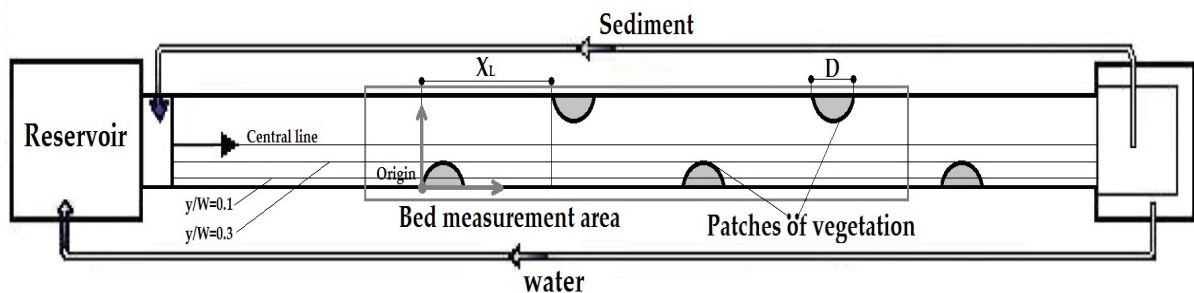


Figure 7.1. Location of patches of vegetation and the details of the experimental channel (Origin of coordinate and longitudinal lines along the channel, which are used to investigate the velocity)

Considering the configuration of the patches in the channel, velocity measurements were done at different longitudinal intervals in 5 different points in each cross section and at 0.2 and 0.8 times of water depth. The mean of two velocities at 0.2 and 0.8 of the flow depth at each point is considered as a depth-averaged velocity. The minimum longitudinal interval for velocity measurements was 19 cm up to 28 cm. Figure 7.2 shows the origin of coordinate and locations of velocity measurements in the channel with the explained configuration of the patches. x and y represents the longitudinal and lateral distance from the origin of

coordinate and horizontal and vertical axes show respectively the non-dimensional longitudinal distance and non-dimensional lateral distance from the origin of coordinate at upstream side of the patch of vegetation. It should be mentioned that the plan of velocity measurements for other configurations is the same and just the longitudinal intervals changes due to the location of the patches in the channel.

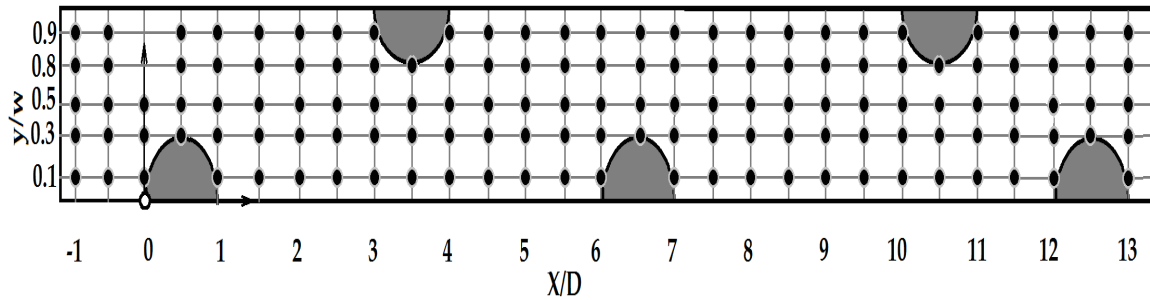


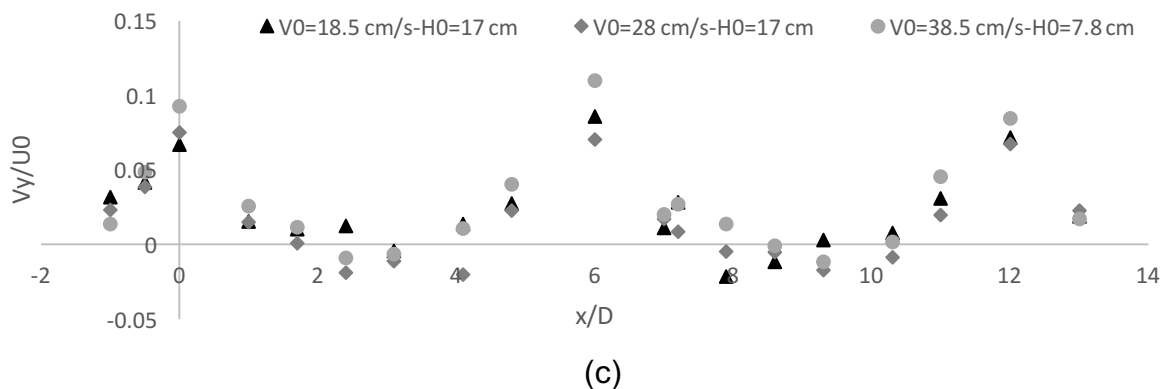
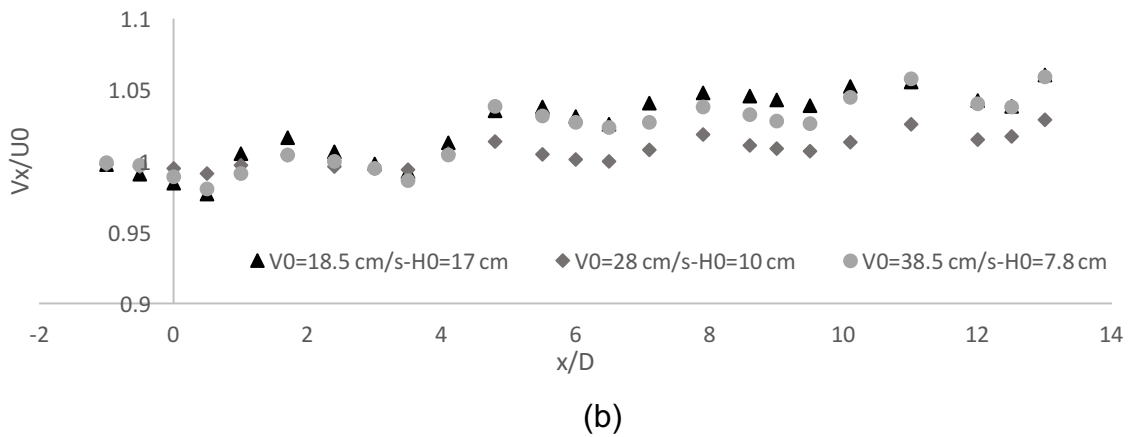
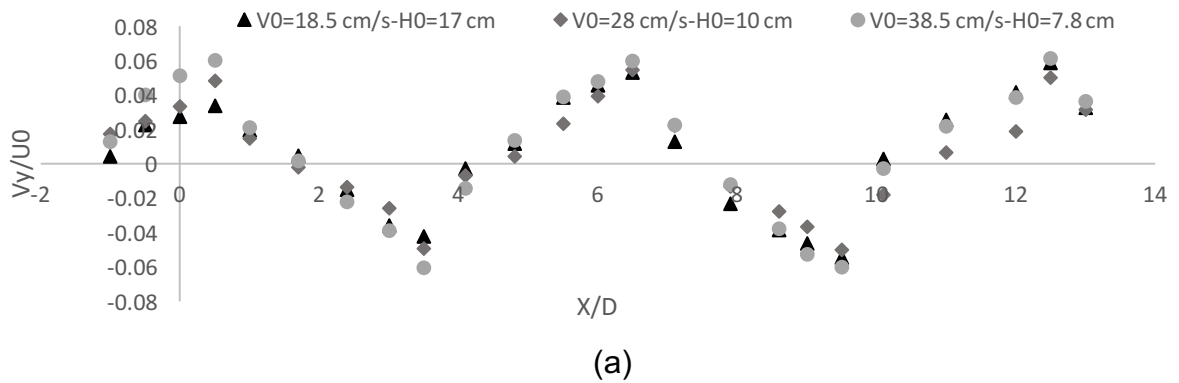
Figure 7.2. Location of velocity measurements along the channel

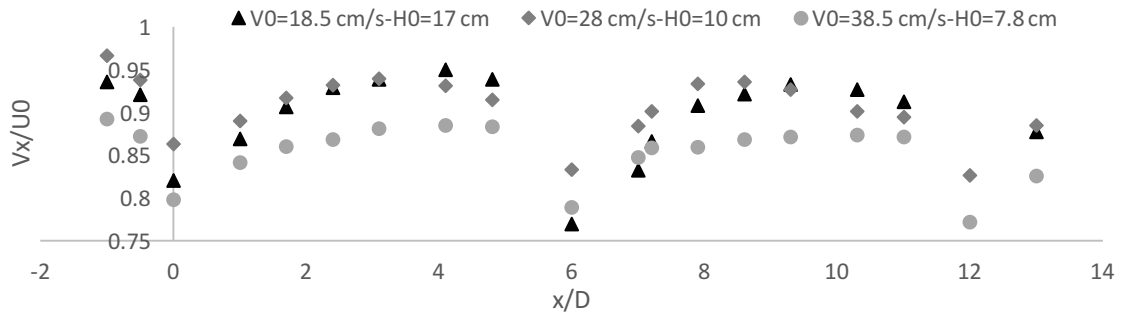
Table 7.1 shows the details of these experiments (U_0 is the depth average velocity, h_0 is the depth of flow and Q_s is the bed load transport without interaction of the patch of vegetation).

Table 7.1. Summary of experiments with mutual patches

test N.	h_0 [cm]	U_0 [cm/s]	Fr N.	Ω_v	D [cm]	t [h]	Q_s [gr/min]
1	17.7	18.5	0.1	0.025	56	9.5	0
2	10.5	28.5	0.3	0.025	56	8.5	150
3	7.8	38.5	0.4	0.025	56	8	950
4	17.7	18.5	0.1	0.05	50	9.5	0
5	10.5	28.5	0.3	0.05	50	8.5	150
6	7.8	38.5	0.4	0.05	50	8	950
7	17.7	18.5	0.1	0.1	38	9.5	0
8	10.5	28.5	0.3	0.1	38	8.5	150
9	7.8	38.5	0.4	0.1	38	8	950
10	9	22	0.2	0.1	50-70	9.5	42
11	9	30	0.3	0.1	50-70	8.5	180
12	9	45	0.5	0.1	50-70	8	1220
13	9	22	0.2	0.05	50-70	9.5	42
14	9	30	0.3	0.05	50-70	8.5	180
15	9	45	0.5	0.05	50-70	8	1220
16	9	22	0.2	0.025	50-70	9.5	42
17	9	30	0.3	0.025	50-70	8.5	180
18	9	45	0.5	0.025	50-70	8	1220

Considering the same three upstream boundary conditions of the experiments with a single patch of vegetation ($(U_0=18.5 \text{ cm/s}, h_0=17.7 \text{ cm})$, $(U_0=28.5 \text{ cm/s}, h_0=10.5 \text{ cm})$, and $(U_0=38.5 \text{ cm/s}, h_0=7.8 \text{ cm})$), here the effects of lateral and longitudinal intervals on velocity distribution and bed profiles are investigated for the patches with density of 0.05. The results of depth-average velocity measurement along the certain lines at different y/W ratio (figure 7.1) are shown in figure 7.3 (a to d).





(d)

Figure 7.3. Depth average component of the velocity along 2 longitudinal axes- (a): transverse velocity along $y/W=0.5$, (b): streamwise velocity along $y/W=0.5$, (c): transverse velocity along $y/W=0.2$ & (d): streamwise velocity along $y/W=0.2$

In figure 7.3, the locations of the patches are between $0 < \frac{x}{D} < 1$, $3 < \frac{x}{D} < 4$, $6 < \frac{x}{D} < 7$,

$12 < \frac{x}{D} < 13$. As it was explained in chapter 4, by approaching the flow to a patch of

vegetation, transverse velocity starts to increase around the area of vegetation and the acceleration rate is a function of the density of vegetation. This acceleration rate is independent from the flow Fr number. This is also obvious from the pattern of component of the velocity in figure 7.3. The acceleration of the transverse velocity initiates from upstream side of the patch and it continues to the wake of the patch. On the other hand, consideration of the size, lateral and longitudinal intervals in installation of the mutual patches is caused the reacceleration of the transverse velocity in the mid-channel on the opposite direction (figure 7.3 a), which provides a meander pattern in velocity distribution. According to the constant density of patches, the acceleration rate of the transverse velocity remains constant. Although for the defined configuration vegetation regions changes the transverse velocity in the mid-channel, the effects of vegetation in the areas close to the opposite banks are less. Due to this reason the decelerated transverse velocity remains almost constant at the wake of the patches of vegetation. This situation continues along the places close to the banks of the channel till the flow reaches to the next patch of vegetation at the downstream part (figure 7.3 c).

By increases of transverse velocity at the upstream edge of the patches, flow starts to deflect to the central part and this process would lead to changes of the direction of the velocity. Generally, the streamwise velocity along the central part of the channel is accelerated in the area beside the vegetation region and by continuing

to move to downstream, the increased velocity is decelerated gradually until it reaches to the next opposite patch. Furthermore, changes of the bed profile and accumulation of sediment behind the vegetation zones would cause a gradual increase of streamwise velocity along the central part of the channel (figure 7-3 b). The scour and deposition observed for these three tests in the area which is shown in figure 7.1 are also presented in figures 7.4 (a to c).

However, the streamwise velocity along the bank sides follows a different scenario. By diversion of the flow to the central part of the channel and penetration of the rest of flow into the vegetation region, the streamwise velocity starts to decelerate and it reaches to its lowest amount at the downstream edges of the patch and accelerates again. Presence of the patches on the opposite side of the channel in this configuration shortened the recovering length, which is required at the wake of a simple patch for the flow to increase to the initial velocity rate (figure 7.3 d).

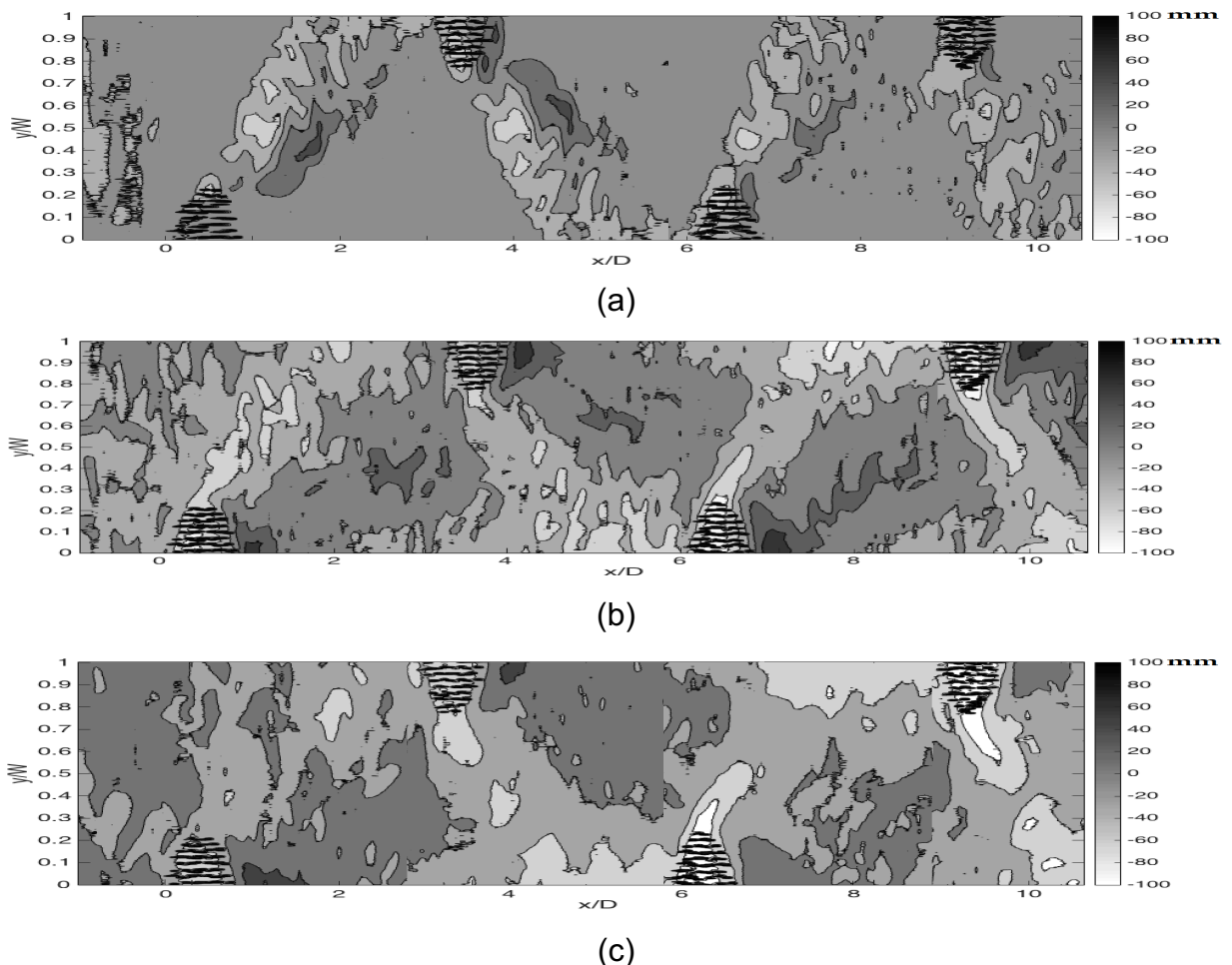
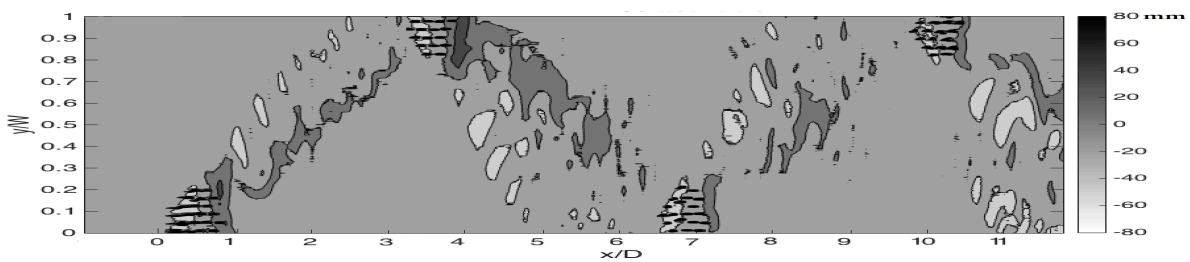


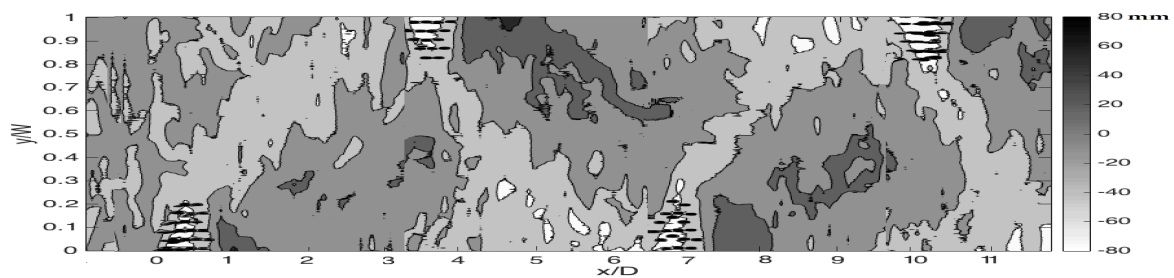
Figure 7.4. bed profile along the experimental channel (density of the patches=0.05, $D=50$ cm)-(a): ($U_0=18.5$ cm/s, $h_0=17.7$ cm), (b): ($U_0=28.5$ cm/s, $h_0=10.5$ cm), and (c): ($U_0=38.5$ cm/s, $h_0=7.8$ cm)

In figure 7.4, flow is in the positive x direction and the lighter parts show regions of scour, while the darker areas represent the deposits. The black circles indicate the position of the cylinders. As it was expected, the scouring starts from the area close to the upstream edges of patches of cylinders and extends across the channel to the opposite bank, which is accompanied by the implementation of a similar semicircle patch of vegetation. The expected meander pattern of scour and deposition along the scanned area proves the capability of the equations 5.6 and 5.7 about the estimation of the lateral and longitudinal effective lengths.

The experiments with the same upstream boundary condition are also run for two other vegetation densities (0.1, 0.025) to validate the reliability of the equation 5.6 and 5.7. Using this particular equations in these experiments, allows us to predict the scouring around the patches of vegetation with different densities on both sides of the channel. According to the diagram equation 5.6 and 5.7, the lateral and longitudinal affected length for the patches with density of 0.025 and 0.56 m diameter is around 1m and 1.83m respectively. Furthermore, both of the lateral and longitudinal affected lengths of the patches with density of 0.1 and 0.38 m diameter are 1m. This length is used to plant the stems along the both sides of the channel. The contour plots of the beds are shown in figures 7.5 and 7.6.



(a)



(b)

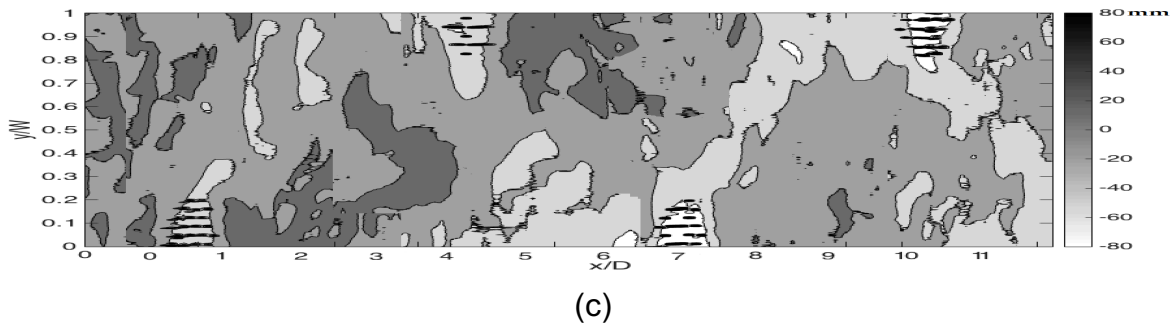


Figure 7.5. bed profile along the experimental channel (density of the patches=0.025, $D=56$ cm)-(a): ($U_0=18.5$ cm/s, $h_0=17.7$ cm), (b): ($U_0=28.5$ cm/s, $h_0=10.5$ cm), and (c): ($U_0=38.5$ cm/s, $h_0=7.8$ cm)

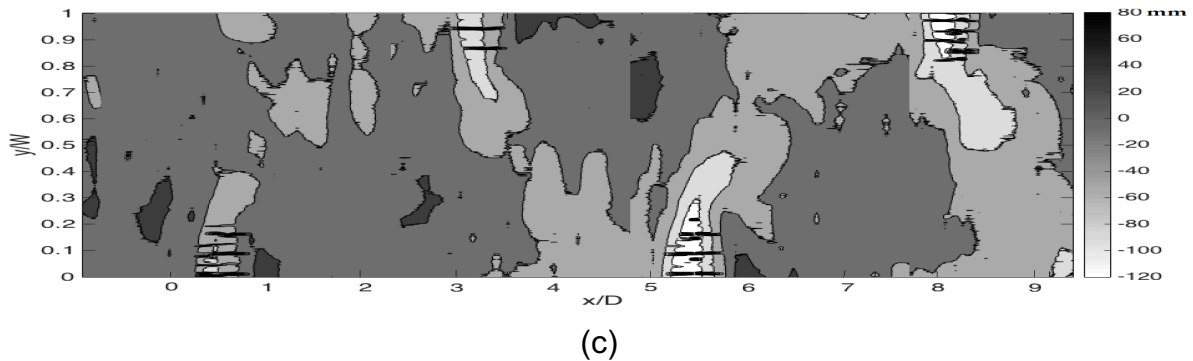
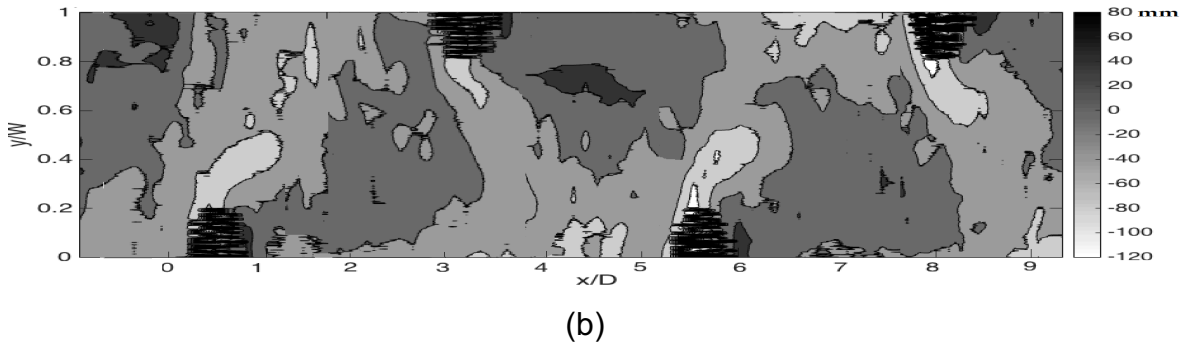
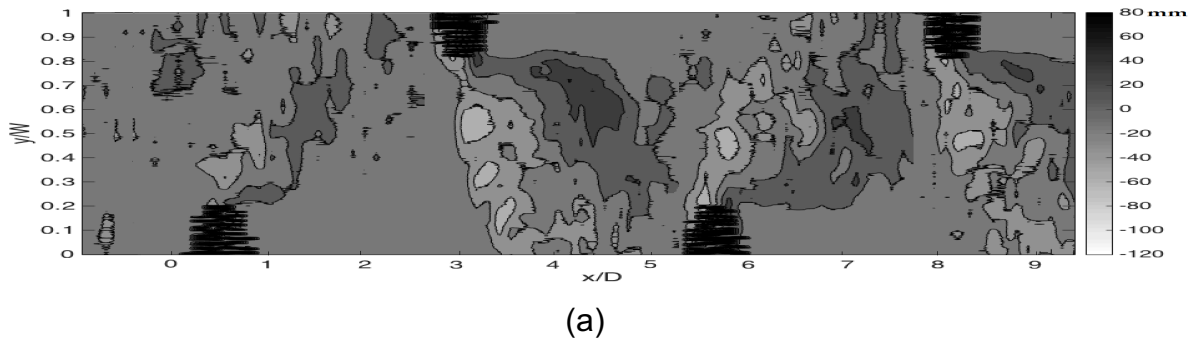


Figure 7.6. bed profile along the experimental channel (density of the patches=0.1, $D=38$ cm)-(a): ($U_0=18.5$ cm/s, $h_0=17.7$ cm), (b): ($U_0=28.5$ cm/s, $h_0=10.5$ cm), and (c):($U_0=38.5$ cm/s, $h_0=7.8$ cm)

Figures 7.5 and 7.6 respectively illustrate bed profiles in the channel with density of the patches of 0.025 and 0.1 through three different channel Fr number, $Fr=0.1$ (case a), $Fr=0.3$ (case b), and $Fr=0.4$ (case c). The general patterns of deposition and erosion are similar in both conditions. This would confirm the precision of the equation 5.6 and 5.7 about the calculation of the lateral and longitudinal effective lengths in order to create a meander pattern in the straight channel. As it was expected in this series of tests, increasing of the stem density is caused deeper scour holes and the deepest scouring for each test is located at about upstream half of the vegetation region. In fact, scour initiate at the front of each patch and intensify within the first half of the patches and then extends across the channel to the opposite side. According to the density of the stems, the second half of the patch could be scoured or deposited.

7.3 Validation of numerical code for mutual patches

By using the calibrated model and to make sure that the simulated results of the numerical code are in reliable agreement with the experimental results, the experiments of mutual patches with density of 0.05 and $Fr=0.4$ is simulated by Delft3D. The simulation process of a channel with mutual patches is similar to simulation of a channel with a simple patch of vegetation, which is explained in chapter 6. For the 2D simulation of the experiments, a rectangular domain with 1-meter width and 14-meter length has been prepared. The computational grids have 185 and 50 cells in the streamwise and transverse direction respectively. The total discharge of 30 L/s is specified for the upstream boundary condition, while the downstream boundary condition is fixed with water level ($h_0=7.8$ cm), which is found by the laboratory's measurements. The initial water level is also specified due to the same water depth measurements. The bed roughness coefficient is $n=0.022$ and location of the vegetation zone and their features implemented by the trachytopo functionality along the channel. The result of depth average velocity over the bed profile around the second patch of vegetation is compared with the experimental data and presented in figure 7.7 (a and b).

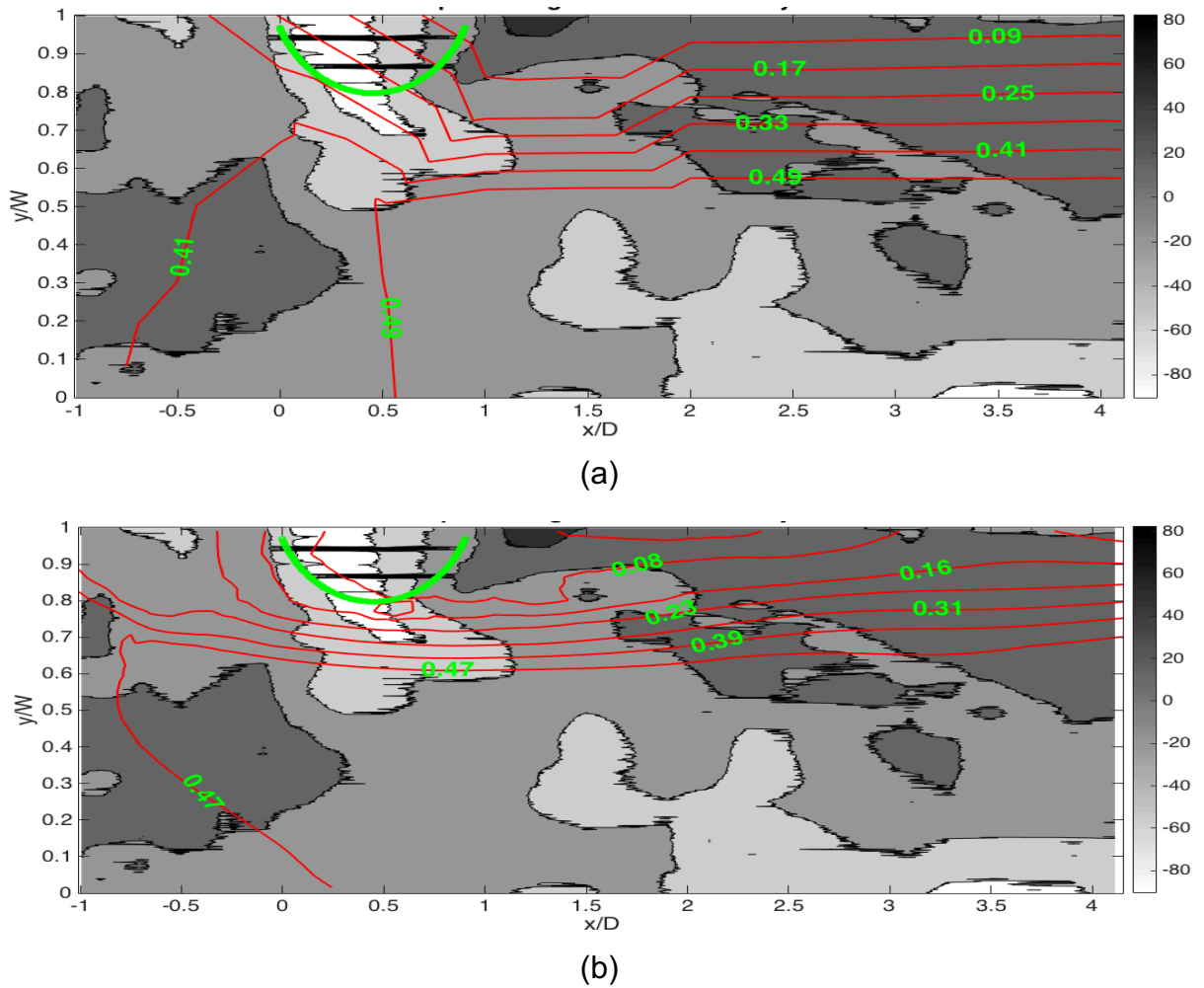
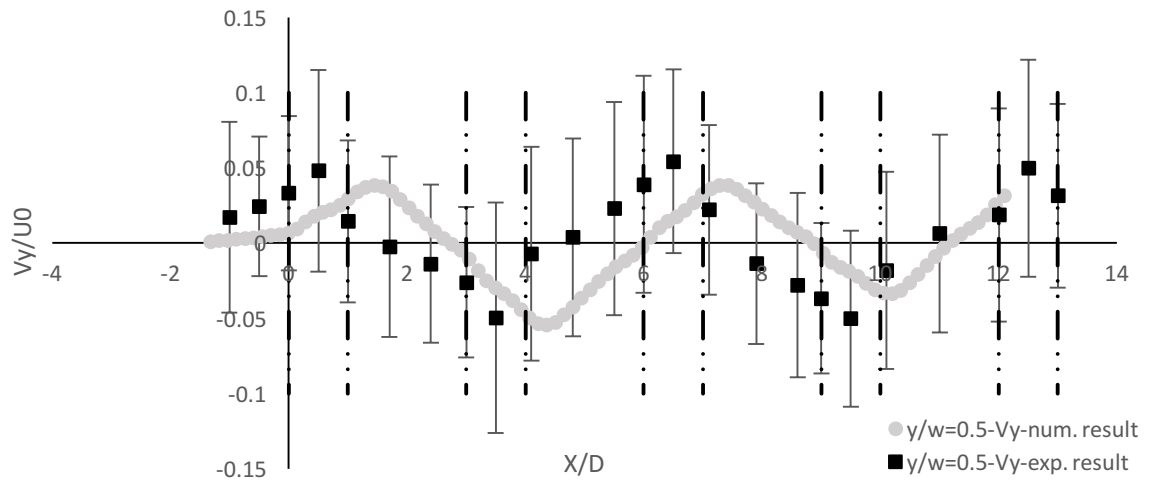
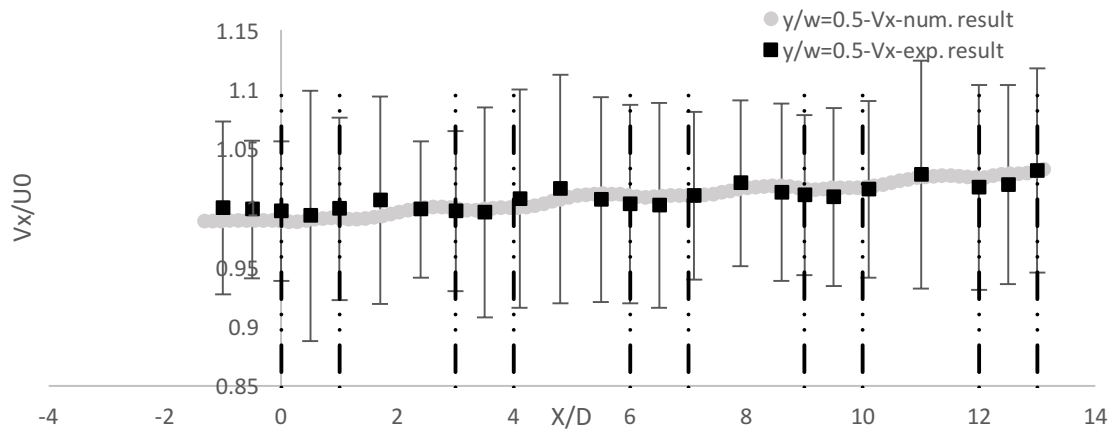


Figure 7.7. Comparison of depth average velocity result of the numerical simulation (density of the patches=0.05, $D=50$ cm) ($U_0=38.5$ cm/s, $h_0=7.8$ cm)- (a): Experimental measurements, (b): Numerical results

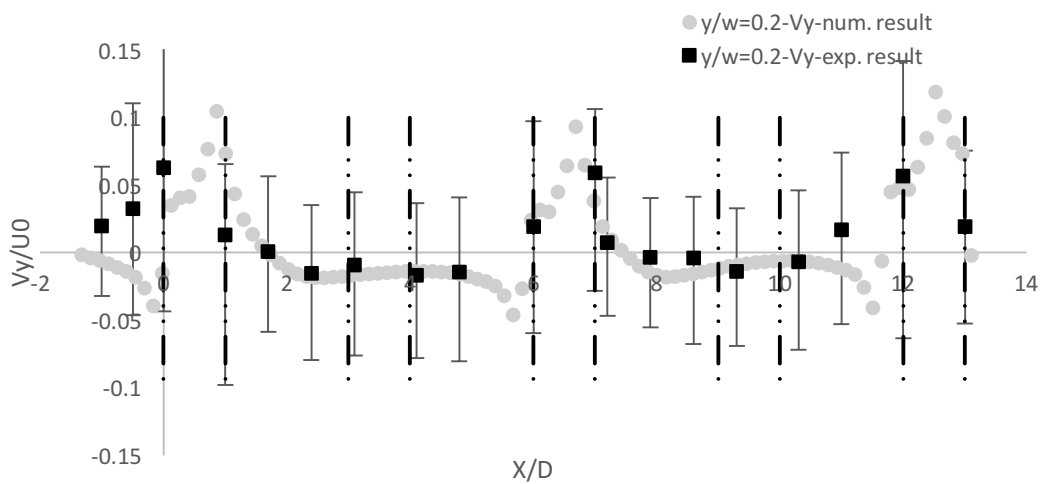
As it can be seen in figure 7.7, the general pattern of velocity distribution around the patches of vegetation is simulated very well for the investigated test. More detail investigations have been done on depth average component of the velocity along the certain lines with different y/W ratio from the origin of coordinates. The comparison of experimental data with numerical results is shown in figure 7.8 (a to d). The dotted lines in figure 7.8 denote the edges of patches. The locations of the patches are between $0 < \frac{x}{D} < 1$, $3 < \frac{x}{D} < 4$, $6 < \frac{x}{D} < 7$, $9 < \frac{x}{D} < 10$, $12 < \frac{x}{D} < 13$.



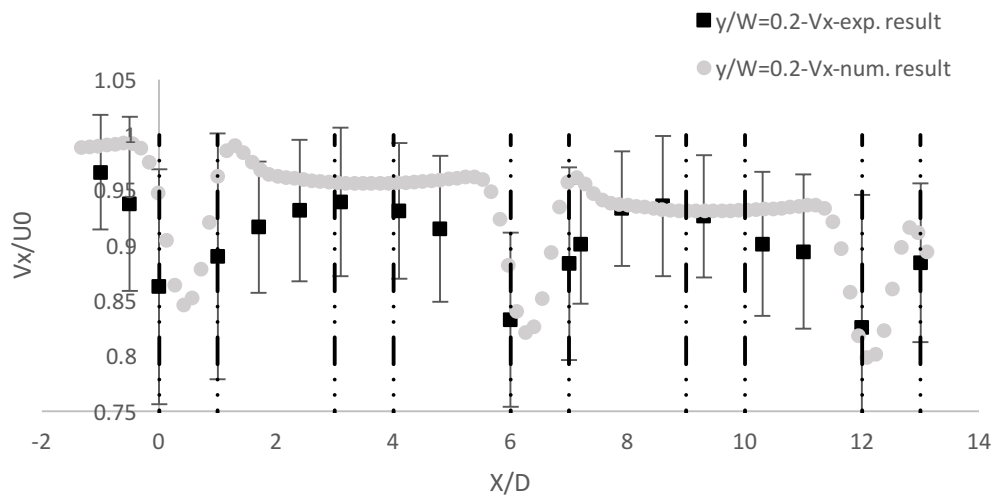
(a)



(b)



(c)



(d)

Figure 7.8. Comparison of simulated depth average component of the velocity along 2 longitudinal axes of $y/W=0.2$, & 0.5 (density of patches= 0.05 , $D=50$ cm, $U_0=28.5$ cm/s, $h_0=10.5$ cm)- (a): transverse velocity along $y/W=0.5$, (b): streamwise velocity along $y/W=0.5$, (c): transverse velocity along $y/W=0.2$ & (d): streamwise velocity along $y/W=0.2$

Figure 7.8 a represents the comparison of the transverse velocity along the central line of the channel. The calculated values of transverse velocity by the model are almost constant with the experimental data. This agreement is also confirmed for streamwise velocity along the central line (figure 7.8 b). Furthermore, the results of transverse and streamwise velocity along the line with $y/W=0.2$ ratio, which passes through the patches is in overall alignment with observed data (figure 7.8 (c and d)) and notably, the numerical code covers the limitation of the experimental data such as the velocity magnitude within patches. In addition, the simulated scour and deposition shows good agreement with the measured data. The result of simulated bed profile for this experiment is shown in figure 7.9.

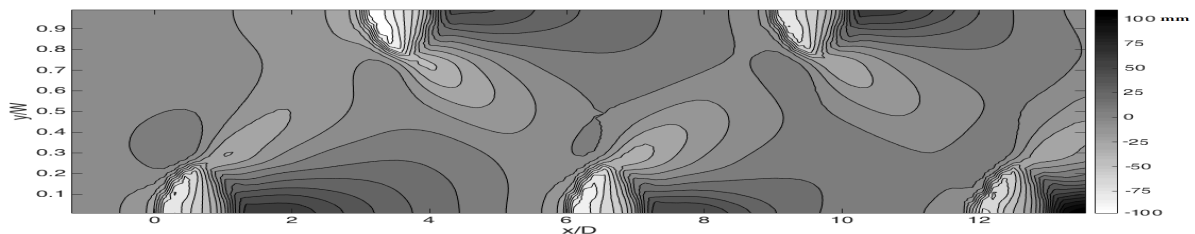


Figure 7.9. bed profile results of the numerical simulation (density of the patches= 0.05 , $D=50$ cm) ($U_0=28.5$ cm/s, $h_0=10.5$ cm)

In order to investigate the result of numerical and experimental result in details, the minimum elevation of the bed in different cross section along the channel is extracted and tracked for both numerical and experimental data and the scouring trend are compared in figure 7.10.

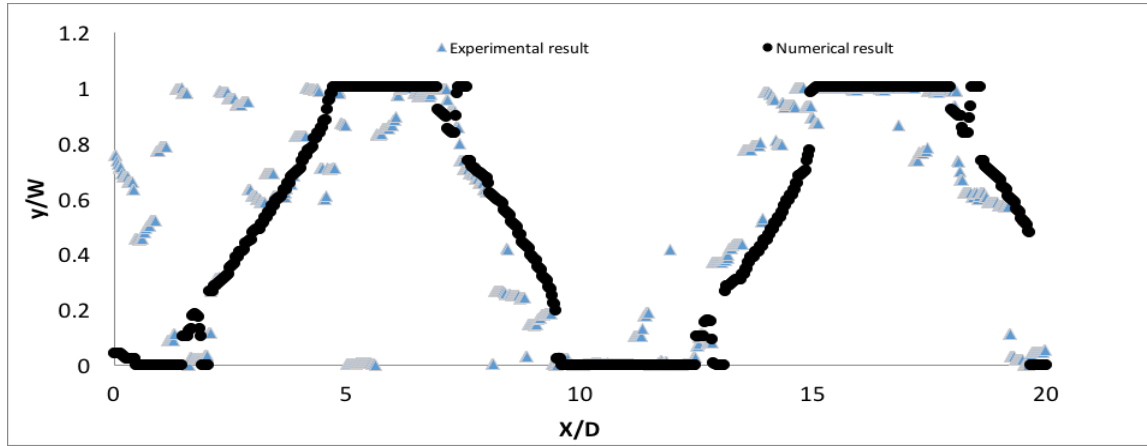


Figure 7.10. Extracted data with minimum bed elevations in all cross sections along the channel

Following the calculated and observed scour regions in figure 7.10 for the explained test, it is found that the computational model can accurately capture the bed profile in the channel. Considering the limitations of experimental flume and in order to investigate the effects of width of the channel on mutual patches and subsequently on bed profile, a set of tests with the constant initial condition ($U_0=28.5$ cm/s, $h_0=10$ cm), and different W/D ratios (1, 2, 3, 4, 6, 8, 10, 12, 14) are simulated for the patches with constant longitudinal spacing X_L . In addition, in order to investigate the effects of the longitudinal distances between the patches, the interval between the patches changed in different simulation in a channel with 1m width, which is equal to X_D for patches with $\Omega=0.05$. The distances are chosen both more than and less than X_L . Table 7.2 illustrates the details of the simulation variables.

Table 7.2 Details of simulation variables

Test	h_0 [cm]	U_0 [cm/s]	Ω	D [cm]	Q_s [gr/min]	Width [m]	Longitudinal intervals [m]
Effects of w/D	10.5	28.5	0.05	50	150	0.5, 1, 1.5, 2, 3, 4, 5, 6, 7	1.45
Effects of L/D	10.5	28.5	0.05	50	150	1	0.75, 1, 1.25, 1.5, 1.75, 2.25, 2.75, 3.25, 3.75, 4.25, 5.25, 6.25

Results of velocity distribution and bed profile are investigated in terms non dimensional lateral distance (W/D) and non-dimensional longitudinal distance (X/D).

7.4 Effects of non dimensional lateral distance (W/D) in a channel

Recently scientists have been tried to characterize the important parameters associated with isolated patches to study the effects of patches in streams. Luhar et al. (2008), proposed the ratio of A_v/A (vegetated plan areas relative to total plan area) to characterize hydrodynamics and mass transport in patches of vegetation in marshes. Vandenbruwaene et al., (2011) introduced the ratio of D/s (diameter of the patch relative to interspatial distance between patches) to investigate the interaction between adjacent patches of *Spartina anglica*. Zong and Nepf (2010, 2011), used the ratio of U_1/U_0 (*depth average velocity immediately behind a circular patch relative to depth average velocity without the effects of vegetation*) to investigate the turbulence dispersion around a circular patch. They also considered $C_D a D$ as a flow blockage to quantify the effects of density of a circular finite patch in flow field.

In this study, the effects of the width of the channel on bed morphology of the channel with patches of vegetation on both sides of the channel is investigated in terms of the non-dimensional (W/D) ratio (W represents the width of the channel and D represents the diameter of the patch of vegetation). The W/D ratio is the key parameter to understanding the distribution of sediment within a partly vegetated channel and the ability of patches of vegetation with different densities at banks of the channel to move sediment and change the morphology of the channel.

Due to the results of the experiments and simulations, the W/D ratio is a sensitive indicator of sediment transport and has significant effects on channel morphology. Consideration of the W/D ratio is necessary for describing channel bed morphology and comparison of ratio values can be used to interpret changes in channel bed forms following the introducing of patches of vegetation in the channel.

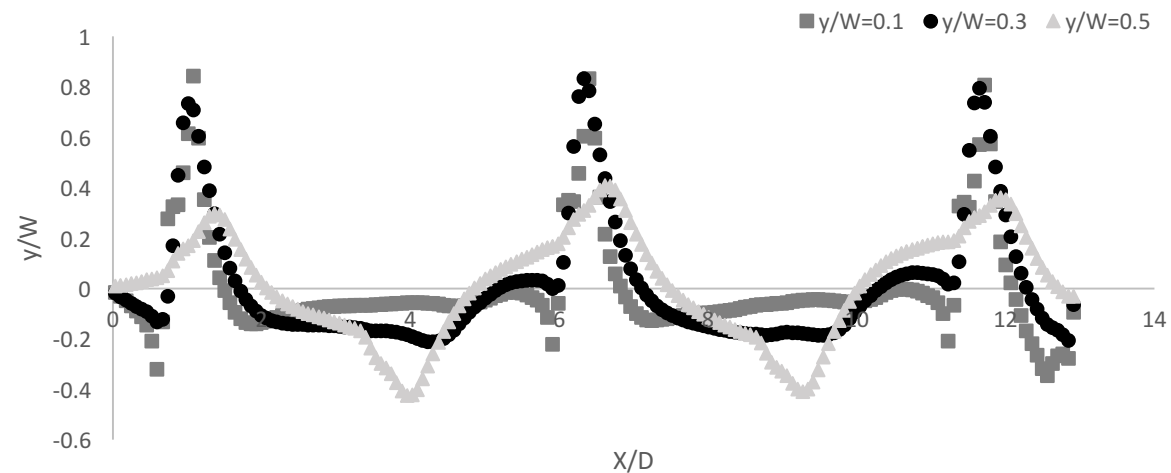
The derived power functions (see chapter 5), used to predict the appropriate longitudinal intervals between the patches and also estimate the width of the channel, which is enough to have the lateral effects of mutual patches of vegetation on opposite banks. Using the W/D ratio as an important factor in

sediment transport, channel responses investigated by describing the velocity impacts and bed profiles with different W/D ratio.

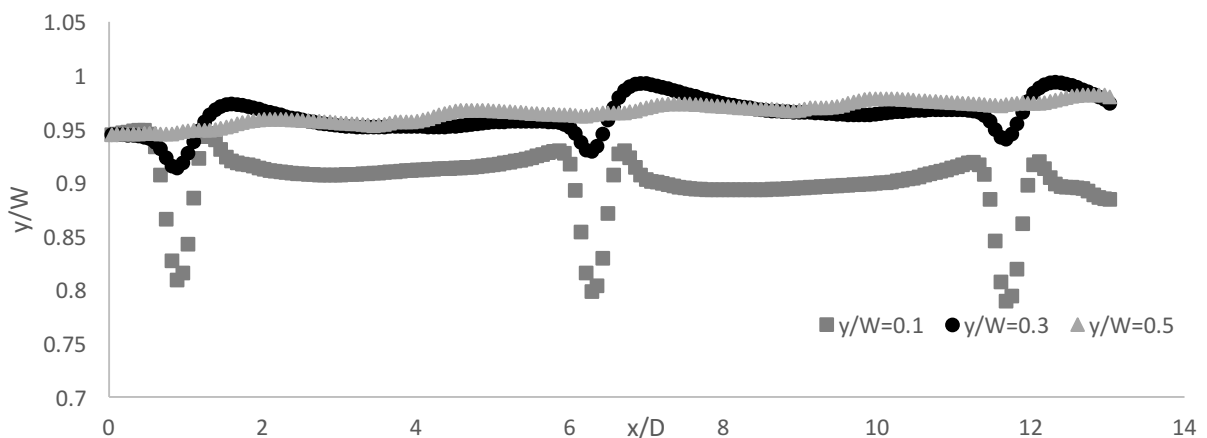
Simulations are accomplished for channels with different values of W/D ratio and equal physical, initial and boundary condition. The density of the patches of vegetation is 0.1, and according to the derived power functions the ratio of longitudinal affected length to diameter of the patch and lateral affected length to patch diameter is 2.7 and 2.6 respectively. In fact, the W/D ratio value of 2.6 is selected as the reference, which is the most frequent value to provide meander pattern on the channel and then the lower and higher rates are compared with it.

7.4.1 Velocity impacts

Velocity analyses are made along the certain lines with different y/W ratio from the origin of coordinates across the channel (figure 7.1). The locations of the patches are between $0 < \frac{x}{D} < 1$, $3 < \frac{x}{D} < 4$, $6 < \frac{x}{D} < 7$, $9 < \frac{x}{D} < 10$, $12 < \frac{x}{D} < 13$.



(a)



(b)

Figure 7.11. components of the velocity along five longitudinal axes of $y/W=0.1, 0.3, \& 0.5$ in the channel with $W/D = X_w/D$, (a): stream-wise velocity (V_x), (b): transverse velocity(V_y)

Stream-wise and transverse component of the velocity are extracted and plotted along these lines to investigate the effects of mutual patches on velocity distribution. Figure 7.11 (a and b) compares the stream-wise and transverse components of the velocity along three longitudinal axes of $y/W= 0.1, 0.3,$ and 0.5 in the channel with W/D ratio equal to X_w/D .

In figure 7.11 (a & b) the vertical axes presents the normalized stream-wise and transverse velocity versus the normalized distance from the origin of coordinate, which is shown in figure 7.1. Stream-wise velocity along the axes clarifies the processes which happen to the flow structure. As it was estimated, along axes which pass through the vegetation area ($y/W=-0.4,$ and 0.4) follows a deceleration beginning about $2D$ upstream side of the patches and continues with acceleration of flow by passing through each vegetation region. But the process is slightly different for the axes closer to the central part of the channel ($y/W=-0.2, 0, 0.2$). For these axes approaching of the flow to the patches is followed by acceleration of stream-wise velocity. This trend eventually starts to decelerate by getting far from each patch till the flow reach to the next opposite patch.

In terms of transverse velocity, the scenario is different and an identical process with different rates happens along considered axes. The transverse velocity starts to increase about one D from the upstream side of each vegetation region and the maximum velocity occurs at a point inside the patch. The position of this point depends on the patch density. By reaching to this point, deceleration of the transverse velocity starts till it reaches to the next patch of vegetation.

Stream-wise and transverse component of the velocity are also plotted along three longitudinal axes of $y/W=-0.4, 0,$ and 0.4 in the channel with different W/D ratio to investigate the effects of non dimensional lateral distance (W/D) and non-dimensional longitudinal distance (X/D) on velocity distribution. Figure 7.12 (a to c) 7.13 (a to c) illustrates variation of stream-wise and transverse velocity respectively under the same explored initial and boundary condition and due to changes of W/D from less than X_w/D to more than $4X_w/D$.

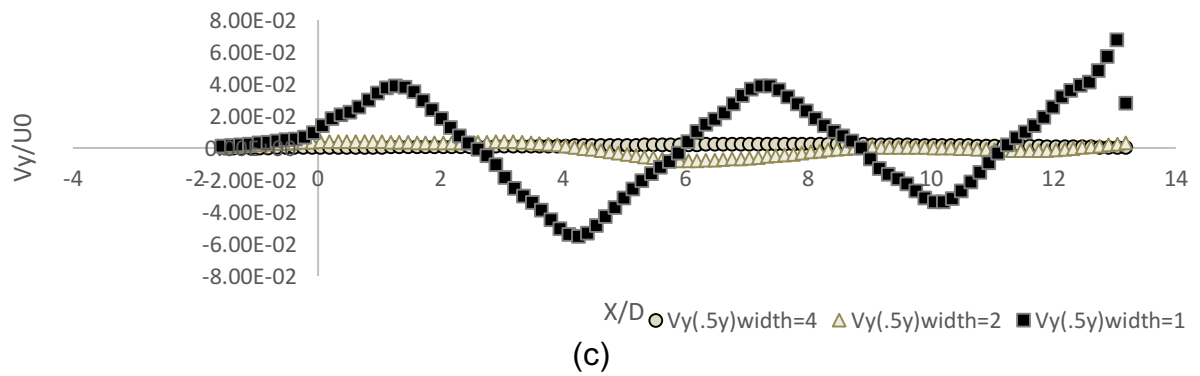
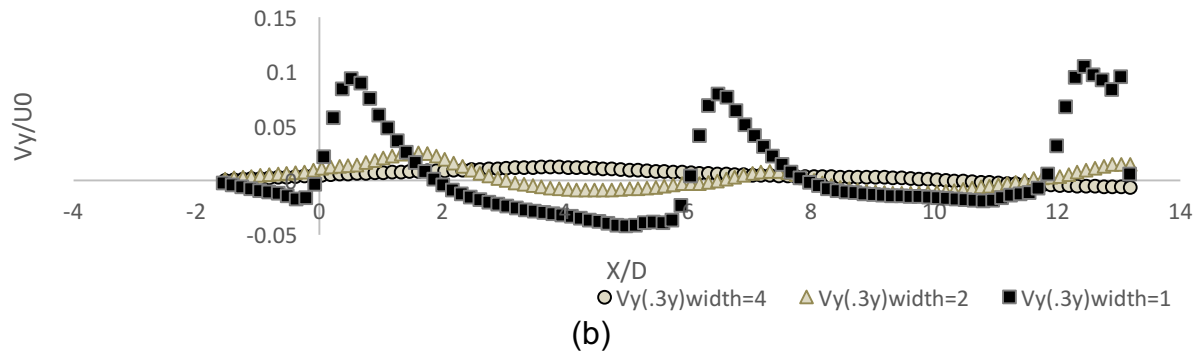
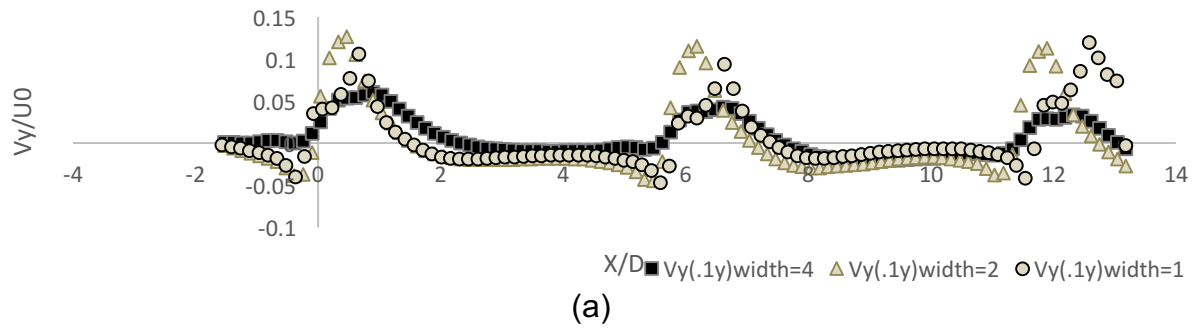
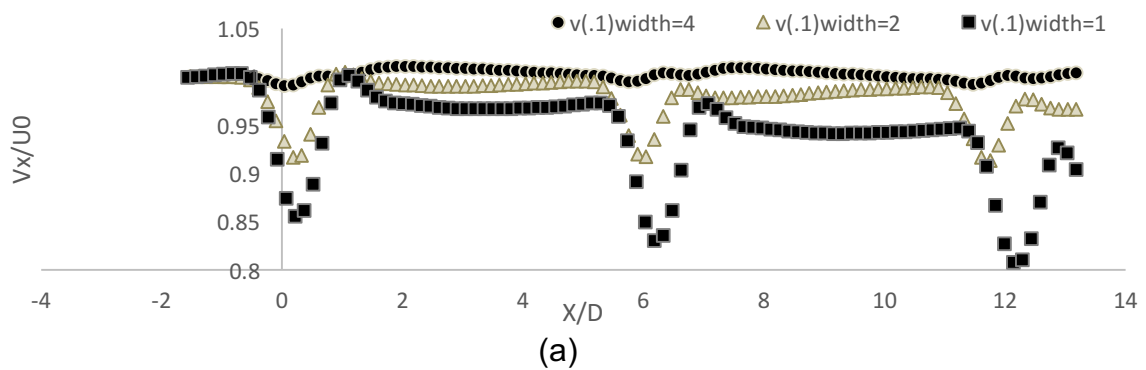


Figure 7.12. Transverse velocity of channels with $W/D < X_w/D$ to $4X_w/D < W/D$, (a): $y/W=0.1$, (b): $y/W=0.3$, (c): $y/W=0.5$



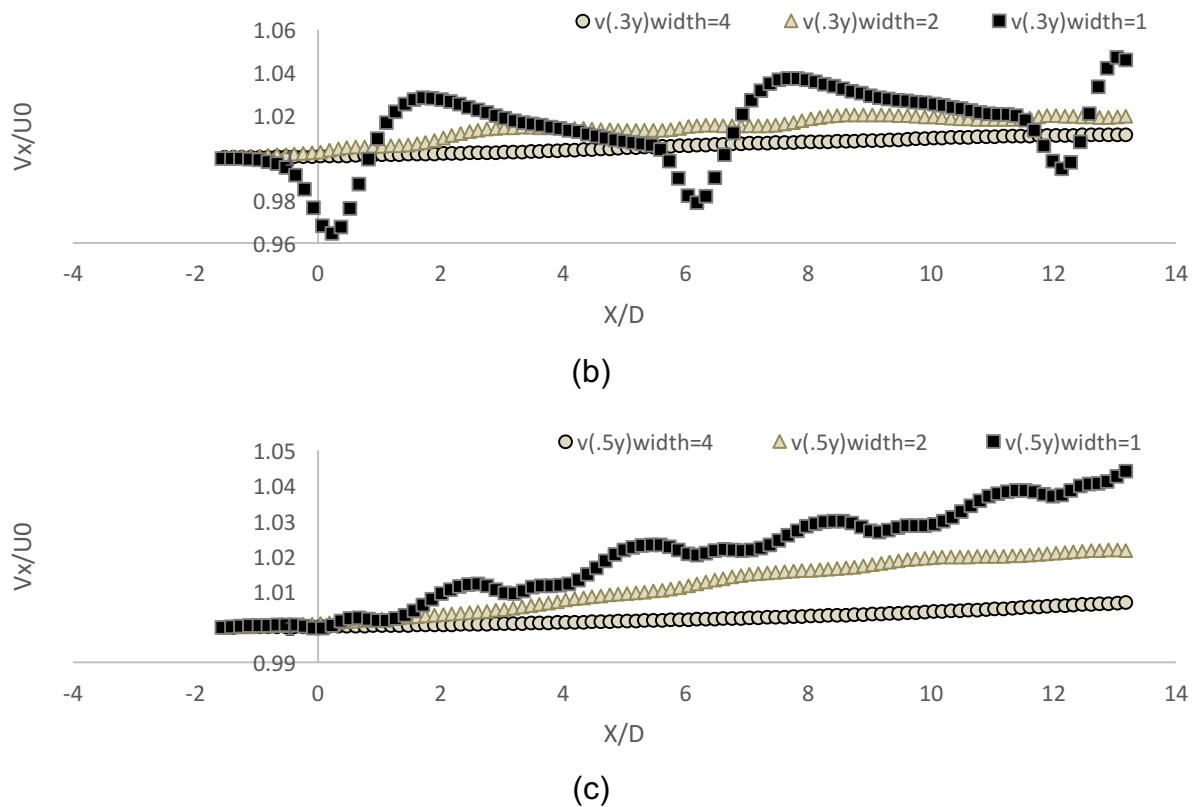


Figure 7.13. Stream-wise velocity of channels with $W/D < X_w/D$ to $4X_w/D < W/D$, (a): $y/W=0.1$, (b): $y/W=0.3$, (c): $y/W=0.5$

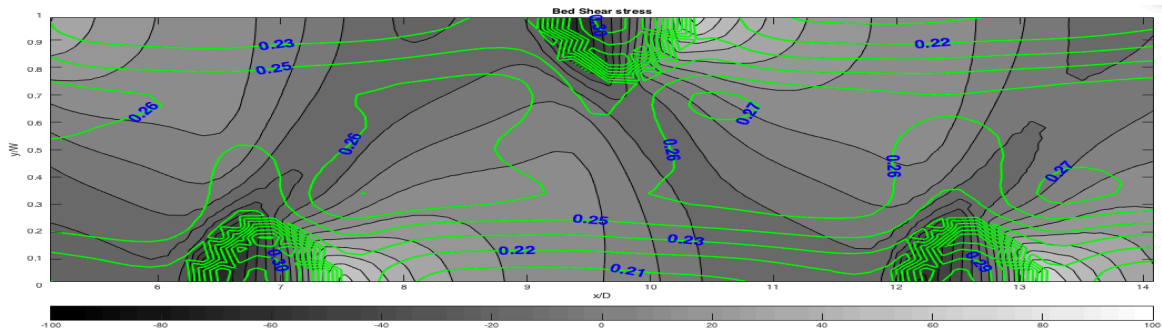
In figure 7.12 and 7.13 (a to c), as it was expected, by increasing the width of the channel the effects of a patch of vegetation on the main part of flow and on the next opposite side decreases. This will cause different velocity distribution and subsequently different bed profiles. In terms the transverse velocity, as it was described in figure 7.3, by approaching to each patch of vegetation, the transverse velocity starts to enhance across the flume. But as it is explored in chapter 5, the maximum lateral effective dominant of each patch is limited and it is a function of vegetation density. Hence, increasing of W/D ratio decreases the impacts of vegetation region in the central and the opposite half of the flume. Considering the figure 7.12 (a & c), the channels with W/D ratio less than X_w/D , process of increasing of transverse velocity passes the central part and reaches to the opposite side of the flume and this would lead to the meander pattern in the velocity field. Furthermore, increasing of W/D ratio to $2X_w/D$ would lead to decreasing of the lateral effects of the patches and the transverse velocity in the regions located in front of the patches across to the channel in the opposite half of the flume remain constant, but the central parts of the channel are still influenced and the transverse velocity follows the increasing process (figure 7.12 b). However, growing the amount of W/D ratio to more than $4X_w/D$ gradually reduces the lateral

effects of the vegetation region and the impacts of the patches of vegetation would be limited to the local scale and does not reach to the central part of the channel.

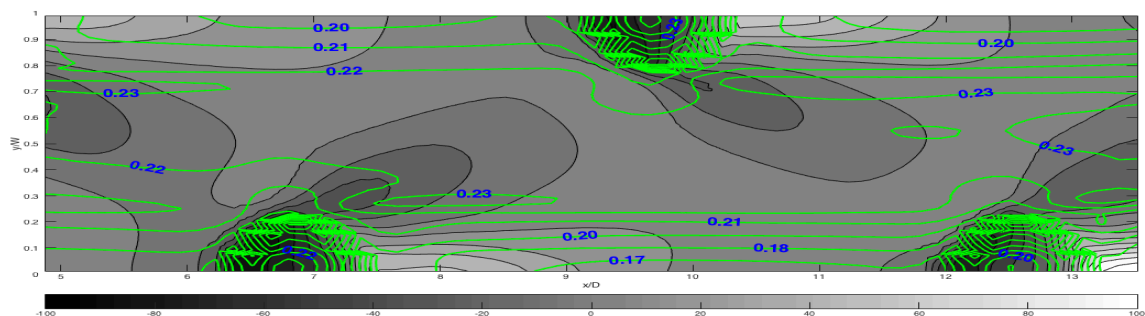
Although the effects of W/D ratio on stream-wise velocities follow the same trend, but the process of velocity fluctuation is different. As it is shown in figure 7.13 b, when $W/D < X_w/D$ the stream-wise velocity on the central line of the channel follows deceleration and acceleration at the upstream and downstream side of each patch respectively. By increasing of the W/D ratio to $2X_w/D$, fluctuation of the stream-wise velocity reduces in the central line of the channel and this shows the reduction of the impacts of vegetation region on central part of the channel. This trend continues almost in channels with W/D equal to $2X_w/D$, but with lower rates. In addition, within channels with W/D greater than $2X_w/D$, the stream-wise velocity on the central line of the channel remains more or less constant.

7.4.2 Bed profile

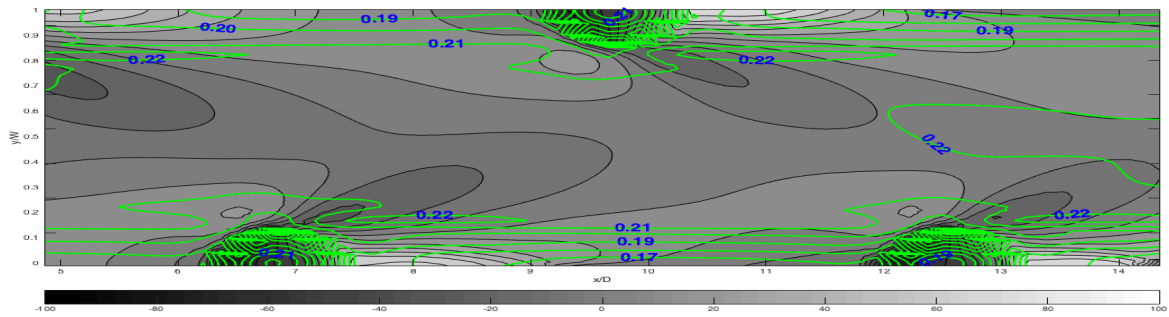
The sediment processes are connected to the main characteristics of the velocity field. Figure 7.14 (a to f) illustrates variation of bed profiles (around the three last patches of vegetation) and calculated bed shear stress by means of equation 3.8 and 3.9 due to changes of W/D from less than X_w/D to more than $4X_w/D$.



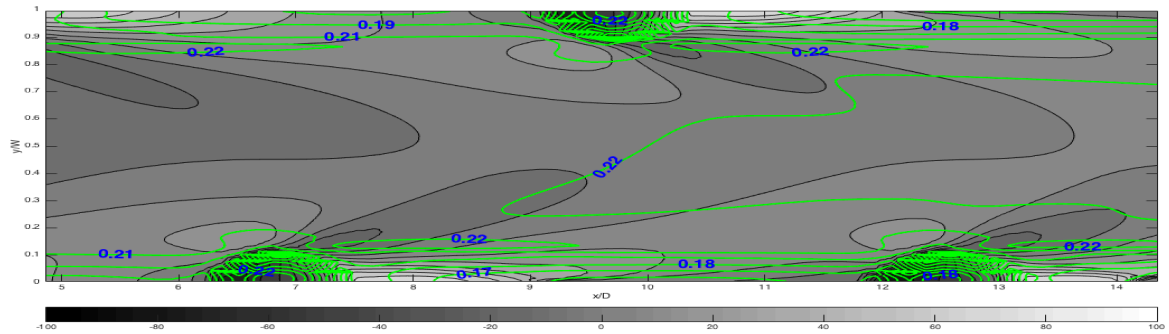
(a)



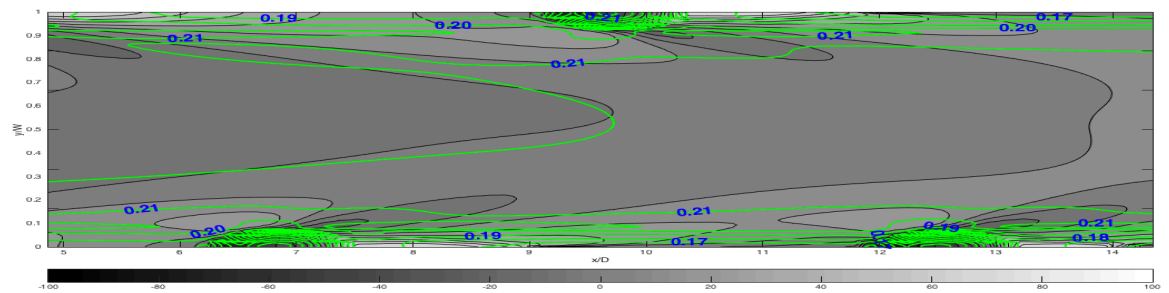
(b)



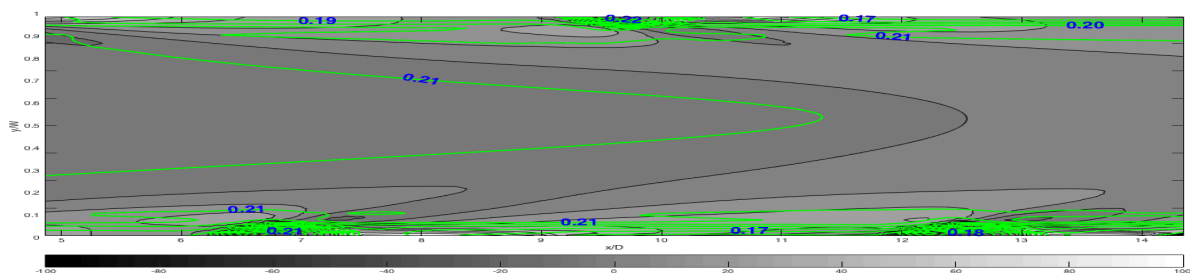
(c)



(d)



(e)



(f)

Figure 7.14. Bed profile of the channels with different W/D ratio and equal physical, initial and boundary condition-(a): $W/D=1$, (b): $W/D=2$, (c): $W/D=3$, (d): $W/D=4$, (e): $W/D=6$, (f): $W/D=10$

The net scouring volume within the channel with lower ratio ($(W/D) < (X_w/D) = 2.6$) shows higher velocity and turbulence in unvegetated regions, which is caused by mutual effects of patches of vegetation. In the other word, the scouring reaches to

the opposite side of the channel at the upstream side of the opposite vegetation region and causes the more turbulence and consequently the extension of scouring in these part of the channel.

As the W/D ratio increases to X_w/D , the scouring extends into the opposite vegetation region and provide a meander bed profile on the channel bed. Increasing of the W/D ratio leads to the changes of the meander bed forms to narrower and deeper channel and finally it tends to change to two smaller channel or a channel with islands in the mid-channel. In fact, the distribution of sediment within channels having high W/D ratio is such that deposition is not only placed in the wake of the vegetation area, but also within the central regions of the channel. As the W/D ratio increases the effects of vegetation finites to the bank of the channel and local erosion around each patch of vegetation. Figure 7.15 presents the effects of W/D ratio in a channel to help to summarize the results.

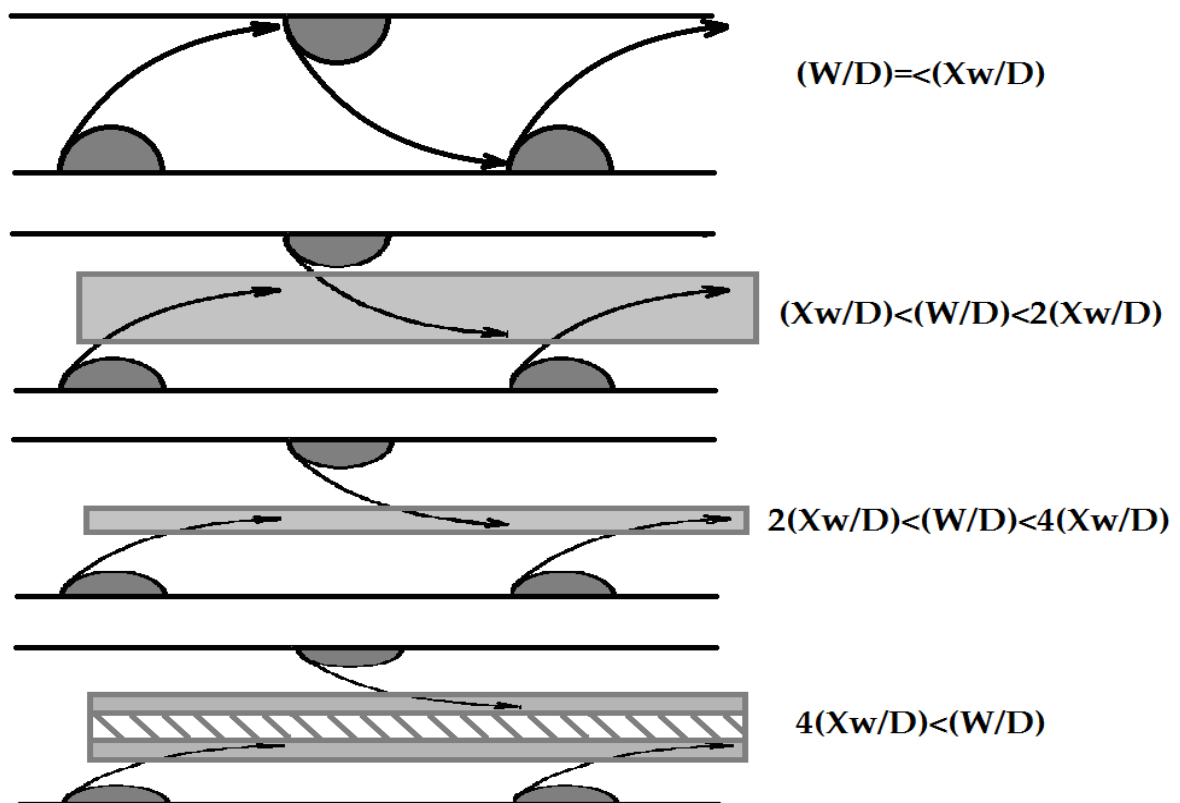


Figure 7.15. Probable bed profile in channels with different W/D ratio

Considering the process explained in figure 7.15 and the results of velocity distribution due to W/D ratio, some criteria has been prepared to predict the bed forms, which can be useful in related river restoration projects.

When the W/D ratio is less than the portion of lateral affected length to D :

-
- Associated erosion with the patch reaches to the other side of the channel.
 - If there are patches on the opposite side, meander bed could be shaped
 - As the ratio decreases, erosion area increases.

But if the portion of W/D comes between X_w/D and it's double, then:

- Associated erosion with the patch passes the mid-channel, but doesn't reach to the opposite side.
- If there are patches on the opposite side, they have less morphological effects on each other.
- As the ratio become closer to the lower range, the channel would be more wide and less deep, but if it increases to the upper range, narrower and deeper channel with more deposits at the wake of the patches would be shaped

If the portion of width to patch diameter comes between double X_w/D and $4X_w/D$, then:

- Associated erosion with the patch doesn't pass the mid-channel.
- If there are patches on the opposite side, narrower channel would be shaped.
- As the ratio increases, erosion area and the depth of water in the mid-channel decreases, because the opposite patches has less effects on the each other and subsequently on the flow

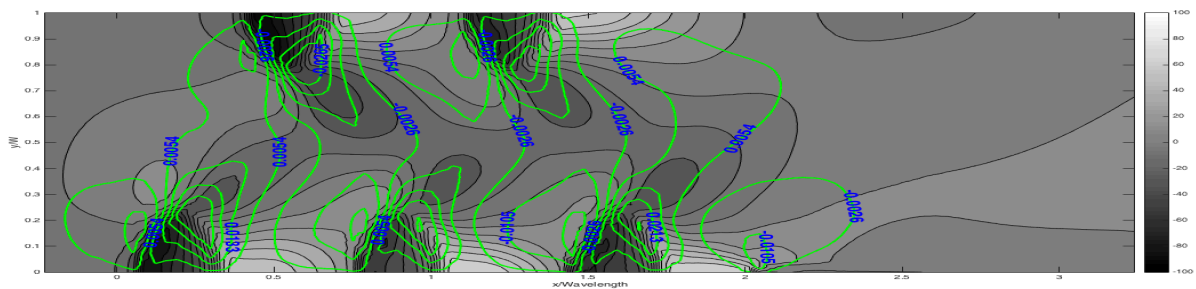
And if the portion of width to patch diameter becomes more than $4X_w/D$

- The main channel mostly acts as two smaller channel, and creation of islands in the mid-channel is possible.
- During the flood seasons the central parts can be help to convey the extra flow.
- As the ratio increases deposits increases and erosion approximately remain constant

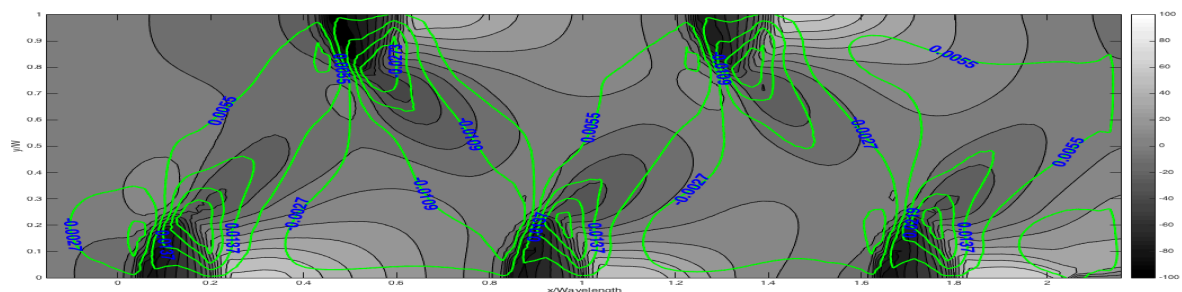
7.5 Effects of non dimensional longitudinal distance (L/D) in a channel

As far as the W/D ratio is equal or less than X_w/D , the diverted flow from one side of the channel can impact the opposite side. On the other hand, the longitudinal interval between patches of stems changes the flow field and subsequently the bed

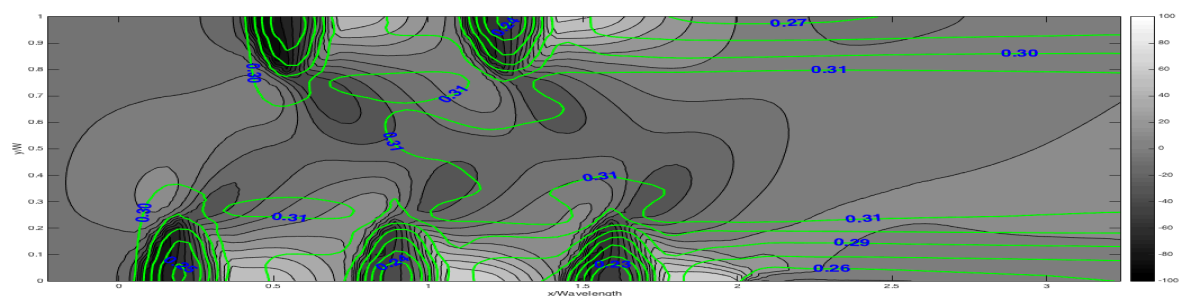
profile. For investigation of effects of longitudinal intervals between the patches, a set of numerical simulations are accomplished in the channel with 1 m width and 30 m length. 5 Patches of 50cm diameter with density of 0.05 are installed along the both sides of the channel with different intervals from $L=0.75$ m to $L=6.75$ m (from upstream edge of a patch to the upstream edge of the next patch) (table 7.2). Due to experimental results, the configuration with intervals of 1.45 m (which is equal to X_L) has been considered as a reference to investigate the bed profile pattern. The result of components of the velocity distributions over bed elevations for typical tests with both more and less longitudinal intervals than the reference test have been illustrated in figures 7.16 (a to d) and 7.17 (a to i). It should be mentioned that the same results for the reference test has been shown in figure (7-14b).



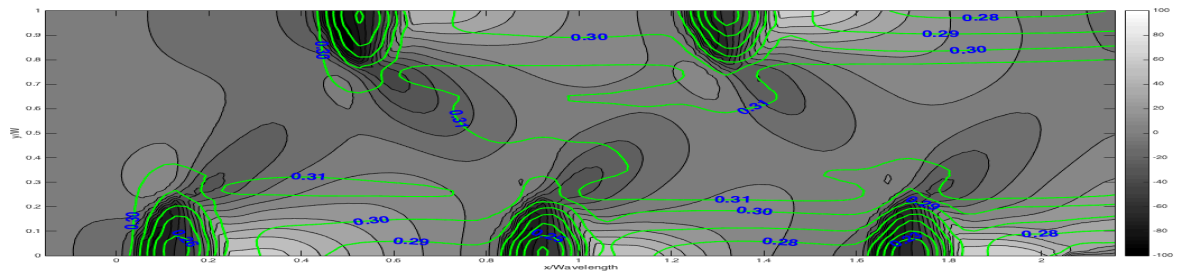
(a)



(b)

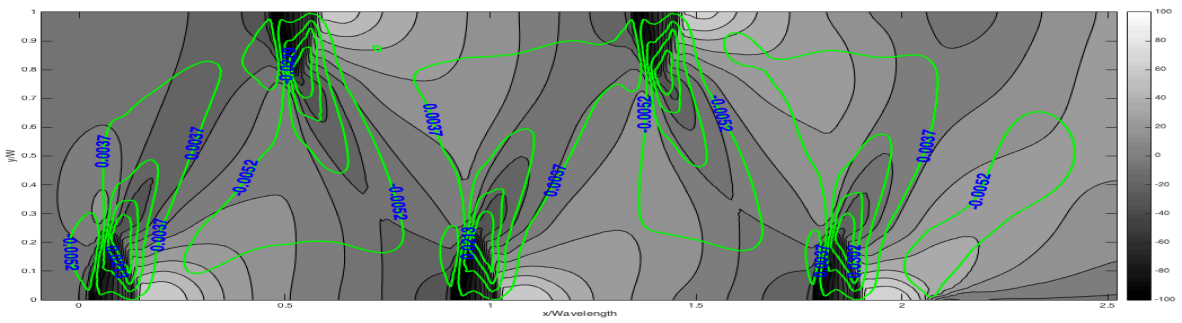


(c)

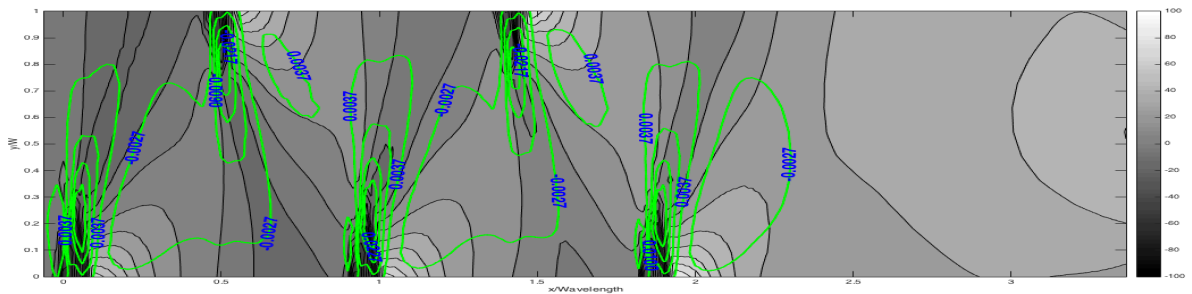


(d)

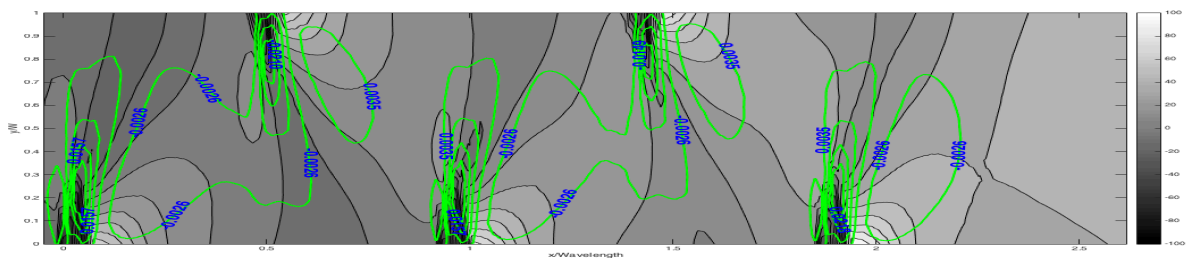
Figure 7.16. Bed profile and distribution of components of the velocity-(a): Transverse velocity $X_L=0.75$; (b): Transverse velocity $X_L=1.25$; (c): Streamwise velocity $X_L=0.75$; d: Streamwise velocity $X_L=1.25$



(a)



(b)



(c)

$X_L=1.75$; (f): Streamwise velocity $X_L=2.75$; (g): Streamwise velocity $X_L=3.75$; (h): Streamwise velocity $X_L=5.25$

In figure 7.16, as it was expected, by decreasing of the longitudinal interval between the patches, the mutual interaction between the vegetated areas increases. In contrast, the increase of the interval would cause less interaction both from the patches of the opposite and the same side. Consequences of the mutual interaction would change the velocity distribution and turbulence in the channel and ultimately modify the bed pattern. When the longitudinal intervals are shorter than X_L , the scour and deposit regions behind the patches interfere with each other and provide different bed forms than meander beds. In fact, if one of the patches is considered (except two first patches), the scour region which is created by the opposite vegetated area and the deposit region that is accumulated by the upstream patch interfere with the patch and as the result a narrower and deeper channel can be formed. But as the longitudinal interval enhances, the mutual impacts of the vegetated areas would decrease, and when this interval exceeds from almost three times of X_L , the mutual influence can be neglected and the patches act separately. This fact can also be proven by investigating the non-dimensional scoured area within one meander wave length (figure 7.18).

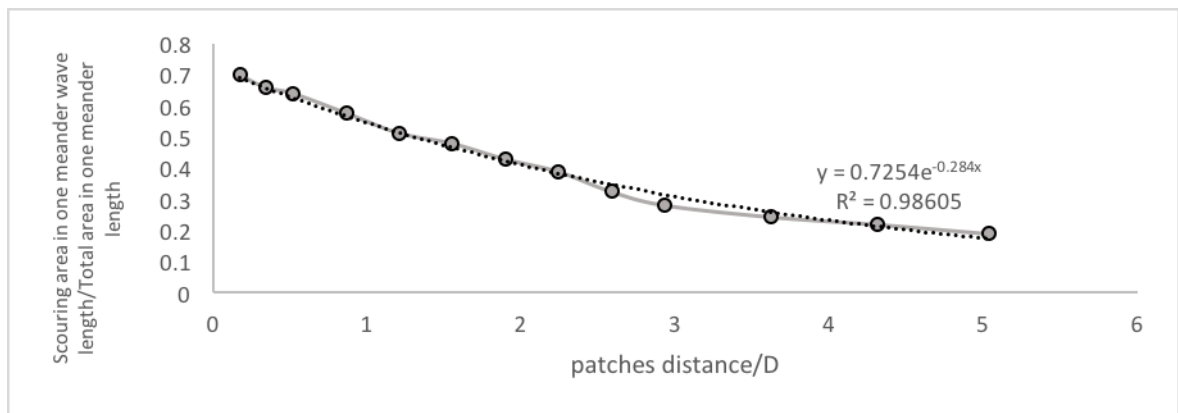
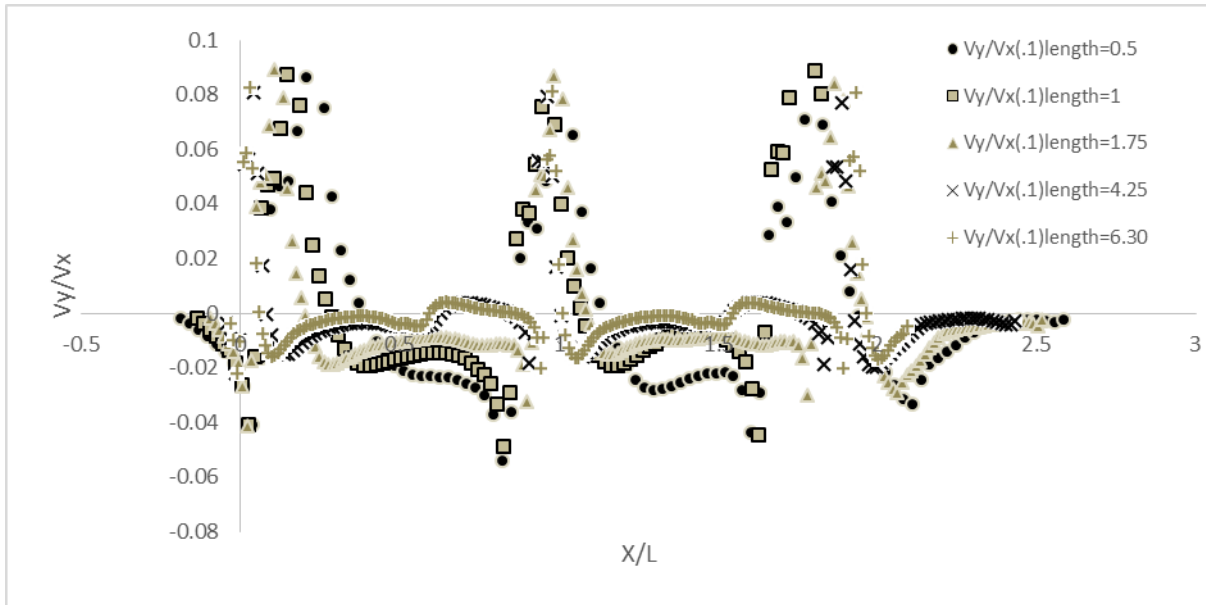
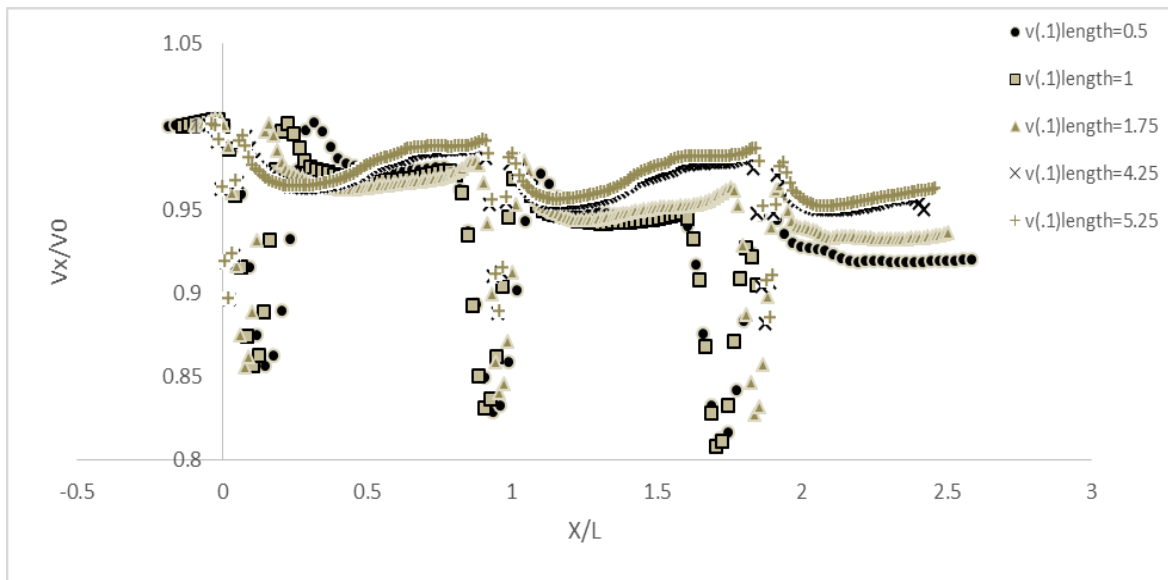


Figure 7.18. Effects of longitudinal intervals on scouring area

By increasing the ratio of longitudinal interval to the longitudinal effective length, the non-dimensional scoured area for one meander wave length decreases exponentially and the rate of the changes become constant for the larger ratios ($L > 3X_L$) which shows that the mutual effect of the vegetated regions is negligible. For more investigation about the velocity distribution, the longitudinal profile of the components of the velocity along $y/w=0.1$ have been plotted in figure 7.19.



(a)



(b)

Figure 7.19. Longitudinal components of the velocity along a channel with $y/w=0.1$ -(a): Transverse velocity; (b): Streamwise velocity

For the tests with shorter intervals increase of the turbulence would causes more scouring between the patches and in response, the depth of the flow increases. but as it is shown in figure 7.19 a, the transverse velocity shows higher fluctuations because of the prompt effects of the patch on the opposite side. In addition, the highest rate of transverse velocity has not effected by the longitudinal spacing between the patches and it shows that the diversion of the flow is not a function of the longitudinal intervals between the vegetated zones. As the intervals become longer, enough space would be provided behind the patches for the flow to

retrieve. However, changes of water depth control the velocity magnitude and as it is shown in figures 7.16 and 7.17 longitudinal intervals between the patches just change the velocity distribution and bed profile while the range of velocity magnitude is almost remains constant.

Given each of this planting provides the preferable river channels with it's special morphological and ecological benefits. Combining these criteria with the effects of the longitudinal intervals between the patches can also help to increase the efficiency of planting. In a channel with $W/D < X_w/D$, when L/D ratio is equal to X_w/D the meander pattern creates on channel bed, but as the L/D ratio becomes less than X_L/D then erosion region within the channel increases and subsequently the depth of the water increases and due to the deposit region behind the patches, narrower and deeper channels can be shaped. As the L/D ratio becomes larger than X_L/D , the mutual interaction between the patches decreases and when this portion becomes almost $3X_L/D$, the mutual effects of the patches can be neglected.

On the other hand, when $W/D > X_w/D$, the scouring caused by the opposite side patches has less effects on the patch and as W/D becomes larger, the mutual effects of the opposite side patch becomes negligible. Also in these cases (if $L/D < 3X_L/D$), the deposit regions of upstream vegetated part may have a direct effect on the patch.

In previous chapters it is mentioned that the vegetation density is a critical parameter which determines flow deflection. As the flow deflection increases, velocity of flow promotes along the outer edges of a patch in the main unvegetated part of the channel. Higher flow velocity in these regions provides stronger vortices and increase erosion. According to the position of patches, the new distinct erosion and deposition pattern in the main unvegetated part of the channel would lead to changes of the channel bed slope. A comparison has been made on the average bed slope of the unvegetated central part of the experimental channel just before and after the installation of patches of vegetation. As expected, increasing of the vegetation density in tests with $W/D = X_w/D$ and $L/D = X_L/D$, causes the linear enhancing of the average bed slope (figure 7.20). Because the vegetation zones in these cases are located immediately at the end of the effective domain of the upstream patch and there is a continuous erosion pattern in the main channel. However, the trend of increasing of the slope accelerates and decelerates due to the position of vegetation zones. For example, in tests with $W/D < X_w/D$ and $L/D = X_L/D$, the effect of vegetation density on increasing of the average bed slope intensify, while in tests with lower ratio of W/D and the same longitudinal intervals it decelerates (figure 7.20 a.). The increasing of the average bed slope in the

investigated tests is mainly because of the mutual interaction of vegetation zones and the acceleration and deceleration rate of it is due to the intensity of the interaction.

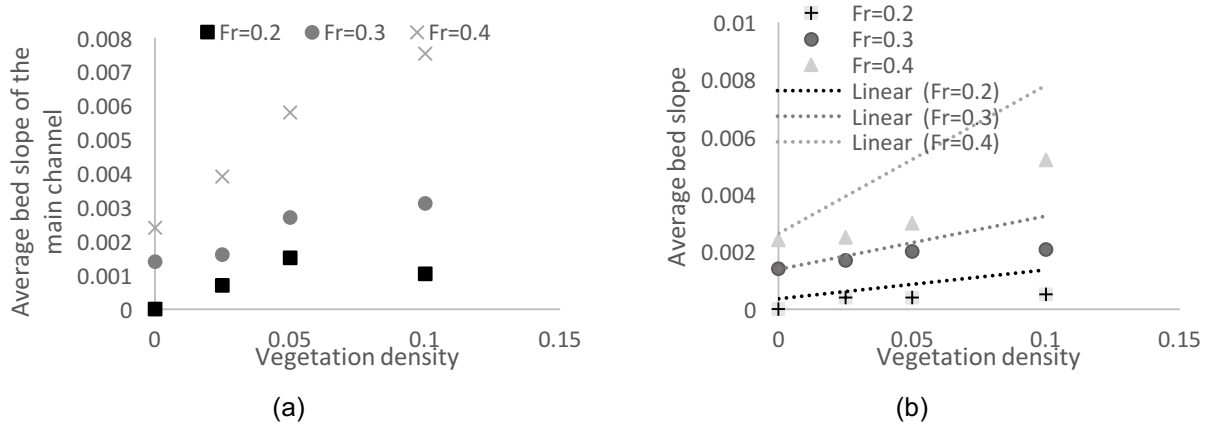


Figure 7.20. (a). Average bed slope of the central part of the experimental channel before and after the installation of patches of vegetation; (b): Comparison of bed slope of the central part and meander part

As the meander pattern is provided through all of the tests in figure 7.20a, further analysis has been done on the average bed slope of the meander pattern, which contains almost the minimum elevation of each cross section. The results show the same trend in increasing of the bed slope by promotion of vegetation density (figure 7.20b).

7.6 Estimation of meander pattern

Sinuosity is the consequence of minimum expenditure of energy and defined as a ratio of longitudinal length to lateral length (Langbein and Leopold 1966, Williams 1986). Sinuosity is directly related to meander geometry characteristics and since it is based on easily observable and interpreted patterns, it can be used to delineate morphologies.

Considering the explained results for the cases with the W/D ratio equal or less than the X_w/D , the bed morphology tends to change to meander shape. Due to this fact and according to the defined relations between effective lengths and the vegetation density, estimation of meander pattern is achievable.

In order to estimate a general pattern for the meandering of the bed, it is assumed that the modified meander bed follows a sinuous pattern. Considering $y=C_1\sin(C_2x)$ for the meander pattern, which is a consequence of introducing of patches of vegetation on bed morphology in cases with W/D less than X_w/D , then C_1 is

proportional to $X_w/2$ and C_2 is proportional to the reverse of X_L and due to the equation 5.6 and 5.7, the following formula can be concluded to estimate the meander pattern of the channel:

$$y=1.57D(\Omega^{0.138})\text{Sin}(x/(0.5D\Omega^{-0.592})) \quad 7.1$$

The equation 7.1 concerns density of the patch and specify the required width for creation of the meander bed profile. The proposed formula is on the basis of the installation of a finite patch of stems in the straight channel. It exploits the longitudinal and lateral affected lengths for the patches with different stem densities and predicts the meander pattern. The formula is then validated by 3 different tests with mutual patches of stems in which the initial and upstream boundary condition is constant but the channel is equipped by 3 various patches of different sizes and densities of stems. The minimum elevation of the bed in different cross section along the channel is used to extract and track the experimental meander bed pattern. Figure 7.21 till 7.23 shows the comparison of graphical experimental results for a single meander wave-length with the same results that calculated by the equation 7.1. The size and position of patches are also illustrated in the same figures. The x-axis is normalized by the patch diameter and the y-axis is normalized by the width of the flume.

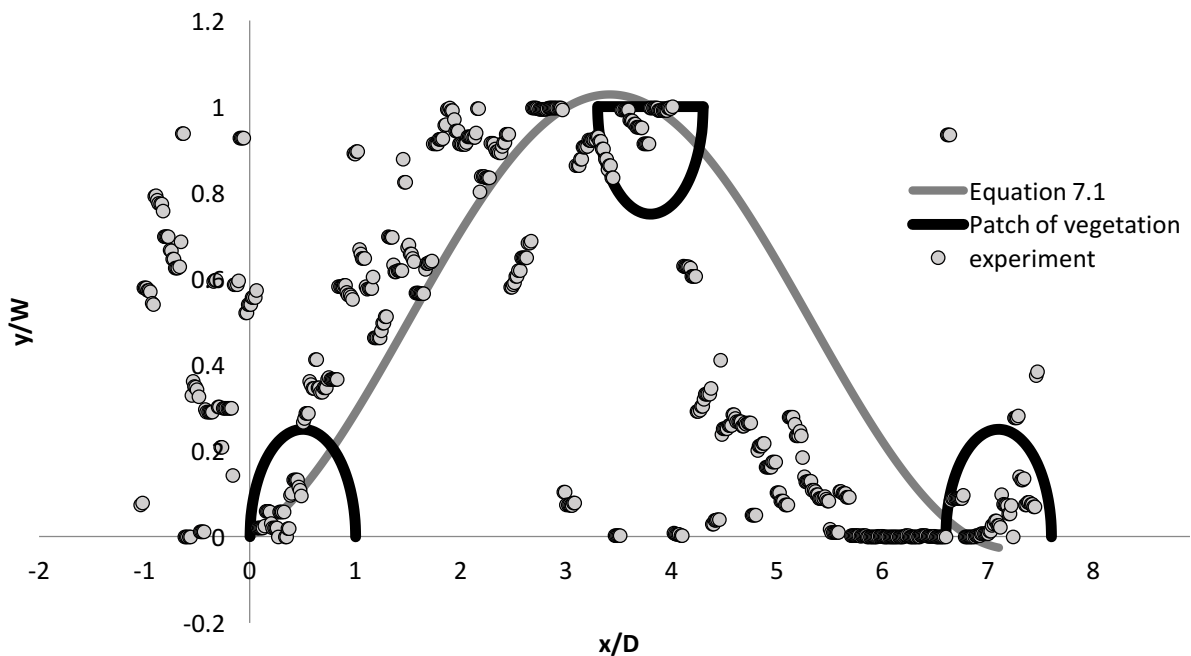


Figure 7.21. Comparison of the meander bed forms along one meander wave-length, $D=0.56\text{m}$, $\Omega_v=0.025$, $Fr=0.3$

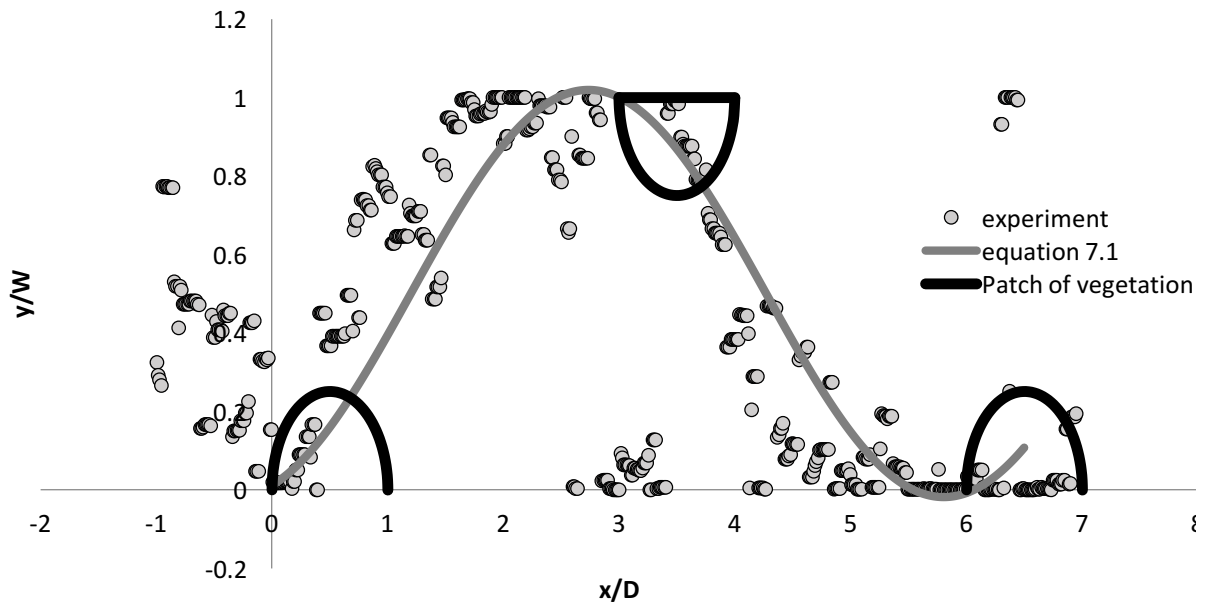


Figure 7.22. Comparison of the meander bed forms along one meander wavelength, $D=0.5\text{m}$, $\Omega_v=0.05$, $Fr=0.3$

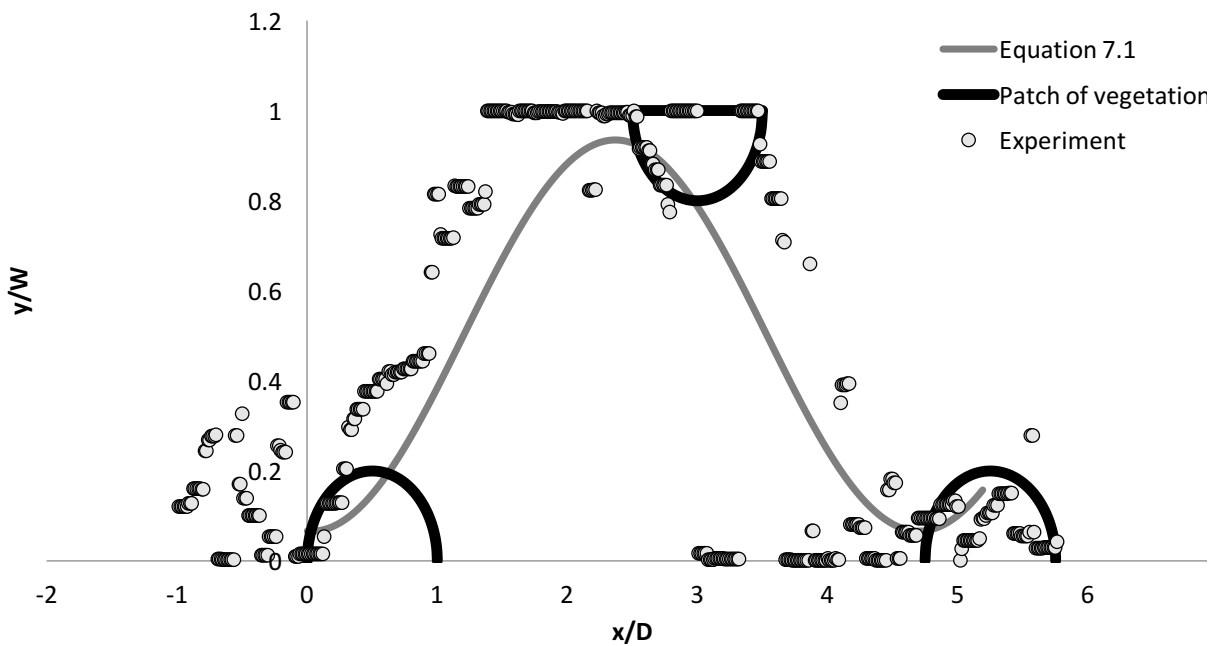


Figure 7.23. Comparison of the meander bed forms along one meander wavelength, $D=0.38\text{m}$, $\Omega_v=0.1$, $Fr=0.3$

Overall, the comparison of results of different tests in figure 7.21 to 7.23 ensures that the equation 7.1 can predict the meander bed in a channel with mutual patches of vegetation. It can be clearly seen that for the considered sizes of patches, increasing of the patch density decreases the meander wavelength and the results of the proposed formula validate the consideration of these

facts. So that, the result of equation 7.1 can be used to investigate the effects of the mutual patches of stems in a channel.

However, in channels with ($W/D \leq X_w/D$) the most important effective parameter of a patch is the density of stems. A small change in vegetation density results in flow sinuosity and consequently the bed meander profile. Using the equation 7.1, to clarify the influence of density of the patch, different range of vegetation density is considered for patches with constant size ($D=0.5\text{m}$) and the calculated bed meander patterns are compared in figure 7.24.

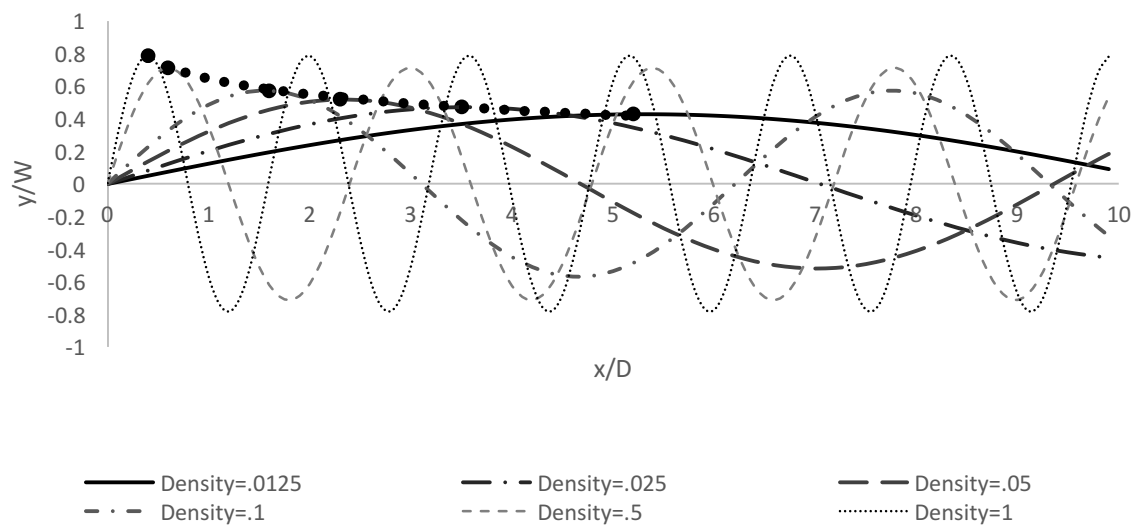


Figure 7.24. Effects of vegetation density on meander pattern

It is assumed that the bed profile in an un-vegetated straight channel almost follows straight lines, but introducing of permeable patches of vegetation changes the straight lines to sinus lines. The line which contains the points of highest flow depth is also considered as the center of the meander bed. In figure 7.24, the black line is the meander pattern of a bed which is created by the lowest magnitude of vegetation density and the dotted gray line shows the meander wave-length which is created by the highest vegetation density. As it was expected, increasing of the vegetation density provide shorter meander wave-length and have more lateral impacts on bed profile. In the other word, the same size denser patches of stems increases sinuosity of flow and cause longer scour holes across the channel. One of the striking features to comment on in meander patterns in figure 7.24 is that even though increases of density enhance the lateral impact exponentially, density promotion has greater impacts on meander wavelength due to the ranges of the densities. For the patches with lower density ($\Omega_v < 0.5$), however increasing of the density reduce the meander wavelength dramatically, while for higher densities

($\Omega_v > 0.5$) the ranges of changes is declined. In figure 7.24 the black dotted line connect the lateral affected lengths of different densities to illustrate the lateral effects of density. For example, by increase of the density from 0.0125 to its double and from 0.5 to its double, the influences of the patch promote up to 10 percent laterally for both of them. But, the impacts of the density on the meander wave length for the same cases are much more for the lower density. To conclude, in restoration projects, considering the reason of changes of the straight bed to meander bed, and due to the physical condition of the site, the size and density of the patch can be determined by the proposed formula.

7.7 Conclusion

The results of the study of a single patch of stems in the first part of experiments show that density and size of the patch has significant impact on velocity distribution and bed morphology. However, in study of a channel with mutual patches of stems, achieving the expected meander pattern of scour and deposition along the scanned area proves the capability of results of the estimation of the lateral and longitudinal effective lengths.

Generally, installation of patches of stems with the proposed intervals (X_w, X_L) on both sides of the channel causes certain changes in velocity distribution and bed topography, which can be classified as follows:

- Acceleration and deceleration of the velocity along the central part of the channel with general enhancement of the velocity magnitude due to changes of the bed profile and accumulation of sediment behind the vegetation zones.
- Deceleration and acceleration of the velocity along the bank sides of the channel with gradual reduction of the velocity magnitude after diversion of the flow to the central part and penetration of the rest of flow into the vegetation region.
- Decreasing of the required length for acceleration and recovering the velocity of the flow at the wake of the patch comparing to a simple patch of stems.
- Constant reacceleration of the transverse velocity in the mid-channel on the opposite direction, which provides a meander pattern in velocity distribution and consequently in bed topography (In case of sediment transportation).

-
- Negligible transverse velocity at the wake of each patch due to less mutual effects of a patch on the areas close to the opposite banks.
 - Extension of the scour region across the channel to the upstream edges of the opposite patch and creation of the meander pattern of scour and deposition on bed profile.

The computational model also can relatively capture the velocity and bed profiles in the vegetated channel and it is used to cover the limitations of experimental flume and investigate the effects of non-dimensional W/D and L/D on bed profile. Both of the W/D and L/D ratios are keys to figuring out the fate of sediments within a channel with side patches of vegetation.

In the channelized rivers, the W/D ratio is a sensitive indicator of sediment transport and has significant effects on channel morphology. Following the introducing of patches of vegetation in the channel and Consideration of the different values of W/D ratio shows it is necessary for prediction of changes in channel bed forms. Increasing of the ratio influence the main part of flow and decreases the mutual effects of the patches and this causes changes in velocity distribution and bed profiles.

For lower ratios of W/D , the scouring extends into the opposite side providing a meander bed profile on the channel bed. If the W/D ratio were to increase, it would lead to the meander bed forms converting into a narrower and deeper channel. This would eventually cause changes to two smaller channels or a channel with islands in the mid-channel. As the W/D ratio increases, the effect of vegetation finites to the bank of the channel also providing with a local erosion around each patch of vegetation. The results based on the varying ratios of W/D are then used to prepare some criteria to predict the bed profiles as a consequence of the implementation of the patches of vegetation and they can be useful in related river restoration projects.

On the other hand, the longitudinal intervals between patches of stems influence the flow field and the bed profile. Generally, the increase and decrease of the L/D causes less and more interaction both from the patches of the opposite and the same side respectively. Consequences of the mutual interaction impact the velocity distribution and turbulence in the channel and ultimately modify the bed topography.

For lower L/D , the scour and deposit regions around each patch interfere with the next one and provide different bed forms than meander beds. In the other word, the created scour region by the opposite patch and the upstream deposit region by the upstream same side patch interfere with the patch and as the result a narrower

and deeper channel can be formed. For higher L/D ratios, the mutual impacts of the vegetated areas decrease and particularly, the scoured area for one meander wave length decreases. When the longitudinal interval exceeds from certain amount the mutual influence is negligible and the patches act separately. The mentioned a certain amount is quantified by X_L and some criteria are proposed to predict the channel bed forms.

Collecting whole the data, in cases with eligible condition of meander bed forms, the general meander pattern is estimated by the proposed formula. This formula can be useful for restoration projects.

8 References

- Afzalimehr, H., Dey, S. 2009. Influence of bank vegetation and gravel bed on velocity and Reynolds stress distributions. *J. Sediment Research*. 24. 236-246.
- Antonarakis, A.S., Richards, K.S., Brasington, J., Bithell, M., Müller, E. 2009. Leafless roughness of complex tree morphology using terrestrial lidar. *J. Water Resources Research*. 45. 1-14.
- Armanini, A., Cavedon, V., Righetti, M. 2010. Sediment transport processes in vegetated streams. 1st European IAHR Congress, Edinburgh.
- Armanini A., Cavedon V., Righetti M. 2010 b. Sediment transport in vegetated rivers, Submitted to *J. Water Resources Research*.
- Arens, S. M. Baas, A., Boxel, J.V. 2001. Influence of reed stem density on foredune development. *J. Earth Surface Protection Landforms*. 26. 1161-1176.
- Baptist, M. J., 2005. Modelling Floodplain Bio-geomorphology. Ph.D. thesis, Delft University of Technology.
- Beeson C.E., Doyle P.F. 1995. Comparison of bank erosion at vegetated and non-vegetated channel bends. *J. Water Resources Bulletin*. 31. 983–990.
- Bennett, S., Wu, W., Alonso, C.V., Wang, S.Y. 2008. Modeling fluvial response to in- stream woody vegetation: implications for stream corridor restoration. *J. Earth Surface Process Landforms*. 33. 890-909.
- Bennett, S. 2004. Effects of emergent riparian vegetation on spatially averaged and turbulent flow within an experimental channel. In *Riparian Vegetation and Fluvial Geomorphology, Water Science Applications Series*, Bennett SJ, Simon A (eds), vol. 8. 29–41.
- Bennett, S., Pirim, T., Barkdoll, B. 2002. Using simulated emergent vegetation to alter stream flow direction within a straight experimental channel. *J. Geomorphology*. 44.115– 693.
- Bouma, T.J., Van Duren, L.A., Temmerman, S., Claverie, T., Blanco-Garcia, A., Ysebaert, T., Herman, P.M.J. 2007. Spatial flow and sedimentation patterns within patches of epibenthic structures: Combining field, flume and modeling experiments. *J. Continental shelf Research* 27, 1020-1045.

-
- Bouteiller, C.L., Venditti, J. 2014. Vegetation-driven morphodynamics adjustments of a sand bed. *Geophysical Research Letters*.41. 1-8.
 - Bridge, J.S. 2003. *River and Floodplains: Forms, Processes, and Sedimentary Record*. Oxford. UK: Blackwell Pub.
 - Brookes, A.S., Brierley, G.J. 2004. Farming realistic river rehabilitation targets in light of altered sediment supply and transport relationships: lessons from East Gippsland, Australia. *J. Geomorphology*. 58. 107-123.
 - Carmo, B.S., Shewin. S.J., Bearman, P.W., Willden, R.H.J. 2011. Flow-induced vibration of a circular cylinder subjected to wake interference at low Reynolds number. *J. Fluids and Structures*.1-32.
 - Chen, S.Ch., Chan, H.Ch., Li, Y.H. 2012. Observations on flow and local scour around submerged flexible vegetation. *J. Advances in Water Resources*. 43. 28-37.
 - Cheng, L., Yong-ming, Sh. 2008. Flow structure and sediment transport with impacts of aquatic vegetation. *J. Hydrodynamics*. 20. 461-468.
 - Cheng, M., Whyte, D.S., Lou, J. 2007. Numerical simulation of flow around a square cylinder in uniform-shear flow. *J. Fluid and Structures*. 23. 207-226
 - Coulthard, T. J. 2005. Effects of vegetation on braided stream pattern and dynamics. *J. Water Resources Research*. 41.
 - Darby, S. E. 1999. Effect of riparian vegetation on flow resistance and flood potential. *J. Hydraulic Engineering*. 125. 443-454.
 - Dargahi, B. 1987. Flow field and local scouring around a cylinder. *Bullten. 137. Research. Institute Tech. Hydraulic Lab., Stockholm , Sweden*.
 - Dargahi, B. 1989. The turbulent flow field around a circular cylinder. *J. Experiments in Fluids* 8. 1-12.
 - Dargahi, B. 1990. Controlling mechanism of local scouring. *J. Hydraulic Engineering* 116. 1197-1214.
 - Dabney, S. M., McGregor, K. C., Grissinger, E. H., Foster, G. R. 1993. *Vegetative Barriers for Runoff and Sediment Control*. *J. Integrated Resources Management and Landscape Modification for Environmental Protection*. 60-70.
 - Downs, P.W., Thorne, C.R. 2000. Rehabilitation of a lowland river: reconciling flood defense with habitat diversity and geomorphological sustainability. *J. Environmental Management* 58. 249–268.

-
- Debnath, K., Manik, M.K., Mazumder, B.S. 2012. Turbulence statistics of flow over scoured cohesive sediment bed around circular cylinder, *J. Advances in Water Resources*. 41. 18–28.
 - Deltares, 2006. Delft3D User Manual, Delft: Deltares.
 - Deltares, 2010. Delft3D User Manual, Delft: Deltares.
 - Dittrich, A., Järvelä, J. 2006. Flow-vegetation-sediment interaction. *J. Water Engineering Research* 6. 123–130.
 - Dosskey, M.G., Vidon, P., Gurwick, N.P., Allan, C.J., Duval, T.P., Lowrance, R. 2010. The role of riparian vegetation in protecting and improving chemical water quality in streams. *J. American Water Resources Association*. 46. 261-277.
 - Edwards, P.J., Kollmann, J., Gurnell, A.M., Petts, G.E., Tockner, K., Ward, J.V. 1999. A conceptual model of vegetation dynamics on gravel bars of a large Alpine river. *J. Wetlands Ecology and Management*. 7. 141–153.
 - Engelund, F., Hansen. E. 1967. A monograph on sediment transport in alluvial streams. Teknisk Forlag,. Copenhagen
 - Everard, M., Quinn, N. 2015. Realizing the value of fluvial geomorphology. *J River Basin Management*, 13:4, 487-500.
 - Fischenich, J.C. 1997. Hydraulic impacts of riparian vegetation. Technical Report EI-97-9.
 - Follett, E.M., Nepf, H.M. 2012. Sediment patterns near a model patch of reedy emergent vegetation. *J. Geomorphology*. 179. 141-151.
 - Ganoulis, j. 2003. Risk-based floodplain management: A case study from Greece. *J. River Basin Management*. 1. 41-47.
 - Gerstner, C.L. 1998. Use of substratum ripples for flow refuging by Atlantic cod, *Gadus morhua*. *J. Environmental Biology of Fishes*. 53. 455-460.
 - Ghisalberti, M., and H. Nepf. 2006. The structure of the shear layer in flows over rigid and flexible canopies. *J Environmental Fluid Mechanics*. 6. 277–301.
 - Ghisalberti, M., and H. Nepf. 2002. Mixing layers and coherent structures in vegetated aquatic flows. *J. Geophysical Research* 107, 1-11.
 - Gurnell. A. 2013. Plants as river system engineers. *Earth Surf. Process. Landforms* 39, 4–25.

-
- Gurnell A., Petts G. 2006. Trees as riparian engineers: the Tagliamento River, Italy. *J. Earth Surface Processes and Landforms* 31. 1558–1574.
 - Gurnell, A.M., Petts, G.E., Hannah, D.M., Smith, B.P.G., Edwards, P.J., Kollmann, J., Ward, J.V. and Tockner, K. 2001. Riparian vegetation and island formation along the gravel-bed Fiume Tagliamento, Italy. *J. Earth Surface Processes and Landforms* 26. 31-62
 - Harrison, S.S.C., Harris, I.T. 2002. The effects of bankside management on chalk stream invertebrate communities. *J. Freshwater Biology*. 47. 2233-2245.
 - Hendriks, I. E., van Duren, L. A. 2006. Turbulence levels in a flume compared to the field: Implications for larval settlement studies. *J. of Sea Research* 55. 15-29.
 - Hey, R.D., Thorne, C.R. 1986. Stable channels with mobile gravel beds. *J. Hydraulic Engineering*. 112(8): 671–689.
 - Hicks, D.M., Shankar, U., Duncan, M.J., Rebuffe, M., Aberle, J. 2006. Use of remote-sensing technology to assess impacts of hydro-operations on a large, braided, gravel-bed river: Waitaki River, New Zealand. IAHS Special Publication, Gravel Bed Rivers.
 - Huai, W., Hu, Y., Zeng, Y., Han, J. 2012. Velocity distribution for open channel flows with suspended vegetation. *J. Advances in Water Resources*. 49. 56–61.
 - Huang, H.Q., & Nanson, G.C. 1997. Vegetation and channel variation; a case study of four small streams in southeastern Australia. *J. Geomorphology* 18. 237–249.
 - Hupp, C.R., Bazemore, D.E. 1993. Temporal and spatial patterns of wetland sedimentation, West Tennessee. *J. Hydrology*. 141. 179-196.
 - Ikeda, S., Izumi, N. 1990. Width and depth of self-formed straight gravel rivers with bank vegetation. *J. Water Resources. Research*. 26. 2353–2364.
 - Ishikawa, Y., Sakamoto, T., Mizuhara, K. 2003. Effect of density of riparian vegetation on effective tractive force. *J. Forest Research* 8. 235–246.
 - Jarvela, J., Aberle, J., Dittrich, A., Rauch, H.P., Schnauder, I. 2006. Flow-vegetation-sediment interaction: Research challenges. *River Flow 2006-Ferreira, Alves, Leal & Cardoso*.

-
- Jarvela, J. 2005. Effect of submerged flexible vegetation on flow structure and resistance. *J. Hydrology* 307. 233–241.
 - Jarvela, J. 2004. Determination of flow resistance caused by non-submerged woody vegetation. *Inter. J. River Basin Management* 2. 61–70.
 - Jeffries R., Darby, S.E., Sear, D.A. 2003. The influence of vegetation and organic debris on flood-plain sediment dynamics: case study of a low-order stream in the New Forest, England. *J. Geomorphology* 51. 61–80.
 - James, C.S., Birkhead, A.L. Jordanova, A.A., O'Sullivan. J.J. 2004. Flow resistance of emergent vegetation. *J. Hydraulic Research* 42. 390–398.
 - Kadlec, R. 1990. Overland flow in wetlands: Vegetation resistance. *J. Hydraulic Eng.*, 116, 691-707.
 - Kirkby, M. 1990. The landscape viewed through models. *J. Geomorphology Supply* 79. 63-81.
 - Kiya, M., Tamura, H., Arie, M. 1980. Vortex shedding from a circular cylinder in moderate-Reynolds-number shear flow. *J. Fluid Mechanics* 101. 721-735.
 - Klaassen, G.J. 2002. Novel approaches in river engineering. In D. Bousmar & Y. Zech (eds), *River Flow 2002*: 27–43. Lisse: Swets & Zeitlinger.
 - Klopstra, D., Barneveld, H. J., Van Noortwijk J. M., Van Velzen, E.H. 1997. Analytical model for hydraulic roughness of submerged vegetation. In *The 27th IAHR Congress, San Francisco, 1997; Proceedings of Theme A, Managing Water: Coping with Scarcity and Abundance*, pages 775-780. American Society of Civil Engineers (ASCE), New York.
 - Kumar, A., Kothiyari, U.C. 2012. Three-dimensional flow characteristics within the scour hole around circular uniform and compound piers, *J. Hydraulic Engineering*, 138. 420–429.
 - Li, R.M., Shen, H.W. 1973. Effect of tall vegetation on flow and sediment. *J. Hydraulics Division* 99. 793–814.
 - Lopez, F., Garcia, M.H. 1998. Open-channel flow through simulated vegetation: Suspended sediment transport modeling. *J. Water Resources Research*. 34. 2341–2352.
 - Luhar, M., Rominger, J., Nepf, H. 2008. Interaction between flow, transport and vegetation spatial structure. *J. Environmental Fluid Mechanics*. 8, 423-429

-
- Maghaddam, F., Kouwen. N. 1997. Non-rigid non-submerged vegetative roughness on floodplains. *J. Hydraulic Engineering*. 123.
 - Meire, D., Kondziolka, J., Nepf. H.M. 2014. Patches in side-by-side configuration: A description of the flow and deposition fields. *River Flow 2014*. Taylor & Francis Group, London. 401-408.
 - Neary, V.S., Bennett, S.J., Diplas, P. 2012. Effects of vegetation on turbulence, sediment transport, and stream morphology. *J. Hydrulic Engineering*. 138. 765-776.
 - Neary, V.S. 2009. Physical habitat requirements for Bivalvia:Unionidea: With a focus on recommendations for habitat enhancement and restoration of selected unionids and their host fish within Buck Creek. Report to Kentucky Fish and Wildlife Service and the Nature Conservancy. Southeastern Aquatic Restoration Program (SARP).
 - Nelson, J.M., Shreve, R.L., McLean, S.R. Drake, T.G. 1995. Role of near-bed turbulence structure in bed load transport and bed form mechanics. *J. Water Resources Research*, 31. 2071-2086.
 - Nepf, H.M. 1999. Drag, turbulence, and diffusion in flow through emergent vegetation. *J. Water Resources Research* 35. 479–489.
 - Nepf, H.M. Sullivan, J.A., Zavistoski, R.A. 1997. A model for diffusion within emergent vegetation, *J. Oceanography* 42. 1735-1745.
 - Nezu, I., Nakagawa, H. 1993. Turbulence in open channel flows, IAHR Monograph, Balkema, Rotterdam.
 - Nicolle, A., Eames, I. 2011. Numerical study of flow through and around a circular array of cylinders. *J. Fluid Mechanics*. 679. 1-31.
 - Perona, p., Camporeale, C., Perucca, E., Savina, M., Molnar, P., Burlando, P., Ridolfi, L. 2009. Modelling river and riparian vegetation interactions and related importance for sustainable ecosystem management. *J. Aquatic Science*. 71. 266 – 278
 - Pietsch, TJ, Nanson GC. 2011. Bankfull hydraulic geometry; the role of in-channel vegetation and downstream declining discharges in the anabranching and distributary channels of the Gwydir distributive fluvial system, southeastern Australia. *Geomorphology* 129. 152–165.
 - Platts, W., Nelson, R.L. 1985. Stream habitat and fisheries response to livestock grazing and instream improvement structures, Big Creek, Utah. *J. Soil and Water Conservation*. 40, 374-379.

-
- Poggi, D., A. Porporato, L. Ridolfi, J. D. Albertson, Katul G. G. 2004. The effect of vegetation density on canopy sub-layer turbulence, *J. Boundary Layer Meteorology*. 111 565–587.
 - Pollock, M. M., Naiman, R. J. Hanley, T. A. 1998. Plant species richness in riparian wetlands-A test of biodiversity theory. *J. Ecology*. 79. 94–105.
 - Righetti, M., Armanini, A. 2002. Flow resistance in open channel flows with sparsely distributed bushes. *J. Hydrology* 269. 55–64.
 - Rominger, J. T., Lightbody, A.F., Nepf H.M. 2011. Effects of added vegetation on sand bar stability and stream hydrodynamics. *J. Hydraulic Engineering*. 136. 994–1002.
 - Rowntree, K.M. Dollar, E.S.J. 1999. Vegetation controls on channel stability in the Bell River, Eastern Cape, South Africa. *J. Earth Surface Processes and Landforms* 24. 127-134.
 - Schlosser, I.J. 1982. Fish community structure and function along two habitat gradients in a headwater stream. *J. Ecological Monographs*. 52. 3395-414.
 - Sear, D.A., Newson, C.L., Throne, C.R. 2003. Guidebook of applied fluvial geomorphology. R and D Technical report FD1914, DEFRA: Flood Management Division, London, UK, 253pp.
 - Sear, D.A. 1994. River Restoration and Geomorphology. *J. Aquatic Conservation-Marine and Freshwater Ecosystems*. 4. 169-177.
 - Seminara, G., Blondeaux, p. 2013. River, Coastal and Estuarine Morphodynamics. Springer Science & Business Media.
 - Shi, Z., Pethick, J., Pye, K. 1995. Flow structure in and above the various heights of a saltmarsh canopy: A laboratory flume study, *J. Coastal Research*, 11, 1204-1209.
 - Shields, A. 1936. Anwendung der Ähnlichkeitsmechanik und der Turbulenzforschung auf die Geschiebebewegung; In *Mitteilungen der Preussischen Versuchsanstalt für Wasserbau und Schiffbau*, Heft 26
 - Shimizu, Y., Tsujimoto, T. 1997. Numerical analysis of turbulent open-channel flow over a vegetation layer using a k-e turbulence model. *J. Hydroscience and Hydraulic Engineering*. 11. 57–67.

-
- Smagorinsky, J. 1993. Large eddy simulation of complex engineering and geophysical flows, in *Evolution of Physical Oceanography*, edited by B. Galperin, and S. A. Orszag, pp. 3-36. Cambridge University Press.
 - Specht, F.-J. 2002. Einfluß von Gerinnebreite und Uferbewuchs auf die hydraulisch-sedimentologischen Verhältnisse naturnaher Fließgewässer. Mitt. des Leichtweiß-Instituts für Wasserbau, Heft 153. TU Braunschweig.
 - Stone, B.M., Hung, T.S. 2002. Hydraulic resistance of flow in channels with cylindrical roughness. *J. Hydraulic Engineering* 128. 500–506.
 - Tal, M., Paola, C. 2007. Dynamic single-thread channels maintained by the interaction of flow and vegetation. *J. Geology* 35. 347–350.
 - Tanino, Y., Nepf, H.M. 2008. Lateral dispersion in random cylinder arrays at high Reynolds number. *J. Fluid Mechanics*. 600. 339–371.
 - Termini, D. 2016. Experimental analysis of the effect of vegetation on flow and bed shear stress distribution in high-curvature bends. *J. Geomorphology*. 274. 1–10
 - Termini, D., Sammartano, V. 2008. Experimental analysis of relations between coherent turbulent structures and formation of bedforms. *J. Hydro-Engineering and Environmental Mechanics* 55. 125-143
 - Thornton, C.I., Abt, S.R., Morris, C.E. & Fischenich, J.C. 2000. Calculating shear stress at channel-overbank interfaces in straight channels with vegetated floodplains. *J. Hydraulic Engineering*. 126. 929–936.
 - Tollner, E.W., Barfield, B.J. Hayes, J.C. 1982. Sedimentology of erect vegetal filters. *J. Hydraulic Div.* 108. 1518–1531.
 - Tsujimoto, T. 1999. Fluvial processes in streams with vegetation. *J. Hydraulic Research*. 37. 789–803.
 - Tsujimoto, T., Kitamura, T., Tsujikura, H. 1998. Development of sand island with vegetation by repetition of flood and low-stage water. 3rd International Conference on Hydro-science and Engineering, Cottbus.
 - Van Rijn, L.C. 1994. Principles of fluid flow and surface waves in rivers, estuaries, seas, and oceans. Aqua publications. Amsterdam. PP395.
 - Vandenbruwaene, W., et al. 2011. Flow interaction with dynamic vegetation patches: Implications for biogeomorphic evolution of a tidal landscape. *J. Geophysics Research*. 116. F01008.

-
- Vargas-Luna, A., Crosato, A., Uijttewaal, W.S.J. 2015. Representing plants as rigid cylinders in experimnets and models. *J. Advances in Water Resources*. 44. 1-18.
 - Vastila, K. 2015. Flow-Plant-Sediment Interactions: Vegetative Resistance Modeling and Cohesive Sediment Processes. Doctoral Dissertations. Aalto University.
 - Watson, C.C., Abt, S.R., Derrick, D. 1997. Willow posts bank stabilization. *J. American Water Resources Association* 33. 293–300.
 - White, K.L., Chaubey, I. 2005. Sensitivity analysis, calibration, and validations for a multisite and multivariable swat model, *J. THE AMERICAN WATER RESOURCES ASSOCIATION. (JAWRA)* 41(5):1077-1089.
 - Wiklund, J.A., Bozinovski, N., Hall, R.I. 2009. Epiphytic diatoms as flood indicators. *J Paleolimnol. J. Paleolimnology*. 44. 25-42.
 - Wilcock, R., Champion, P., Nagels, J., Crocker, G. 1999. The influence of aquatic macrophytes on the hydraulic and physicochemical properties of a New Zealand lowland stream. *J. Hydrobiologia*. 416. 203–214.
 - Wilson, C. A. 2007. Flow resistance models for flexible submerged vegetation, *J. Hydrology*. 342, 213–222.
 - Wilson, L.G. 1967. Sediment removal from flood water by grass filtration. *Transactions of the ASAE*. 10. 35-37.
 - Wu, F.C., Shen, H.W., Chou, Y.J. 1999. Variation of roughness coefficients for unsubmerged and submerged vegetation. *J. of Hydraulic Engineering* 125. 934–942.
 - Yager, E.M., Schmeckle, M.W. 2013. The influence of vegetation on turbulence and bed load transport. *J. Geophysical Research*, 118, 1585-1601.
 - Zong, L., Nepf., H. 2011. Vortex development behind a finite porous obstruction in a channel. *J. Fluid Mechanic*.1-24.
 - Zong, L., Nepf, H.M. 2010. Flow and deposition in and around a finite patch of vegetation. *J. Geomorphology* 116, 363–372.

9 Appendix A: parameter settings

This appendix deals with important parameters used to simulate the flow in the flume.

9.1 Numerical setting

One of the most vital parameters to start the simulation in Delft3D is the time step (Δt). A suitable value as the first estimation of time step for simulations can be calculated using the Courant number, which implies that flow particles should move within less than or equal to two grid cells in each time step size. The Courant number can be defined:

$$CFL = \frac{\Delta t \sqrt{gH}}{\{\Delta x, \Delta y\}} \quad (9-1)$$

Where Δt is the time step, $(\Delta x, \Delta y)$ is the grid size in x and y direction respectively. Courant number should be less than 10. The additional limitation also applies to depth average models:

$$Cr = \frac{u \cdot \Delta t}{\Delta x} < 1 \quad (9.2)$$

According to the grids with dimensions from 1cm to 15 cm, and using the velocity range of 0.15 m/s up to 0.5 m/s, the time steps have chosen less than 1s. Smaller time steps did not significantly affect results. Table 9.1 represents the key parameters used for simulation of the straight channel with patches of vegetation.

Table 9.1 Applied parameters in simulations

Hydrodynamic Parameters		Value
Domain (* .mor), (* .dep)	Grid parameters	Rectangular ($\Delta x/\Delta y < 2$)
	Bathymetry	Smoothed bed
	Layer	1
Time frame	Time step	$\Delta t < 1$ [s]
Initial conditions	Initial uniform water level	Uniform water level
Boundaries	Upstream condition	Total discharge=30 [lit/s]

(* .bnd), (* .bct)	Downstream condition	Uniform water level
Physical parameters	Gravitational acceleration	$g=9.81$ [m ² /s]
	Fluid density	$\rho_w=1000$ [kg/m ³]
	Bed roughness	$C=20-25$ [m ^{0.5} /s]
	Wall condition	Free
	Uniform horizontal eddy viscosity	$Vicouv= 10^{-3}-10^{-2}$ [m ² /s]
	Uniform horizontal eddy diffusion	$Dicouv= 10^{-3}-10^{-2}$ [m ² /s]
	Depth specified	corners
	Depth at grid cell center	Max
	Threshold depth	$Thresh=5$ [cm]
Morphodynamic parameters		
Sediment (* .sed)	Type	Non-cohesive sand
	Specific Density	$RhoSol=2600$ [kg/m ³]
	Dry bed density	$CDryB= 1600$ [kg/m ³]
	Median sediment diameter	$SedDia (D_{50})= 0.5$ [mm]
	Initial sediment thickness	$IniSedThick= 25$ [cm]
Sediment formula (* .tra)	calibration coefficient	$\alpha= 8$
	Constant(I)	$b= 0$
	Constant(II)	$c= 1.5$
	ripple factor or efficiency factor	$\mu= 1$
	critical mobility factor	$\theta_{cr}= 0.047$
Morphology (* .mor)	Morphological scale factor	$MorFac= 1$
	Spin-up interval	$MorStt= 240$ [min]
	Minimum depth for sediment computations	$SedThr= 5$ [cm]
Trachytopo (* .tdf), (* .taf)	Vegetation height	$h_v= 30$ [cm]
	Vegetation density	$n= 0.025-0.05-0.1$ [1/m]
	Stem diameter	$d= 1$ cm
	Drag coefficient	$C_D=$ equation (6-1)

	Chézy roughness for bed in vegetation area	$C=10-15 [m^{0.5}/s]$
--	--	-----------------------

10 Appendix B: Experimental results

According to the figure 2.3, all of the velocity measurements were done by ADV in the flume done at 0.2 and 0.8 times of water depth. Considering the data analysis in chapter 4, in this appendix experimental results of velocity measurements are presented. At first profiles of components of the velocity are illustrated and then the ranges of them are presented.

10.1 Streamwise velocity

Profiles of streamwise velocity for experiments with a single patch of vegetation ($0.025 < \Omega_v < 0.1$) both near the bed and near the surface are presented in figures 10.1 to 10.6.

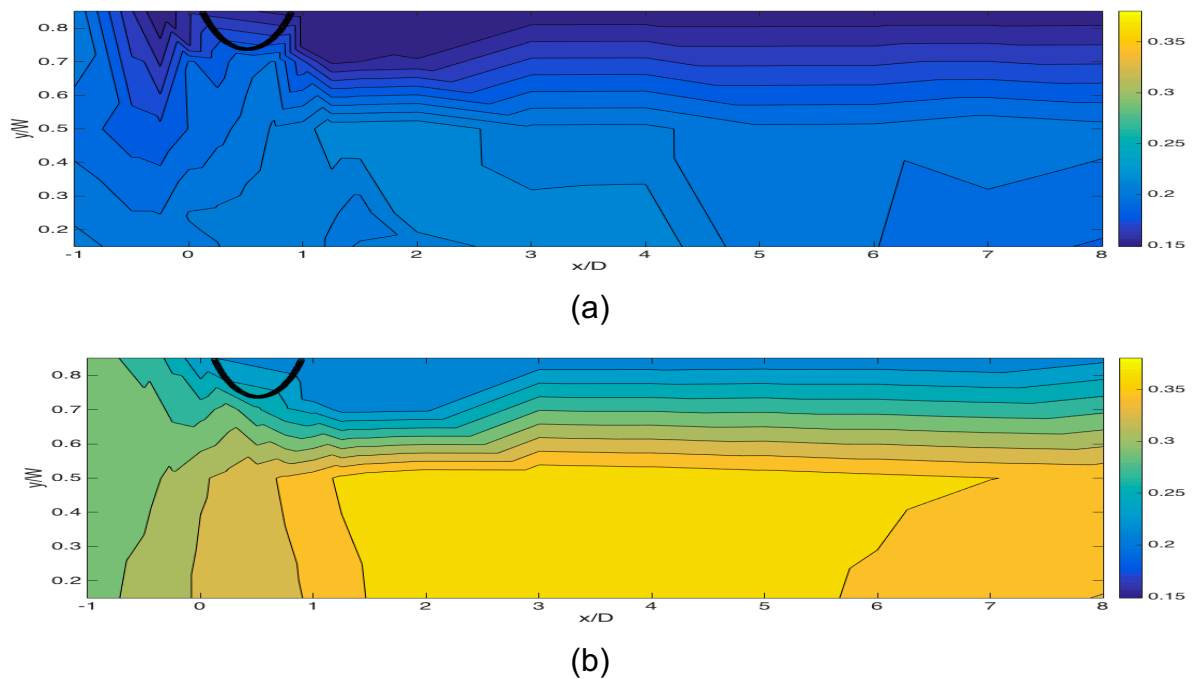
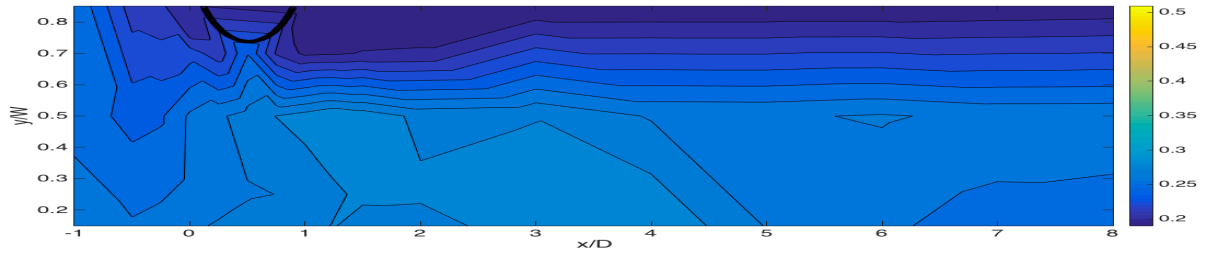
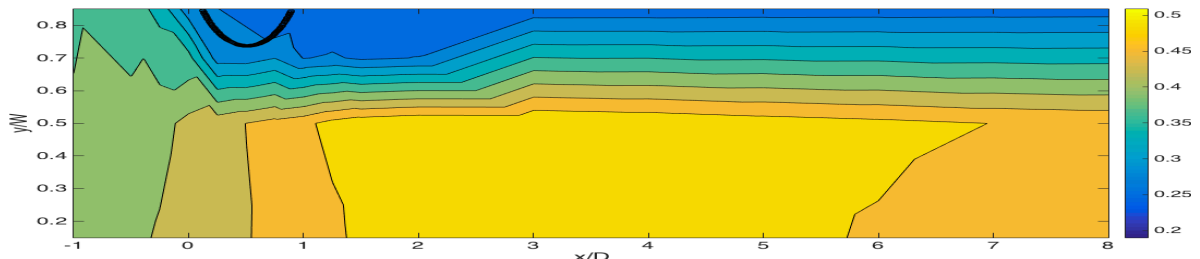


Figure 10.1. Plan view of the streamwise component of the velocity with Fr number=0.3 and $\Omega_v=0.025$, A: at 0.2 h, B: at 0.8h

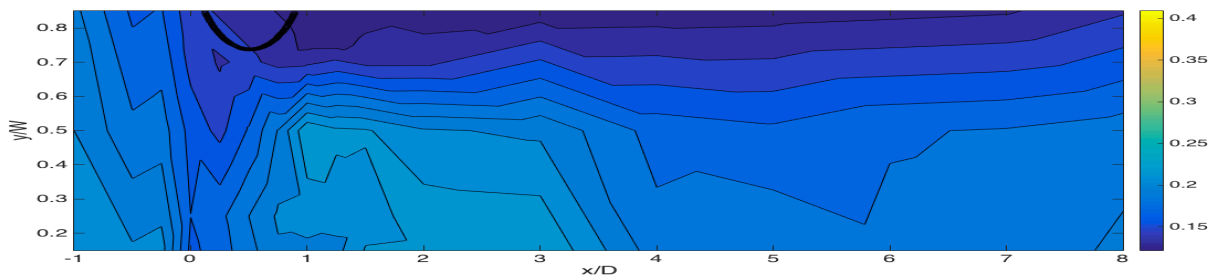


(a)

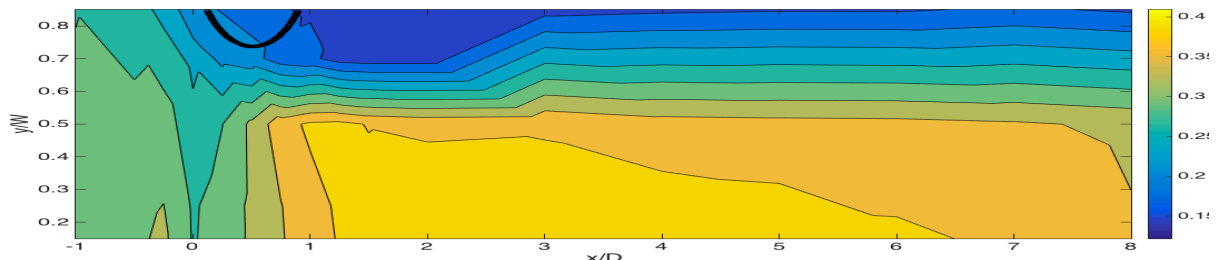


(b)

Figure 10.2. Plan view of the streamwise component of the velocity with Fr number=0.4 and $\Omega_v=0.025$, A: at 0.2 h, B: at 0.8h

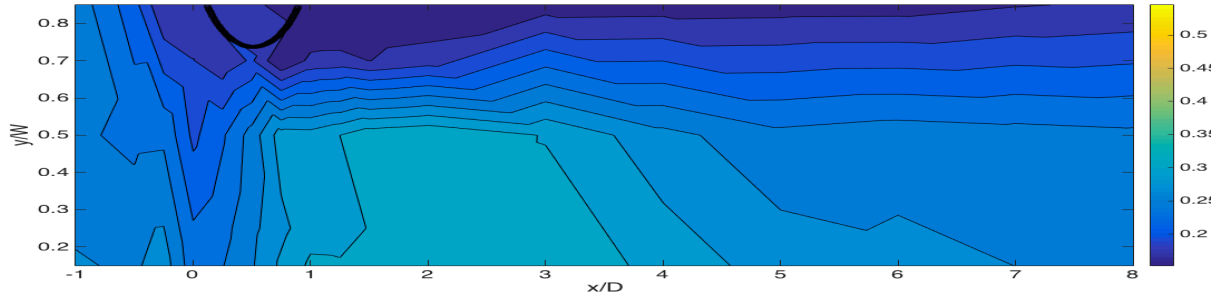


(a)

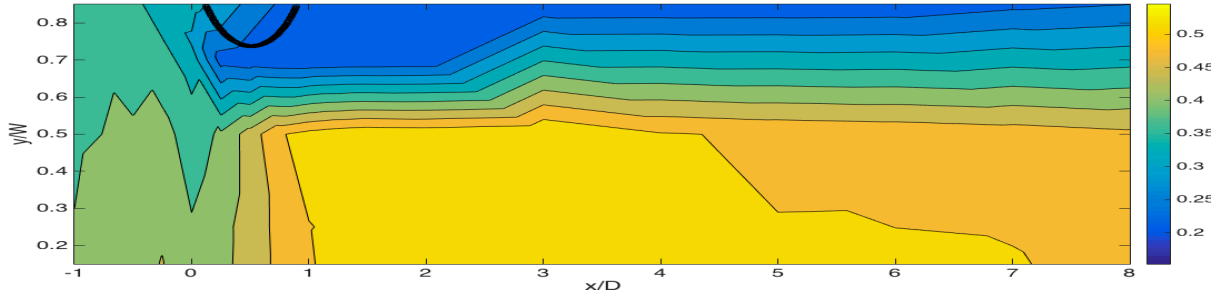


(b)

Figure 10.3. Plan view of the streamwise component of the velocity with Fr number=0.3 and $\Omega_v=0.05$, A: at 0.2 h, B: at 0.8h

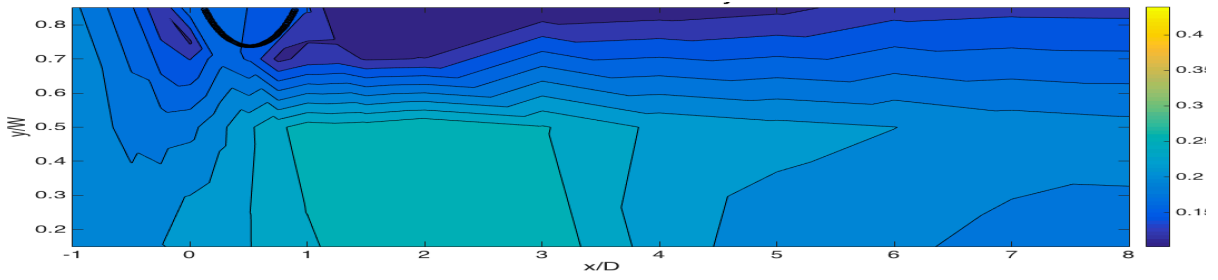


(a)

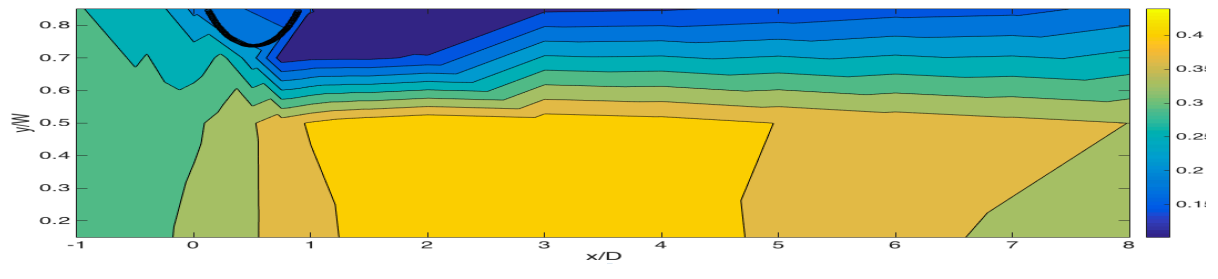


(b)

Figure 10.4. Plan view of the streamwise component of the velocity with Fr number=0.4 and $\Omega_v=0.05$, A: at 0.2 h, B: at 0.8h

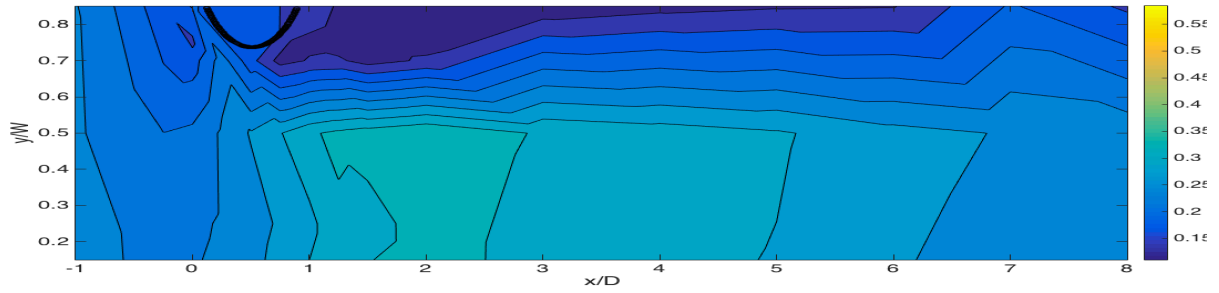


(a)

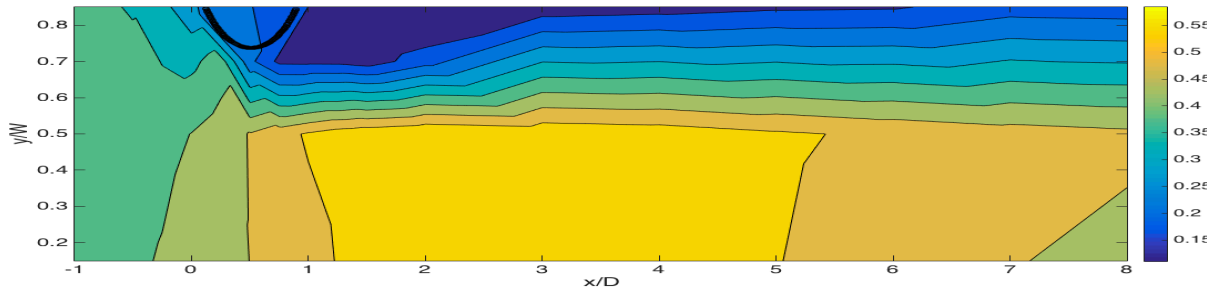


(b)

Figure 10.5. Plan view of the streamwise component of the velocity with Fr number=0.3 and $\Omega_v=0.1$, A: at 0.2 h, B: at 0.8h



(a)

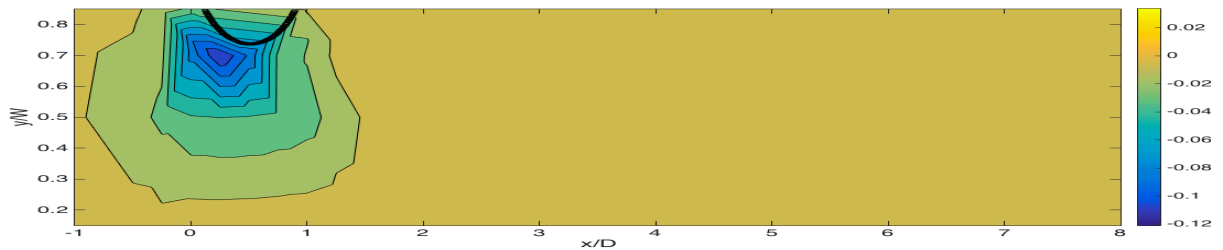


(b)

Figure 10.6. Plan view of the streamwise component of the velocity with Fr number=0.4 and $\Omega_v=0.1$, A: at 0.2 h, B: at 0.8h

10.2 Transverse velocity

profiles of transverse velocity for experiments with a single patch of vegetation ($0.025 < \Omega_v < 0.1$) both near the bed and near the surface are presented in figures 10.7 to 10.12.



(a)

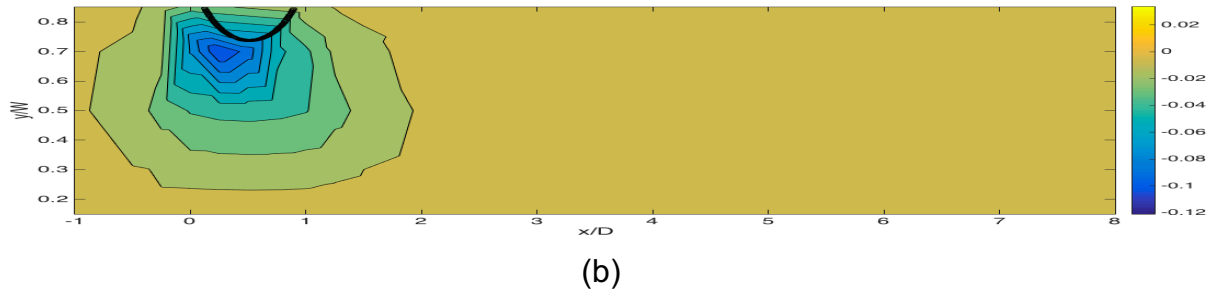


Figure 10.7. Plan view of the transverse component of the velocity with Fr number=0.3 and $\Omega_v=0.025$, A: at 0.2 h, B: at 0.8h

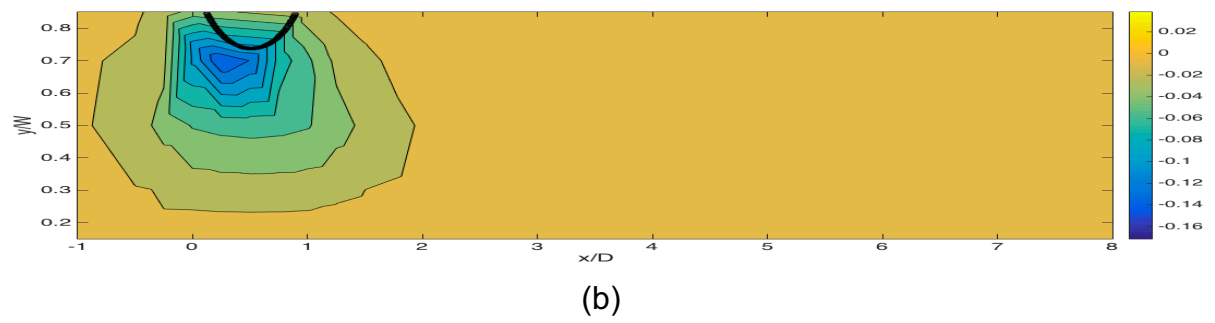
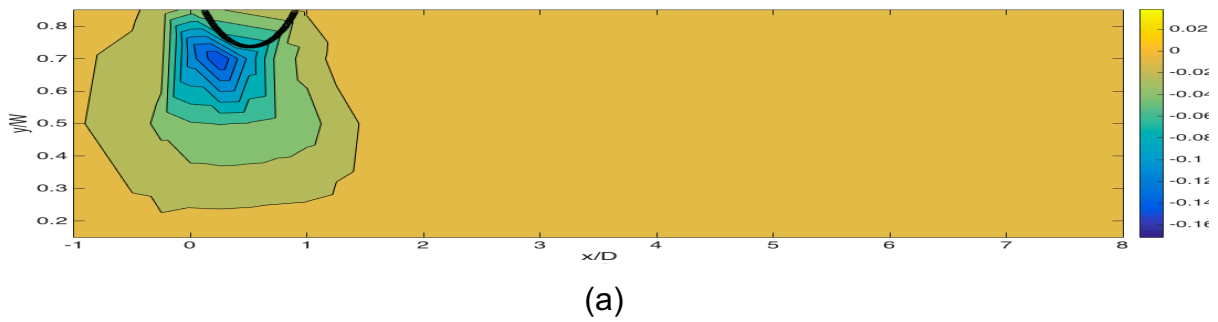
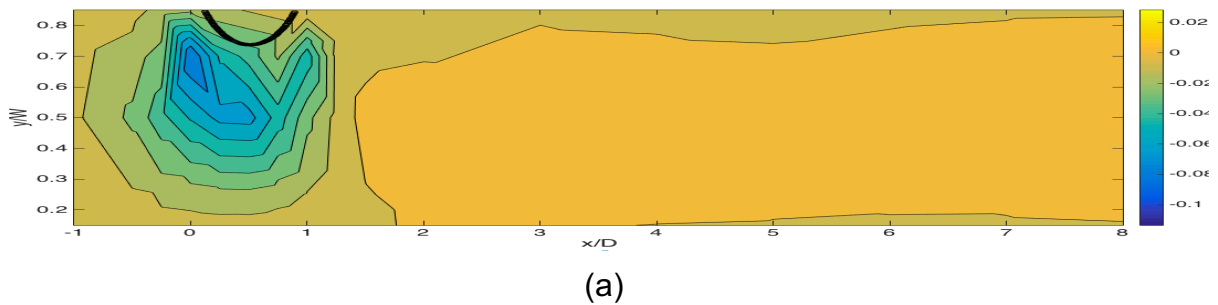


Figure 10.8. Plan view of the transverse component of the velocity with Fr number=0.4 and $\Omega_v=0.025$, A: at 0.2 h, B: at 0.8h



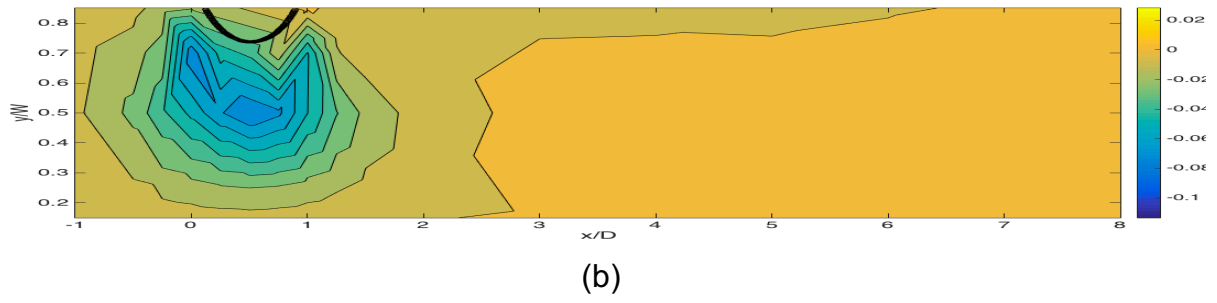


Figure 10.9. Plan view of the transverse component of the velocity with Fr number=0.3 and $\Omega_v=0.05$, A: at 0.2 h, B: at 0.8h

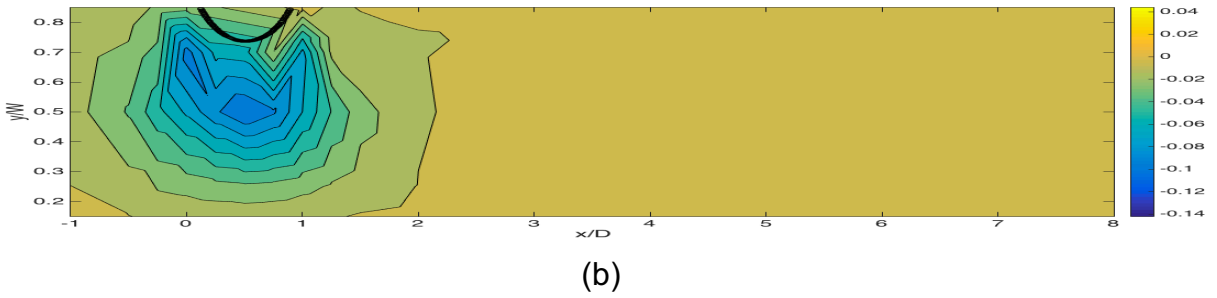
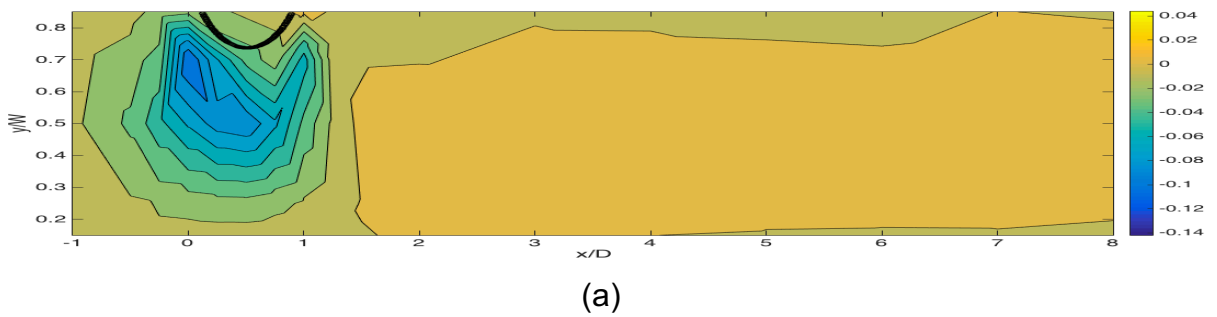
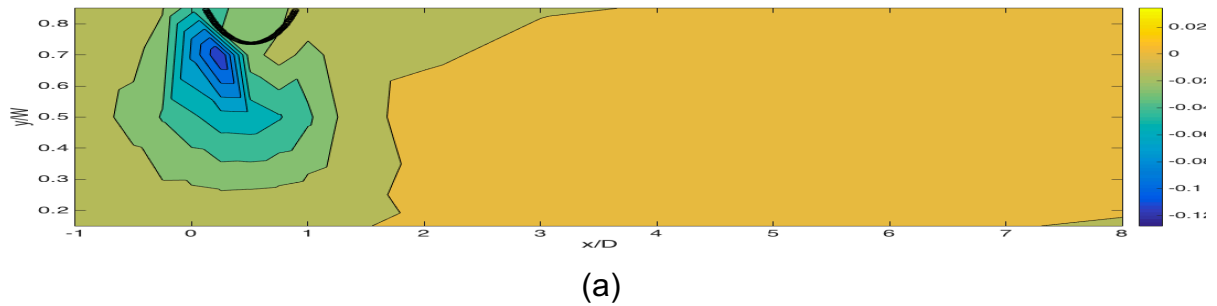


Figure 10.10. Plan view of the transverse component of the velocity with Fr number=0.4 and $\Omega_v=0.05$, A: at 0.2 h, B: at 0.8h



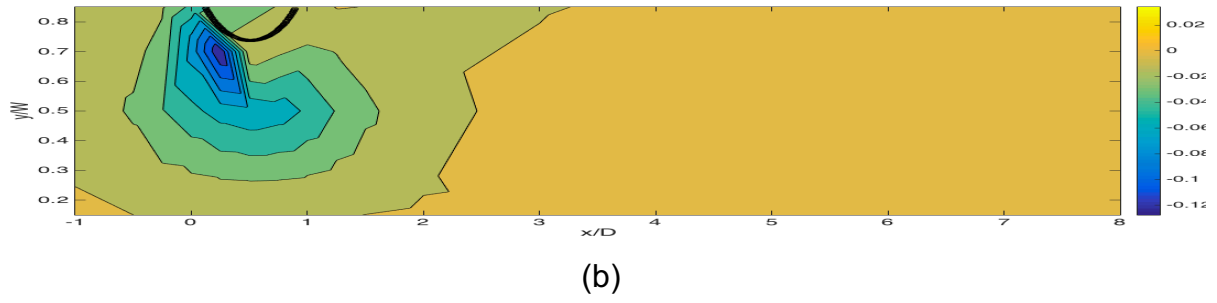


Figure 10.11. Plan view of the transverse component of the velocity with Fr number=0.3 and $\Omega_v=0.1$, A: at 0.2 h, B: at 0.8h

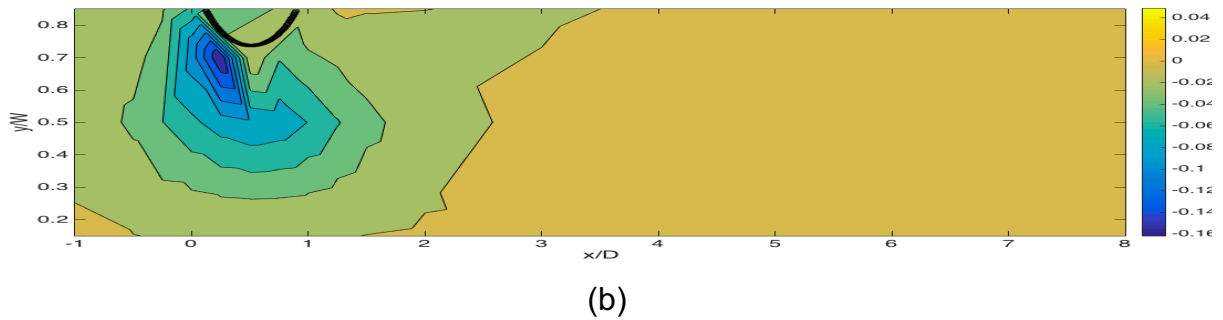
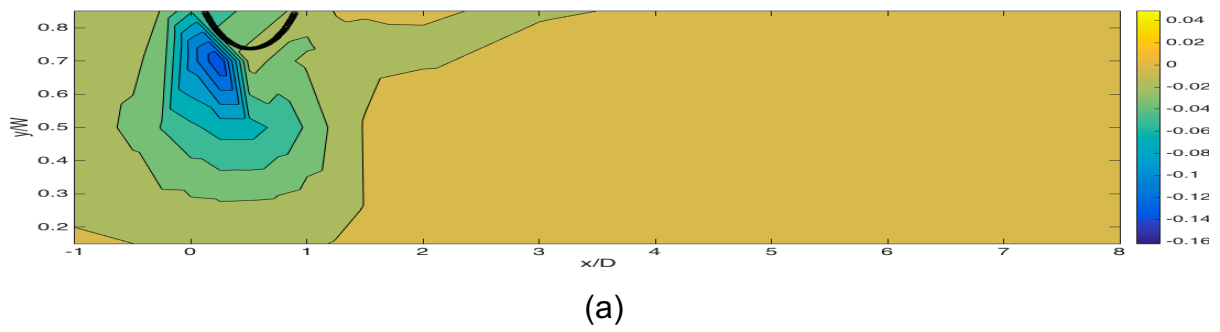
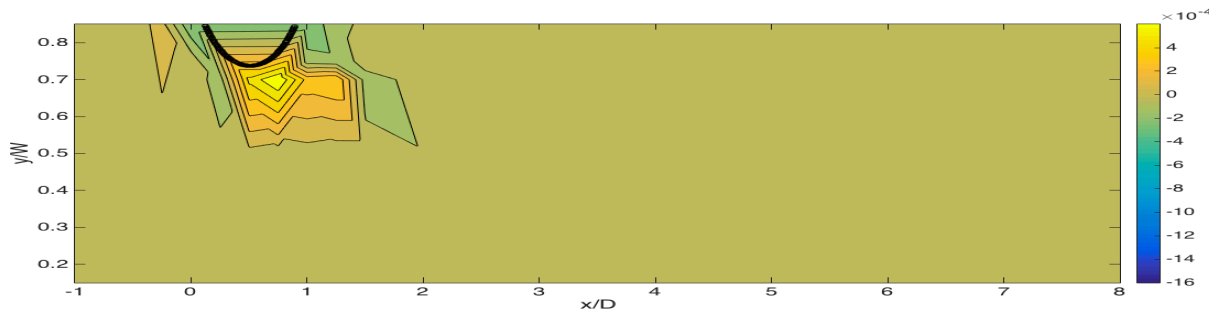


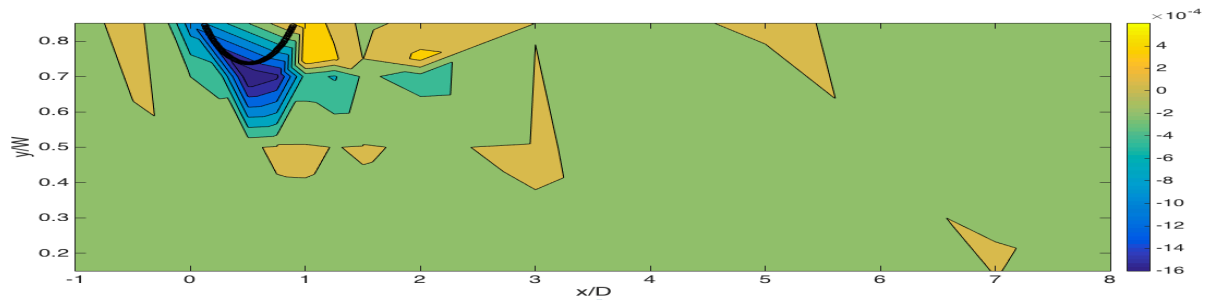
Figure 10.12. Plan view of the transverse component of the velocity with Fr number=0.4 and $\Omega_v=0.1$, A: at 0.2 h, B: at 0.8h

10.3 Vertical velocity

Profiles of vertical velocity for experiments with a single patch of vegetation ($0.025 < \Omega_v < 0.1$) both near the bed and near the surface are presented in figures 10.13 to 10.18.

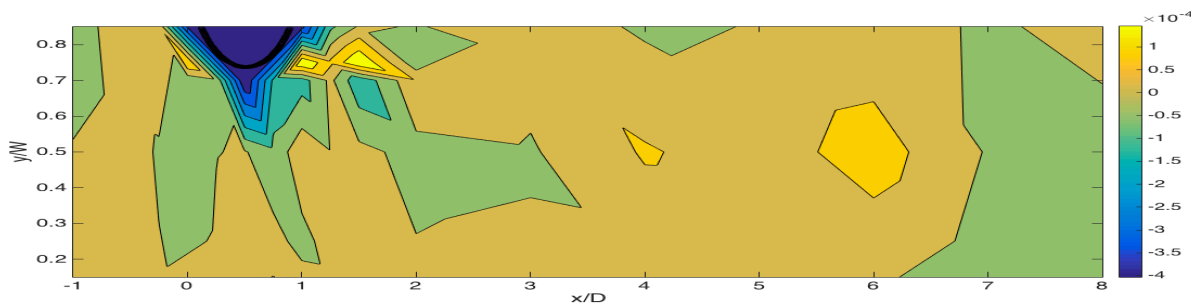


(a)

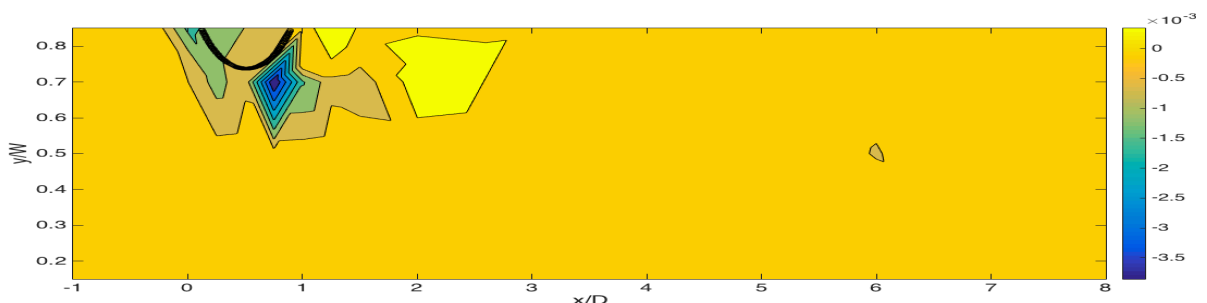


(b)

Figure 10.13.. Plan view of the vertical component of the velocity with Fr number=0.3 and density of the patch of vegetation=0.025, A: at 0.2 h, B: at 0.8h

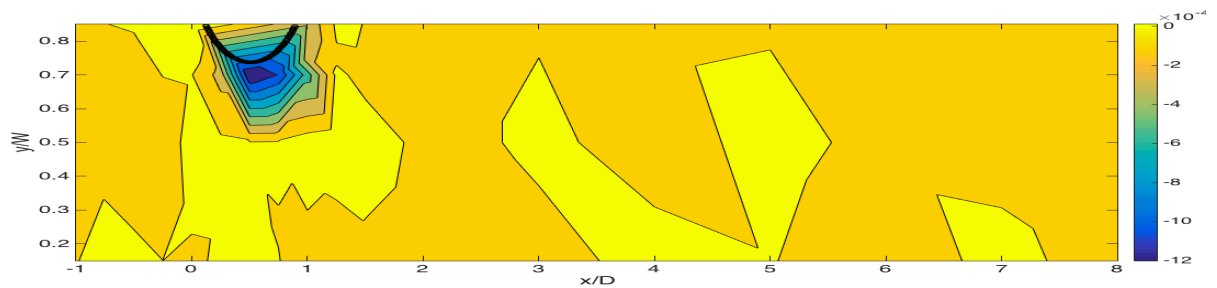


(a)

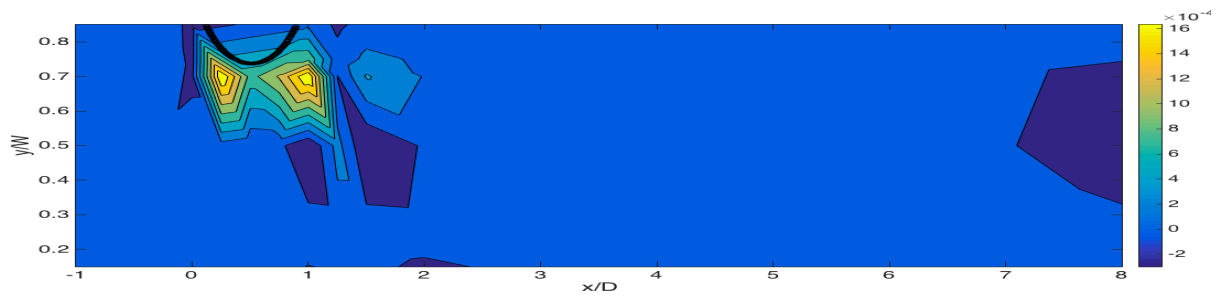


(b)

Figure 10.14.. Plan view of the vertical component of the velocity with Fr number=0.4 and density of the patch of vegetation=0.025, A: at 0.2 h, B: at 0.8h

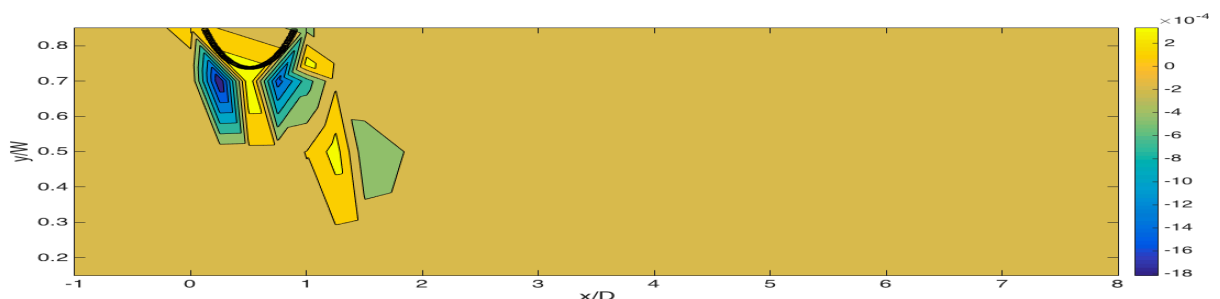


(a)

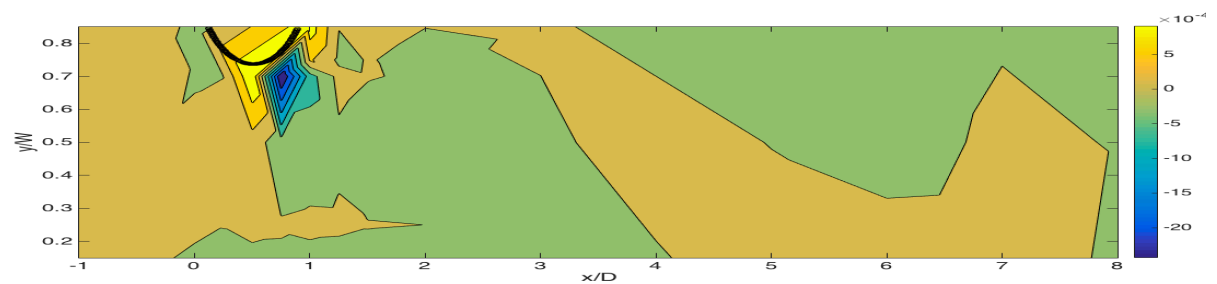


(b)

Figure 10.15. Plan view of the vertical component of the velocity with Fr number=0.3 and density of the patch of vegetation=0.05, A: at 0.2 h, B: at 0.8h

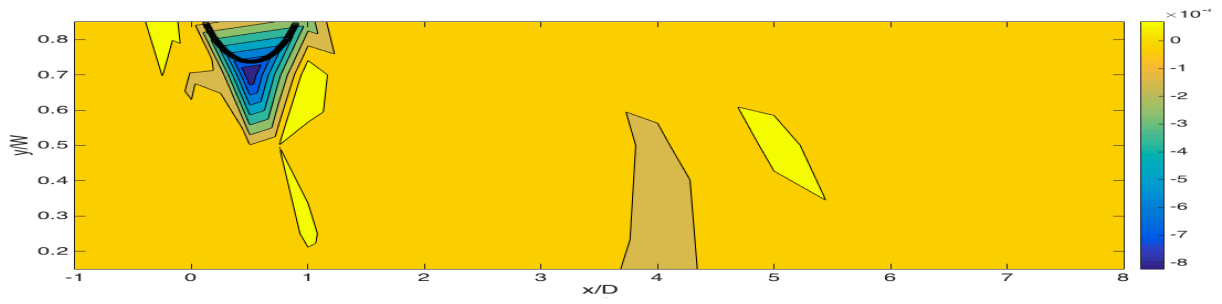


(a)

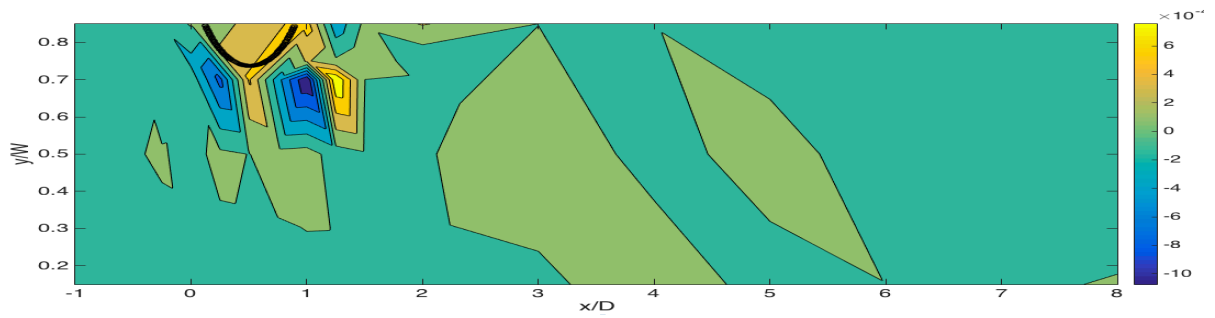


(b)

Figure 10.16. Plan view of the vertical component of the velocity with Fr number=0.4 and density of the patch of vegetation=0.05, A: at 0.2 h, B: at 0.8h

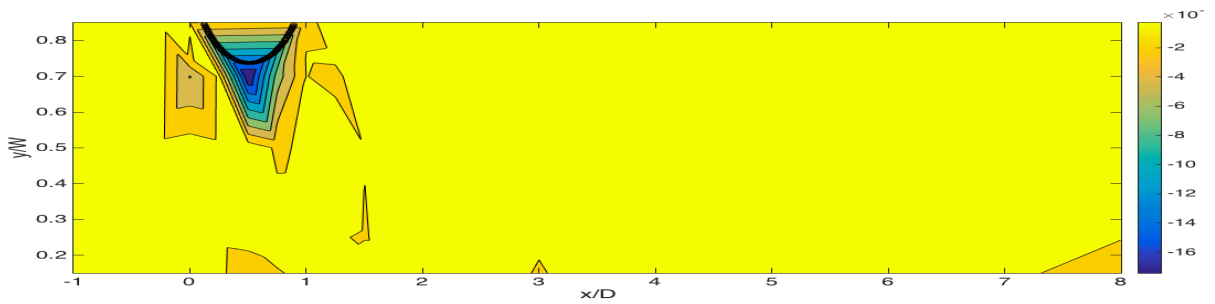


(a)

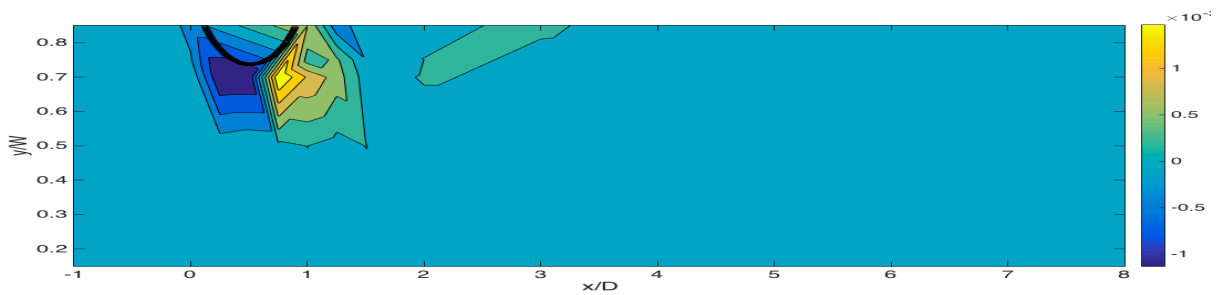


(b)

Figure 10.17. Plan view of the vertical component of the velocity with Fr number=0.3 and density of the patch of vegetation=0.1, A: at 0.2 h, B: at 0.8h



(a)



(b)

Figure 10.18. Plan view of the vertical component of the velocity with Fr

number=0.4 and density of the patch of vegetation=0.1, A: at 0.2 h, B: at 0.8h

10.4 Ranges of velocities

Figures 10.19 to 10.21 present the range of different components of the velocity for experiments with a single patch of vegetation ($0.05 < \Omega_v < 0.1$)

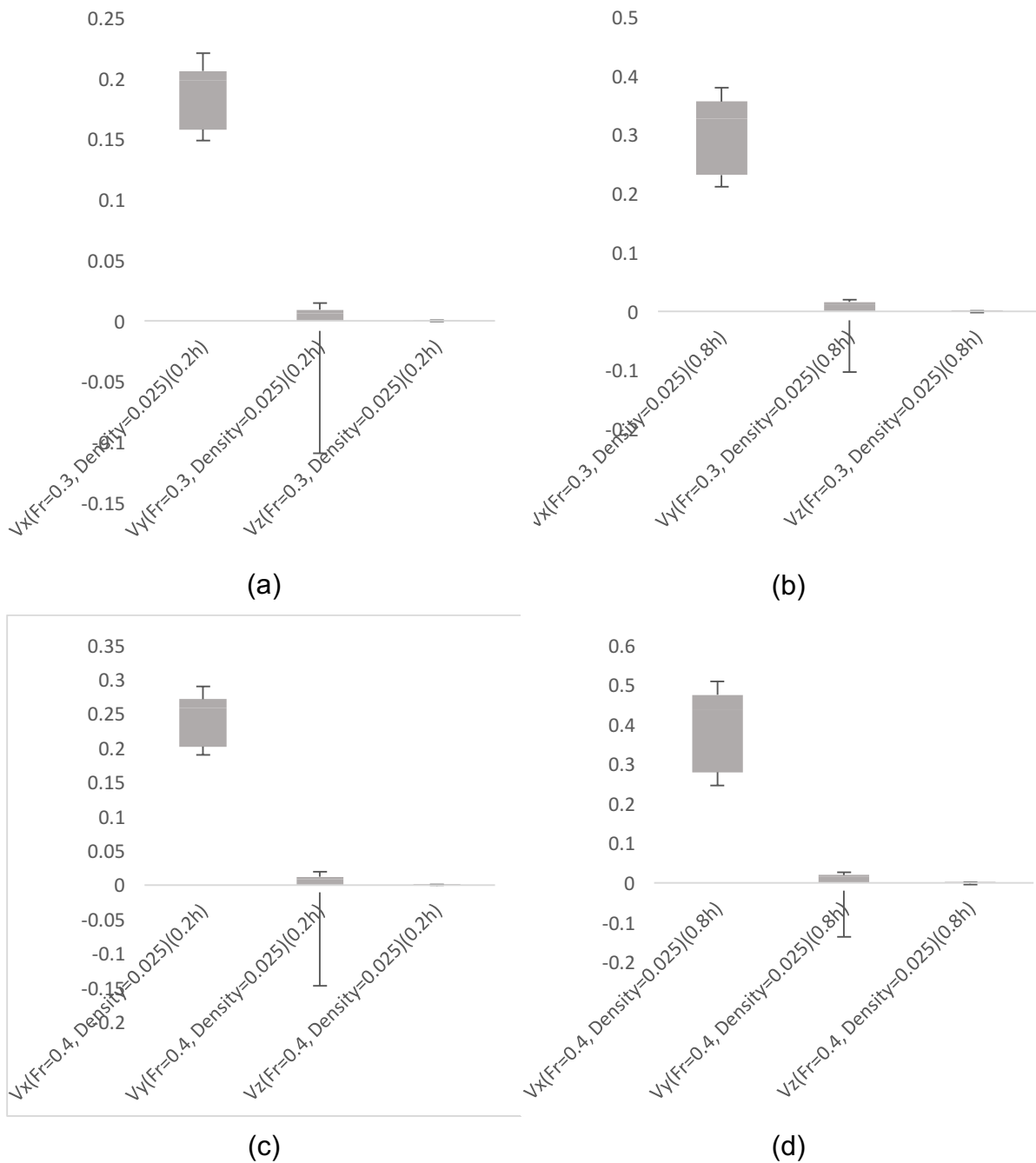


Figure 10.19. Ranges of velocity components. a: $Fr=0.3, \Omega=0.025$, at 0.2h; b:

Fr=0.3, $\Omega=0.025$, at 0.8h; c: Fr=0.4, $\Omega=0.025$, at 0.2h; d: Fr=0.4, $\Omega=0.025$, at 0.8h

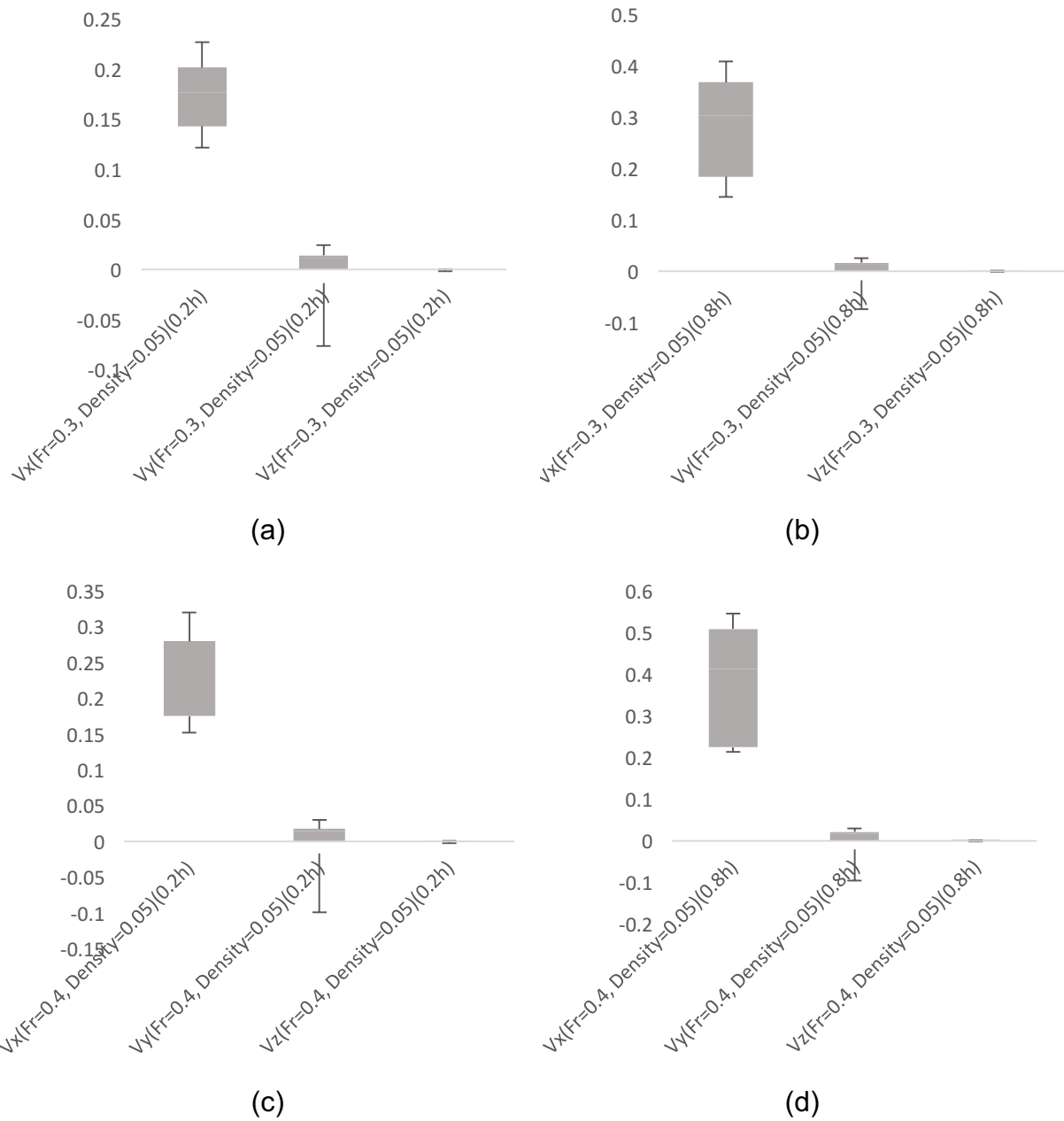


Figure 10.20. Ranges of velocity components. a: Fr=0.3, $\Omega=0.05$, at 0.2h; b: Fr=0.3, $\Omega=0.05$, at 0.8h; c: Fr=0.4, $\Omega=0.05$, at 0.2h; d: Fr=0.4, $\Omega=0.05$, at 0.8h

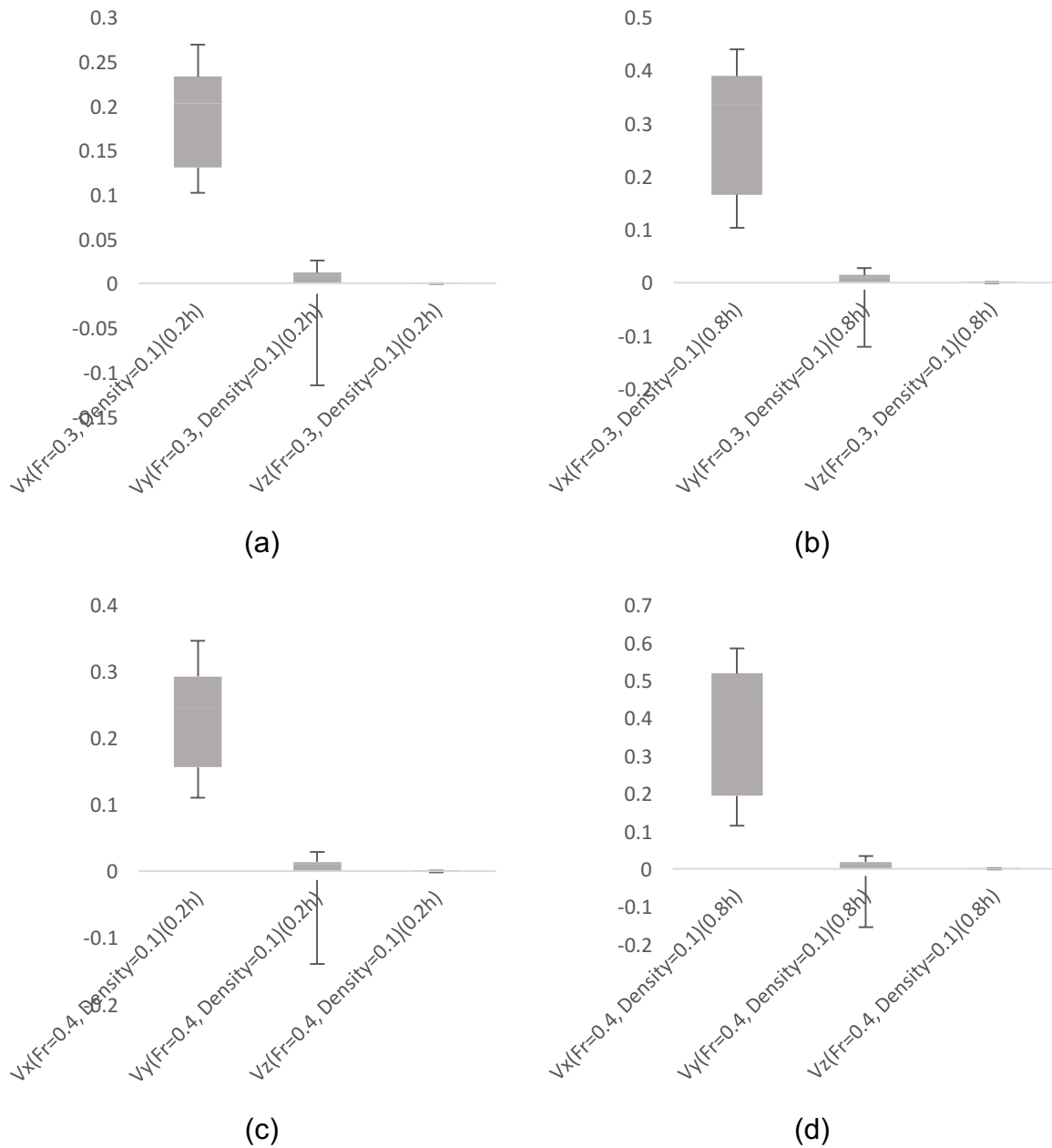


Figure 10.21. Ranges of velocity components. a: $Fr=0.3, \Omega=0.1$, at 0.2h; b: $Fr=0.3, \Omega=0.1$, at 0.8h; c: $Fr=0.4, \Omega=0.1$, at 0.2h; d: $Fr=0.4, \Omega=0.1$, at 0.8h